PNNL-16198

Pacific Northwest
National Laboratory
Operated by Battelle for the
U.S. Department of Energy

Carbon Tetrachloride Flow and Transport in the Subsurface of the 216-Z-18 Crib and 216-Z-1A Tile Field at the Hanford Site: Multifluid Flow Simulations and Conceptual Model Update

M. Oostrom
M. L. Rockhold
P. D. Thorne
G. V. Last
M. J. Truex

October 2006

Prepared for the U.S. Department of Energy
under Contract DE-AC05-76RL01830

DISCLAIMER

PACIFIC NORTHWEST NATIONAL LABORATORY
operated by
BATTELLE
for the
UNITED STATES DEPARTMENT OF ENERGY
under Contract DE-AC05-76RL01830

Printed in the United States of America

Available to DOE and DOE contractors from the
Office of Scientific and Technical Information,
P.O. Box 62, Oak Ridge, TN 37831-0062;
ph: (865) 576-8401
fax: (865) 576-5728
email: reports@adonis.osti.gov

Available to the public from the National Technical Information Service,
U.S. Department of Commerce, 5285 Port Royal Rd., Springfield, VA 22161
ph: (800) 553-6847
fax: (703) 605-6900
email: orders@ntis.fedworld.gov
online ordering: http://www.ntis.gov/ordering.htm


This document was printed on recycled paper.
(8/00)

PNNL-16198

Carbon Tetrachloride Flow and Transport in the Subsurface of the 216-Z-18 Crib and 216-Z-1A Tile Field at the Hanford Site: Multifluid Flow Simulations and Conceptual Model Update

M. Oostrom
M. L. Rockhold
P. D. Thorne
G. V. Last
M. J. Truex

October 2006

Prepared for
the U.S. Department of Energy
under Contract DE-AC05-76RL01830

Pacific Northwest National Laboratory
Richland, Washington 99352

Abstract

Past practices resulted in the discharge of carbon tetrachloride (CT, tetrachloromethane) to the 216-Z-9, 216-Z-1A, and 216-Z-18 waste sites in the 200-PW-1 Operable Unit in the 200 West Area of the U.S. Department of Energy's (DOE's) Hanford Site in Washington State. Fluor Hanford, Inc. is conducting a Comprehensive Environmental Response, Compensation, and Liability Act (CERCLA) remedial investigation/feasibility study (RI/FS) for the 200-PW-1 Operable Unit. As part of this overall effort, Pacific Northwest National Laboratory was contracted to improve the conceptual model of how CT is distributed in the Hanford 200 West Area subsurface through use of numerical flow and transport modeling. This work supports the DOE's efforts to characterize the nature and distribution of CT in the 200 West Area and to subsequently select an appropriate final remedy.

Three-dimensional modeling was conducted with layered models to further develop the conceptual model of CT distribution in the vertical and lateral direction beneath the 216-Z-1A tile field and 216-Z-18 cribs and to investigate the effects of soil vapor extraction (SVE). Base case and sensitivity analysis simulations considered migration of dense, nonaqueous phase liquid (DNAPL) consisting of CT and co-disposed organics in the subsurface beneath the two disposal sites as a function of the properties and distribution of subsurface sediments and of the properties and disposal history of the waste. Simulations of CT migration were conducted using the Subsurface Transport Over Multiple Phases (STOMP) simulator.

Simulation results support a conceptual model for CT distribution where CT in the DNAPL phase is expected to have migrated primarily in a vertical direction below the disposal trench. None of the simulations predicted that CT in the DNAPL phase would move across the water table below the 216-Z-18 site. Movement of CT in the DNAPL phase across the water table below the 216-Z-1A site was only predicted in simulations with smaller disposal areas and larger volumes, compared to the base case simulation, and in isotropic porous media. Because uncertainties in disposal area and volume exist, movement of CT in the DNAPL phase across the water table in the subsurface below the 216-Z-1A site should be considered as a possibility. However, even if DNAPL moved across the water table in the past, there may not currently be a DNAPL phase in the groundwater beneath the 216-Z-1A site because of dissolution. Results also show that the Hanford 1a geologic unit, located just beneath the 216-Z-1A and 216-Z18 disposal areas, retains more CT DNAPL within the vadose zone during infiltration and redistribution than other hydrologic units. During simulated SVE operations, CT in this unit remained in the subsurface while DNAPL in other layers was effectively removed. Additional characterization of the Hanford 1a unit below the two disposal sites would provide valuable information about the quantity of DNAPL phase CT remaining in the vadose zone. A significant amount of the disposed CT DNAPL may have partitioned to the vapor phase and subsequently into water and sorbed phases. As for the 216-Z-9 site, it is predicted that any continued migration of CT from the vadose zone to the groundwater is likely to occur through interaction of vapor phase CT with the groundwater and not through continued DNAPL migration. The results indicated that SVE appears to be an effective technology for vadose zone remediation, but additional effort is needed to improve simulation of the SVE process through an enhanced understanding of rate-limited volatilization.

Executive Summary

Carbon tetrachloride (CT) was discharged to waste sites that are part of the 200-PW-1 Operable Unit in the 200 West Area of the U.S. Department of Energy's (DOE's) Hanford Site in Washington State. Fluor Hanford, Inc. is conducting a Comprehensive Environmental Response, Compensation, and Liability Act (CERCLA) remedial investigation/feasibility study (RI/FS) for the 200-PW-1 Operable Unit. The RI/FS process and remedial investigations for the 200-PW-1, 200-PW-3, and 200-PW-6 Operable Units are described in the Plutonium/Organic-Rich Process Condensate/Process Waste Groups Operable Unit RI/FS Work Plan. As part of this overall effort, Pacific Northwest National Laboratory (PNNL) was contracted to improve the conceptual model of how CT is distributed in the Hanford 200 West Area subsurface through use of numerical flow and transport modeling. This work supports the DOE's efforts to characterize the nature and distribution of CT in the 200 West Area and to subsequently select an appropriate final remedy.

Three-dimensional modeling was conducted with layered models to refine and update the conceptual model of CT distribution in the vertical and lateral direction beneath the 216-Z-1A tile field and 216-Z18 crib and to investigate the effects of Soil Vapor Extraction (SVE) as a CT remediation option. Simulations targeted migration of dense, nonaqueous phase liquid (DNAPL) consisting of CT and co-disposed organics in the subsurface beneath the two disposal sites as a function of the properties and distribution of subsurface sediments and of the properties and disposal history of the waste. The geological representation of the computational domain was extracted from a larger EarthVision™ geologic model of the 200 West Area subsurface. Simulations of CT migration were conducted using the Water-Oil-Air mode of the Subsurface Transport Over Multiple Phases (STOMP) simulator (White and Oostrom 2006). The simulations considered disposal of liquid waste at the 216-Z-1, Z-2, and Z-3 sites, prior to disposal at the 216-Z-1A and 216-Z18 sites.

A total of 34 three-dimensional simulations have been conducted based on a layered EarthVision™ geologic model, which is an interpretation of available geologic data. These simulations consist of one base case simulation and 33 sensitivity analysis simulations. These simulations examined the infiltration and redistribution of CT from 1954 through 1993, just before the SVE treatment began. A second series of simulations examined the impact of SVE on the carbon tetrachloride distribution in the subsurface over the time period of 1993 to 2005. The simulations were completed on the Environmental Molecular Sciences Laboratory (EMSL) MPP2 supercomputer.

Results of the simulations, summarized below, refer to movement of CT through the different geological layers in the subsurface beneath the disposal sites. The first geologic unit encountered is the H1a unit, a near surface unit of the Hanford Formation that is present in some locations in the 200 West Area. The next units encountered are the H1 and H2 units of the Hanford formation, respectively. The Cold Creek unit (CCU) underlies the H2 unit and is significant in that it contains a fine-grained silt layer and a caliche layer. These layers have significantly different hydraulic properties and can retain more CT than other units in the vadose zone. The Ringold E unit is below the CCU. The water table is located in the Ringold E unit about 20 m below the CCU.

Results of Base Case Simulation

Simulated DNAPL movement at the 216-Z-1A site for the base case simulation parameter values shows DNAPL movement only as deep as the CCU and DNAPL does not move across the water table. CT disposal at the 216-Z-1A site impacts the groundwater only through vapor and aqueous phase migration. Similarly, simulated DNAPL movement is limited at the 216-Z-18 site with DNAPL not penetrating any deeper than the H2 unit. CT disposal at the 216-Z-18 site has a limited impact on the groundwater through vapor and aqueous phase migration. The limited movement of DNAPL at these two disposal sites is partially due to the presence of the H1a unit just below the disposal site. The properties of this unit are such that DNAPL is retained to a greater extent than in the H1 and H2 units below. The H1a unit is not present at the 216-Z-9 site where previous simulations (Oostrom et al. 2004 and 2006) showed much more significant vertical movement of DNAPL.

Results of Sensitivity Simulations

The categories of sensitivity simulations conducted in this modeling effort included 1) Disposal Site Area (footprint), 2) DNAPL Volume, 3) DNAPL Properties and Porous Media Properties Related to CT, 4) Porous Media Properties of the H1a Unit, 5) Porous Media Properties of the Cold Creek Unit, and 6) Porous Media Properties of all Units. Key results of these sensitivity simulations are summarized in the following paragraphs.

Sensitivity simulations with decreased disposal site area (infiltration area) showed significantly different results than for the base case. In all three sensitivity cases, DNAPL was predicted to move across the water table beneath the 216-Z-1A site, and the DNAPL moved deeper into the H2 unit beneath the 216-Z-18 site. Increasing the DNAPL volume (category 2) also increased DNAPL penetration in the subsurface. When DNAPL volume was doubled, DNAPL was predicted to move across the water table beneath the 216-Z-1A site. Sensitivity simulations where the DNAPL properties or properties related the CT (e.g., solubility, partitioning coefficient) did not result in any DNAPL movement across the water table. Some of these sensitivity cases did change the distribution of CT within the subsurface by changing the distribution of CT between the DNAPL, vapor, aqueous, and sorbed phases. Porous media properties of the H1a unit or the CCU also impact the distribution of CT in the subsurface, but none of the sensitivity simulations for these units resulted in DNAPL moving across the water table. However, the sensitivity case where the anisotropy ratio was globally lowered to a value of 1:1 for all units and the case where the horizontal and vertical permeability of all units was increased by a factor of 10 showed significant changes in the simulated DNAPL migration and overall distribution of CT compared to the base case. The lower anisotropy ratio resulted in simulation of a large quantity of DNAPL crossing the water table beneath the 216-Z-1A site.

Of importance, some of the sensitivity simulations that showed DNAPL moving across the water table are the results of changes in parameters for which there is a large uncertainty in the actual value. For instance, the actual infiltration area is not well known and if this area were smaller than what was selected for the base case, DNAPL may have moved across the water table beneath the 216-Z-1A site. Similarly, there is some uncertainty in the volume of DNAPL disposed and the porous media property values. Thus, interpretation of the results reported herein should consider both the base case and the sensitivity simulations.

Results of Soil Vapor Extraction Simulations

The simulations of SVE showed similar results to what has been previously reported in Oostrom et al. (2004 and 2006) in that the model appears to predict extraction of more CT by SVE than has been observed in the field. There are several possible reasons for the discrepancy between observed and simulated results, including uncertainties in flow rates, fluid-media properties, and disposal history (e.g., volumes, rates, and timing). The differences may also result from the current simulations being based on equilibrium phase partitioning, meaning simulations do not account for any rate-limited (kinetic) interfacial mass transfer effects. However, the SVE simulation results suggest that SVE will be effective for removing CT from the permeable units of the Hanford and Ringold Formation and that residual CT will be predominantly located in the CCU, H1a unit or in other silt lenses. Thus, SVE can be effective at removing the driving force for future CT migration to the groundwater because this migration must occur through these permeable units.

Conceptual Model Implications

The simulations results reported herein generally support the conclusions reported by Oostrom et al. (2004; 2006).

- *Where is CT expected to accumulate?* CT DNAPL accumulates in the finer-grain sediments of the vadose zone but does not appear to pool on top of these layers. From the 216-Z-1A and 216-Z-18 modeling effort, CT DNAPL accumulates in the finer-grained sediments of the vadose zone such as the CCU and the H1a unit.

- *Where would continuing liquid CT sources to groundwater be suspected?* Migration of DNAPL CT tends to be preferentially vertically downward below the disposal area. Considerable lateral movement of DNAPL CT is not likely. However, significant lateral migration of vapor CT occurs. From the 216-Z-1A and 216-Z-18 modeling effort, DNAPL movement to the groundwater is not likely below the 216-Z-18 site. None of the simulations reported here show any movement of DNAPL across the water table below the 216-Z-18 site. DNAPL movement to the groundwater is possible below the 216-Z-1A site, although only 5 of the 35 simulation show such DNAPL movement to below the water table.

- *What is the estimated distribution and state of CT in the vadose zone?* The majority of the CT was typically a DNAPL or in the sorbed phase in 1993. Heterogeneities, however, as shown in the results reported herein, tend to increase the amount of CT present in the vapor and related water and sorbed phases compared to the DNAPL phase. The center of mass for CT in the vadose zone was typically directly beneath the disposal area and within the CCU. From the 216-Z-1A and 216-Z-18 modeling effort, similar to the CT below the 216-Z-9 site, the majority of the CT was typically a DNAPL or sorbed to the solid phase in 1993 for both the 216-Z-1A and 216-Z-18 sites. The center of mass for CT in the vadose zone was typically directly beneath the disposal area and within the CCU.

- *How does SVE affect the distribution of CT in the vadose zone?* The 216-Z-1A and 216-Z-18 modeling effort directly supports the conclusions of the 216-Z-9 modeling results. The simulations predict that SVE effectively removes CT from the permeable layers of the vadose zone. Finer-grain porous media with larger moisture contents, such as the CCU sediments, are less affected by SVE.

- *Where would DNAPL contamination in groundwater be suspected?* The 216-Z-1A and 216-Z-18 modeling effort directly supports the conclusions of the 216-Z-9 modeling results, although DNAPL is only predicted to move across the water table under certain sensitivity conditions for the 216-Z-1A site. Simulations indicate that migration of DNAPL is primarily in the vertical direction such that DNAPL, if present in the groundwater, would be most likely expected in a zone distributed around the centerline of the disposal area.

Updates to the previous conceptual model depicted in the RI/FS Work Plan (DOE 2004) are listed below and are consistent with conceptual model shown in the recent RI report (DOE 2006).

1. No lateral movement of DNAPL to under Plutonium Finishing Plant (PFP) is likely.
2. The zones of persistent CT mass in the vadose zone are primarily the CCU and H1a geologic units.
3. Large vertical and lateral density-driven movement of vapor occurred in the past.
4. DNAPL penetration to groundwater is likely to have occurred at the 216-Z-9 site, possible at the 216-Z-1A site, and unlikely at the 216-Z-18 site.
5. DNAPL penetration to the groundwater from undocumented releases is unlikely.
6. The phase distribution of CT changes over time due to volatilization, interaction of gas-phase CT with pore water and aqueous-phase CT with sorbed phase, DNAPL dissolution in groundwater, and the impact of soil vapor extraction.

Simulation results from the 216-Z-1A and 216-Z-18 modeling effort herein and from Oostrom et al. (2004 and 2006) were also compared to available field data. Key conclusions from this comparison are listed below.

- High soil concentrations and predicted areas with high DNAPL saturations are spread vertically within a relatively small lateral area within about 30 m of the disposal area footprint.

- Measured groundwater concentrations are higher and the high groundwater concentrations are spread deeper in the aquifer beneath the 216-Z-9 site compared to the 216-Z-1A and 216-Z-18 sites. This observation correlates to modeling results where the CT flux to the groundwater at the 216-Z-9 site was significantly higher than the flux at the 216-Z-1A and 216-Z-18 sites. Modeling results showing a larger number of sensitivity simulations with DNAPL flux to groundwater and deeper penetration of DNAPL within the aquifer beneath the 216-Z-9 site compared to the other two disposal areas are also consistent with these observations.

Model results can also be compared to this field data to evaluate reasonable scenarios for how CT entered the groundwater. For instance, with 100,000 kg of CT that entered the aquifer (based on the estimate in Murray et al. 2006), only by combining the estimates of CT mass flux to the groundwater from simulation sensitivities (not the base cases) that show DNAPL crossing the water table predict a combined mass of CT (216-Z-9, Z-18, and Z-1A) in the aquifer similar to the estimated CT mass. The average CT mass of dissolved CT that has been transported across the water table (a measure of the impact of vapor phase transport to the groundwater table and pore water from the vadose zone entering the groundwater) for all three sites through 1993 is approximately 5,000 – 10,000 kg. The accumulated CT mass in the aquifer would be significantly lower than the mass of CT in the groundwater estimated by Murray et al. (2006) if only aqueous and vapor phase CT and no DNAPL phase entered the groundwater. This assessment indicates that it is likely that DNAPL CT has entered the groundwater. The simulation

results herein and in Oostrom et al. (2004; 2006) show that the most likely location of significant DNAPL movement across the water table is below the 216-Z-9 site.

Research Recommendations

- For the simulations described for the 216-Z-9 disposal site (Oostrom et al. 2004; 2006), the CCU silt and carbonate units accumulated and retained relatively large amounts of DNAPL CT. The simulation results presented in this report show that considerable accumulation is predicted in the H1a unit, located directly below the two disposal sites. Sensitivity simulations show that DNAPL flow behavior in this unit is largely affected by permeability and porosity. Additional characterization of the H1a unit hydraulic properties would yield an enhanced estimate for that unit's ability to retain CT DNAPL.

- Similar to the results shown in Oostrom et al. (2006), the simulated SVE yields are strongly affected by the assumption of equilibrium phase partitioning. None of the simulations in this report account for any rate-limited (kinetic) interfacial mass transfer effects. Laboratory and theoretical investigations into the kinetic behavior of CT mass transfer between DNAPL and the aqueous, gas, and sorbed phases are necessary to develop a science-based model for CT mass transfer.

Acknowledgments

The parallel processing simulations on the MPP2 supercomputer were performed under a Computational Grand Challenge Application project, “Multifluid Flow and Multicomponent Reactive Transport in Heterogeneous Subsurface Systems,” at the Molecular Science Computing Facility (MSCF) in the William R. Wiley Environmental Molecular Sciences Laboratory (EMSL), a national scientific user facility sponsored by the U.S. Department of Energy’s Office of Biological and Environmental Research and located at the Pacific Northwest National Laboratory, in Richland, Washington.

The residual DNAPL saturations were obtained in the Subsurface Flow and Transport Experimental Laboratory at the W. R. Wiley Environmental Molecular Sciences Laboratory. Development of the experimental procedures to determine residual DNAPL saturations was funded by the Remediation and Closure Science Project, through the U.S. Department of Energy’s Richland Operations Office.

Contents

Figures

Tables

1.0 Introduction

Plutonium recovery operations within the Z-Plant aggregate area (Plutonium Finishing Plant [PFP]) at the Hanford Site resulted in organic and aqueous wastes that were disposed at several cribs, tile fields and French drains. The organic waste consisted of carbon tetrachloride (CT) mixed with lard oil, tributyl phosphate (TBP), and dibutyl butyl phosphonate (DBBP). The main disposal areas were the 216-Z-9 trench, 216-Z-1A tile field, and 216-Z-18 crib. The location of the disposal sites can be found in Figure 3.1. The three major disposal facilities received a total of about 13,400,000 L of liquid waste containing 363,000 to 580,000 L of CT. Assuming a maximum CT aqueous solubility of 800 mg/L and a fluid density of 1.59 g/cm^3, the 13,400,000 L of liquid waste would be able to contain approximately 6,700 L of CT in dissolved form. This indicates the majority of the CT entered the subsurface as an organic liquid. Although a considerable amount of the disposed CT is assumed to remain in the vadose zone as a residual liquid, the physical processes describing the formation of residual dense, nonaqueous phase liquid (DNAPL) in the vadose zone are not well understood and have not previously been incorporated into multi-fluid flow simulators.

Two remediation technologies have been applied near the PFP facility. Between 1992 and 2000, about 76,500 kg (48,100 L) of CT was removed using a soil-vapor extraction (SVE) system in the vadose zone. In addition, a pump-and-treat system for the unconfined aquifer removed 4,570 kg (2,870 L) of CT from groundwater between 1996 and 2000.

Between 1996 and 2000, dissolved CT concentrations increased at several groundwater extraction wells located in the northern part of the PFP complex. The persistence of the contamination suggests that a continuing DNAPL source may be present in the vadose zone or groundwater. Further remedial action decisions require the identification of any continuing sources of CT beneath the PFP (DOE 2001).

Several conceptual models have been proposed to explain the behavior of CT mixtures in the subsurface. The conceptual models were summarized as follows (DOE 2004):

1. Downward migration of CT through disposal facilities and underlying soil column to groundwater, with lateral migration of groundwater to the PFP.

2. Downward migration of CT at the disposal site through underlying soil column to the Cold Creek unit (CCU; see Chapter 3 for a discussion of the geology), with lateral migration along the top of the unit toward the PFP. In addition, CT also moves vertically to the groundwater and laterally to the PFP.

3. Downward migration from an unknown source.

4. Vapor migration from major disposal sites to groundwater, followed by lateral movement to the PFP.

5. A combination of options 1 through 4.

A series of three-dimensional multifluid flow simulations was conducted by Oostrom et al. (2004; 2006) with the STOMP simulator (White and Oostrom 2006) to examine the impact of parameter varia-

tion on the migration of CT in the subsurface beneath the 216-Z-9 disposal area over the period from 1954 to 1993, when SVE was initiated in the area. The numerical models were configured using available information regarding the hydrogeology, measured fluid properties for the likely mixtures of disposed organic liquid (e.g., mixtures of CT, lard oil, TBP, and DBBP), and estimates of hydrologic boundary conditions. The hydrogeologic setting was configured by assembling a geologic model based on interpretations of borehole geologic information at the regional and local scale. The geologic model was constructed using the EarthVision™ (Dynamic Graphics, Inc., Alameda, CA) software to provide a means for three-dimensional interpolation of borehole geologic information and to establish an electronic format for the geologic model that enabled porous media properties to be readily mapped to the numerical model grid. Fluid properties for relevant organic liquid mixtures were determined in the laboratory as part of the DOE's Remediation and Closure Science Project (Oostrom et al. 2004). Simulation results of water flow from a regional scale model were used to establish the boundary conditions for the local model that was used to simulate DNAPL movement. Appropriate ranges for organic liquid and water disposal conditions for the local model were established based on a thorough review of historical information. The multifluid flow and transport simulations lead to the following adjustments of the conceptual model:

- *Where is CT expected to accumulate?* CT DNAPL accumulates in the finer-grain sediments of the vadose zone but does not appear to pool on top of these layers.

- *Where would continuing liquid CT sources to groundwater be suspected?* Migration of DNAPL CT tends to be preferentially vertically downward below the disposal area. Considerable lateral movement of DNAPL CT is not likely. However, significant lateral migration of vapor phase CT occurs.

- *What is the estimated distribution and state of CT in the vadose zone?* The majority of the CT was typically a DNAPL or in the sorbed phase in 1993. Heterogeneities, however, as shown in the results reported by Oostrom et al. (2006) tends to increase the amount of CT present in the vapor, water, and sorbed phases compared to the DNAPL phase. The center of mass for CT in the vadose zone was typically directly beneath the disposal area and within the CCU.

- *How does SVE affect the distribution of CT in the vadose zone?* SVE effectively removes CT from the permeable layers of the vadose zone. SVE previously applied in the 216-Z-9 trench area has likely removed a large portion of CT initially present in the permeable layers within the large radius of influence of the extraction wells. Finer-grain porous media with larger moisture contents, such as the CCU sediments, are less affected by SVE.

- *Where would DNAPL contamination in groundwater be suspected?* Simulations indicate that migration of DNAPL is primarily in the vertical direction such that DNAPL, if present in the groundwater, would be most likely expected in a zone distributed around the centerline of the disposal area.

This report describes three-dimensional subsurface modeling of CT in the vicinity of the 216-Z-1A and 216-Z-18 disposal sites. The modeling includes a base case simulation using the best available data and a sensitivity analysis in which disposal infiltration area, disposal volume, DNAPL properties, and porous media hydraulic properties were varied. The SVE remediation process was included for the base case simulation and several sensitivity analysis simulations. In this report the fundamentals of the

numerical model STOMP (White and Oostrom 2006) is described in Chapter 2 followed by a discussion of the geological model in Chapter 3. Chapter 4 outlines the choice of boundary and initial conditions, as well as porous medium and fluid properties for all simulations. The results are reported in Chapter 5 and an updated conceptual model is presented in Chapter 6.

2.0 STOMP Simulator and Constitutive Relations

The water-oil-air operational mode of the STOMP simulator (White and Oostrom 2006) was used to simulate multi-fluid flow and transport beneath the 216-Z-1A and 216-Z-18 disposal sites. The fully implicit integrated finite difference code has been used to simulate a variety of multi-fluid systems (e.g., Hofstee et al. 1998, Oostrom et al. 1997, 1999, 2003; Oostrom and Lenhard 1998; Schroth et al. 1998; White et al. 2004). In this section, a brief overview is presented of the governing equations and solution methods. Details of the simulation can be found in White and Oostrom (2006).

The applicable governing equations are the component mass-conservation equations for water, organic compounds, and air, expressed as, respectively:

$$\frac{\partial}{\partial t}\left[n_D \omega_l^w \rho_l s_l\right] = -\nabla F_l^w + \dot{m}^w \tag{2.1a}$$

$$\frac{\partial}{\partial t}\left[\sum_{\gamma=l,n}\left(n_D \omega_\gamma^o \rho_\gamma s_\gamma\right) + \left((1-n_T)\omega_s^o \rho_s\right)\right] = -\sum_{\gamma=l,n}\left\{\nabla F_\gamma^o + \nabla J_\gamma^o\right\} + \dot{m}^o \tag{2.1b}$$

$$\frac{\partial}{\partial t}\left[\sum_{\gamma=l,g}\left(n_D \omega_\gamma^a \rho_\gamma s_\gamma\right)\right] = -\sum_{\gamma=l,g}\left\{\nabla F_\gamma^a + \nabla J_\gamma^a\right\} + \dot{m}^a \tag{2.1c}$$

where

$$F_\gamma^w = -\frac{\omega_\gamma^w \rho_\gamma k_{rl} k}{\mu_\gamma}\left(\nabla P_\gamma + \rho_\gamma g_z\right) \text{ for } \gamma = \text{l,g,} \tag{2-1d}$$

$$F_\gamma^o = -\frac{\omega_\gamma^o \rho_l k_{r\gamma} k}{\mu_\gamma}\left(\nabla P_\gamma + \rho_\gamma g_z\right) \text{ for } \gamma = \text{l,n,g} \tag{2.1e}$$

$$F_\gamma^a = -\frac{\omega_\gamma^a \rho_\gamma k_{r\gamma} k}{\mu_\gamma}\left(\nabla P_\gamma + \rho_\gamma g_z\right) \text{ for } \gamma = \text{l,g} \tag{2.1f}$$

$$J_\gamma^w = -\tau_\gamma n_D \rho_\gamma s_\gamma \frac{M^w}{M_\gamma} D_\gamma^w \nabla \chi_\gamma^w \text{ for } \gamma = \text{l,g} \tag{2.1g}$$

$$J_\gamma^o = -\tau_\gamma n_D \rho_\gamma s_\gamma \frac{M^o}{M_\gamma} D_\gamma^o \nabla \chi_\gamma^o \text{ for } \gamma = \text{l,n,g} \tag{2.1h}$$

$$J_\gamma^a = -\tau_\gamma n_D \rho_\gamma s_\gamma \frac{M^a}{M_\gamma} D_\gamma^a \nabla \chi_\gamma^a \text{ for } \gamma = \text{l,g} \tag{2.1i}$$

The subscripts l, n, g, and s denote aqueous, NAPL, gas and solid phase, respectively; the superscripts w, o, and a denote water, organic compound, and air components, respectively; t is time (s), n_D is the diffusive porosity, n_T is the total porosity, ω is the component mass fraction, ρ is the density (kg/m^3), s is the actual liquid saturation, V is the volumetric flux (m/s), J is the diffusive-dispersive mass flux vector (kg/m^{2}s), m is the component mass source rate (kg/m^{3}s), k is the intrinsic permeability (m^2), $k_{r\gamma}$ is the relative permeability of phase γ, μ is the viscosity (Pa s), P is the pressure (Pa), g_z is the gravitational vector (m/s^2), τ is the tortuosity, M is the molecular weight (kg/mole), D is the diffusive-dispersive tensor (m^2/s), and χ is the component mole fraction. The partitioning between the aqueous and solid phases is described by a linear exchange isotherm through a constant distribution coefficient.

The governing partial differential equations (Equations 2.1a, 2.1b, and 2.1c), are discretized following the integrated-volume finite difference method by integrating over a control volume. Using Euler backward-in-time differencing, yielding a fully implicit scheme, a series of nonlinear algebraic expressions is derived. The algebraic forms of the nonlinear governing equations are solved with a multi-variable, residual-based Newton-Raphson iterative technique where the Jacobian coefficient matrix is composed of the partial derivatives of the governing equations with respect to the primary variables.

Assuming that the aqueous phase never disappears, the primary variable for the water equation is always the aqueous pressure. For the oil equation, the primary variable is P_n when free NAPL is present, s_n when only entrapped NAPL is present, and the component mole fraction when no NAPL is present. For the air equation, the primary variable is P_a. The algebraic expressions are evaluated using upwind interfacial averaging to fluid density, mass fractions, and relative permeability. User specified weights (i.e., arithmetic, harmonic, geometric, upwind) are applied to the remaining flux components. For the simulations described in this report, harmonic averages were used for all other flux components, while the maximum number of Newton-Raphson iterations was sixteen, with a convergence factor of 10^{-6}.

Secondary variables, those parameters not directly computed from the solution of the governing equations, are computed from the primary variable set through the constitutive relations. A complete overview of these relations can be found in White and Oostrom (2000). In this section, only the relations between relative permeability, fluid saturation, and capillary pressure (k-S-P) pertinent to the reported simulations are described. The used k-S-P relations consist of the Brooks and Corey (1964) S-P relations in combination with the k-S relations derived from the Burdine (1953) or Mualem (1976) model, modified with adjustments for the gas phase permeability using the theory presented by Klinkenberg (1941). A discussion of these relations and a new theory for residual saturation formation has been provided by Lenhard et al. (2004). In these relations, the effects of fluid entrapment and residual saturation formation have been included.

The k-S-P relations distinguish between actual, effective, and apparent saturations. Actual saturations are defined as the ratio of fluid volume to diffusive pore volume. Effective saturations represent normalized actual saturations based on the pore volumes above the irreducible or minimum saturation of the wetting fluid (i.e., aqueous phase liquid). Effective saturations for the aqueous phase, NAPL, and gas phase and total liquid, are defined according to Equation (2.2):

$$\bar{s}_l = \frac{s_l - s_{rl}}{1 - s_{rl}} \tag{2.2a}$$

$$\bar{s}_n = \frac{s_n}{1 - s_{rl}} \tag{2.2b}$$

$$\bar{s}_g = \frac{s_g}{1 - s_{rl}} \tag{2.2c}$$

$$\bar{s}_t = \frac{s_l + s_n - s_{rl}}{1 - s_{rl}} \tag{2.2d}$$

where s_{rl} is the irreducible aqueous phase saturation. Apparent saturations are defined in terms of effective saturations. Apparent saturations represent the effective saturation of the fluid plus the effective saturations of fluids of lesser wettability entrapped within the wetting fluid. In the simulator, it is assumed that fluid wettability follows the sequence: water > NAPL > air (Leverett 1941). Fluids of lesser wettability can potentially be trapped by NAPL or aqueous phase and NAPL can be entrapped by the aqueous phase.

In a three-phase system, the apparent total-liquid saturation is considered to be a function of the air-NAPL capillary pressure, and the apparent aqueous phase saturation a function of the NAPL-water capillary pressure, as follows:

$$\bar{\bar{s}}_t = \left[\frac{P_d}{\beta_{gn} P_{gn}}\right]^{\lambda} \quad \text{for} \quad \beta_{gn} P_{gn} > P_d \tag{2.3a}$$

$$\bar{\bar{s}}_t = 1 \quad \text{for} \quad \beta_{gn} P_{gn} \le P_d \tag{2.3b}$$

$$\bar{\bar{s}}_l = \left[\frac{P_d}{\beta_{nl} P_{nl}}\right]^{\lambda} \quad \text{for} \quad \beta_{nl} P_{nl} > P_d \tag{2.3c}$$

$$\bar{\bar{s}}_l = 1 \quad \text{for} \quad \beta_{nl} P_{nl} \le P_d \tag{2.3d}$$

where P_d is the air-entry pressure, P_{gn} the gas phase – NAPL capillary pressure, P_{nl} the NAPL – aqueous phase capillary pressure, γ is a pore-size distribution factor, and β_{gn} and β_{nl} are interfacial tension dependent scaling factors, defined as $\beta_{gn} = \left(\sigma_{gn} - \sigma_{nl}\right)/\sigma_{gn}$ and $\beta_{nl} = \left(\sigma_{gn} - \sigma_{nl}\right)/\sigma_{nl}$, respectively. The nature of these relations is discussed by Lenhard (1994). For aqueous-gas phase systems, Equations (2.3) are replaced by

$$\bar{\bar{s}}_l = \left[\frac{P_d}{P_{gl}}\right]^{\lambda} \quad \text{for} \quad P_{gl} > P_d \tag{2.4a}$$

$$\bar{\bar{s}}_l = 1 \quad \text{for} \quad P_{gl} \le P_d \tag{2.4b}$$

3.0 Geologic Model

Development of a geologic model for the 216-Z-18 and 216-Z-1A disposal sites was completed in two stages. First, a regional-scale geologic model was developed to support groundwater flow modeling and set the boundary conditions for the more detailed local model. Then a detailed site-specific scale geologic model was developed to support detailed flow and transport simulations for the two disposal sites.

3.1 Site-Specific Geologic Model Development

The boundaries of the regional geologic model domain were selected such that primary recharge or discharge areas were included within the domain. The regional model domain included important liquid disposal areas: the 216-U-14 ditch to the east, the 216-U-pond to the south, the 200-ZP-1 injection wells to the west, and the old 216-T-4 pond to the north. The extent of the regional and the site-specific models are shown in Figure 3.1. The site-specific model extent is 597 m in the East-West and 612 m in the South-North direction. To support the development of a site-specific geologic model for high-resolution groundwater modeling of the 216-Z-1A and 216-Z-18 disposal facilities, a detailed analysis was conducted of borehole data in and immediately adjacent to these sites (Figures 3.2 and 3.3). This detailed data analysis was supplemented by previous site-specific interpretations of the geologic framework beneath the 216-Z-1A site.

The Hanford Well Information System (HWIS) indicates that 109 boreholes are in the immediate vicinity of the 216-Z-1A site while 26 boreholes are in the immediate vicinity of the 216-Z-18 site. There are a number of cone penetrometer testing (CPT) and Geoprobe® boreholes in the area. These boreholes, however, tend to be very shallow and generally lack samples and direct observation/data on the sediments penetrated. Thus, our analyses focused mostly on 57 traditionally drilled and sampled boreholes where physical descriptions (i.e., geologist's logs), laboratory data from drill cuttings and samples, and geophysical logs are available. These boreholes had the highest quality and most comprehensive data sets.

The analysis of borehole data was initiated with the assembly and entry of raw data sets for each selected borehole. These data were entered in to the Hanford Borehole Geologic Information System (HBGIS), a web-based relational database system with configuration control that provides systematic entry, management, and dissemination tools for borehole geologic data with configuration control (Last et al. 2002). The data entered for a particular borehole is dependent on the types of data available for that borehole. However, the raw data generally consists of general borehole information (location, elevation, etc.), driller's logs, geologist's logs, geophysical logs, and laboratory data from physical and geochemical analyses of borehole samples. The primary sources for these data are shown in Table 3.1. These data were assembled and systematically translated into electronic form and entered into HBGIS using internal PNNL procedures, DO-06, -07, and -09 as found in manual PNL-MA-567 (PNNL, 1995). The HBGIS website(http://hbgis.emsl.pnl.gov/HBGIS/login.jsp) provides a graphical user interface to browse and download the raw data for use in generating log plots and to support preparation of geologic cross sections.

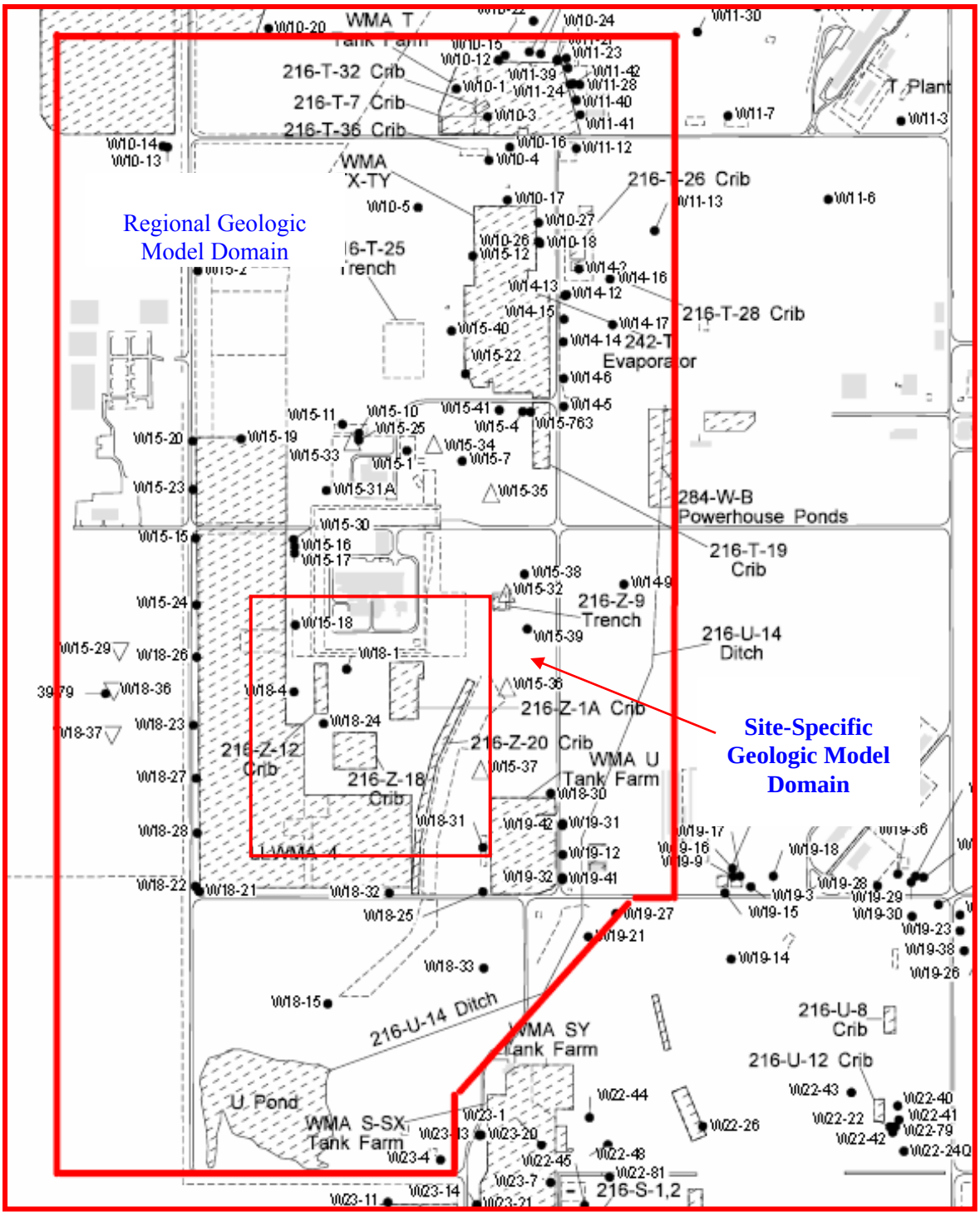

Figure 3.1. Outline of Regional and Site-Specific Geologic Model Domains

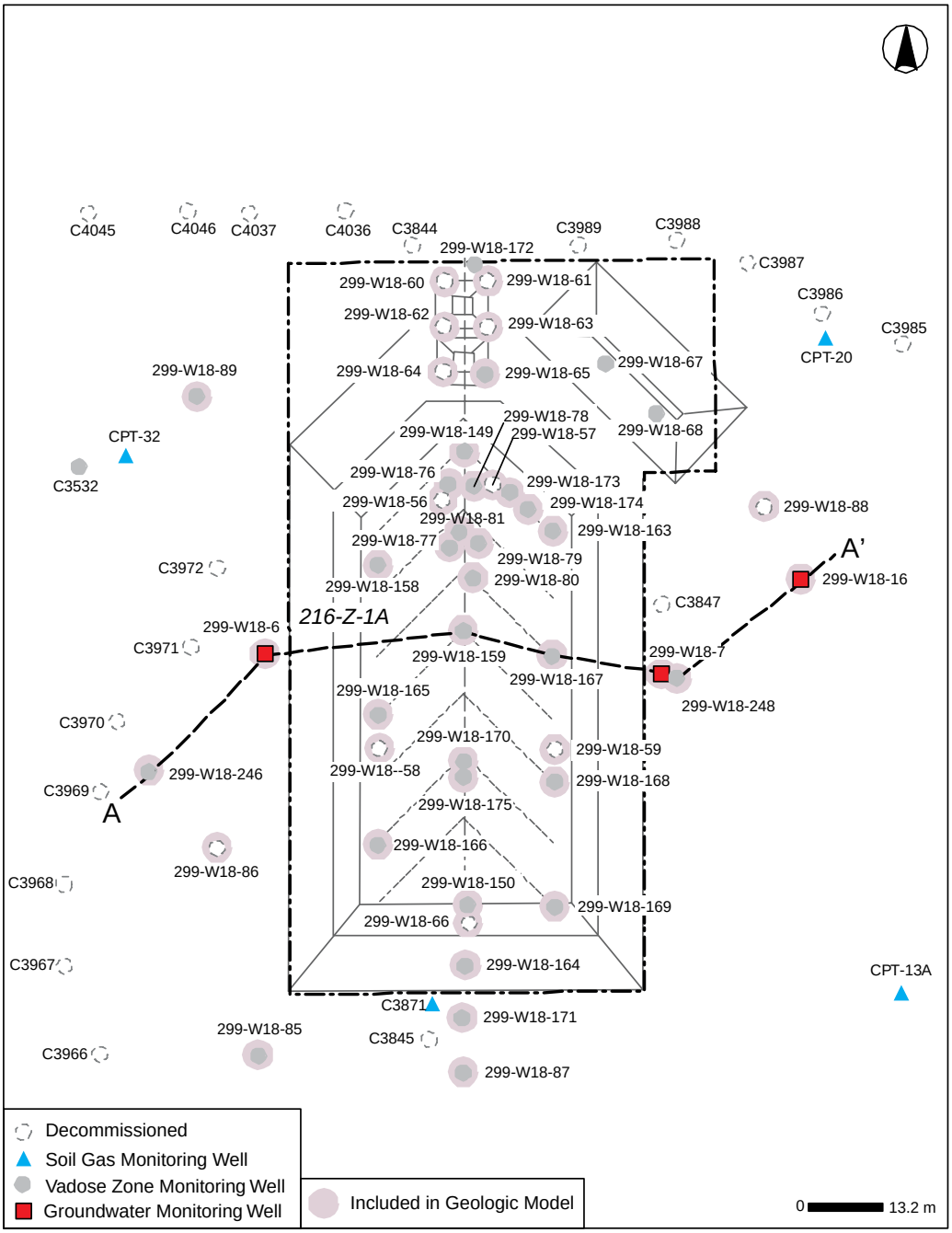

Figure 3.2. Borehole/Well Locations in the Vicinity of the 216-Z-1A Tile Field

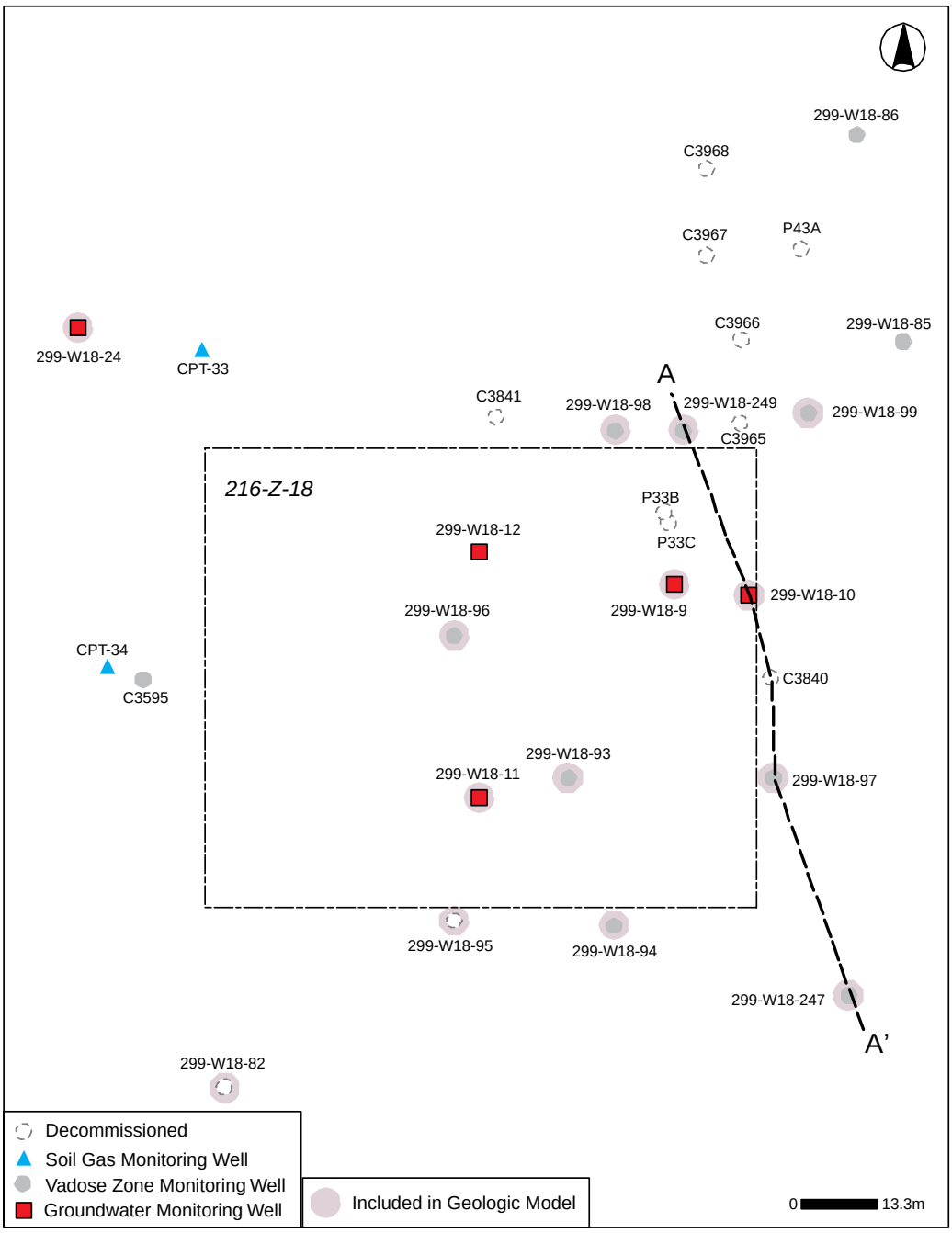

Figure 3.3. Borehole/Well Locations in the Vicinity of the 216-Z-18 Crib

Table 3.1. Borehole Geologic Data Sources

Raw Data Type	Primary Data Source	Secondary Data Source	Other Supplementary Data Sources
Location Coordinates	HWIS Interface-Survey Information-Horizontal		
Casing Elevation	HWIS Interface-Survey Information-Vertical		
Ground Surface Elevation	HWIS Interface-Survey Information-Vertical-DISC_Z	Calculated using stickup taken from HWIS Interface-Document Types-As-built, Well Summaries	Calculated using stickup taken from HWIS Interface-Well History Information-Inspection Logs; or using a default stickup of 0.91 m
Driller's Logs	HWIS Interface-Document Types-Other Well Records	PNNL's Well Log Library	
Geologist's Borehole Logs	HWIS Interface-Document Types-Other Well Records	PNNL's Well Log Library	Published and unpublished reports, field and laboratory notebooks.
Borehole Geophysics (earliest digital data available)	– New boreholes: Hanford Geophysical Logging Project Website (http://gj.em.doe.gov/hanf/) – Older boreholes: PNNL Log Database (http://boreholelogs.pnl.gov/)	Digital data in project files (e.g., digitized from analog strip charts)	Analog strip charts from PNNL Well Log Library, published and unpublished reports
Laboratory Particle-Size and $CaCO_3$ Data	Virtual Library – ROCSAN Data Module		Published and unpublished reports, laboratory notebooks.
Laboratory Moisture Content Data			Published and unpublished reports, laboratory notebooks.

Once the raw data sets for each selected borehole were assembled and translated into electronic form, some manipulation of the data sets was conducted to derive additional data sets (e.g., the sand:mud ratio), adjust for differences in reference elevations (e.g., account for stickup), and/or graphically portray the data. Selected data sets were then plotted side-by-side in graphical log plots to aid synergistic interpretation of all data sets for a given borehole. Correlation lines were added to correlate changes across multiple data sets. The choice of where to draw the correlation lines and the interpretation of these changes relative to key stratigraphic contacts and/or changes in lithologic/facies was based on the professional judgment of a qualified/licensed geologist, or their assistant, using all available data. Log plots and data from individual boreholes were often compared with the log plots and data from surrounding boreholes to improve consistency and confidence in the interpretations.

Detailed cross sections were constructed by hand using interpreted and raw data for selected boreholes in and adjacent to each facility. Figures 3.4 and 3.5 illustrate the cross-sections for the 216-Z-1A and 216-Z-18 sites, respectively. Interpretations were made of the fine-scale facies variations (based in part on sediment size classifications and sedimentary structures). The larger-scale stratigraphic contacts were then adjusted to honor the major lithologic changes that were correlated between multiple boreholes. Once the cross sections were prepared, the correlation lines and lithofacies/stratigraphic contacts for each borehole were revisited and adjusted where appropriate. The depth of the principal stratigraphic contacts for each borehole was assembled in to an *Excel* spreadsheet and combined with corresponding information (e.g., top of casing elevation and the stickup of the top of casing above ground surface) to calculate contact elevations. All raw borehole geologic data are in feet, thus, all analysis was done in feet and then converted to meters. A summary of the pertinent borehole/well information and geologic contacts for those wells included in the geologic model for the 216-Z-1A and 216-Z-18 sites is provided in Table 3.2.

Borehole geologic data are of variable quality and there are many sources of uncertainty associated with these data and interpretation of the geologic units, their lateral continuity, and their thicknesses. The principal source of uncertainty for identification of geologic units and their contacts is the quality of the drilling, sampling, and descriptive logging techniques used during installation of the borehole, as well as the availability of borehole geophysical logs and laboratory data from borehole samples. Many boreholes installed prior to the 1980s were drilled without a geologist present to describe the drilling cuttings and samples. For these boreholes, only driller's logs are available and their quality varies significantly. Furthermore, subtle differences and gradational changes between geologic facies and across stratigraphic units make delineation and correlation of individual facies and sediment packages difficult. Potentially significant sources of uncertainty come from poor survey and depth control. Of particular concern is the ground surface elevation at the time of drilling and sampling, the reference point elevation at the time of borehole geophysical logging or other measurements, and the accuracy of depth measurements. Multiple survey estimates for some wells suggest that the uncertainty in ground surface elevation could be as much as 2.4 m. This can impart a significant error in the slopes of the geologic contacts. The ground surface elevations used in this report were calculated using the following set of logic rules (see Table 3.1).

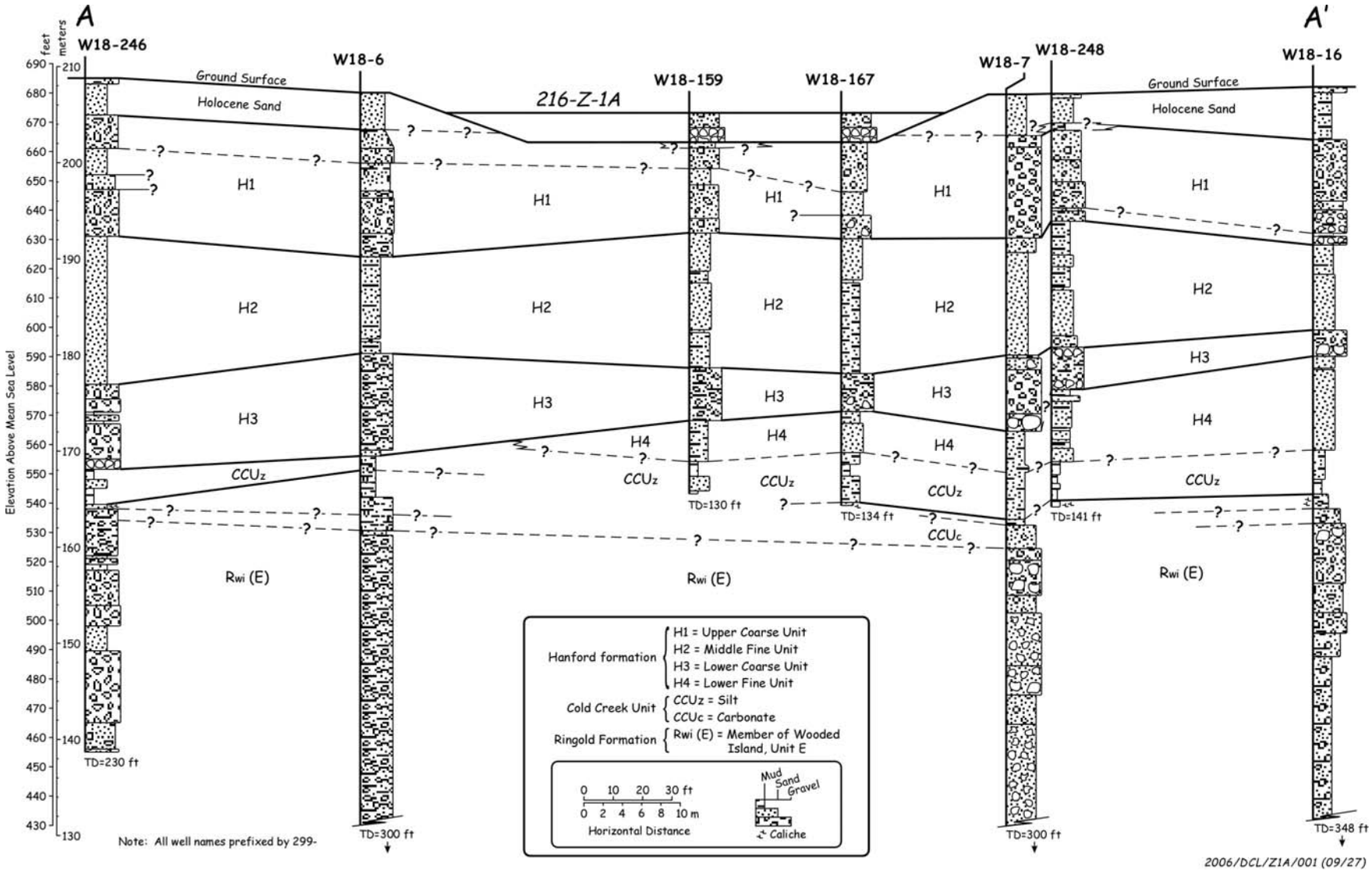

Figure 3.4. Cross Section Through 216-Z-1A Tile Field (see Figure 3.2 for Cross-Section Location)

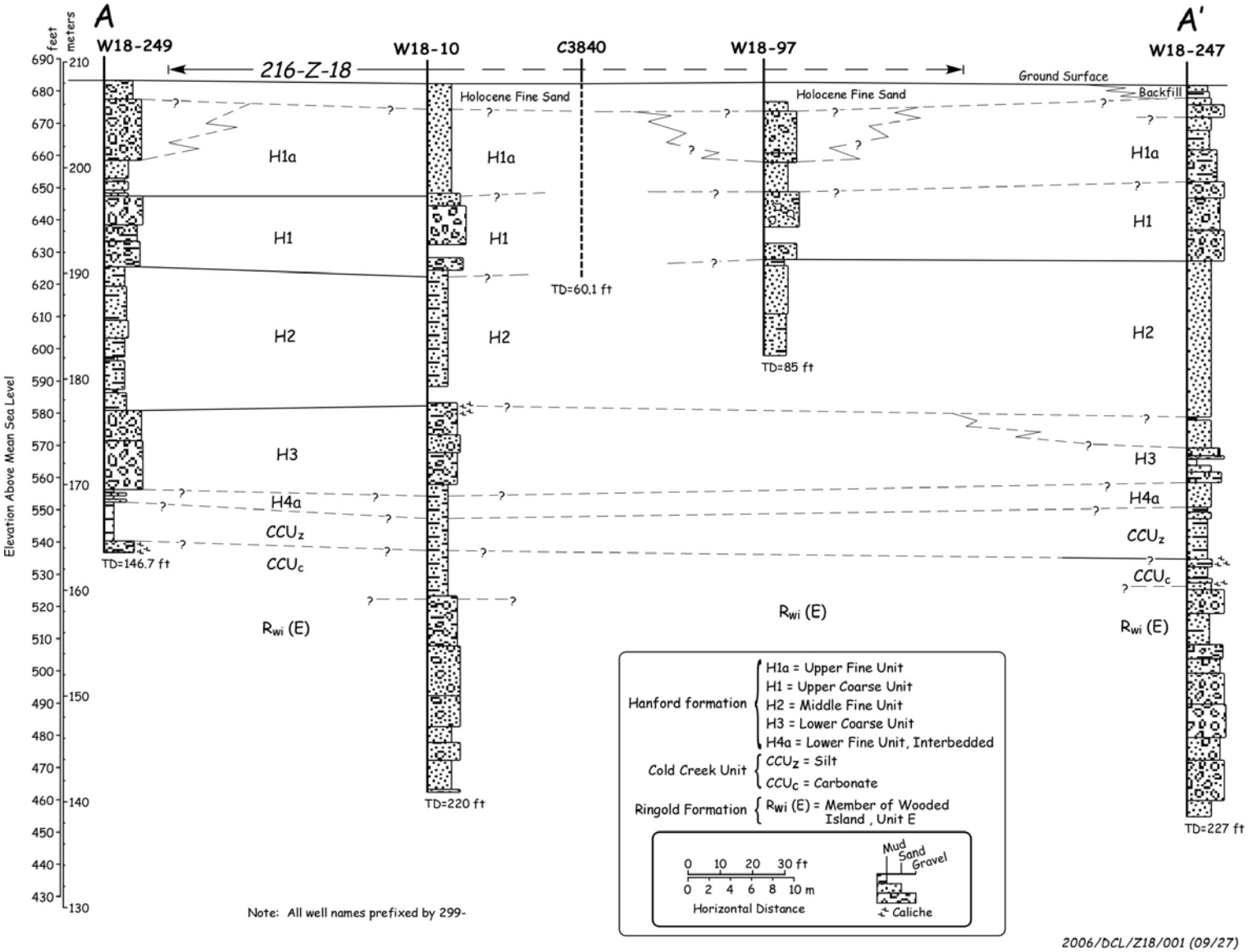

Figure 3.5. Cross Section Through 216-Z-18 Crib (see Figure 3.3 for Cross-Section Location)

Table 3.2. Borehole/Well Information and Elevation of Geologic Contacts Beneath the 216-Z-1A and 216-Z18 Sites

Well ID	Well Name	Drill Date	Drill Depth (m)	Casing Stickup		Horizontal Coordinates (NAD83(91))		Vertical Elevation (NAVD88)			Holocene		Hanford Formation						Cold Creek Unit		Ringold Formation				Saddle Mountains Formation
				Stickup from Inspection Logs (m)	Stickup from As Built (m)	Northing (m)	Easting (m)	Top Of Casing (m)	DISC_Z (Brass Cap) (m)	Best Estimate Ground Surface Elevation (m)	Backfill	Eolian Sand	Upper Sand Unit	Upper Gravelly Unit	Middle Fine Sand Unit	Lower Gravelly Unit	Lower Sandy Unit	Lower Fine Sandy Unit	Silt Unit	Carbonate Unit	Member of Taylor Flats	Member of Wooded Island, Unit E	Member of Wooded Island, Lower Mud	Member of Wooded Island, Unit A	Elephant Mountain Member
216-Z-1A																									
A7523	299-W18-6	01/15/64	91.4	0.8	0.8	135412.825	566513.075	208.123	No value	207.3	NP	207.4	-	203.1	192.4	180.2	172.3	NP	166.8	163.2	NP	160.1	ETD	-	-
A7524	299-W18-7	01/13/64	91.4	0.8	ND	135409.803	566580.971	207.816	207.057	207.1	NP	207.1	NP	202.8	190.0	179.9	NP	-	169.3	167.7	NP	161.7	ETD	-	-
C4303	299-W18-16	10/20/04	106.1	ND	ND	135425.690	566605.050	208.580	207.887	207.9	207.9	207.3	-	202.4	191.4	182.6	179.9	-	170.1	165.5	NP	162.5	ETD	-	-
A7539	299-W18-56	03/31/49	45.7	ND	ND	135439.422	566543.288	205.468	No value	204.6	204.6	-	-	201.5	191.2	175.9	171.3	-	168.3	164.9	-	160.4	ETD	-	-
A7540	299-W18-57	03/31/49	45.7	ND	ND	135441.881	135441.881	205.569	No value	204.7	204.7	-	-	201.9	191.3	177.5	171.4	-	168.4	163.8	160.8	159.2	ETD	-	-
A7541	299-W18-58	03/31/49	45.7	ND	ND	135396.732	566532.425	204.874	No value	204.0	204.0	-	-	201.2	189.0	173.2	169.2	-	166.2	163.1	-	158.6	ETD	-	-
A7542	299-W18-59	03/25/49	45.7	ND	ND	135396.808	566562.593	205.242	No value	204.3	-	204.3	-	203.1	191.2	175.1	172.3	-	169.3	163.2	NP	160.4	ETD	-	-
A7543	299-W18-60	04/30/49	45.7	ND	ND	135476.905	566543.498	207.373	No value	206.5	206.5	-	-	200.4	193.1	182.4	171.7	-	169.3	167.1	163.2	ETD	-	-	-
A7544	299-W18-61	04/30/49	45.7	ND	ND	135476.924	566551.116	207.318	No value	206.4	206.4	-	-	200.6	192.1	181.4	173.2	-	169.2	165.6	-	164.0	ETD	-	-
A7545	299-W18-62	04/30/49	46.0	ND	ND	135468.982	566543.518	207.214	No value	206.3	206.3	-	-	200.5	192.0	182.8	172.2	-	169.1	165.5	163.0	ETD	-	-	-
A7546	299-W18-63	04/30/49	45.7	ND	ND	135469.001	566551.136	207.221	No value	206.3	206.3	-	-	201.1	190.5	181.3	170.7	-	169.1	165.8	-	161.5	ETD	-	-
A7547	299-W18-64	04/30/49	45.7	ND	ND	135461.363	566543.537	207.211	No value	206.3	206.3	-	201.1	197.5	191.1	179.8	171.6	-	168.5	165.5	163.9	ETD	-	-	-
A7548	299-W18-65	04/30/49	45.7	ND	ND	135461.157	566550.687	207.720	No value	206.8	206.8	-	-	201.6	192.5	181.8	172.7	-	169.6	168.1	-	165.1	ETD	-	-
A7549	299-W18-66	04/30/49	45.7	ND	ND	135366.906	566547.736	205.011	No value	204.1	204.1	-	0.0	202.3	190.7	175.5	170.6	-	166.0	166.0	-	162.0	ETD	-	-
A7559	299-W18-76	03/28/67	5.9	0.3	ND	135441.910	566544.323	205.655	No value	205.4	205.4	-	202.1	ETD	-	-	-	-	-	-	-	-	-	-	-
A7560	299-W18-77	03/30/67	7.6	0.1	ND	135431.162	566544.972	205.369	No value	205.3	205.3	-	-	202.5	ETD	-	-	-	-	-	-	-	-	-	-
A7561	299-W18-78	03/30/67	5.2	0.2	ND	135441.801	566548.713	205.605	No value	205.4	205.5	-	201.8	ETD	-	-	-	-	-	-	-	-	-	-	-
A7562	299-W18-79	03/30/67	7.0	0.1	ND	135431.644	566549.436	205.370	No value	205.3	205.3	-	202.3	ETD	-	-	-	-	-	-	-	-	-	-	-
A7563	299-W18-80	03/31/67	6.6	0.1	ND	135425.927	566548.767	205.265	No value	205.1	205.2	-	202.1	ETD	-	-	-	-	-	-	-	-	-	-	-
A7564	299-W18-81	04/03/67	12.5	1.0	ND	135434.168	566546.238	206.199	No value	205.2	205.2	-	202.2	196.1	ETD	-	-	-	-	-	-	-	-	-	-
A7568	299-W18-85	08/05/69	45.7	0.9	ND	135343.986	566512.133	208.284	No value	207.4	NP	207.4	-	205.9	191.9	176.2	-	-	167.8	164.0	ETD	-	-	-	-
A7569	299-W18-86	08/21/69	45.7	0.7	0.9	135379.643	566504.409	209.420	No value	208.5	208.5	-	207.0	204.2	190.2	176.8	NP	-	167.4	164.6	ETD	-	-	-	-
A7570	299-W18-87	09/05/69	45.7	0.7	0.7	135341.157	566546.827	207.520	No value	206.8	NP	206.8	-	205.3	188.8	178.1	-	-	169.0	161.4	ETD	-	-	-	-
A7571	299-W18-88	09/19/69	45.7	0.8	0.9	135438.239	566598.682	208.289	No value	207.4	NP	207.5	-	203.5	192.5	182.5	180.0	-	169.1	165.4	ETD	-	-	-	-
A7572	299-W18-89	10/21/69	45.7	0.9	0.9	135456.982	566501.077	208.762	No value	207.8	-	-	207.9	203.6	191.1	178.0	NP	-	169.1	165.5	-	163.7	ETD	-	-
A7632	299-W18-149	04/12/74	28.0	0.6	0.3	135447.523	566547.007	206.099	No value	205.8	205.5	-	201.8	199.4	191.5	181.1	ETD	-	-	-	-	-	-	-	-
A7633	299-W18-150	06/30/73	39.0	0.9	0.9	135370.302	566547.472	205.275	204.979	205.0	205.0	NP	201.0	196.8	190.7	175.7	171.5	NP	168.1	ETD	-	-	-	-	-
A7641	299-W18-158	09/08/77	39.9	0.8	0.6	135428.187	566532.337	206.113	No value	205.5	205.5	-	-	201.7	191.2	176.5	171.7	-	169.8	ETD	-	-	-	-	-
A7642	299-W18-159	01/31/78	39.6	0.3	0.3	135416.930	566547.038	205.574	No value	205.2	205.2	NP	-	202.2	192.8	178.7	173.2	NP	169.0	ETD	-	-	-	-	-
A7645	299-W18-163	02/28/77	49.7	0.8	0.8	135433.972	566562.210	206.097	No value	205.3	205.3	NP	200.8	195.6	191.6	179.0	173.6	-	169.4	166.3	ETD	-	-	-	-
A7646	299-W18-164	02/01/77	46.6	0.9	ND	135359.471	566547.207	207.826	No value	206.9	206.9	-	201.7	195.6	192.3	176.7	171.5	-	168.2	163.6	161.5	ETD	-	-	-
A7647	299-W18-165	03/31/77	41.1	0.9	0.9	135402.403	566532.425	205.970	No value	205.0	205.0	-	201.4	195.6	191.0	175.8	171.5	-	168.2	164.2	ETD	-	-	-	-
A7648	299-W18-166	04/30/77	41.8	0.8	0.8	135380.206	566532.323	205.673	No value	204.8	204.8	NP	201.2	195.1	192.0	172.8	170.1	-	167.7	163.7	ETD	-	-	-	-
A7649	299-W18-167	05/31/77	40.8	1.0	1.0	135412.556	566562.190	206.197	No value	205.2	205.2	NP	-	202.2	192.1	178.1	174.1	0.0	169.8	164.7	ETD	-	-	-	-
A7650	299-W18-168	06/30/77	39.9	1.0	1.0	135391.142	566562.572	205.840	No value	204.8	204.8	NP	201.5	194.3	191.9	174.4	173.8	-	168.3	ETD	-	-	-	-	-
A7651	299-W18-169	09/30/77	40.2	0.9	0.9	135369.787	566562.410	205.830	No value	204.9	204.9	NP	199.4	194.1	189.4	177.5	174.3	-	169.7	ETD	-	-	-	-	-
A7652	299-W18-170	09/21/77	9.1	1.1	ND	135394.261	566547.122	206.028	No value	204.9	204.9	-	201.9	195.8	ETD	-	-	-	-	-	-	-	-	-	-
A7653	299-W18-171	08/09/77	41.5	0.8	0.8	135350.503	566546.525	207.644	No value	206.9	206.9	-	199.6	195.6	191.6	177.3	-	-	169.1	ETD	-	-	-	-	-
A7655	299-W18-173	10/24/77	15.5	1.0	ND	135440.700	566554.641	206.327	No value	205.3	205.3	-	201.4	194.1	191.0	ETD	-	-	-	-	-	-	-	-	-
A7656	299-W18-174	04/27/93	40.1	ND	ND	135437.384	566558.208	205.946	No value	205.0	204.9	NP	200.7	194.6	190.6	179.2	172.5	-	168.5	165.3	ETD	-	-	-	-
A7657	299-W18-175	12/07/77	39.6	0.9	0.9	135392.144	566547.078	205.774	No value	204.9	204.9	NP	NP	201.9	190.6	-	-	-	168.6	ETD	-	-	-	-	-
A7726	299-W18-246	03/23/92	70.1	0.3	ND	135392.613	566492.988	209.327	208.774	208.8	208.8	208.2	NP	205.0	192.3	176.9	NP	NP	168.1	164.4	NP	162.8	ETD	-	-
A7728	299-W18-248	05/26/92	43.0	ND	ND	135408.957	566583.704	207.970	207.189	207.2	207.2	206.9	NP	203.7	193.9	180.8	176.4	-	168.9	165.0	ETD	-	-	-	-
216-Z-18																									
A7526	299-W18-9	12/13/68	67.1	0.9	0.9	135302.121	566472.961	209.111	No value	208.2	NP	NP	208.2	198.5	190.6	175.6	NP	169.8	167.8	163.7	160.1	156.4	ETD	-	-
A4931	216-W18-10	12/11/68	67.1	0.9	ND	135300.687	566485.910	208.870	No value	208.0	NP	208.0	205.5	197.3	189.7	177.5	NP	169.0	166.8	163.8	NP	159.2	ETD	-	-
A7527	299-W18-11	01/04/69	67.1	1.0	1.0	135265.616	566439.603	209.468	No value	208.5	208.5	NP	203.9	197.8	190.2	175.2	ND	169.8	168.2	163.3	161.2	159.7	ETD	-	-
A4936	299-W18-24	08/10/87	73.1	0.7	0.7	135346.316	566370.843	209.697	209.038	209.0	NP	209.0	203.9	197.5	187.7	174.9	NP	NA	168.8	163.6	-	160.6	ETD	-	-
A7565	299-W18-82	ND	44.5	73.1	ND	135216.029	566395.551	209.579	No value	136.4	136.4	-	134.9	129.6	122.1	102.9	-	97.4	95.9	NR	NR	ETD	-	-	-
A7576	299-W18-93	02/08/72	42.7	1.0	ND	135269.393	566454.950	209.349	No value	208.3	-	208.4	204.5	198.4	193.1	174.2	-	170.3	167.5	ETD	-	-	-	-	-
A7577	299-W18-94	02/10/72	24.4	1.0	ND	135244.013	566462.690	209.088	No value	208.1	-	208.1	206.3	197.1	190.1	ETD	-	-	-	-	-	-	-	-	-
A7578	299-W18-95	02/15/72	24.4	1.0	~3	135244.988	566435.266	209.429	No value	208.4	NP	208.4	206.0	197.7	191.3	ETD	-	-	-	-	-	-	-	-	-
A7579	299-W18-96	02/18/72	45.7	0.9	0.9	135293.826	566435.228	209.060	No value	208.2	NP	208.2	206.1	197.5	192.1	176.5	-	169.2	166.5	163.5	ETD	-	-	-	-
A7580	299-W18-97	02/24/72	25.9	0.8	~3	135269.490	566490.243	208.857	No value	208.1	-	208.1	205.4	197.7	191.3	ETD	-	-	-	-	-	-	-	-	-
A7581	299-W18-98	02/29/72	24.4	0.9	~3	135328.927	566462.509	209.118	No value	208.3	-	208.3	206.4	199.1	190.6	ETD	-	-	-	-	-	-	-	-	-
A7582	299-W18-99	03/08/72	41.1	0.9	~3	135331.723	566496.307	208.908	No value	208.0	NP	208.0	205.2	198.8	192.4	176.0	NP	-	167.7	ETD	-	-	-	-	-
A7581	299-W18-247	05/06/92	69.2	ND	ND	135231.658	566503.137	208.679	207.789	207.8	207.8	206.6	204.8	198.7	191.2	173.5	NP	170.2	167.9	163.0	NP	160.3	ETD	-	-
A7729	299-W18-249	07/31/92	44.7	ND	ND	135329.008	566474.500	208.843	208.292	208.3	NP	208.3	206.5	197.3	190.6	177.1	NP	169.6	168.4	164.7	ETD	-	-	-	-

NA = Not Applicable
ND = Not Documented
NP = Not Present
'-' = Not Determined
EDT = Exceeds Total Depth

1. If HWIS contained a DISC_Z value,[1] then that value was used as a proxy for the ground surface elevation.

2. Otherwise, the ground surface elevation was calculated from the HWIS vertical survey value (assumed to be top of casing) minus the stickup value taken from as-built documents found in HWIS. If multiple stickup values were found, then professional judgment was used to select the most representative stickup value.

3. If a stickup value was not available from the "as built" documents found in HWIS, the stickup value found in Inspection Log documents in HWIS was used to calculate the ground surface elevation. If multiple stickup values were found, then professional judgment was used to select the best stickup value.

4. If a stickup value could not be found in either the "as built" document or Inspection Log documents, then a default stickup value 0.91 m was used to calculate the ground surface elevation.

The spacing and accuracy of depth-discrete observations/samples can also have a significant effect on the interpretation of the depth and thickness of geologic units. Drill cuttings and samples have routinely been collected at 1.5 m intervals. However the accuracy of depth measurements for these samples and observations is rather uncertain due to the variability in measurement techniques used by various drillers. The resulting uncertainty associated with interpretation of the depth and thickness of geologic units is estimated to be within the range of 0.7 to 3 m. Borehole geophysical logging data can help to significantly reduce depth uncertainties for geologic units with a distinct geophysical signature. A minor source of uncertainty contributing to the accuracy of depth measurements is the straightness and plumbness of the borehole. This source of uncertainty is deemed to be rather minor because most boreholes have been shown to have only minor deviations when casing liners and/or groundwater pumps have been installed.

There is also uncertainty in interpreting the geometric shape of the various geologic units (particularly within the cataclysmic flood deposits of the Hanford formation). While depth-discrete observations and samples are vertically spaced 1.5 m or less apart, the horizontal spacing between adjacent observations and samples is generally 10 to 100 times that distance. Even at the 216-Z-1A site, where borehole coverage is about the best available for any site at Hanford, the uncertainty in correlating geologic contacts between boreholes and interpreting where changes in facies and pinchouts occur, is expected to be in the range of 10s of meters. Further contributing to this uncertainty, is the potential for some wells/boreholes to be miss-labeled, and thus, the geologic information for those boreholes could be assigned to the incorrect location. For instance, it is believed that wells 299-W18-6 and 299-W18-7 were mislabeled in the field shortly after they were drilled and completed. A comparison of the scintillation and total gamma geophysical logs with geologic descriptions in the driller's logs and borehole sample data (i.e., granulometric and calcium carbonate data), suggests that the geophysical logs labeled as being for well 299-W18-6 correlate better with the geologic materials labeled as being from 299-W18-7 and visa versa. Thus, for this analysis, we have used the driller's log, granulometric data, and calcium carbonate data labeled as being from well 299-W18-6 for the location of well 299-W18-7 as labeled in the field and as documented in HWIS. Likewise, we used the driller's log, granulometric data, and calcium

[1] The DISC_Z field in HWIS is generally understood to contain surveyed elevations of the brass cap located on the concrete pad at or just above the ground surface.

carbonate data labeled as being from well 299-W18-7 for the location of well 299-W18-6 as labeled in the field and as documented in HWIS. Note that the geophysical logs were kept with the wells as they were labeled and located in the field and in HWIS.

3.2 Geologic Framework Beneath the 216-Z-1A and 216-Z-18 Facilities

The geologic framework beneath the 216-Z-1A and 216-Z-18 facilities can be represented by a sequence of 5 major stratigraphic units. From oldest to youngest, these are the Saddle Mountains Formation (of Miocene age), the Ringold Formation (of Miocene/Pliocene age), the CCU (Pliocene-Pleistocene), the Hanford formation (Pleistocene), and undifferentiated Holocene deposits. Each of the sedimentary sequences overlying the Saddle Mountains Formation can be further subdivided into a number of lithofacies or subunits. Table 3.3 (modified from Oostrom et al. 2004 and Last and Rohay 1993) illustrates the dominant grain size, calcium carbonate content, and gross gamma activity for the principal sedimentary sequences and lithofacies overlying the basalt bedrock.

1. **Saddle Mountains Formation**. The Saddle Mountains Formation forms the bedrock beneath the site. Its uppermost member, the Elephant Mountain Member lies at a depth of approximately 161 m, and slopes to southwest at a rate of about 0.015 (or 15 m/100 m). This medium- to fine-grained tholeiitic basalt essentially acts as a no-flow boundary at the floor of the unconfined aquifer

2. **Ringold Formation**. The basalt bedrock is overlain by the Ringold Formation, a sedimentary sequence of fluvial-lacustrine clay, silt, sand, and granule to cobble gravel deposited by the ancestral Columbia River. Beneath the 216-Z-9 site, the Ringold Formation has been subdivided into three subordinate units. From oldest to youngest, these are: 1) Unit A – fluvial sandy gravel; 2) the Lower Mud Unit – a sequence of paleosols and lake deposits, consisting of muddy medium to fine sand; and 3) Unit E – semi-indurated fluvial muddy sand gravel.

3. **Cold Creek Unit**. Overlying the Ringold Formation is the CCU. Locally, this unit is differentiated into the Cold Creek carbonate layer and the Cold Creek silt layer. The Cold Creek carbonate layer, formerly described as the caliche (or calcrete), is a fine- to coarse-grained, calcium-carbonate cemented paleosol that developed on top of the Ringold Formation. Overlying the Cold Creek carbonate layer is the Cold Creek silt layer formally referred to as the "Early Palouse Soil." This unit consists of cohesive, compact, massive to laminated and stratified fine-grained sand and silt (e.g., Sandy Mud).

4. **Hanford Formation**. Rohay et al. (1994) locally subdivided the Hanford formation into five mapable units (from oldest to youngest): 1) a lower fine-grained unit, 2) a lower coarse-grained unit, 3) a middle fine-grained unit, 4) an upper coarse-grained unit, and 5) an upper fine-grained unit. These units vary in thickness and distribution, with the lower coarse-grained unit thinning and pinching out towards the northwest as the lower fine-grained unit thickens. The upper fine-grained unit is rather difficult to differentiate from Holocene surface deposits and appears to be fairly spotty in its distribution. The five units are:

   (a) **Lower Fine Unit**. The lower fine-grained unit is believed to be equivalent to the H4 unit described by Lindsey et al. (1994 a, b). This unit appears to be a sequence of coarse to medium sand to silty fine to very fine sand, with some silt to silty-clayey sand lenses. It is moderate to well sorted and described as brown, olive brown, and/or light brownish gray with weak to strong

reaction to HCl. This unit varies in thickness from about 4.3 to 9.7 meters thinning and eventually pinching out beneath the western side of the 216-Z-1A tile field. Locally, a sequence of interbedded fine sand and silt that can be differentiated at the base of this unit, can be identified beneath portions of the 216-Z-18 crib.

Table 3.3. Typical Particle-Size, Calcium Carbonate, and Gamma Log Activity for the Principal Stratigraphic Units Beneath the 216-Z-1A and 216-Z-18 Disposal Facilities (after Oostrom et al. 2004)

Formation / Unit	Lithofacies or Facies Association	Borehole /Depth (m)	Folk Classification / Description	Gravel >2 mm Wt. %	Very Coarse Sand 1-2 mm Wt. %	Coarse Sand 0.5-1 mm Wt. %	Medium Sand 0.25-0.5 mm Wt. %	Fine Sand 0.125-0.25 mm Wt. %	Very Fine Sand 0.063-0.125 Wt. %	Mud (Silt + Clay) <0.063 Wt. %	CaCO3 Content Wt. %	Relative Gross Gamma Activity
Holocene Deposits (HD)	Backfill	299-W15-95 3.0 m	gravelly medium SAND	11.9	0.6	16.8	52.5	11.9	3.3	3.1	0.5	Low - Moderate
	Sand (Fine-Grained, Massive, Well Sorted)	299-W15-5 3.0 m	slightly muddy, fine to very fine SAND	0.0	0.7	4.9	13.1	30.9	33.9	16.5	0.5	Moderate
Hanford formation (HF)	Upper Fine, H1a (Sand Dominated)	299-W18-85 4.6 m	gravelly, very coarse to coarse SAND	20.5	39.0	20.0	7.1	4.5	3.0	5.9	0.5	Low
	Upper Coarse, H1 (Gravel Dominated)	299-W18-85 12.2 m	sandy GRAVEL	50.1	24.6	15.9	4.3	1.8	1.1	2.1	0.6	Low
	Fine, H2 (Sand Dominated)	299-W15-95 19.8 m	coarse to medium SAND	3.5	14.0	30.5	29.1	10.4	4.8	7.7	1.5	Low - Moderate
	Lower Coarse, H3 (Gravel Dominated)	299-W18-85 36.6 m	muddy, sandy, GRAVEL	46.7	17.8	9.0	6.9	5.1	3.7	10.8	1.1	Low
	Lower Sand, H4 (HF-SD)	299-W15-95 26.8 m	slightly muddy, medium to fine SAND	1.9	4.8	9.8	21.2	35.6	14.0	12.6	1.2	Low-Moderate
	Interbedded	299-W15-95 27.1 m	sandy MUD	0.0	0.1	0.4	2.4	11.8	46.9	38.4	1.3	
Cold Creek Unit (CCU)	Silt (Fine-Grained, Laminated, to Massive)	299-W15-85 42.7 m	sandy MUD	0.5	1.4	6.0	10.1	6.3	13.3	62.3	2.5	High
	Carbonate (Coarse to Fine-Grained, Carbonate Cemented)	299-W15-5 38.1 m	calcareous, gravelly, muddy, SAND	21.6	10.6	7.6	8.8	9.2	9.9	32.4	12.8	Moderate to High
Ringold	Member of Taylor Flats (Upper)	299-W15-5 45.7 m	slightly muddy, slightly gravelly, coarse to medium SAND	7.3	8.3	22.5	30.5	10.3	6.7	14.5	4.0	Low
	Member of Wooded Island, Unit E	299-W15-5 56.4 m	muddy, sandy, GRAVEL	58.7	12.4	4.0	7.9	7.3	3.8	5.9	0.3	Low-Moderate
	Member of Wooded Island, Lower Mud	299-W15-5 137.2 m	muddy, medium to fine SAND	0.9	2.4	5.5	21.4	21.6	14.0	34.3	1.6	Moderate to High
	Member of Wooded Island, Unit A	299-W15-5 147.8 m	sandy GRAVEL	40.1	33.4	17.1	4.5	1.2	1.2	2.6	0.3	Low-Moderate

* After DOE 2002

(b) **Lower Coarse Unit**. The lower coarse-grained unit is described in geologists' borehole logs as being an unconsolidated gravel, sandy gravel, and/or silty sandy gravel with up to 95% gravel. These materials are described as poorly sorted and bedded, with some openwork and clast supported gravels. Some silt and $CaCO_3$ coatings were noted on some of the clasts giving rise to moderate reaction to HCl. Two thin 1.5 cm thick sandy silt to silt sand lenses were noted in well 299-W-18-246. This unit is equivalent to the H3 unit described by Lindsey et al. (1994a, b). The general thickness of this unit is highly variable ranging from about 3.4 to 10.7 m and generally thins to the east.

(c) **Middle Fine Unit**. The middle fine-grained unit appears to be a sequence of interbedded sand and slightly silty/clayey sand. This sequence is believed to be equivalent to the Hanford H2 unit of Lindsey et al. (1994a, b). Bedding, where noted, is described as <1 cm to 2.4 cm thick. The slightly silty/clayey sand beds are describes as moderate to poorly sorted with up to 25% silt and mostly fine to very fine sand and with similar mineralogy to that of the sand beds. Rohay et al. (1994) indicated that clastic dikes have been encountered in this unit. The general thickness of this unit varies over the study area and ranges from about 8.8 to 15.2 m.

(d) **Upper Coarse Unit**. The upper coarse-grained unit is a sequence of open framework gravel to coarse to medium sand. It is believed to be equivalent to the Hanford H1 unit of Lindsey et al. (1994a, b). Beneath the eastern portion of the 216-Z-1A site, the unit appears to consist of two distinct sediment packages, the lower most sediment package fines upward from poorly sorted open framework gravel to well sorted medium sand. Above this fining upward sequence lies another gravel dominated sediment package. This sediment package grades upward to a gravelly coarse sand, and finally to a moderate to well sorted medium sand. Two thin silty fine sand beds were encountered near the top of this sequence in well 299-W18-246. To the east beneath the 216-Z-1A site the two sediment packages seem to loose their definition and transition into a sequence of gravelly coarse to medium sand. The overall thickness of this upper coarse unit is fairly uniform at about 9.1 to 12.8 m.

(e) **Upper Fine Unit**. The upper fine-grained unit is discontinuous across the study area and is not recognized in the immediate vicinity of the 216-Z-1A site. However, it is present beneath the 216-Z-18 Crib. This unit generally consists of very coarse to medium sand to slightly pebbly very coarse sand, with some silty stringers. The general thickness of this unit beneath the 216-Z-18 ranges from about 6 to 9 m.

5. **Holocene Deposits**. The surface of the study area, where undisturbed, is blanketed by a sequence of slightly silty to silty fine to very fine Holecene Eolian sand. This material is described as brown to dark gray brown, well sorted, and with moderate to no reaction to HCl. This unit appears to range from about 3 m to perhaps as much as 5.5 m. The 216-Z-1A and 216-Z-18 sites were excavated in to the underlying Holocene Sand and upper Hanford units. Stockpiles of sediment created during excavation were used as backfill in and around these facilities. These backfill materials are described as poorly sorted gravelly medium sand to sandy gravel. The backfill materials are discontinuous and are highly localized in areas around the waste disposal facilities, underground pipelines, and well/storage pads. Backfill thickness ranges from less than 0.6 m beneath well/storage pads, to 3.6 m beneath the 216-Z-1A site.

To create a consistent database of geologic contacts, all pertinent data sets were mapped to a single set of hydrostratigraphic units. These hydrostratigraphic units have also been mapped to the new Standardized Stratigraphic Nomenclature (DOE 2002). To enhance the level of detail, the 5 main hydrostratigraphic units were subsequently divided into 14 units: Backfill, Holocene Sand, Hanford Upper Fine, Hanford 1, Hanford 2, Hanford Lower Gravel, Hanford Lower Sand, Cold Creek silt, Cold Creek carbonate, Upper Ringold, Ringold E, Ringold Lower Mud, Ringold A, and Elephant Mtn. Basalt.

3.3 EarthVision™ Geologic Model

EarthVision™ software was used to create a three-dimensional model of the geologic units. The EarthVsion™ model consists of a "faces" file that represents each unit as a zone within a solid three-dimensional block. The surface of each unit is defined by an XYZ grid with XY spacing of 5 m. The model domain is 597 m wide and 612 m long. Figure 3.1 shows the model domain and also shows the location of the PFP, the three major CT disposal sites, U Pond, and the 216-U-14 ditch. The faces file can be sampled using utilities provided in the EarthVision™ software to create input files for numerical flow models. Fourteen units were originally defined for the EarthVision™ model. However, based on revised geological interpretations, the Hanford lower-fines were combined with the Hanford lower-sand unit. The uppermost unit is "backfill," which only occurs in a few locations. The unit below this, which is the first extensive unit, includes both the Holocene Sand and the Hanford Upper Fine units. These units were lumped together into the H1a unit because they are texturally similar.

The following procedure was used to build and revise the geologic model:

1. Grids representing the tops of extensive units (present over most of the model domain) were created based on the elevation picks from wells. Control points were added in areas where data were sparse, particularly on the edges of the model domain to control extrapolation.

2. Thickness (isopach) grids were calculated for less extensive geologic units based on the thickness measured at wells and zero thickness for the not present (NP) flags in the well data. For these less extensive units, it was assumed that the unit was not present in areas where there were no data for the unit.

3. Starting from the base of the model, grids for the top elevation of each less extensive geologic unit were calculated by adding the thickness grid to the elevation grid for whichever unit exists below it.

4. The model was examined to determine if any units had incorrectly "pinched-out" because the top of a deeper unit was being extrapolated above the elevation of the well pick. If this occurred, control points were added to control top of the deeper unit.

The geologic modeling procedure was an iterative process because examination of the model identified wells where elevation picks were inconsistent. The geologic data were then reevaluated by reviewing/evaluating the raw borehole data to determine whether the picks were valid.

The EarthVision™ model is displayed in series of figures. A cutout through both the 216-Z-1A and 216-Z-18 sites is show in Figure 3.6. Locations of West-East and South-North cross sections within the STOMP computational domain through the two sites are given in Figure 3.7. Figure 3.8 and 3.9 show

cross-section through the 216-Z-1A site, while Figures 3.10 and 3.11 depict cross sections through the 216-Z-18 site. Figure 3.12 through 3.22 show top views of the main hydrostratigraphic units.

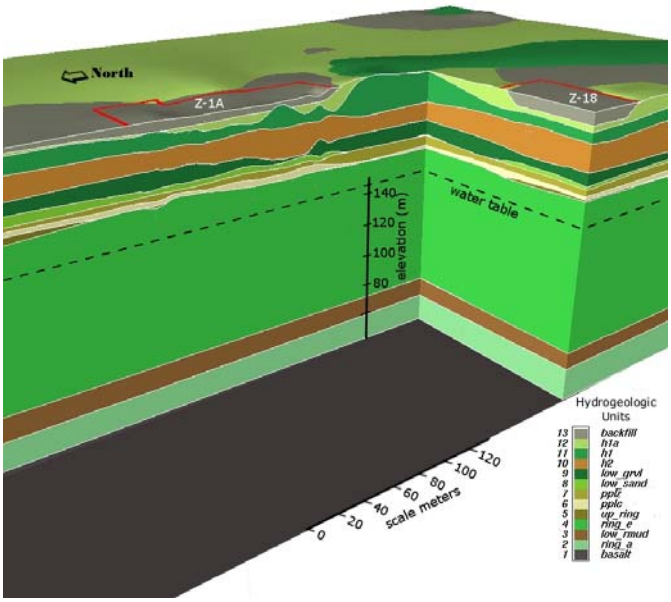

Figure 3.6. Three-Dimensional Geologic Model with a Cut-Out Beneath the 216-Z-18 and 216-Z-1A Sites

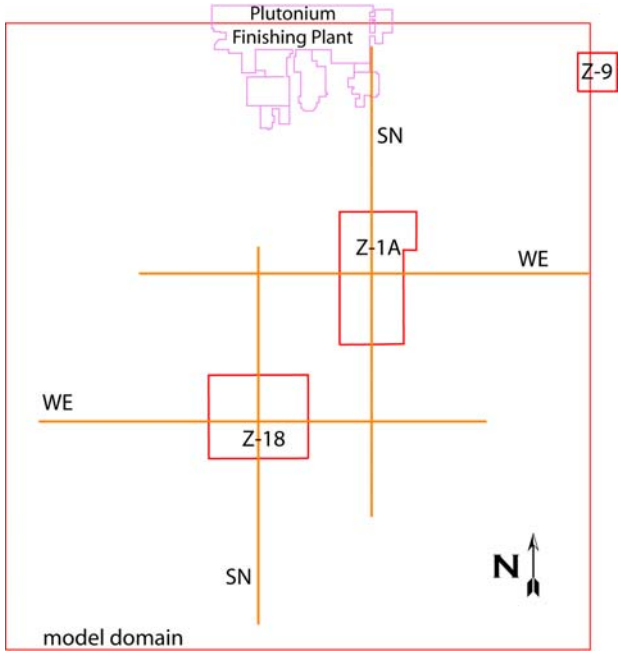

Figure 3.7. STOMP Computational Domain and Location of Cross Sections Through the Disposal Sites

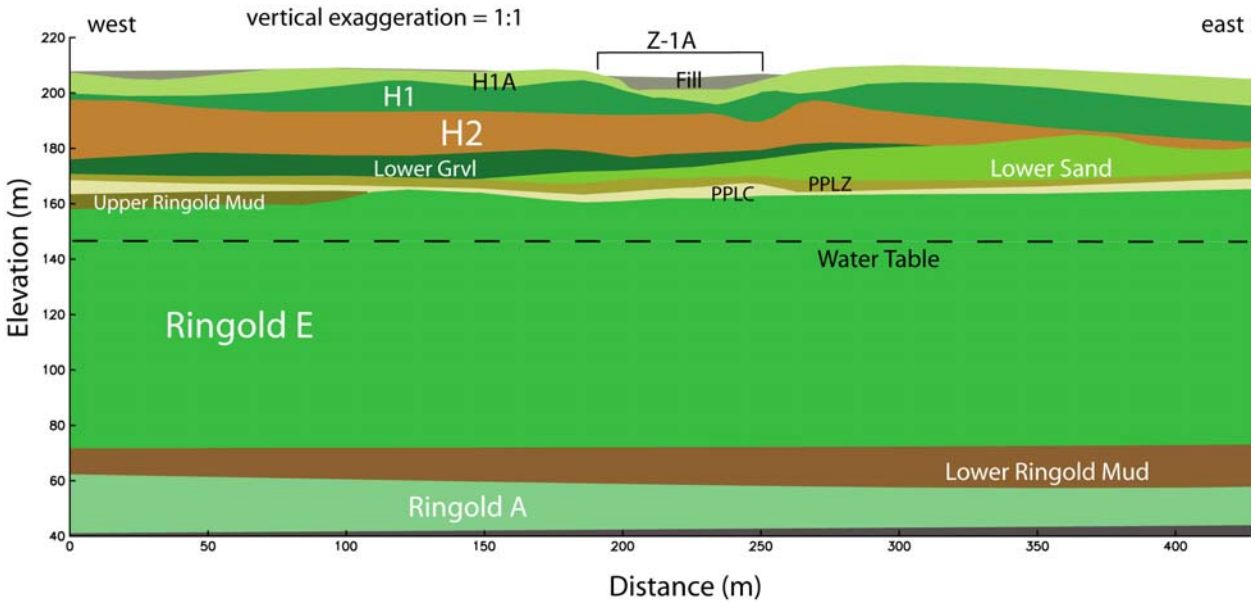

Figure 3.8. West-East Cross Section Through 216-Z-1A Tile Field

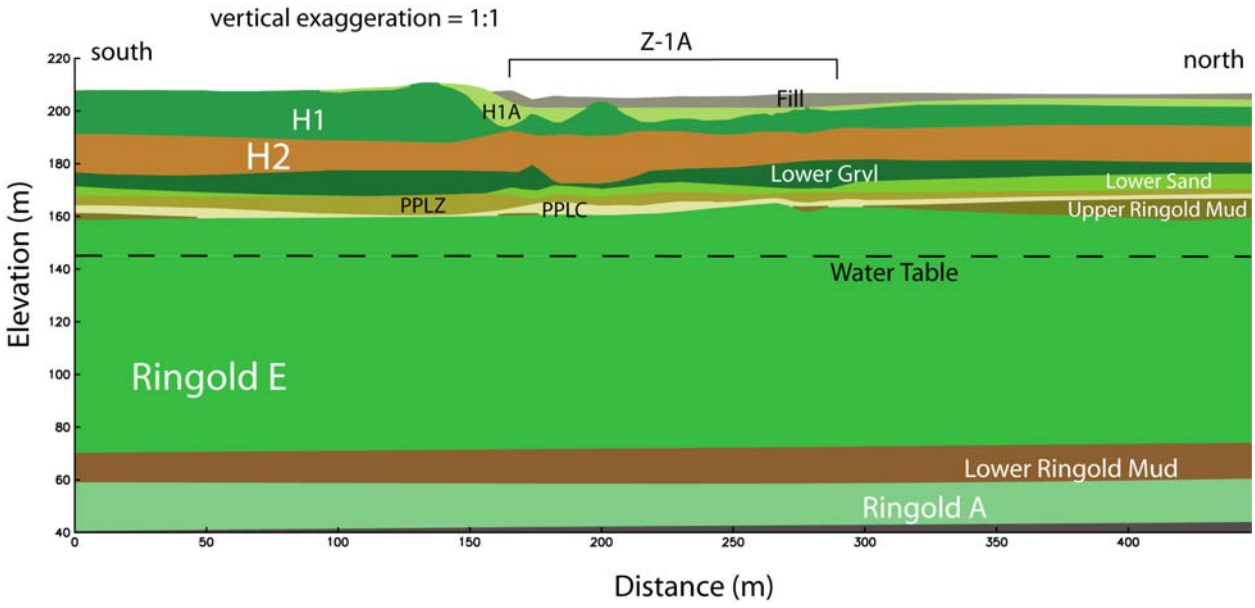

Figure 3.9. South-North Cross Section Through 216-Z-1A Tile Field

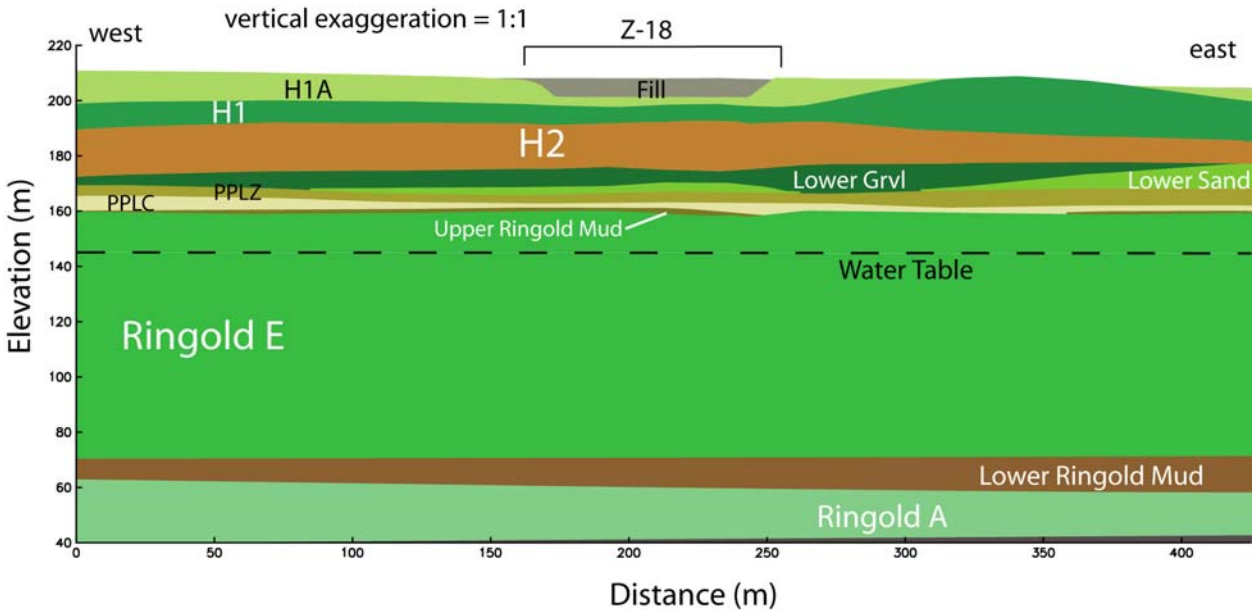

Figure 3.10. West-East Cross Section Through 216-Z-18 Tile Field

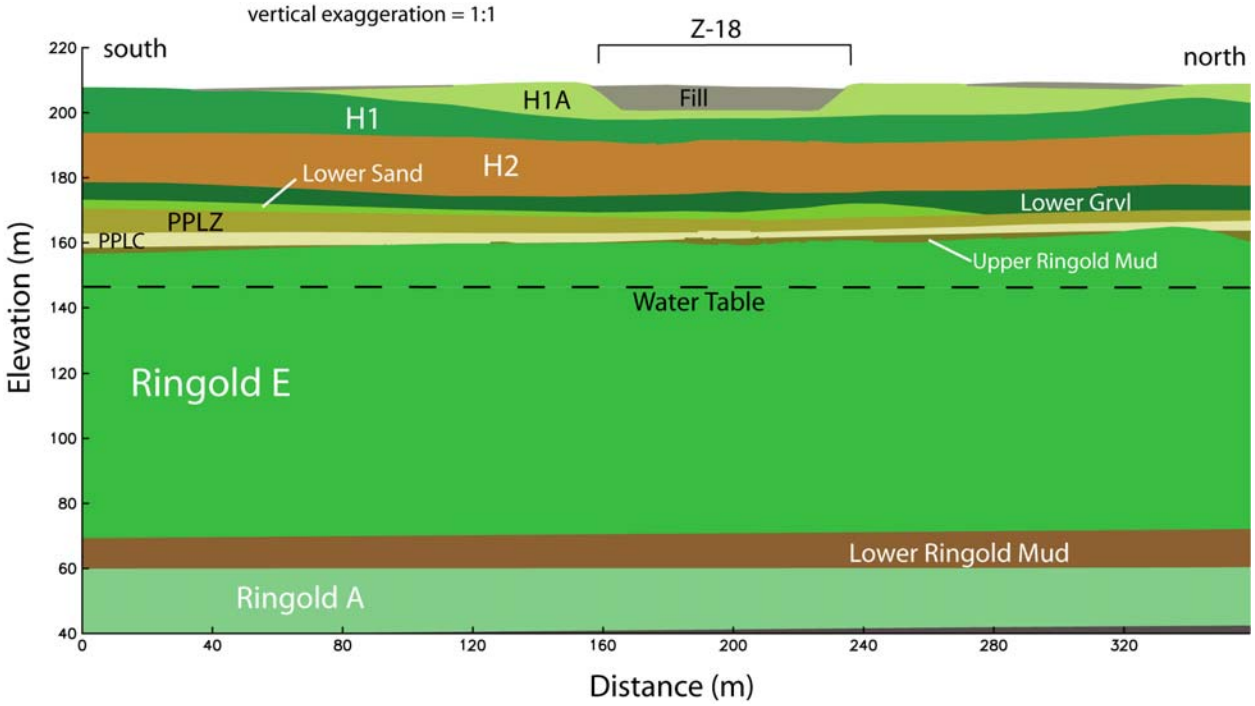

Figure 3.11. South-North Cross Section Through 216-Z-18 Tile Field

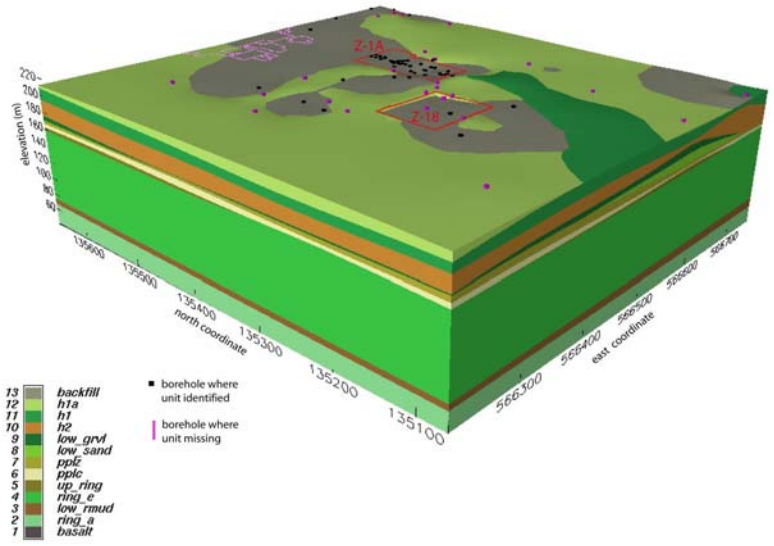

Figure 3.12. Extent of Backfill Unit in Computational Domain

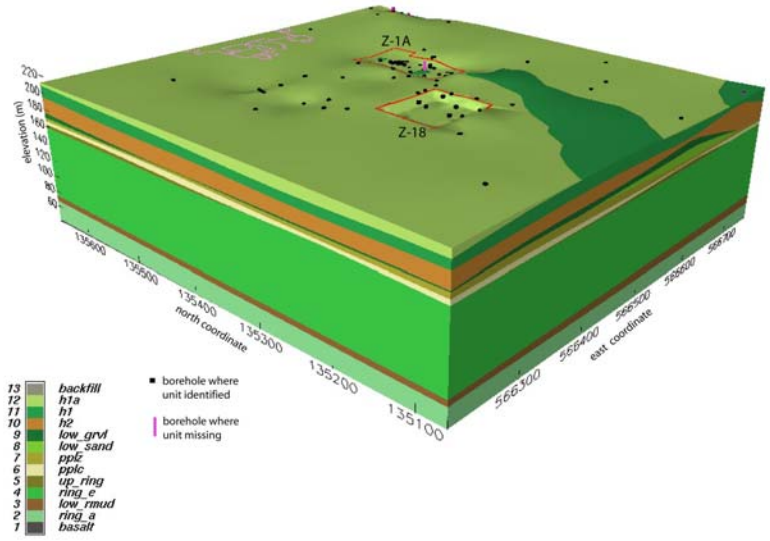

Figure 3.13. Extent of H1a Unit in Computational Domain

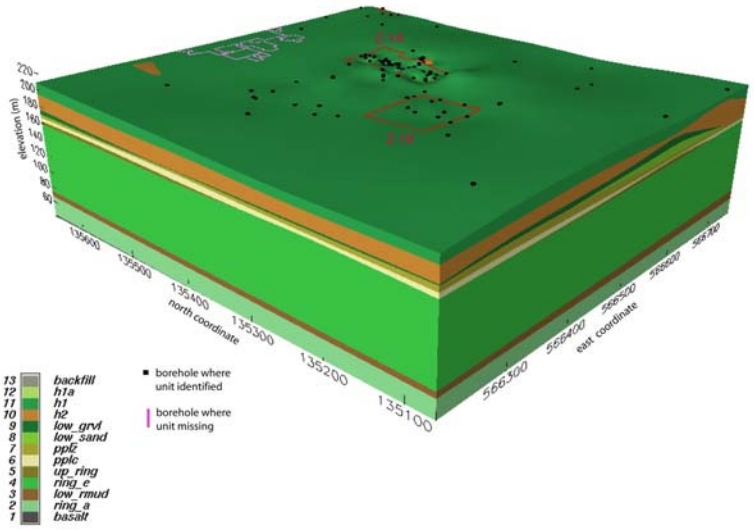

Figure 3.14. Extent of H1 Unit in the Computational Domain

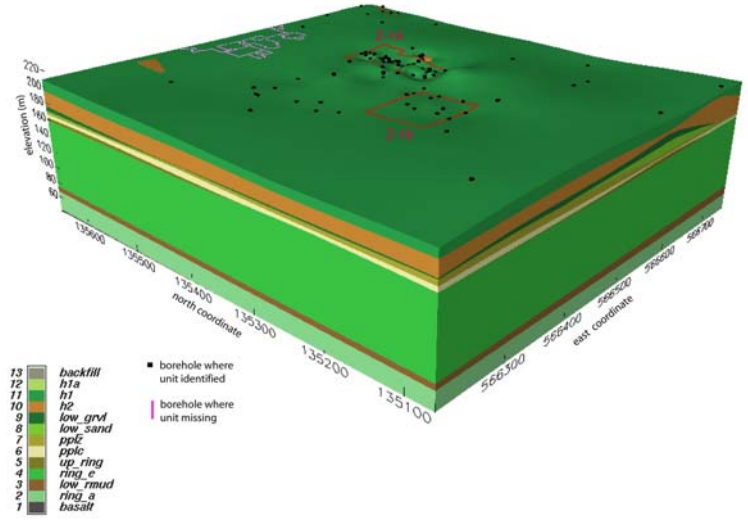

Figure 3.15. Extent of H2 Unit in the Computational Domain

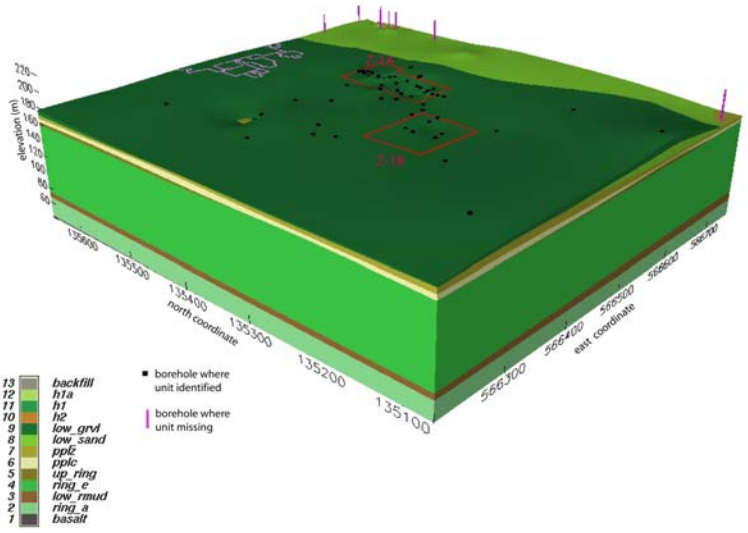

Figure 3.16. Extent of Lower Gravel Unit in the Computational Domain

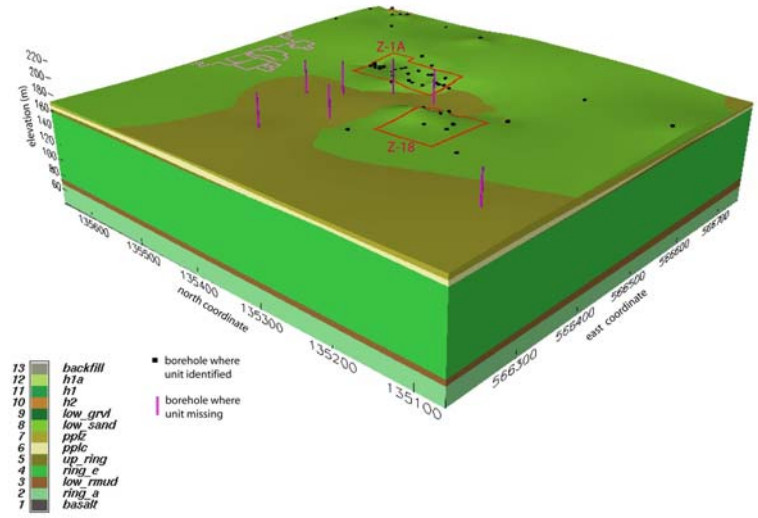

Figure 3.17. Extent of Lower Sand Unit in the Computational Domain

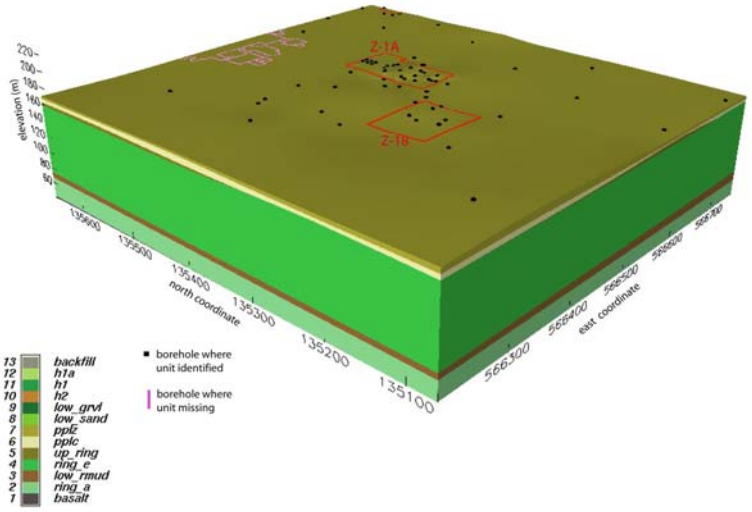

Figure 3.18. Extent of Cold Creek Silt Unit in the Computational Domain

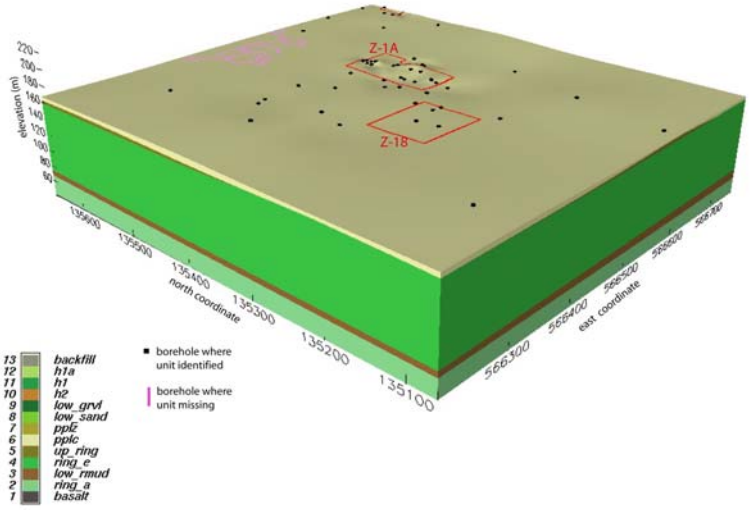

Figure 3.19. Extent of Lower Cold Creek Caliche Unit in the Computational Domain

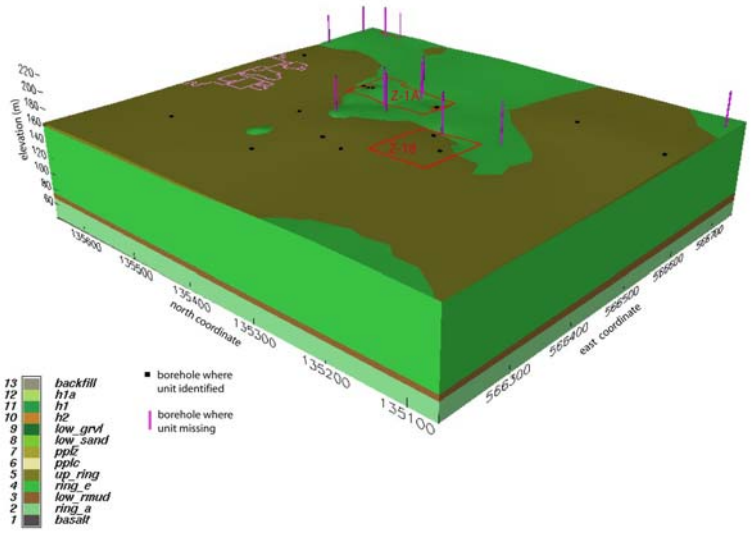

Figure 3.20. Extent of Upper Ringold Unit in the Computational Domain

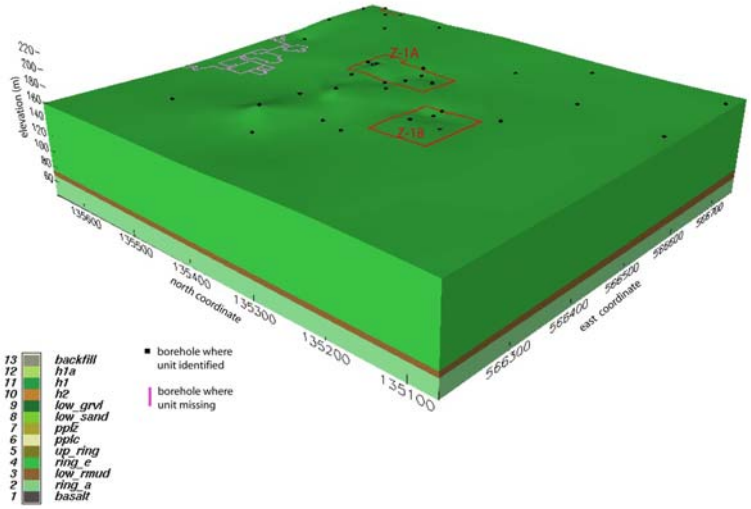

Figure 3.21. Extent of Ringold E Unit in the Computational Domain

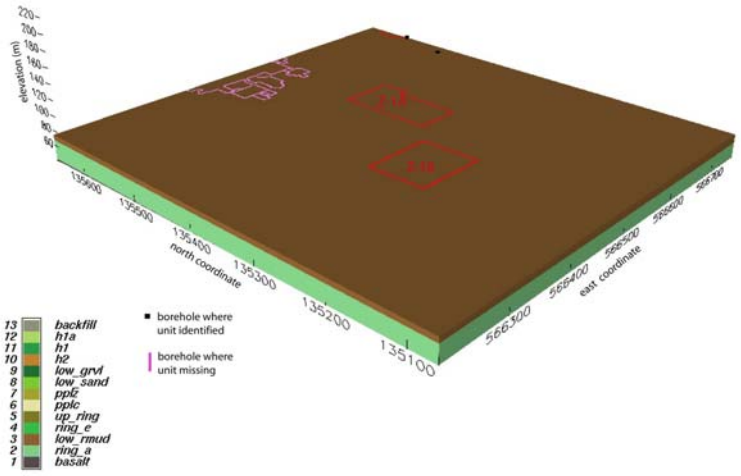

Figure 3.22. Extent of Lower Ringold in the Computational Domain

4.0 Overview of Simulations

Simulations were conducted in two phases. The first set of simulations examined the infiltration and redistribution of CT from the time of disposal through 1993, just prior to the initiation of the SVE treatment. The second phase of simulations examined the impact of SVE on the CT distribution in the subsurface over the time period of 1993 to 2007.

4.1 Infiltration/Redistribution Simulations

A total of 34 three-dimensional simulations were conducted for the infiltration/redistribution assessment. The simulations consist of one base case simulation and a sensitivity analysis consisting of 33 simulations. The computational domain was discretized into 49 x 50 x 85 = 208,250 nodes. Since the water-air-oil mode was used, this number of nodes translates into 3 x 208,250 = 624,750 unknowns. The simulation time period was from 1948 – 1993.

4.1.1 Base Case Simulation

The simulations include fluid infiltration from the 216-Z-1, 216-Z-2, 216-Z-3, 216-Z-1A, and 216-Z-18 disposal facilities. The first three sites, located in the northern part of the 219-Z-1A site footprint (Figure 3.2) received aqueous waste only. The 216-Z-1A and 216-Z-18 sites received both aqueous waste and DNAPL. The aqueous phase and DNAPL volumes reported in this section are obtained from Anderson (1976) and Rohay et al. (1994). The fluid distribution information is listed in Table 4.1 for the aqueous phase disposal sites, Table 4.2 for 216-Z-1A, and Table 4.3 for 216-Z-18. Although the majority of the aqueous waste from 216-Z-1, 216-Z-2, and 216-Z-3 were disposed well before DNAPL was released at the 216-Z-1A and 216-Z-18 sites, the releases are included in the model because the magnitude of the combined volume discharged at the three aqueous waste sites was approximately 2.1×10^8 L, which is almost 25 times the volume disposed of at the 216-Z-1A and 216-Z-18 sites combined. It is expected that this volume, released between 1949 and 1960, would have resulted in elevated water saturations during CT infiltration and redistribution in later years.

The modeled area of the 216-Z-1 and 216-Z-2 sites combination was 40 m^2, while the modeled area of the 216-Z-3 site was assumed to be 160 m^2. The modeled areas for the 216-Z-18 and 216-Z-1A sites were estimated from drawings presented in Rohay et al. (1994). For the 216-Z-18 site, it was estimated that each of the four disposal trenches was 60-m long with a disposal area of 1 m^2 per m trench length, for a total area of 240 m^2. The modeled area of the 216-Z-1A tile field was estimated by adding the length of the vitrified clay distributor pipes from Figure A-2 in Rohay et al. (1994) and allowing a disposal area of 1 m^2 per m pipe length, yielding an area of approximately 480 m^2. The base case simulation takes into account that during the disposal period for DNAPL at this site (1964 - 1969), a 5-cm-diameter stainless steel pipe was used to divide the tile field into three operational sections (216-Z-1AA, 216-Z-1AB, and 216-Z-1AC). The disposal periods for each operation section, each with an area of 160 m^2, were obtained from Anderson (1976) and are listed in Table 4.3.

Table 4.1. Discharged Aqueous Waste Volumes for the 216-Z-1, 216-Z-2, and 216-Z-3 Sites. Following Anderson (1976), the discharges for the 216-Z-1 and 216-Z-2 sites are combined into one area.

216-Z-1 and 216-Z-2		216-Z-3	
Year	Volume (L)	Year	Volume (L)
1949	5.55E6	1952	9.90E6
1950	1.12E7	1953	1.41E7
1951	1.12E7	1954	1.44E7
1952	5.55E6	1955	3.32E7
1966	1.00E5	1956	2.91E7
1967	4.00E3	1957	3.40E7
1968	3.80E4	1958	3.50E7
1969	6.00E4	1959	8.70E6
Total	**3.37E7**	**Total**	**1.78E8**

Table 4.2. Discharged Aqueous Waste and DNAPL Volumes for the 216-Z-18 Site

Year	Aqueous Phase Volume (L)	DNAPL Volume (L)
From 4/1969	5.50E5	2.20E4
1970	7.69E5	3.00E4
1971	8.84E5	3.40E4
1972	1.24E6	5.00E4
Through 4/1973	3.66E5	1.40E4
Total	**3.72E6**	**1.47E5**

The following fluid and porous media properties were used for the base case simulation.

DNAPL properties:

Fluid properties were measured in the EMSL Subsurface Flow and Transport Experimental Laboratory based on average fluid composition of 8.8% TBP, 14.7% DBBP, 2.9% lard oil, and 73.6% CT.

Density: 1,426 kg/m^3
Viscosity: 1.11 x 10^{-3} Pa s
Vapor pressure: 10,830 Pa
Surface tension (air-DNAPL): 25.1 dynes/cm
Interfacial tension (water-DNAPL): 15.2 dynes/cm
CT aqueous phase solubility: 720 mg/L
CT gas phase concentration: 108,300 ppmv

Table 4.3. Discharged Aqueous Waste and DNAPL Volumes for the 216-Z-1A Site

Year	Aqueous Phase Volume (L)	DNAPL Volume (L)
1949	6.00E4	-
1950	1.00E5	-
1951	1.00E5	-
1952	1.00E5	-
1953	1.00E5	-
1954	1.00E5	-
1955	1.00E5	-
1956	1.00E5	-
1957	1.00E5	-
1958	1.00E5	-
1959	4.00E4	-
1960 - 4/1963	-	-
Z-1AA		
5/1964 - 12/1964	4.20E5	2.00E4
1965	9.20E5	4.10E4
1/1966 – 5/1966	5.40E5	2.52E4
Z-1AB		
6/1966 – 12/1966	9.60E5	4.48E4
1/1967 – 9/1967	9.40E5	3.94E4
Z-1AC		
10/1967 – 12/1967	2.53E5	1.06E4
1968	1.00E6	4.50E4
1/1969 – 4/1969	1.55E5	7.00E3
Total	6.21E6	2.42E5

Porous media present in domain (bottom to top):
Ringold A
Lower Mud
Ringold E
Upper Ringold
Cold Creek C
Cold Creek Z
Lower Sand
Lower Gravel
Hanford 2
Hanford 1
Hanford 1a
Backfill

Sorption:

A linear equilibrium K_d of 0.2 mL/g was applied to all porous media.

Hydraulic properties:

Retention parameters, porosities, and hydraulic conductivities were obtained from Khaleel et al. 2001 and Khaleel and Freeman (1995). The published van Genuchten (1980) saturation-pressure parameters were converted to equivalent Brooks-Corey (1964) parameters using the algorithms presented by Lenhard et al. (1989). The Brooks-Corey (1964) and van Genuchten (1980) parameter values are listed in Table 4.4 and 4.5, respectively.

Permeability anisotropy ratio:

10:1

Boundary and initial conditions:

On the top boundary, atmospheric gas pressure was assumed in conjunction with a 0.5 cm/yr water flux (recharge). For the South, North, West, and East boundary, fluctuating water table boundary conditions were imposed for the water mass balance equation below the water table and zero-flux boundary conditions were applied above the water table. The time variant boundary conditions for the water mass balance equation at the South and North boundary (water table information) were similar to the conditions imposed on the domain for the 216-Z-9 studies (Oostrom et al. 2004; 2006).

The resulting boundary conditions yielded a ground water flow direction from south to north. Neumann boundary conditions were imposed for water and DNAPL discharges for the 216-Z-9 trench area during the years that these liquids were disposed. The flow rates are listed in the section associated with the specific input parameters for each simulation case. DNAPL was allowed to move freely across all boundaries. The initial gas and aqueous phase pressure distributions in the domain at 1948 were obtained by conducting a 10,000-yr simulation using the interpolated 1948 water levels at the South and North boundary and a recharge rate of 0.5 cm/yr. It was assumed that in 1948 no DNAPL was present in the domain.

Table 4.4. Horizontal Saturated Hydraulic Conductivity (K_s), Porosity, and Retention Parameter Values (Brooks-Corey λ, h_d, and irreducible water saturation, s_{rl}) of Stratigraphic Units

Stratigraphic Units	K_s (cm/s)	Porosity	Brooks and Corey h_d (cm)	Brooks and Corey λ	s_{rl}
Ringold A	5.73E-3	0.0770	71.3	0.52	0.1299
Lower Mud	1.16E-8	0.0770	71.3	0.52	0.1299
Ringold E	5.73E-3	0.0770	71.3	0.52	0.1299
Upper Ringold	5.73E-3	0.0770	71.3	0.52	0.1299
Cold Creek C	6.72E-3	0.3203	36.3	0.61	0.2451
Cold Creek Z	1.48E-4	0.4238	120.0	0.79	0.0967
Lower Sand	1.87E-2	0.3359	4.7	0.78	0.0747
Lower Gravel	3.00E-2	0.2720	23.0	0.75	0.1471
Hanford 2	5.85E-3	0.3653	14.1	0.95	0.0846
Hanford 1	5.00E-2	0.1660	7.7	0.54	0.1386
Hanford 1A	5.98E-4	0.4478	58.1	0.71	0.1740
Backfill	1.5E-2	0.2620	22.0	0.36	0.3646

Table 4.5. Horizontal Saturated Hydraulic Conductivity (K_s), Porosity, and Retention Parameter Values (van Genuchten α, n, and irreducible water saturation, s_{rl}) of Stratigraphic Units for Simulations

Stratigraphic Units	K_s (cm/s)	Porosity	Van Genuchten α (1/cm)	Van Genuchten n	s_{rl}
Ringold A	5.73E-3	0.0770	0.0090	1.6210	0.1299
Lower Mud	1.16E-8	0.0770	0.0090	1.6210	0.1299
Ringold E	5.73E-3	0.0770	0.0090	1.6210	0.1299
Upper Ringold	5.73E-3	0.0770	0.0090	1.6210	0.1299
Cold Creek C	6.72E-3	0.3203	0.0173	1.7705	0.2451
Cold Creek Z	1.48E-4	0.4238	0.0052	2.0671	0.0967
Lower Sand	1.87E-2	0.3359	0.1338	2.0475	0.0747
Lower Gravel	3.00E-2	0.2720	0.0270	1.9940	0.1471
Hanford 2	5.85E-3	0.3653	0.0448	2.3553	0.0846
Hanford 1	5.00E-2	0.1660	0.0830	1.6600	0.1386
Hanford 1A	5.98E-4	0.4478	0.0107	1.9229	0.1740
Backfill	1.5E-2	0.2620	0.0320	1.4000	0.3646

4.1.2 Sensitivity Analysis Simulations

A total of 33 sensitivity analysis simulations were conducted for the infiltration/redistribution assessment. The simulations are categorized in six groups, depending on the imposed change.

I. *Disposal Site Area*

a. Infiltration area 20% of base case area for both aqueous phase and DNAPL.
b. Infiltration area 10% of base case area for both aqueous phase and DNAPL.
c. Infiltration area 100% of base case area for aqueous phase and 10% for DNAPL.

II. *DNAPL Volume*

a. 1.25 x DNAPL volume base case for both sites.
b. 1.5 x DNAPL volume base case for both sites.
c. 2 x DNAPL volume base case for both sites.

III. *DNAPL Properties and Porous Media Properties Related to CT*

a. Fluid properties of disposed DNAPL equal to properties of pure CT.

Density: 1594 kg/m^3
Viscosity: 0.97x10^{-3} Pa s
Vapor pressure: 11,950 Pa
Surface tension (air-DNAPL): 26.2 dynes/cm

Interfacial tension (water-DNAPL): 40.8 dynes/cm
CT aqueous phase solubility: 800 mg/L
CT gas phase concentration: 120,000 ppmv

b. Properties of DNAPL reflecting DNAPL composition of 50% CT, 10% lard oil, 20% DBBP, and 20% TBP. This DNAPL composition reflects the lowest CT percentage of the disposed DNAPL.

Density: 1260 kg/m^3
Viscosity: 1.357×10^{-3} Pa s
Vapor pressure: 8,250 Pa
Surface tension (air-DNAPL): 24.2 dynes/cm
Interfacial tension (water-DNAPL): 11.8 dynes/cm
CT aqueous phase solubility: 550 mg/L
CT gas phase concentration: 82,300 ppmv

c. A DNAPL vapor pressure of 5,415 Pa.

d. A DNAPL vapor pressure of 2,708 Pa.

e. A CT solubility of 360 mg/L

f. A CT solubility of 180 mg/L

g. A K_d partitioning coefficient of 0.0 mL/g.

h. A K_d partitioning coefficient of 0.1 mL/g.

i. A K_d partitioning coefficient of 0.4 mL/g.

j. Laboratory measured maximum residual NAPL saturation for Cold Creek silt (0.13), Hanford Sand (0.10), Lower Gravel (0.05), and Ringold E material (0.11). For the other materials, a maximum residual of 0.1 was assumed.

k. Measured and assumed maximum residual DNAPL saturation times 1.25.

IV. Porous Medium Properties of H1a Unit

a. Permeability of H1 unit (5.0E-2 cm/s)
b. Porosity of H1 unit (0.166)
c. Air-entry pressure head of H1 unit (7.7 cm)
d. All porous media properties of H1 unit

V. Porous Medium Properties of Cold Creek Unit

a. 0.1 x base case permeability
b. 0.1 x base case permeability and $\sqrt{10}$ x the air-entry pressure head.
c. 10 x base case permeability.
d. 10 x base case permeability and $1/\sqrt{10}$ x the base case air-entry pressure.

VI. Porous Medium Properties of all Units

a. Anisotropy ratio of 1:1.
b. Anisotropy ration of 20:1
c. 1.25 x base case porosity
d. 0.75 x base case porosity
e. 2 x base case air-entry pressure head
f. 0.5 x base case air-entry pressure head
g. 10 x base case permeability
h. 0.1 x base case permeability

4.2 SVE Simulations

Rohay (2002) describes the details of the field SVE campaigns for the 200-PW-1 Operable Unit, which includes the 216-Z-9 trench, 216-Z-1A tile field, and 216-Z-18 crib. There are 46 wells available for SVE in this operable unit, with well diameters ranging from 5 to 20 cm. During the active SVE campaigns, each system extracted soil vapor simultaneously from multiple wells open either above and/or below the CCU. Details on the operation of the well field can be found in Rohay (2002) and Oostrom et al. (2004; 2006).

A total of seven simulations for the period 1993 – 2007 were conducted to investigate the effect of well location, extraction rate, and vapor pressure on CT removal during SVE operations. The base case fluid and porous medium property values are used for all simulations in this section. The initial conditions of these simulations are the base case 1993 conditions. The SVE simulations are:

1. Extraction from all wells.

2. Extraction from wells with screens located in 216-Z-1A Cold Creek Silt: W18-159, -165, -166, -167, -178, and -174.

3. Extraction from wells located near water table near the 216-Z-18 trench: W18-10, -11, and -12.

4. Extraction from well W18-96 only, located below the 216-Z-18 trench.

5. Extraction from well W18-165 only, located below the 216-Z-1A tile field.

6. Extraction from well W18-246 (located west of 216-Z-1A and north of 216-Z-18)

7. Extraction with 25% of the rate.

8. Extraction from all wells and hydraulic properties of H1a the same as for H1.

4.3 Undocumented Discharge Simulations

The conceptual model for CT behavior in the subsurface of the 200 West Area includes downward migration of CT as a DNAPL or dissolved in the aqueous phase to groundwater from an undocumented source (DOE 2004). To address this issue, two types of simulations were conducted.

1. A series of simulations was conducted to estimate the volume of DNAPL needed to reach the groundwater for each of the three DNAPL waste sites. For each site, the infiltration rate of the base case simulation was modified in an iterative manner, while keeping the disposal area and duration unchanged, to find the minimum volume of discharged DNAPL that would yield DNAPL movement across the water table by 1993. The computed volumes are assumed to be indicative of the size of undocumented discharge volumes needed at a typical disposal facility to reach the saturated zone.

2. Assuming that an undocumented discharge might result from an accidental spill, various spills were simulated for two generalized three-dimensional geologic domains. For the first representation, the H1a, H1, H2, and Lower Sand units are assumed to be each 8 m thick. Located below the Lower Sand unit, the Cold Creek silt and caliche units are both 3-m thick. The Ringold E unit is the lowest unit of the simplified computational domain. The water table is located at 65 m below the surface. The first domain represents the subsurface of the 216-Z-1A and 216-Z-18 sites. The second domain is similar to the first with the exception that the H1a unit is not present. Instead, the H1 unit is 16-m thick. The second domain is assumed to represent the subsurface of the 216-Z-9 site (Oostrom et al. 2004, 2006). For each geologic representation, a total of nine simulations were conducted. All spills are assumed to have occurred on a 1 m^2 area, with volumes of 0.2, 2, and 10 m^3, and a spill duration of 1 hour, 1 day, and 10 days. A spill size of 0.2 m^3 is equivalent to approximately a one 208.2-L drum. For each simulation, the maximum DNAPL penetration depth was recorded.

5.0 Results and Discussion

5.1 Base Case Results

Before DNAPL was disposed at the 216-Z-1A and 216-Z-18 sites, large volumes of aqueous phase were released at the 216-Z-1 and 216-Z-2 sites between 1949 and 1953 and the 216-Z-3 site between 1952 and 1960 (Table 4.1). These three sites, located on the footprint of the 216-Z-1A site, have received a combined volume of 212,000 m^3 of aqueous phase through 1960. The combined liquid waste to the 216-Z-1A site from 1964 through 1969 and to the 216-Z-18 site from 1969 through 1973 was 9,120 m^3. Because of the considerable size of the initial aqueous phase waste releases and the location of the disposal sites, liquid waste emanating from the 216-Z-1, 216-Z-2, and 216-Z-3 sites have been included. The effect of the initial water disposal are shown in Figures 5.1 through 5.3, where the differences in water saturations between 1953, 1960, and 1964, respectively, with the 1948 steady-state water saturations are shown. Figure 5.1 depicts the water saturation differences after the 33,500 m^3 liquid waste disposal at the 216-Z-1 and 216-Z-2 sites was completed in 1953. The figure shows increased saturations by up to 70% below the northern part of the 216-Z-1A. The 1960 plot (Figure 5.2) shows water saturation differences directly after the 178,000 m^3 distribution to the 216-Z-3 has ended. The contribution from this site, located about 40 m to the east of the shown cross-section, was able to increase saturation over a 150 x 150 m area, all the way to the water table. The plot showing the differences at 1964 (Figure 5.3) shows that the saturation differences had decreased considerable after four years of inactivity. As expected, the CCU sediments were able to retain the disposed water longer than the other units. The 216-Z-1A tile field received approximately 5,260 m^3 liquid waste between 1964 and 1970, while the waste stream to the 216-Z-18 crib totaled 3,860 m^3 between 1969 and 1974. Plots showing the differences in water saturation between 1948 for 1970 and 1974 are presented in Figures 5.4 and 5.5, respectively. The figures show that the effects from earlier water disposal have dissipated and that most of that water has drained from the CCU and the elevated water saturations are primarily the result of the aqueous phase disposal at the two DNAPL waste sites. Over time, the disposed water continues to flow downward and laterally through capillary forces. In 1993, at the beginning of SVE operations, elevated water saturations are only predicted to occur in the CCU (Figure 5.6).

DNAPL infiltration at the 216-Z-1A site occurred between 1964 and 1970, while the 216-Z-18 site received waste from 1969 through 1974. Disposal at the 216-Z-1A site occurred at three sub-sites: 216-Z-1AA, 216-Z-1AB, and 216-Z-1AC. Each of the three sites received waste for approximately 2 years out of the total of six years that DNAPL waste was disposed at the 216-Z-1A site. Details of the disposal history can be found in Chapter 4. Simulated DNAPL saturations at the end of 1966, 1968, 1970, 1974, 1984, and 1993 are shown in Figures 5.7, 5.8, 5.9, 5.10, 5.11, and 5.12, respectively. Figures 5.7, 5.8, and 5.9 reflect the change in disposal location within the 216-Z-1A site as the DNAPL body is getting larger in a southerly direction with time. In 1970, DNAPL has moved into the Lower Sand unit but not yet into the CCU. Figure 5.9 also shows DNAPL saturations after the first year of disposal at the 216-Z-18 site indicating DNAPL infiltrating from the four individual cribs that comprise the 216-Z-18 site. At the end of the 216-Z-18 site disposal period (1974), the infiltrated DNAPL from this site has just started to move into the H2 unit (Figure 5.10). This figure also shows that below the 216-Z-1A site, DNAPL has entered the CCU silt. After 1974 no aqueous phase or DNAPL were disposed at either site. Figures 5.11 and 5.12 show the DNAPL redistribution at 1984 and 1993 respectively. The plots for this base case simulation show that the DNAPL under the 216-Z-1A site primarily remains in the

H1a unit, H2 unit, and CCU. No DNAPL has moved across the water table by 1993. Below the 216-Z-18 site, the DNAPL has not moved below the H2 unit by 1993. The sequence of plots presented in Figures 5.7 through 5.12 clearly indicates that the disposed DNAPL remained below the footprints of both sites.

The CT gas concentrations in 1970, 1974, 1984, and 1993 are shown in Figures 5.13, 5.14, 5.15, and 5.16, respectively. The figures show that the gas plume grows rapidly and spreads out over the lower-permeability CCU and later in time over the water table. The CT component of the DNAPL is causing the density of the gas phase to increase because the gas density of air saturated with CT in the DNAPL used in the simulations was approximately 1.8 g/L at 20^{o} C, compared with an ambient gas density of 1.2 g/L. The difference in gas density causes density-driven advection to move considerable amounts of CT downward in the vapor phase. Top views of the gas concentrations in the middle of the CCU are shown in Figure 5.17 and 5.18 for 1974 and 1993, respectively. The plots show that CT vapors appear in the CCU below the 216-Z-1A site before arriving below the 216-Z-18 site. By 1993, the plume has become rather extensive in the horizontal directions and its size clearly exceeds the footprints of both disposal sites. CT in the gas phase arrives at the water table approximately 10 years after arriving at the CCU. CT gas concentrations at the first unsaturated node above the water table are shown in Figures 5.19 and 5.20, for 1984 and 1993, respectively. Since the CT gas arrived later at this level, the horizontal extension is less pronounced than in the CCU.

The CT mass distribution over the DNAPL, sorbed, aqueous phase, liquid phase phases are shown in Figure 5.21. The plot shows that after the infiltration periods for the disposal sites (1964-1974), the total CT mass in the computational domain remained practically unchanged through 1993, meaning that only a small amount of CT mass has left the domain in the various phases. After DNAPL infiltration ceased, the CT mass in the DNAPL phase slowly decreased, while the CT mass in the other phases increased. Note that the sorbed CT mass is larger than the CT mass in the gas and aqueous phases. The relative contribution of the sorbed CT mass and the dissolved, and gas phases can be illustrated by a simple distribution calculation. The calculation assumes that an excess of CT DNAPL phase is in equilibrium with the other phases under unsaturated conditions. In this case, the sum of the sorbed and CT mass in the gas and aqueous phases per unit volume is given by

$$\left(1-n_D\right)\rho_s S + \theta_g C_g + \theta_l C_l \tag{5.1}$$

where the subscripts *g* and *l* denote the gas and aqueous phase, respectively, n_D is the porosity, ρ_s is the particle density (M/L^3), *S* is the sorbed CT mass per unit mass of porous medium (M/M), θ is the volumetric content, and *C* the concentration (M/L^3). Assuming a linear sorption isotherm with $S = K_d C_l$, where K_d (L^3/M) is an equilibrium partitioning coefficient, Eq. (5.1) can be rewritten to

$$\left(1-n_D\right)\rho_s K_d C_l + \theta_g C_g + \theta_l C_l \tag{5.2}$$

With the following data, appropriate for the subsurface and DNAPL properties used in the STOMP simulation: n_D = 0.25, ρ_s = 2650 kg/m^3, K_d = 2 x 10^{-4} m^3/kg, θ_g = 0.2, C_g = 0.73 kg/m^3 θ_l = 0.05, and C_l = 0.72 kg/m^3. These values result in a computed sorbed CT mass of 0.3975 kg/m^3, gas phase CT mass of 0.146 kg/m^3, and aqueous phase CT mass of 0.036 kg/m^3. The total CT mass per cubic meter is 0.5795

kg for which 3.64 x 10^{-4} m^3 (364 mL) liquid CT is needed. In this particular example, the sorbed CT mass > gas CT mass > aqueous phase CT mass, which is consistent with Figure 5.21.

The CT DNAPL phase mass distribution of the hydrostratigraphic units for 1960-1993 is shown in Figure 5.22 for the combined sites. The plot shows that the H1a unit contains the most CT in the DNAPL phase throughout the simulation period. Note that the influence of the H1a unit was not observed in the 216-Z-9 simulations (Oostrom et al. 2004; 2006) because this unit is not present below that disposal facility based on the available geologic data. Since the CT DNAPL in the H1a unit is so large, several sensitivity cases were executed to investigate the influence of several hydraulic parameters on CT DNAPL flow in that unit. The results of these simulations are shown in Section 5.2.4. Figure 5.22 also shows that the H2 unit retains considerable volumes of CT DNAPL, while all CT DNAPL has been removed from the H1 unit before 1985. Other units above the CCU containing DNAPL are the Lower Sand and Lower Gravel units. The lowest layer with CT DNAPL is the CCU silt. No CT DNAPL was transported to the CCU caliche.

CT mass distributions over the phases for each of the two individual sites are shown in Figure 5.23 for the 216-Z-1A site and in Figure 5.24 for the 216-Z-18 site. The plots, reflecting the disposed DNAPL volumes, show similar trends as found for the figure combining the phase distributions for both sites (Figure 5.21). CT mass distributions over the hydrostratigraphic units for each individual site are shown in Figure 5.25 and Figure 5.26 for the 216-Z-1A and 216-Z-18 sites, respectively. These two figures show distributions quite different from the plot combining the two sites (Figure 5.22). For the 216-Z-1A site, the H2 unit contains the most DNAPL, followed by the H1a unit. Below the 216-Z-18 site, DNAPL is not able to penetrate lower than the H2 and the vast majority of the DNAPL is located in the H1a. This plot quantitatively describes what can be visually observed in Figures 5.7 through 5.12.

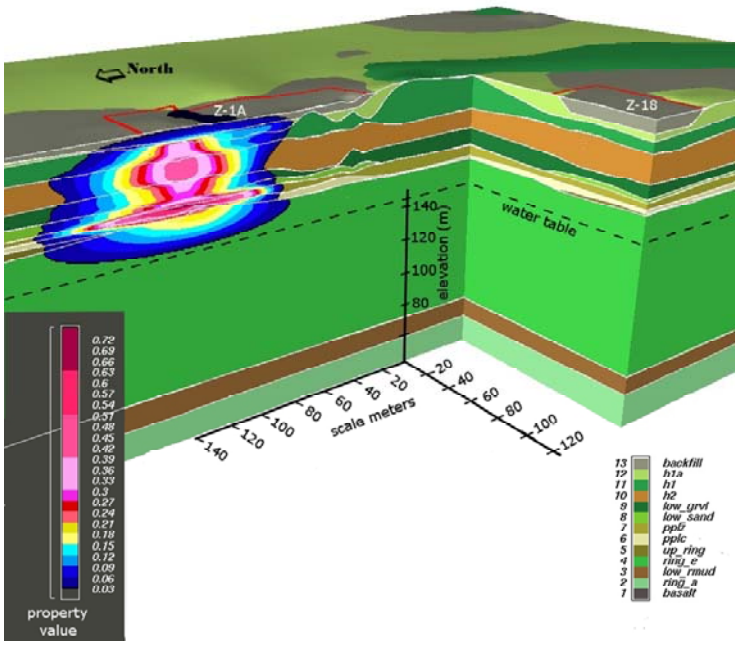

Figure 5.1. Differences in Water Saturations Between 1953 and 1948 (Base Case)

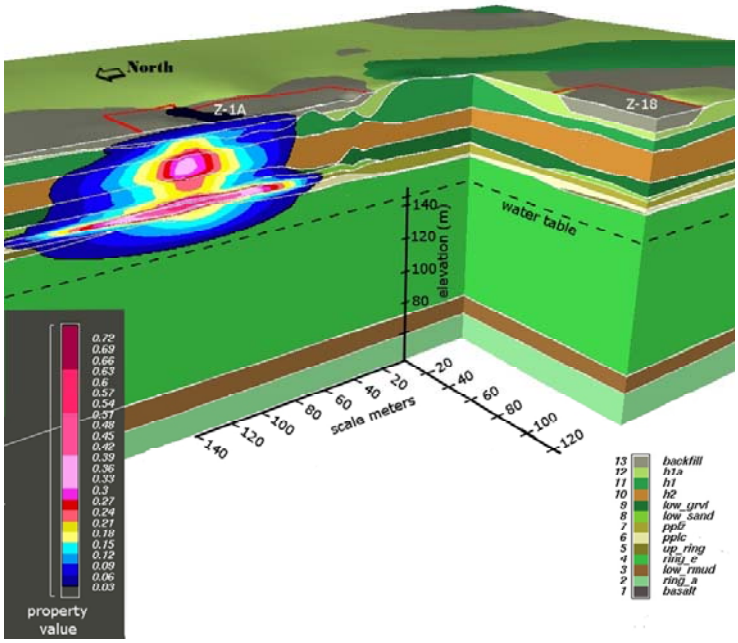

Figure 5.2. Differences in Water Saturations Between 1960 and 1948 (Base Case)

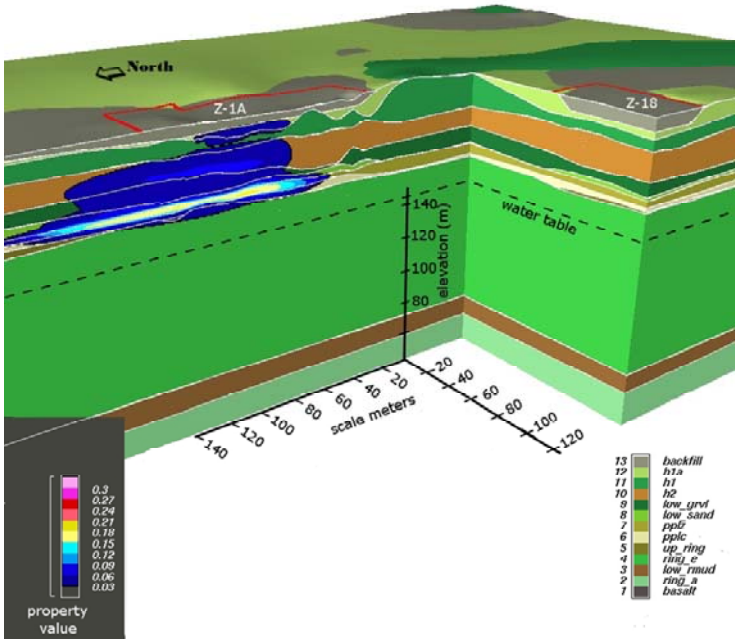

Figure 5.3. Differences in Water Saturations Between 1964 and 1948 (Base Case)

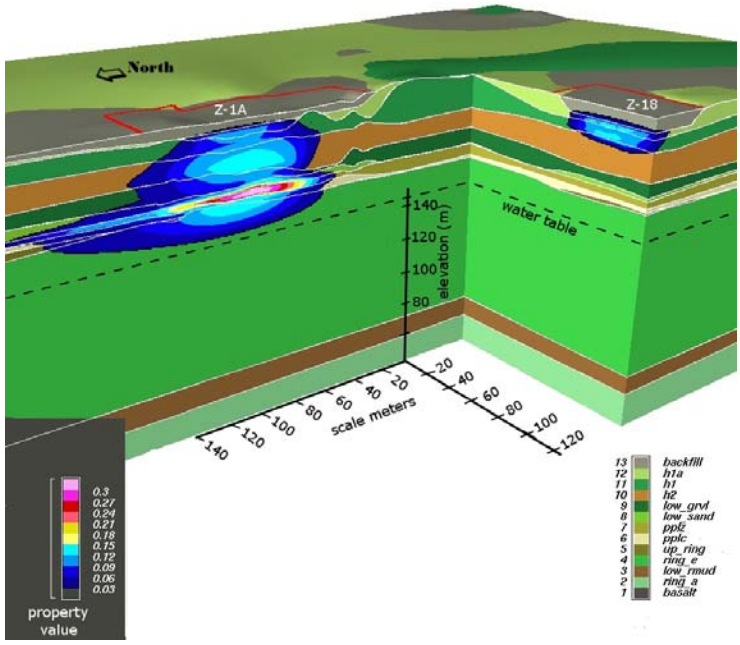

Figure 5.4. Differences in Water Saturations Between 1970 and 1948 (Base Case)

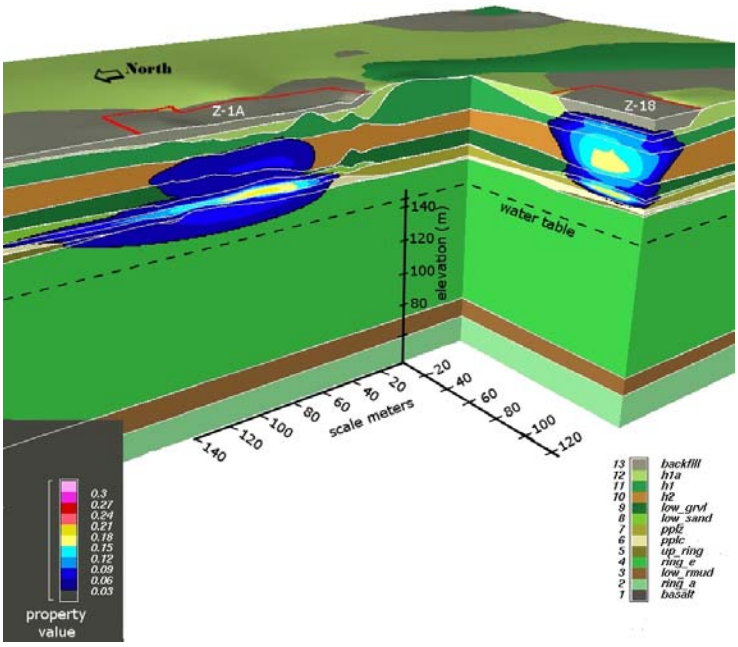

Figure 5.5. Differences in Water Saturations Between 1974 and 1948 (Base Case)

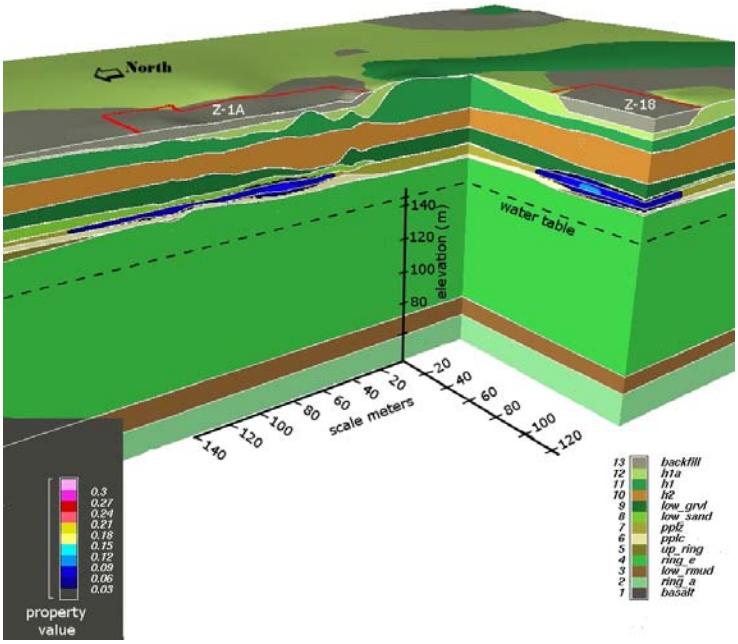

Figure 5.6. Differences in Water Saturations Between 1993 and 1948 (Base Case)

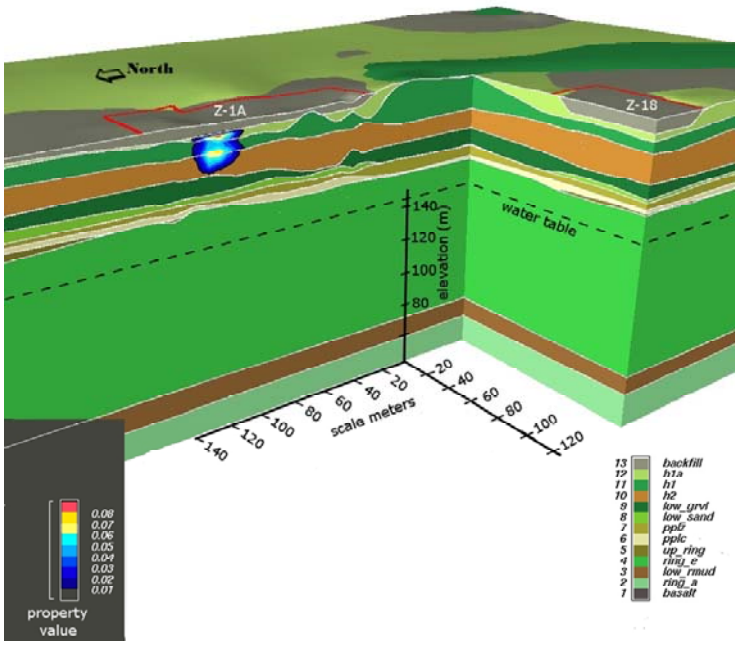

Figure 5.7. DNAPL Saturations at 1966 (Base Case)

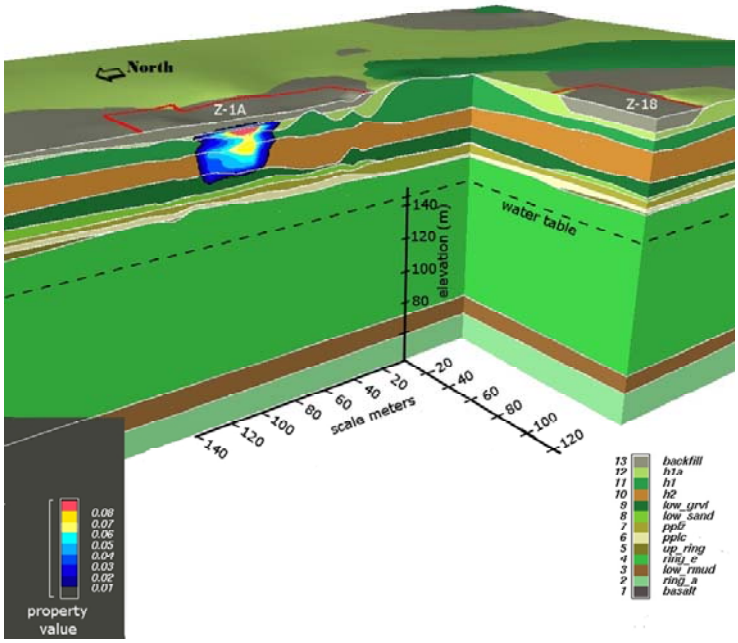

Figure 5.8. DNAPL Saturations at 1968 (Base Case)

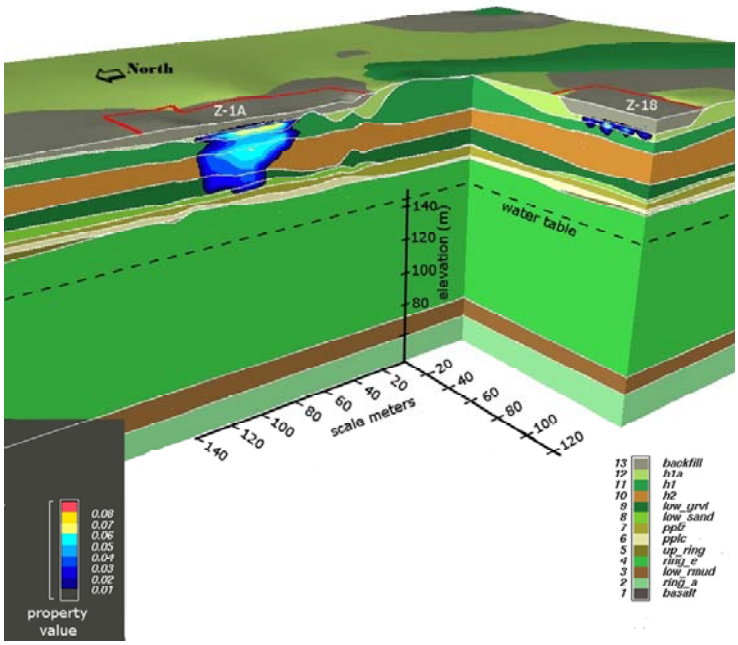

Figure 5.9. DNAPL Saturations at 1970 (Base Case)

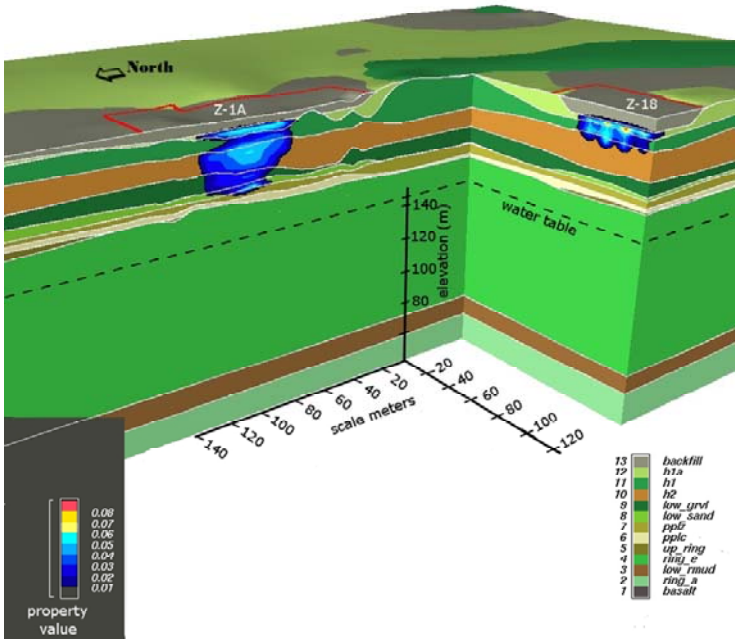

Figure 5.10. DNAPL Saturations at 1974 (Base Case)

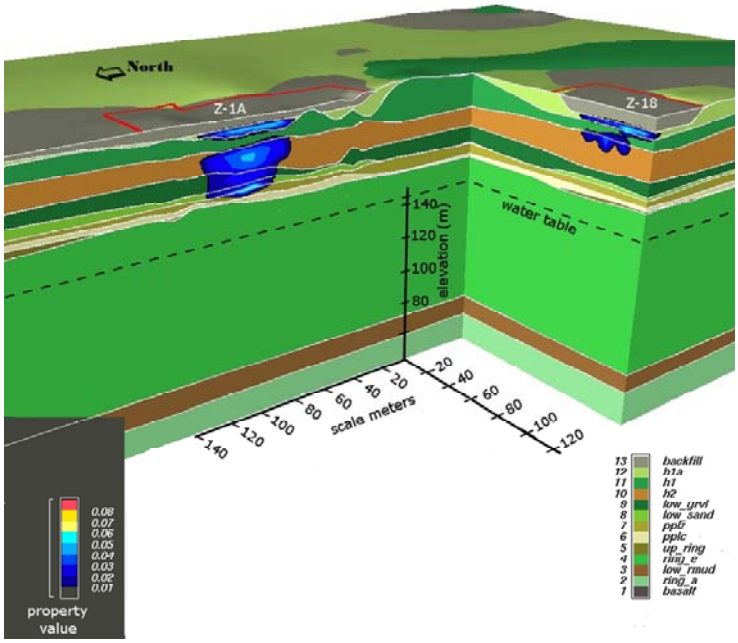

Figure 5.11. DNAPL Saturations at 1984 (Base Case)

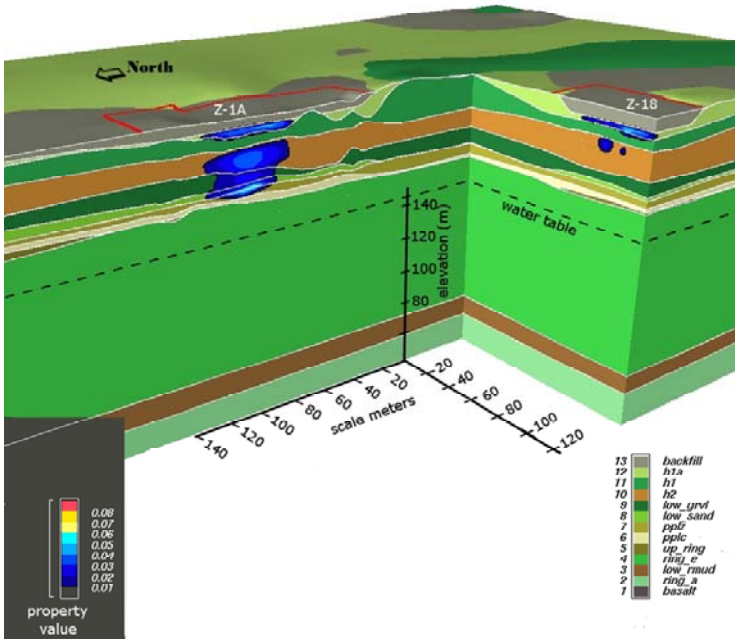

Figure 5.12. DNAPL Saturations at 1993 (Base Case)

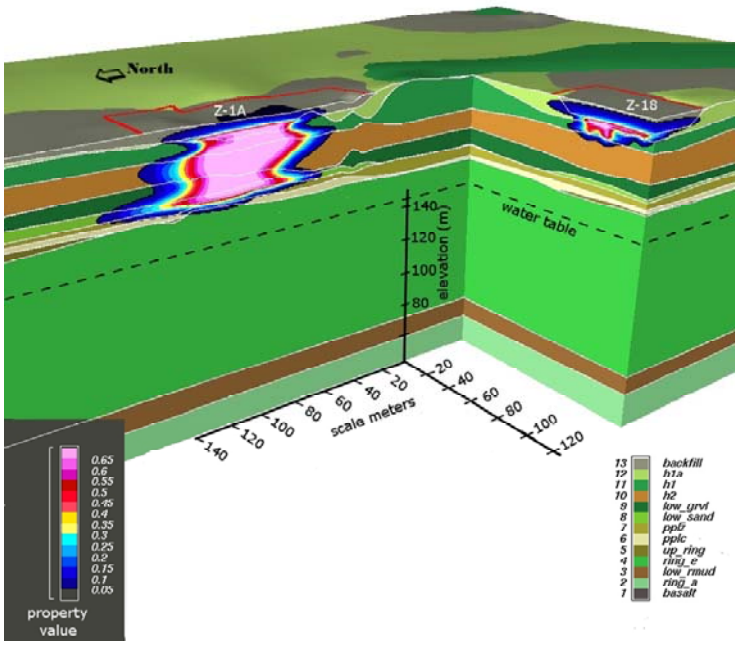

Figure 5.13. CT Gas Concentrations (g/L) at 1970 (Base Case) (0.1 g/L is equivalent to 12,000 ppmv at standard temperature and pressure)

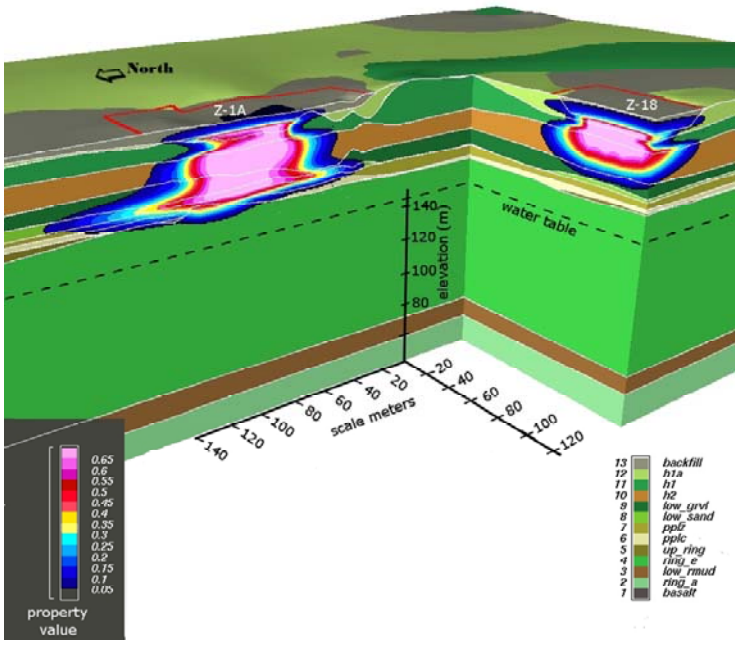

Figure 5.14. CT Gas Concentrations (g/L) at 1974 (Base Case) (0.1 g/L is equivalent to 12,000 ppmv at standard temperature and pressure)

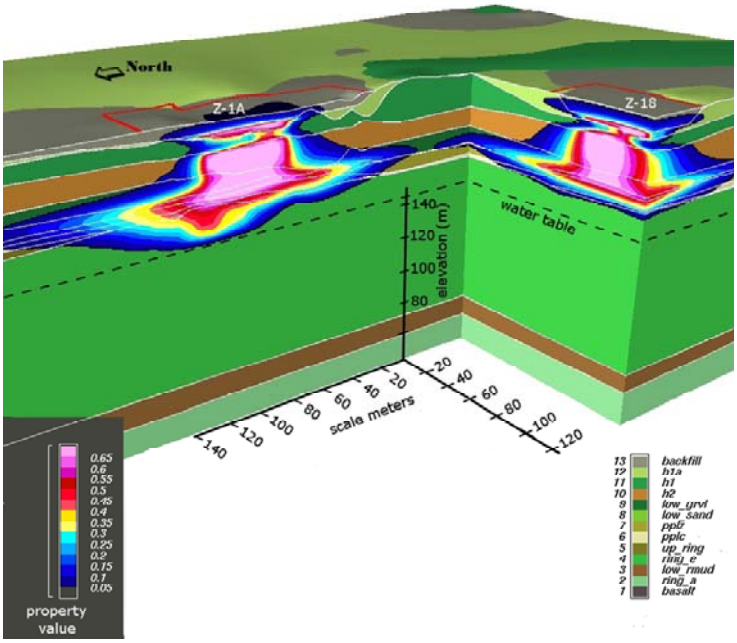

Figure 5.15. CT Gas Concentrations (g/L) at 1984 (Base Case) (0.1 g/L is equivalent to 12,000 ppmv at standard temperature and pressure)

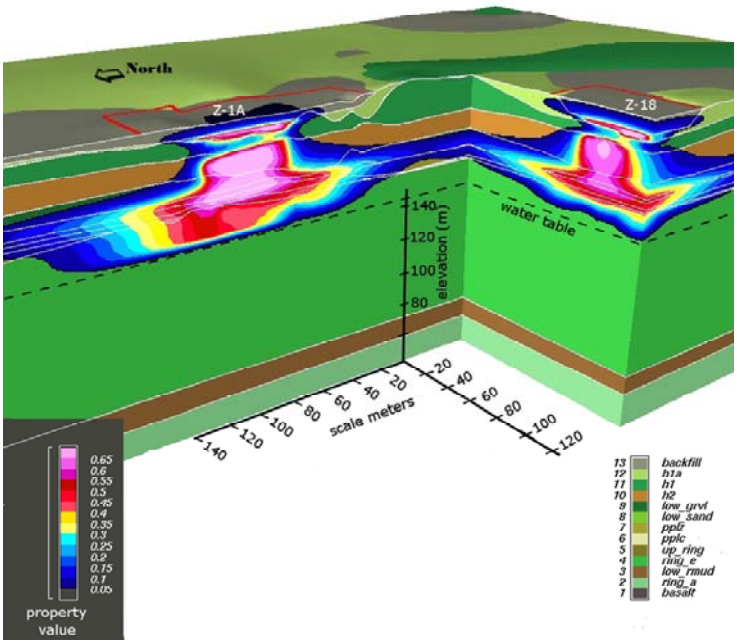

Figure 5.16. CT Gas Concentrations (g/L) at 1993 (Base Case) (0.1 g/L is equivalent to 12,000 ppmv at standard temperature and pressure)

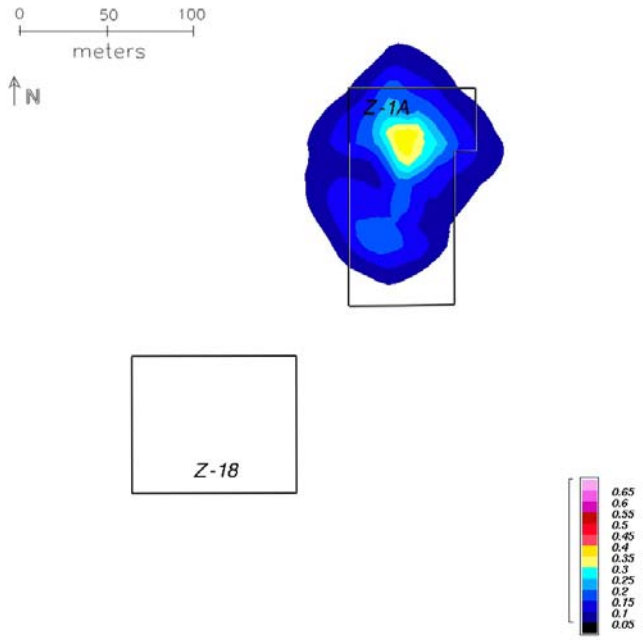

Figure 5.17. Top View of CT Gas Concentrations (g/L) in Cold Creek Unit at 1974 (Base Case) (0.1 g/L is equivalent to 12,000 ppmv at standard temperature and pressure)

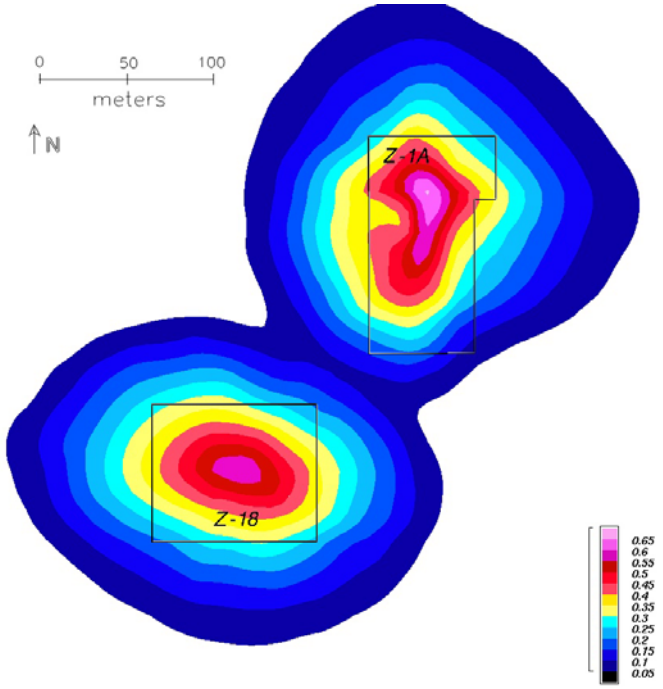

Figure 5.18. Top View of CT Gas Concentrations (g/L) in Cold Creek Unit at 1993 (Base Case) (0.1 g/L is equivalent to 12,000 ppmv at standard temperature and pressure)

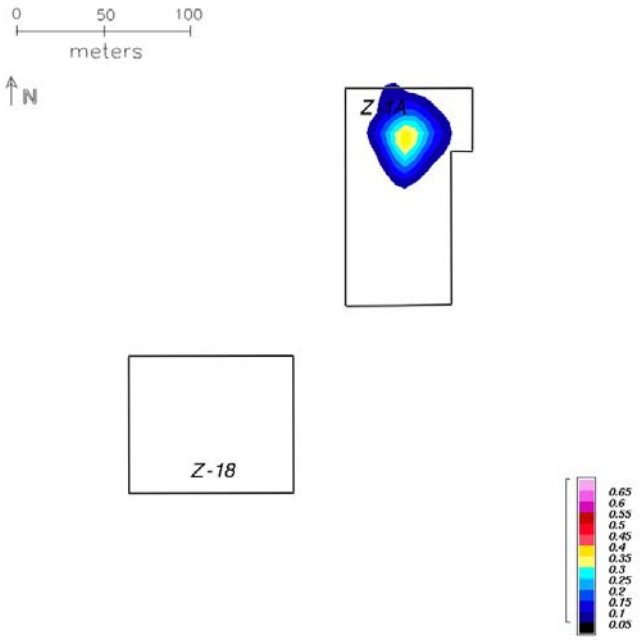

Figure 5.19. Top View of CT Gas Concentrations (g/L) Above Water Table at 1984 (Base Case) (0.1 g/L is equivalent to 12,000 ppmv at standard temperature and pressure)

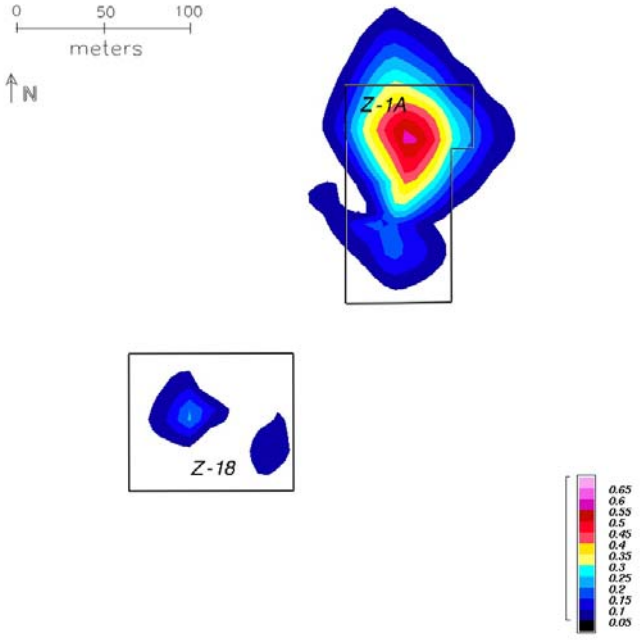

Figure 5.20. Top View of CT Gas Concentrations (g/L) Above Water Table at 1993 (Base Case) (0.1 g/L is equivalent to 12,000 ppmv at standard temperature and pressure)

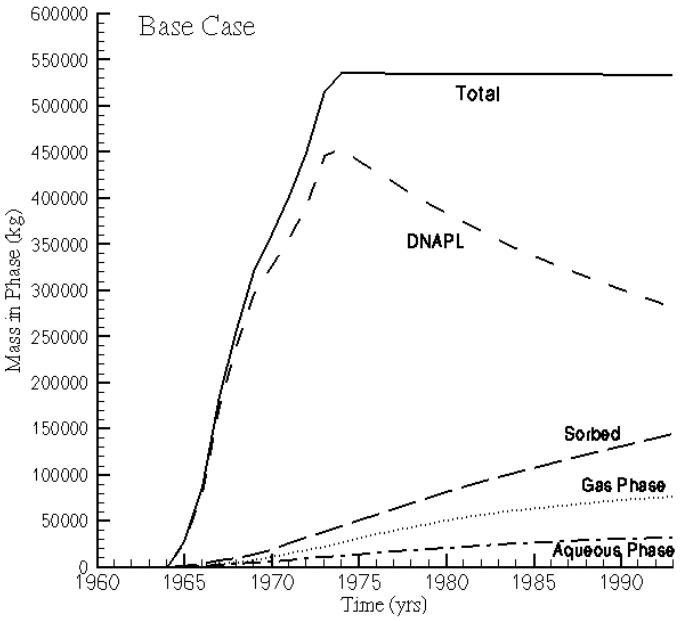

Figure 5.21. CT Mass Distribution Over the DNAPL, Sorbed, Aqueous, and Gas Phases for 1960 – 1993 (Base Case)

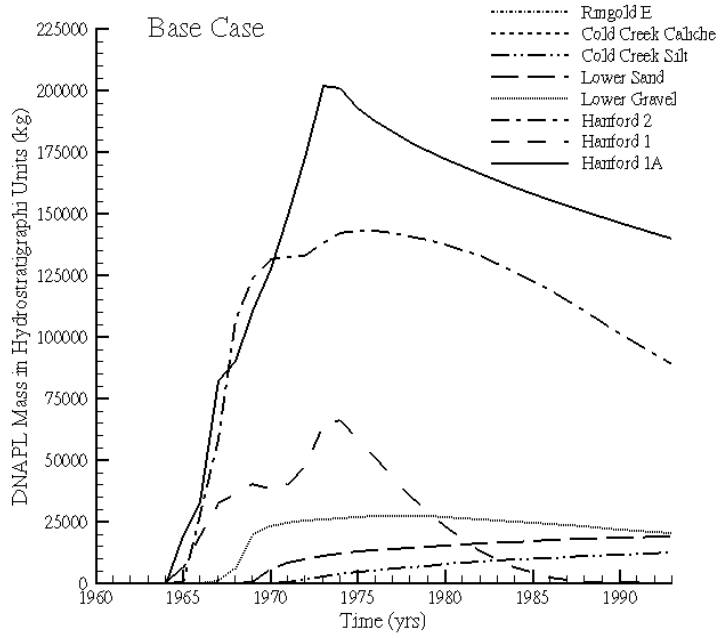

Figure 5.22. DNAPL CT Mass Distribution Over the Hydrostratigraphic Units for 1960 – 1993 (Base Case)

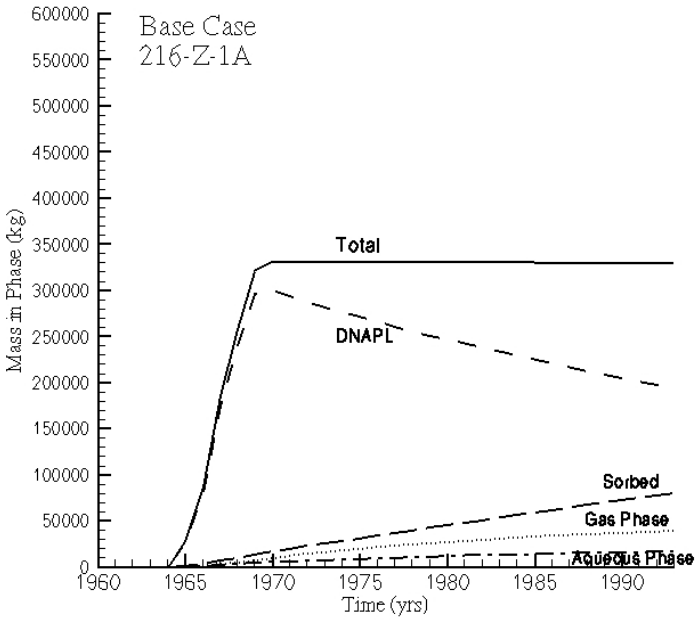

Figure 5.23. CT Mass Distribution Over the DNAPL, Sorbed, Aqueous, and Gas Phases for 1960 – 1993 (Base Case, 216-Z-1A Site)

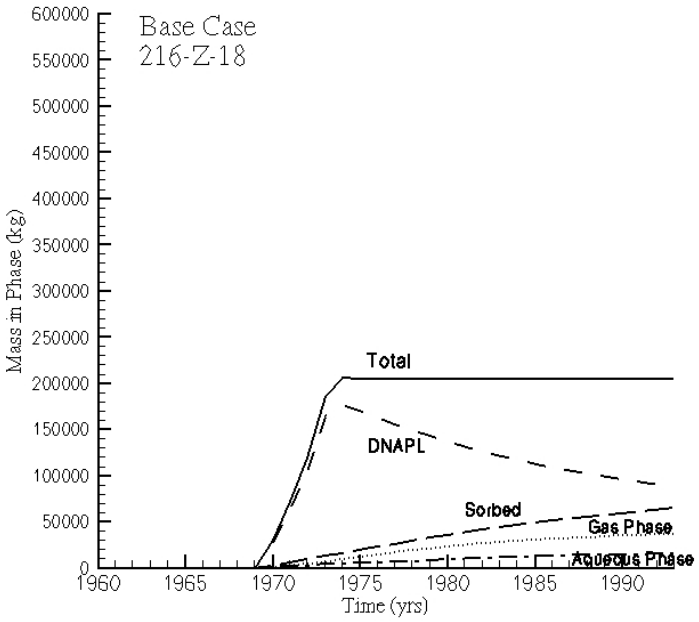

Figure 5.24. CT Mass Distribution Over the DNAPL, Sorbed, Aqueous, and Gas Phases for 1960 – 1993 (Base Case, 216-Z-18 Site)

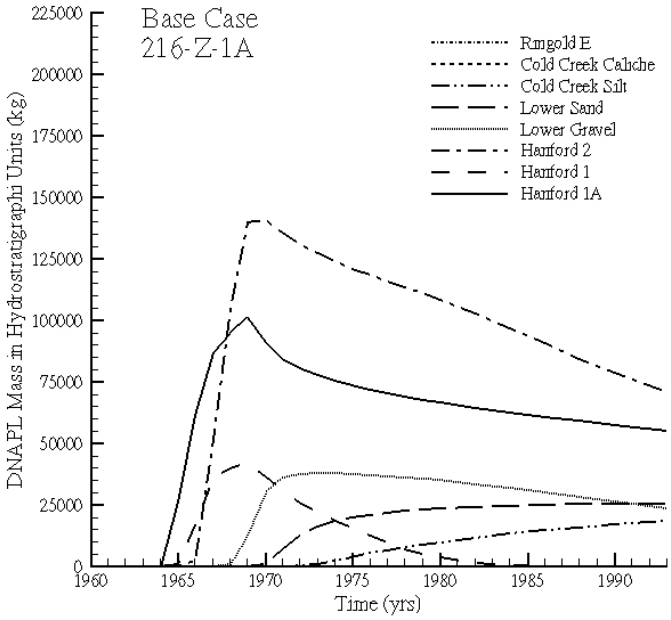

Figure 5.25. DNAPL CT Mass Distribution Over the Hydrostratigraphic Units for 1960 – 1993 (Base Case, 216-Z-1A Site)

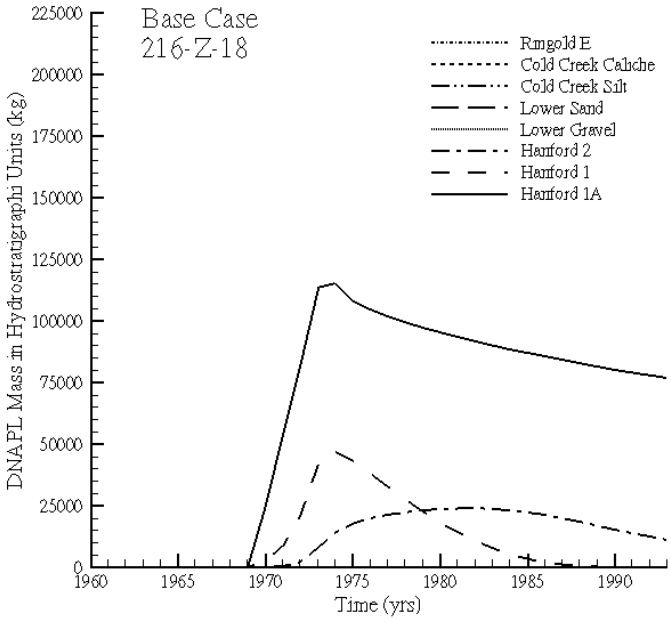

Figure 5.26. DNAPL CT Mass Distribution Over the Hydrostratigraphic Units for 1960 – 1993 (Base Case, 216-Z-18 Site)

5.2 Sensitivity Analysis Results

A total of 33 sensitivity simulations were conducted in six categories, depending on the imposed variation. The categories are 1) Disposal Site Infiltration Area, 2) DNAPL Volume, 3) DNAPL Properties and Porous Media Properties Related to CT, 4) Porous Media Properties of the H1a Unit, 5) Porous Media Properties of the Cold Creek Unit, and 6) Porous Media Properties of all Units. Moment-method statistics of these simulations and a comparison with the base case results are presented in Section 5.3. In this section, the results of the sensitivity simulations are discussed in general terms, with special emphasis on simulations which yielded markedly different results than the base case simulation. Included in the discussion are data on DNAPL vadose zone retention (Table 5.1) and DNAPL movement across the water table (Table 5.2).

Table 5.1. Total DNAPL Mass Inventory and DNAPL Mass in Vadose Zone at 1993, as a Percentage of Total Inventory

Simulation	Total DNAPL Mass Inventory (kg)	DNAPL Mass (kg) in Vadose Zone at 1993	DNAPL Mass (kg) in Vadose Zone at 1993 as a Percentage of Inventory
Base Case	5.37e5	2.81e5	52
I-a	5.37e5	3.16e5	59
I-b	5.37e5	3.29e5	61
I-c	5.37e5	3.31e5	62
II-a	6.71e5	3.83e5	57
II-b	8.06e5	4.89e5	61
II-c	1.74e6	7.10e5	69
III-a	6.00e5	2.97e5	50
III-b	4.47e5	2.99e5	67
III-c	5.37e5	4.21e5	78
III-d	5.37e5	4.81e5	90
III-e	5.37e5	2.86e5	53
III-f	5.37e5	2.89e5	54
III-g	5.37e5	2.85e5	53
III-h	5.37e5	2.83e5	53
III-i	5.37e5	2.76e5	51
III-j	5.37e5	2.92e5	54
III-k	5.37e5	3.02e5	56
IV-a	5.37e5	1.66e5	31
IV-b	5.37e5	2.49e5	46
IV-c	5.37e5	2.67e5	50
IV-d	5.37e5	1.99e5	37
V-a	5.37e5	2.85e5	53
V-b	5.37e5	2.85e5	53
V-c	5.37e5	2.66e5	50
V-d	5.37e5	2.67e5	50

Table 5.1. (contd)

Simulation	Total DNAPL Mass Inventory (kg)	DNAPL Mass (kg) in Vadose Zone at 1993	DNAPL Mass (kg) in Vadose Zone at 1993 as a Percentage of Inventory
VI-a	5.37e5	1.97e5	37
VI-b	5.37e5	4.33e5	81
VI-c	5.37e5	2.91e5	54
VI-d	5.37e5	2.66e5	50
VI-e	5.37e5	2.74e5	51
VI-f	5.37e5	2.83e5	53
VI-g	5.37e5	1.71e4	3
VI-h	5.37e5	4.81e5	90

Table 5.2. Time for DNAPL to Reach the Water Table, CT DNAPL Mass and Dissolved CT Mass Transported Across the Water Table at 1993. CT DNAPL that moved across water table originated from the 216-Z-1A site.

Simulation	Time (yr) for DNAPL to Reach Water Table	CT DNAPL Mass (kg) Moved Across Water Table at 1993	Dissolved CT Mass Moved Across Water Table at 1993
Base Case	-	0	317
I-a	24	14	416
I-b	19	87	418
I-c	14	948	729
II-a	-	0	445
II-b	-	0	539
II-c	13	1,040	622
III-a	-	0	453
III-b	-	0	112
III-c	-	0	0
III-d	-	0	0
III-e	-	0	788
III-f	-	0	1,143
III-g	-	0	5,345
III-h	-	0	1,054
III-i	-	0	40
III-j	-	0	51
III-k	-	0	47
IV-a	-	0	766
IV-b	-	0	513
IV-c	-	0	489
IV-d	-	0	617
V-a	-	0	0
V-b	-	0	0

Table 5.2. (contd)

Simulation	Time (yr) for DNAPL to Reach Water Table	CT DNAPL Mass (kg) Moved Across Water Table at 1993	Dissolved CT Mass Moved Across Water Table at 1993
V-c	-	0	2,237
V-d	-	0	2.254
VI-a	6	45,570	2.076
VI-b	-	0	2,310
VI-c	-	0	0
VI-d	-	0	234
VI-e	-	0	336
VI-f	-	0	543
VI-g	-	0	4,387
VI-h	-	0	0

5.2.1 Disposal Site Area

Three alternative disposal site area simulations were conducted. For case I-a, the infiltration area was 20% of the base case for both fluids while for case I-b, the area was only 10% of the base case. In case I-c, the base case infiltration area was used for the aqueous phase while a 10% area was assumed for the DNAPL. In all three cases, DNAPL was predicted to move across the water table beneath the 216-Z-1A site, although the volume was considerable higher in Case I-c than for the other two cases. As can be seen in Figure 5.27 the DNAPL body under the 216-Z-1A site for case I-c showed less spreading than for the base case (Figure 5.12), while the DNAPL body under the 216-Z-18 site has penetrated much deeper into the H2 unit. As a result, the CT vapor plume for this case is slightly smaller (Figure 5.28) than the base case vapor plume (Figure 5.13). The CT mass distribution curves over the phases of all three disposal area cases have similar shapes as the base case, which is illustrated in Figure 5.29 for case I-c. However, since less DNAPL spreading occurred due to more concentrated releases, more CT remained as a DNAPL in the subsurface (Table 5.1). The CT mass distribution over the hydrostratigrahic units for these cases is different than for the base case (Figure 5.22). The results of case I-c (Figure 5.30) show that, compared to the base case, less CT DNAPL remains in the H1a, but considerably more in the H2 unit and both the CCU silt and CCU caliche. The reduced infiltration area yielded larger DNAPL relative permeabilities and more rapid downward movement.

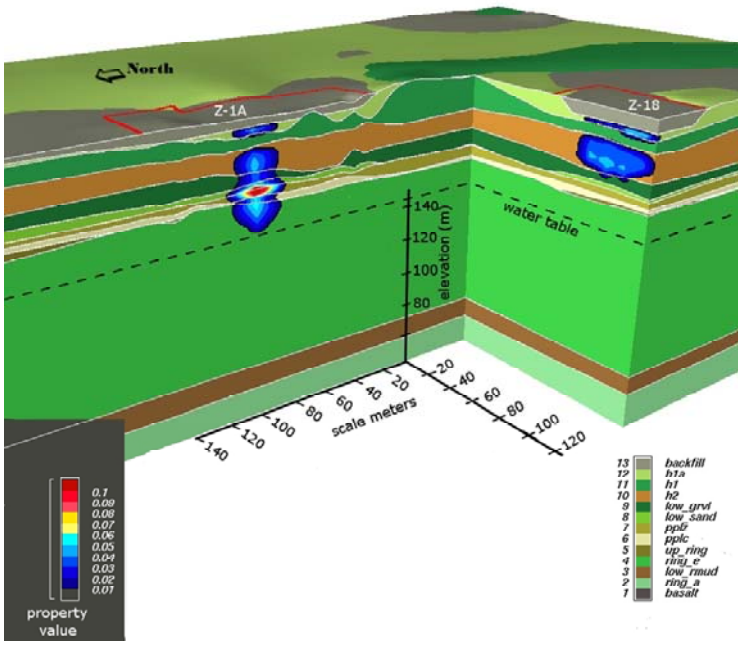

Figure 5.27. DNAPL Saturation at 1993 for Sensitivity Case I-c

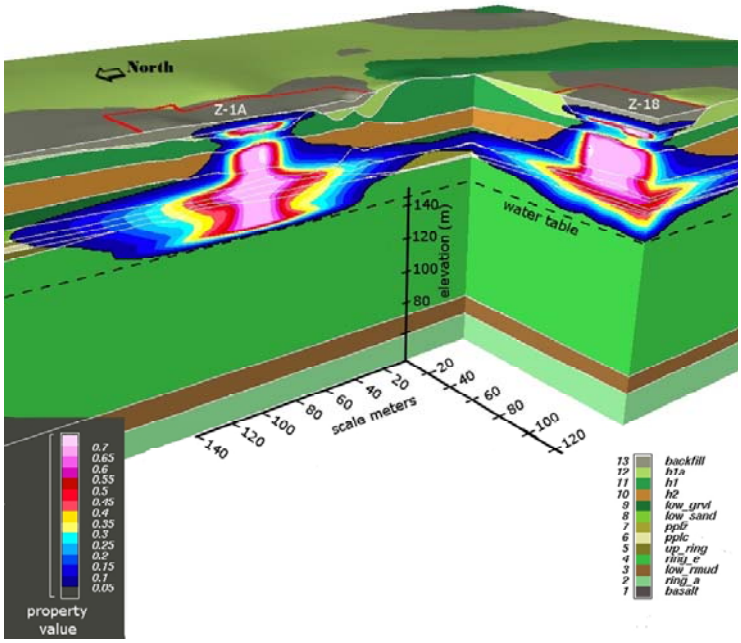

Figure 5.28. CT Gas Concentrations (in g/L) at 1993 for Sensitivity Case I-c (0.1 g/L is equivalent to 12,000 ppmv at standard temperature and pressure)

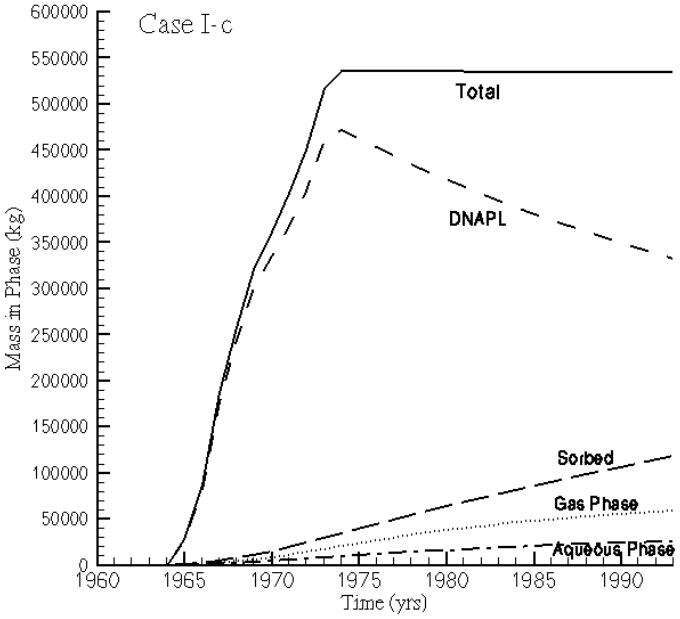

Figure 5.29. CT Mass Distribution Over the DNAPL, Sorbed, Aqueous, and Gas Phases for 1960 – 1993 (Case I-c)

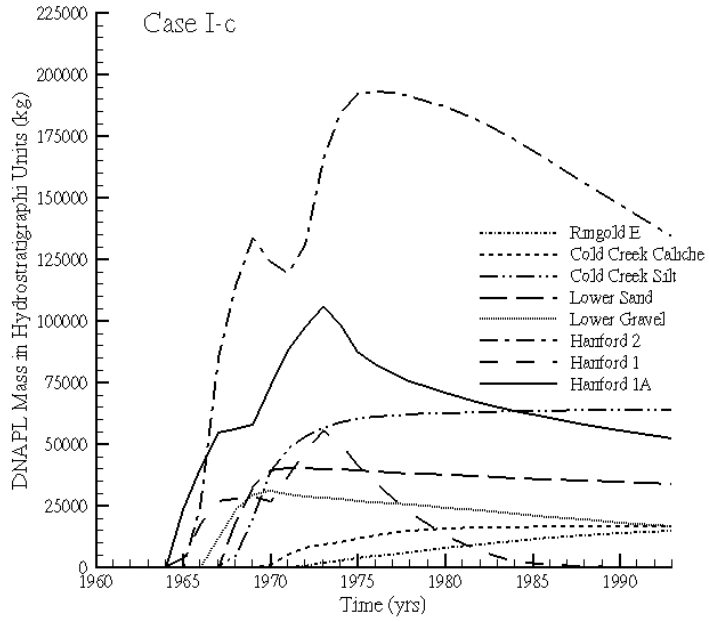

Figure 5.30. DNAPL CT Mass Distribution Over the Hydrostratigraphic Units for 1960 – 1993 (Case I-c)

5.2.2 DNAPL Volume

The implications of varying DNAPL volumes was investigated through three simulations with 1.25 (case II-a), 1.5 (case II-b), and 2 (case II-c) times the base case volume. Although the CT DNAPL mass retained in the vadose zone increased as a percentage of the inventory with volume size (Table 5.1), only case II-c shows CT DNAPL movement across the water table (Table 5.2). DNAPL phase saturations and CT gas phase concentrations for case II-c are shown in Figure 5.31 and 5.32, respectively. Compared to Figure 5.12 for the base case, Figure 5.31 shows DNAPL penetration into the CCU and the Ringold E unit by 1993. The resulting CT gas phase plume from case II-c is not considerably larger than the base case (Figure 5.16), although the plume contains larger areas with relatively higher CT concentrations.

The CT mass distributions over the phases (Figure 5.33) indicated the larger amount of disposed DNAPL compared to the base case (Figure 5.21). As a percentage of the inventory, less sorbed CT and CT in the aqueous and gas phases but more DNAPL are in the domain by 1993 compared to the base case. The CT DNAPL distribution over the hydrostratigraphic units (Figure 5.34) shows a considerable presence in the CCU and Ringold E unit, as is also obvious from Figure 5.31. In fact, the distribution shown in Figure 5.34 is closer to the situation depicted by Figure 5.30 for case I-c.

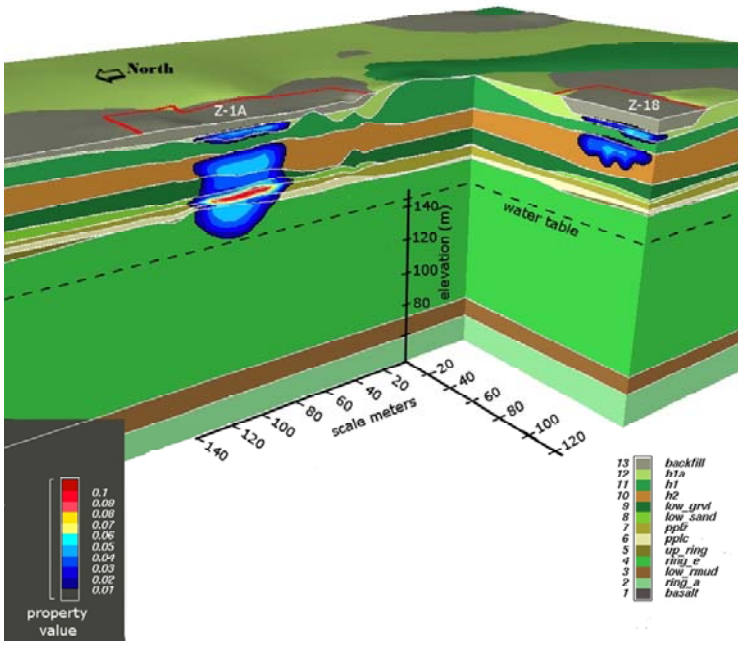

Figure 5.31. DNAPL Saturation at 1993 for Sensitivity Case II-c

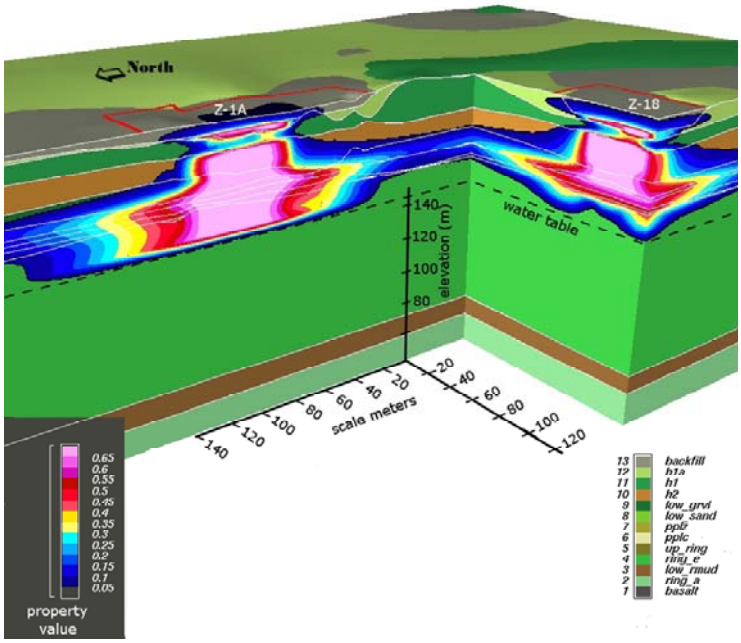

Figure 5.32. CT Gas Concentrations (in g/L) at 1993 for Sensitivity Case II-c (0.1 g/L is equivalent to 12,000 ppmv at standard temperature and pressure)

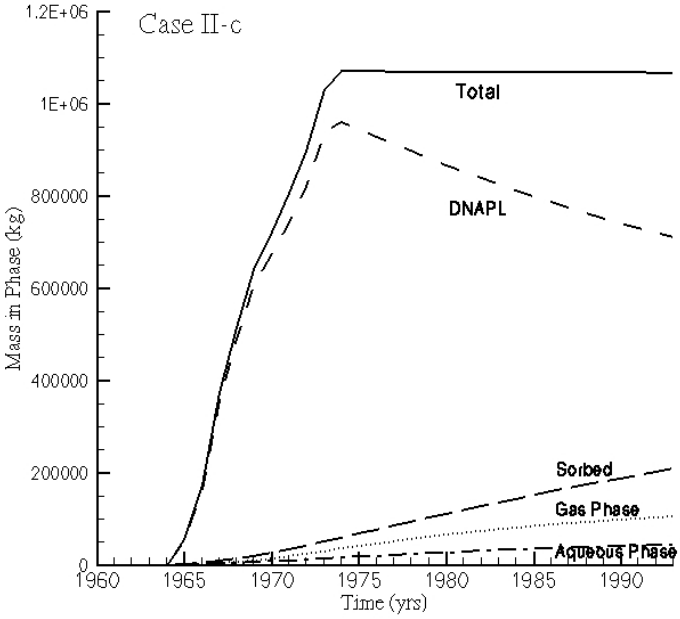

Figure 5.33. CT Mass Distribution Over the DNAPL, Sorbed, Aqueous, and Gas Phases for 1960 – 1993 (Case II-c)

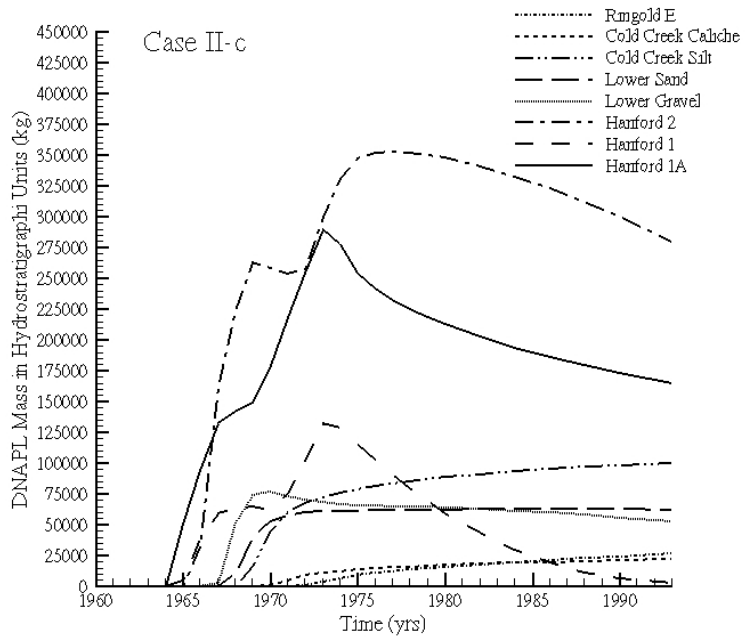

Figure 5.34. DNAPL CT Mass Distribution Over the Hydrostratigraphic Units for 1960 – 1993 (Case II-c)

5.2.3 DNAPL Properties and Porous Media Properties Related to CT

Multiple simulations were conducted to study the impact of DNAPL properties (density, viscosity, vapor pressure, and aqueous solubility), sorption, and residual DNAPL saturation on subsurface flow and transport below the two disposal sites. The simulations in this section are:

a. Fluid properties of disposed DNAPL equal to properties of pure CT.

b. Properties of DNAPL reflecting DNAPL composition of 50% CT, 10% lard oil, 20% DBBP, and 20% TBP.

c. A DNAPL vapor pressure of 5,415 Pa.

d. A DNAPL vapor pressure of 2,708 Pa.

e. A CT solubility of 360 mg/L.

f. A CT solubility of 180 mg/L.

g. A K_d partitioning coefficient of 0.0 mL/g.

h. A K_d partitioning coefficient of 0.1 mL/g.

i. A K_d partitioning coefficient of 0.4 mL/g.

j. Laboratory measured maximum residual DNAPL saturation for CCU silt (0.13), Hanford Sand (0.10), Lower Gravel (0.05), and Ringold E material (0.11). For the other materials, a maximum residual of 0.1 was assumed.

k. Measured and assumed maximum residual DNAPL saturation times 1.25.

The data in Table 5.1 show that except for cases III-b, III-d, and III-d, the CT DNAPL remaining in the vadose zone at 1993 is comparable with the base case. The reason these three cases report higher values of the remaining CT DNAPL is directly related to the lower vapor pressure in these cases. None of the cases in this category showed movement of CT in the DNAPL phase across the water table (Table 5.2).

The simulation results for cases III-a, III-b, III-j, and III-k show that DNAPL movement for these cases do not significantly differ from the base case. Although the DNAPL composition changes the CT phase distribution and CT DNAPL distribution over the hydrostratigraphic units somewhat, the changes are relatively minor. The simulations including a residual DNAPL saturation also produce results that are fairly close to the base case results as the maximum DNAPL saturations during the infiltration and redistribution stages are relatively small so that the residual mass in the units is typically less than a few percent.

The effect of a lower vapor pressure was investigated in case III-c and III-d. The DNAPL saturations and CT gas phase plume at 1993 are shown in Figure 3.35 and 3.36 for case III-d. Figure 3.35 depicts a larger DNAPL body than for the base case (Figure 5.12). In contrast, the CT gas phase plume for case

III-d is smaller than the CT gas phase plume for the base case and the concentrations are lower (Figure 5.16). Figure 5.37 shows a strong reduction in the CT gas phase mass and an increase in the CT DNAPL phase mass. Because less DNAPL volatilizes, more CT moves downwards and laterally as a DNAPL. As a result, the DNAPL body at 1993 is rather extensive with similar penetration into the CCU silt as the base case.

The simulations with lower solubility (cases III-e and III-f) result in relative minor differences in DNAPL body positioning in 1993 (Figure 5.39) but a more limited aqueous phase CT plume (Figure 5.40). The phase distributions (Figure 5.41) show a decrease in the CT mass in the aqueous phase and in the sorbed mass. The latter is explained by realizing that the sorbed mass is directly related to the aqueous phase concentration (see Equations 5.1 and 5.2). CT DNAPL phase mass distributions over the hydrostratic units (Figure 5.42) do not show major differences with the base base.

The effects of sorption were evaluated with case III-g, -h, and –I (see Figures 5.43 through 5.48). The simulation with zero sorption (case III-g) caused a large increase in the CT gas phase plume (Figure 5.44) but not in the DNAPL configuration (Figures 5.43 and 5.46). As a result, the CT phase distribution (Figure 5.45) shows relatively more CT partitioning into the gas and aqueous phases. For simulation III-i, with a portioning coefficient twice as large as for the base case, the sorbed mass at 1993 is approximately 175,000 kg (Figure 5.47), while the CT DNAPL distribution is not significantly affected (Figure 5.48).

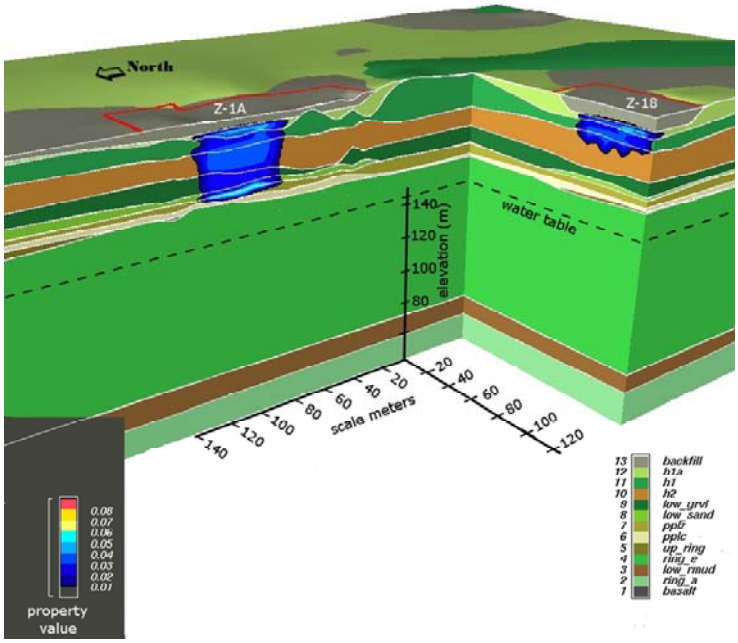

Figure 5.35. DNAPL Saturations at 1993 for Sensitivity Case III-d

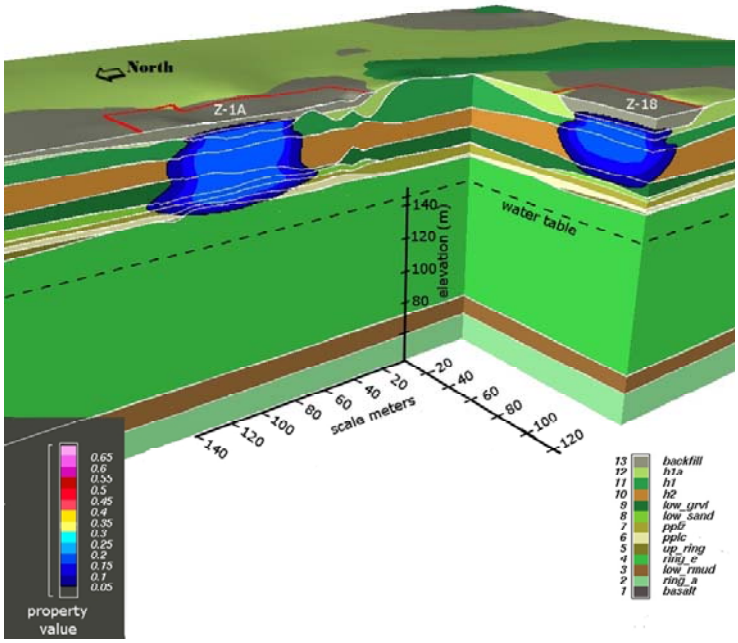

Figure 5.36. CT Gas Concentrations (in g/L) at 1993 for Sensitivity Case III-d (0.1 g/L is equivalent to 12,000 ppmv at standard temperature and pressure)

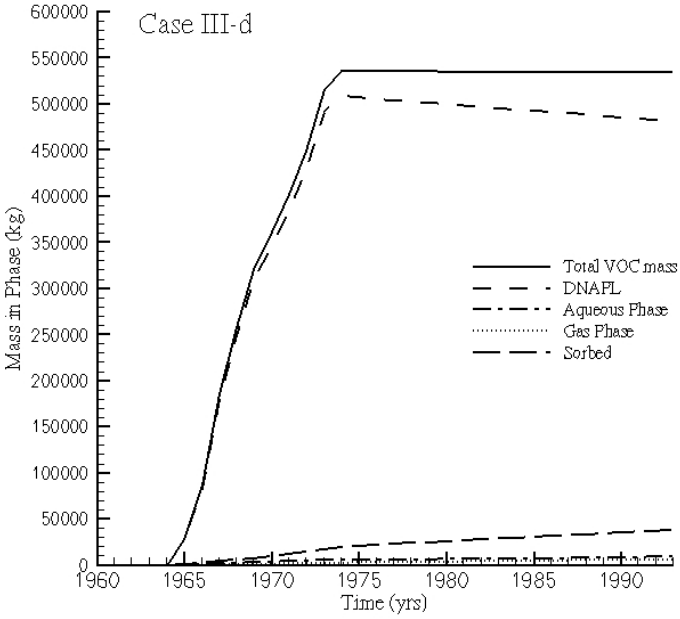

Figure 5.37. CT Mass Distribution Over the DNAPL, Sorbed, Aqueous, and Gas Phases for 1960 – 1993 (Case III-d)

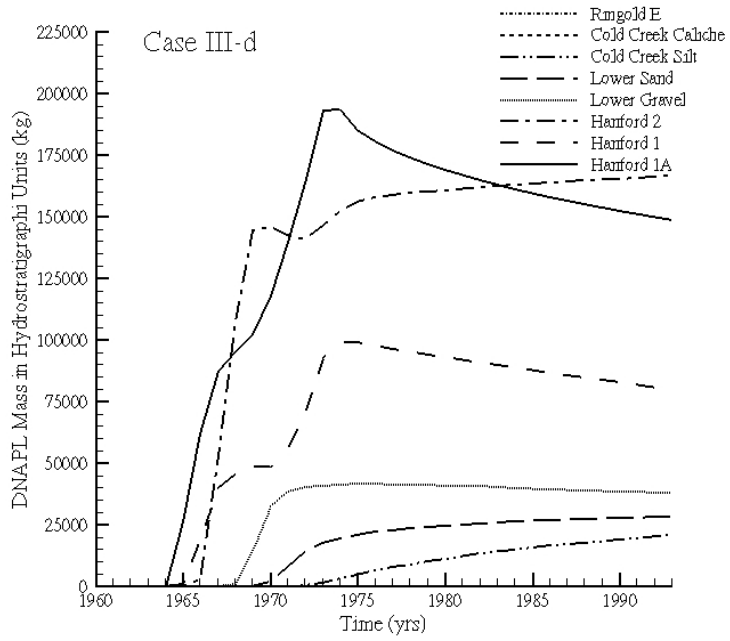

Figure 5.38. DNAPL CT Mass Distribution Over the Hydrostratigraphic Units for 1960 – 1993 (Case III-d)

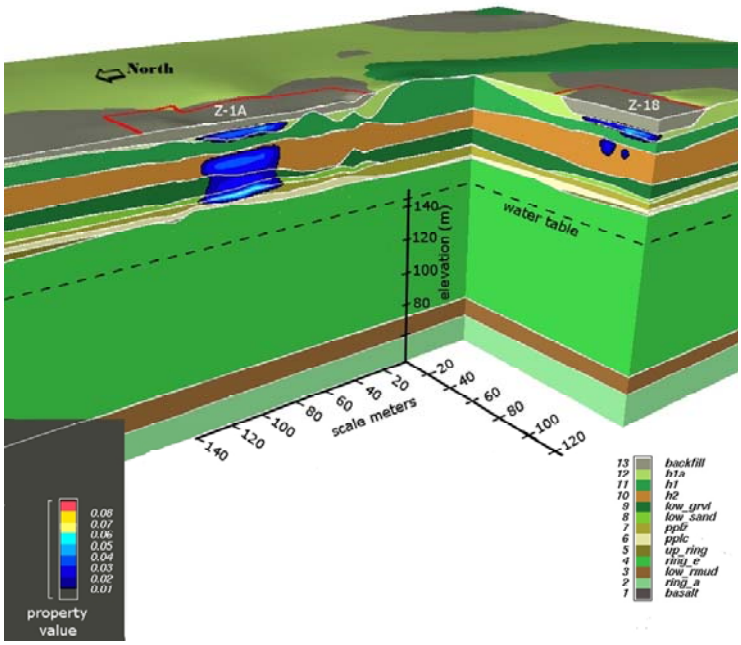

Figure 5.39. DNAPL Saturations at 1993 for Sensitivity Case III-f

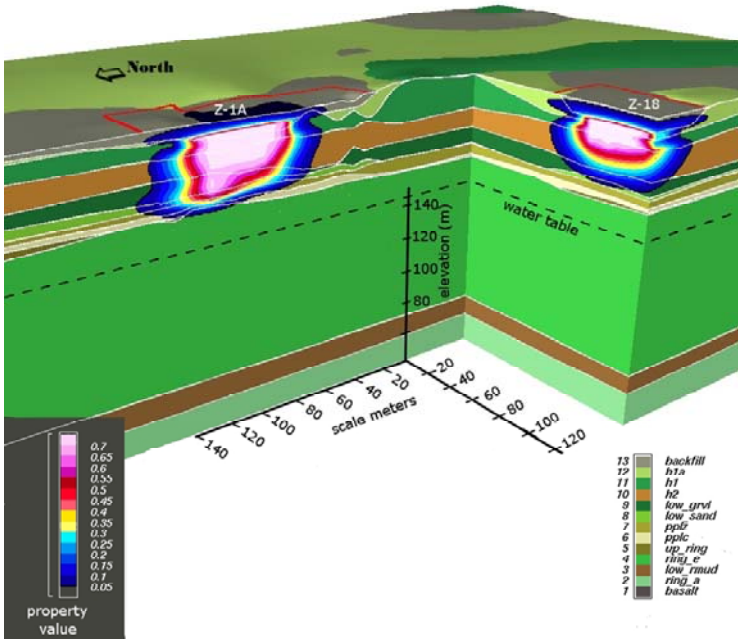

Figure 5.40. CT Aqueous Concentrations (in g/L) at 1993 for Sensitivity Case III-f

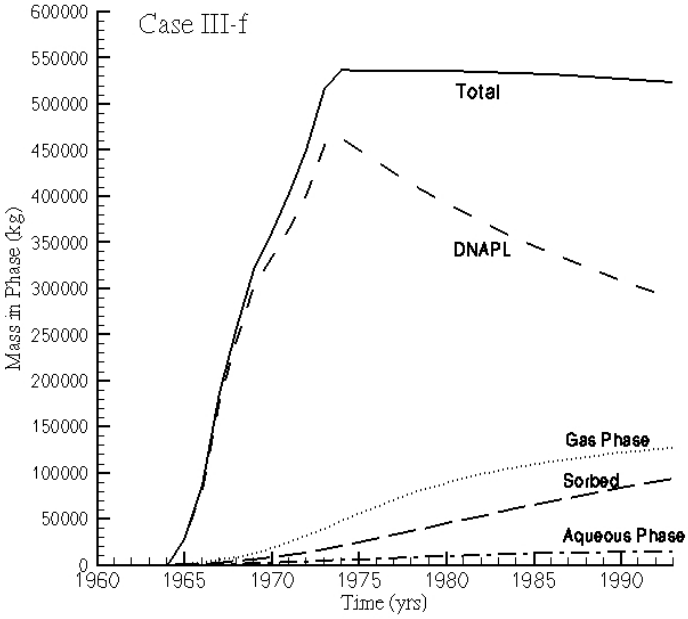

Figure 5.41. CT Mass Distribution Over the DNAPL, Sorbed, Aqueous, and Gas Phases for 1960 – 1993 (Case III-f)

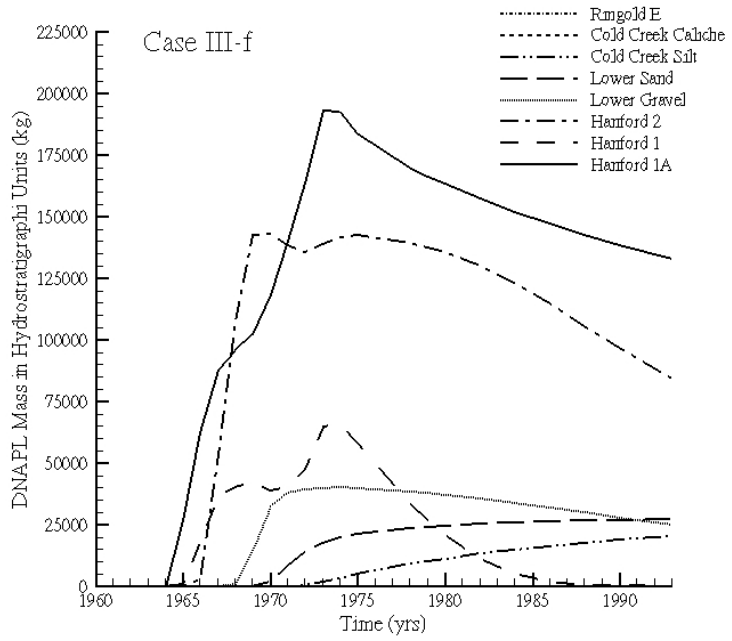

Figure 5.42. DNAPL CT Mass Distribution Over the Hydrostratigraphic Units for 1960 – 1993 (Case III-f)

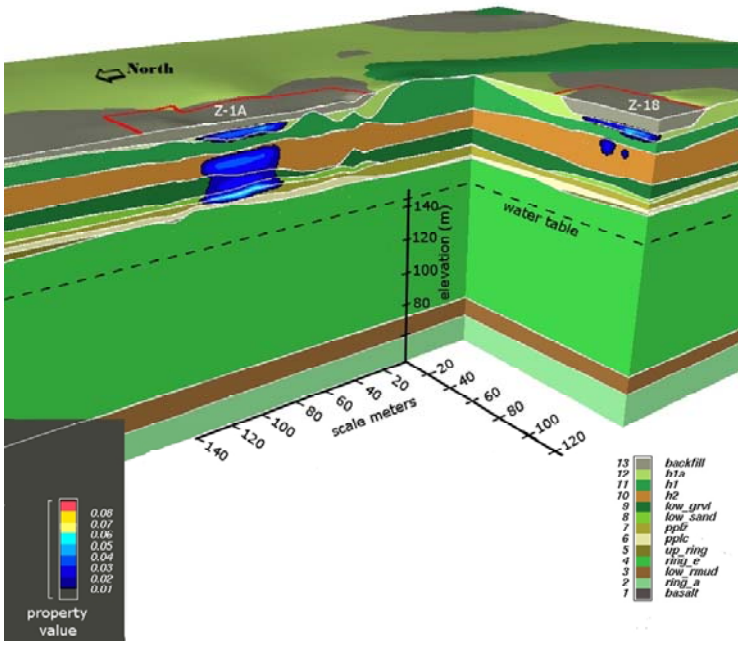

Figure 5.43. DNAPL Saturations at 1993 for Sensitivity Case III-g

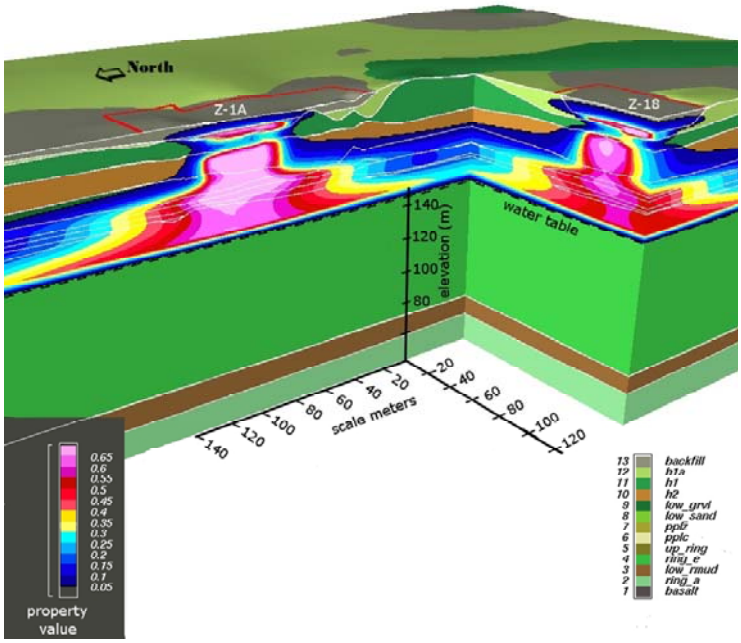

Figure 5.44. CT Gas Concentrations (in g/L) at 1993 for Sensitivity Case III-g (0.1 g/L is equivalent to 12,000 ppmv at standard temperature and pressure)

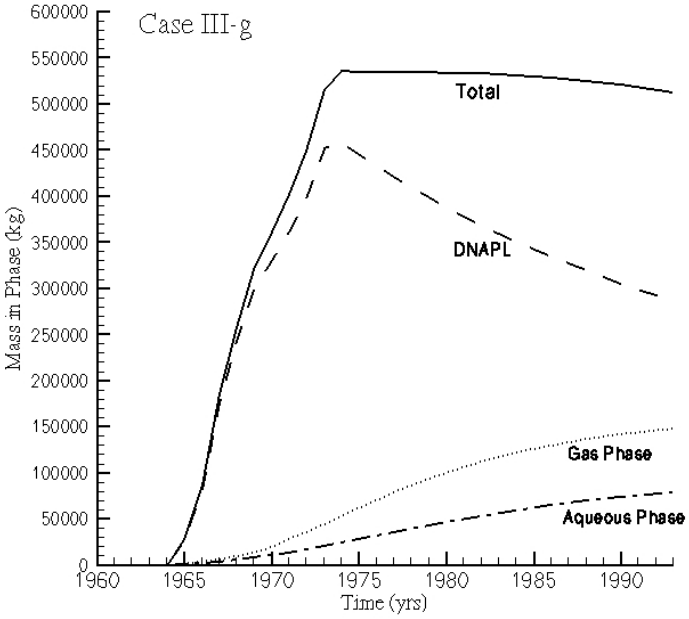

Figure 5.45. CT Mass Distribution Over the DNAPL, Sorbed, Aqueous, and Gas Phases for 1960 – 1993 (Case III-g)

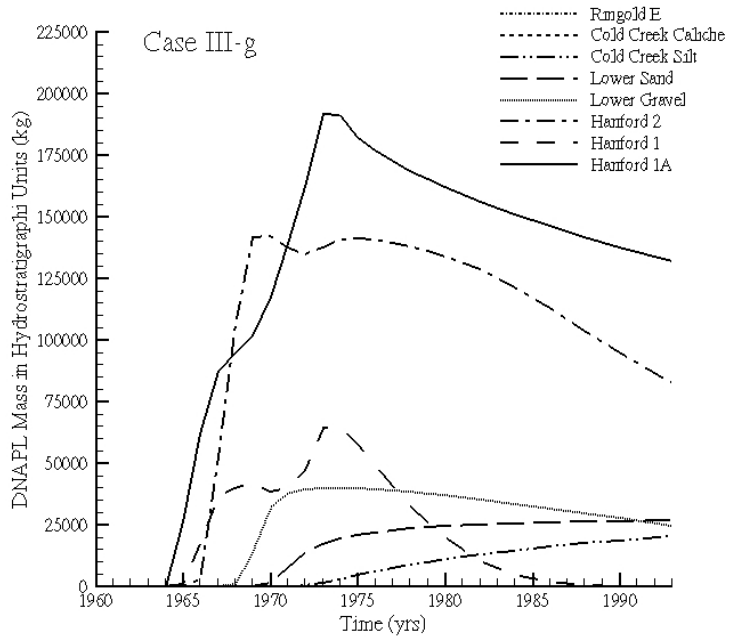

Figure 5.46. DNAPL CT Mass Distribution Over the Hydrostratigraphic Units for 1960 – 1993 (Case III-g)

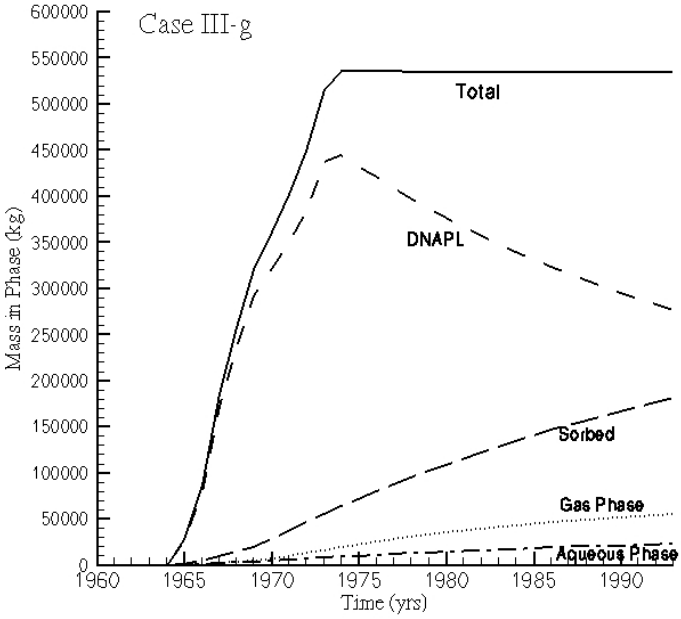

Figure 5.47. CT Mass Distribution Over the DNAPL, Sorbed, Aqueous, and Gas Phases for 1960 – 1993 (Case III-i)

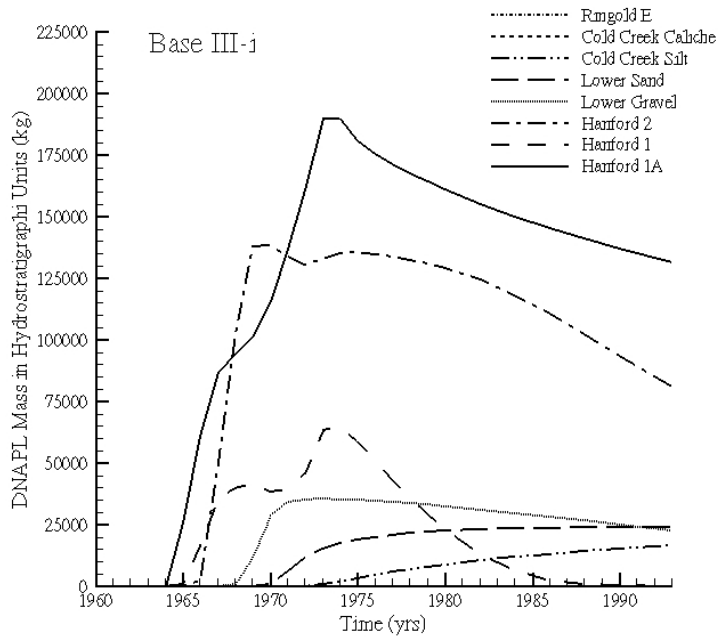

Figure 5.48. DNAPL CT Mass Distribution Over the Hydrostratigraphic Units for 1960 – 1993 (Case III-i)

5.2.4 Porous Medium Properties of H1a Unit

The base case simulation indicated the importance of the H1a unit on DNAPL flow and transport. The H1a unit, located directly below the two disposal sites, has been assigned the properties of Hanford Fine Sand (see Table 3.1 in Oostrom et al. 2004) and has a considerably lower permeability than the underlying H1 sediments, but a larger porosity and entry pressure (Table 4.4 and 4.5). Note that the H1a was not observed below the 216-Z-9 site for the simulations described in Oostrom et al. 2004; 2006. Because there is considerable uncertainty about the properties of the H1a in this model, hydraulic properties of the H1a unit are varied in the four simulations in this category. In case IV-a, IV-b, and IV-c, the permeability, porosity, and air-entry pressure of the underlying H1 unit was assigned to the H1a unit, respectively. For case IV-d, all hydraulic properties of the H1a are equal to those of the H1 unit.

The simulations in this category all show a reduced amount of CT DNAPL in the vadose zone compared to the base case at 1993 (Table 5.1). No DNAPL was transported to the water table, although the dissolved CT mass transported into the saturated zone were larger than for the base case (Table 5.2). Of the three parameters varied in the simulations, the increase in permeability had the largest effect on CT DNAPL flow and CT transport in the gas phase. The decrease in air-entry pressure head for case IV-c only resulted in relatively small changes. The latter result is not unexpected because the domain above the water table remained at a total-liquid saturation less than 0.6 through the DNAPL infiltration and redistribution process. The results for case IV-d are shown in Figures 5.49 through 5.52. The plot with DNAPL saturations (Figure 5.49) show that most of the DNAPL has drained from the H1a underneath both disposal sites, which is in contrast with the findings for the base case (Figure 5.12). The CT gas phase plume of this sensitivity case (Figure 5.50) reaches a similar extension as the base case (Figure 5.16) although no vapors are present in the H1a unit. Differences between this case and the base case are minor in terms of CT phase distributions over time (Figure 5.51). However, the main differences between case IV-d and the base case become obvious in Figure 5.52 where the H2 layer is the unit containing the majority of the DNAPL throughout the infiltration and redistribution periods until 1993. In this case, some DNAPL actually shows up in the CCU caliche.

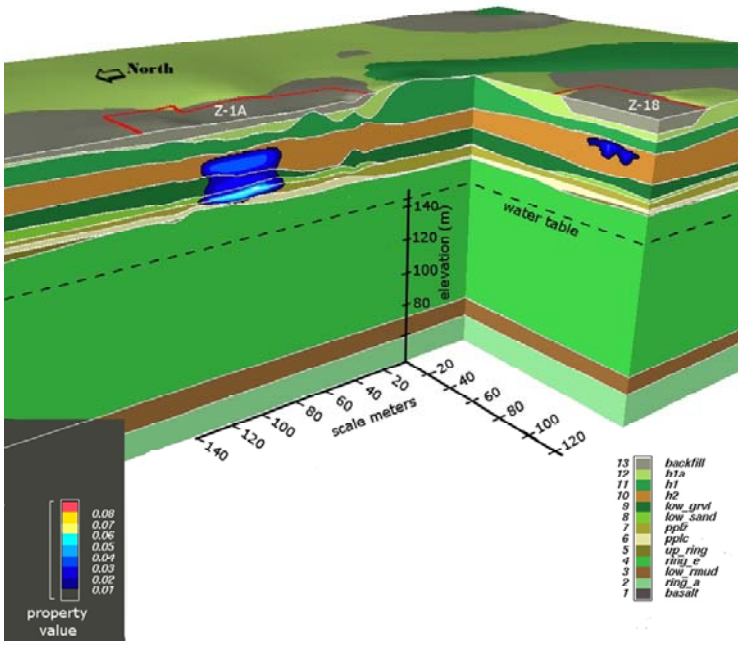

Figure 5.49. DNAPL Saturation at 1993 for Sensitivity Case IV-d

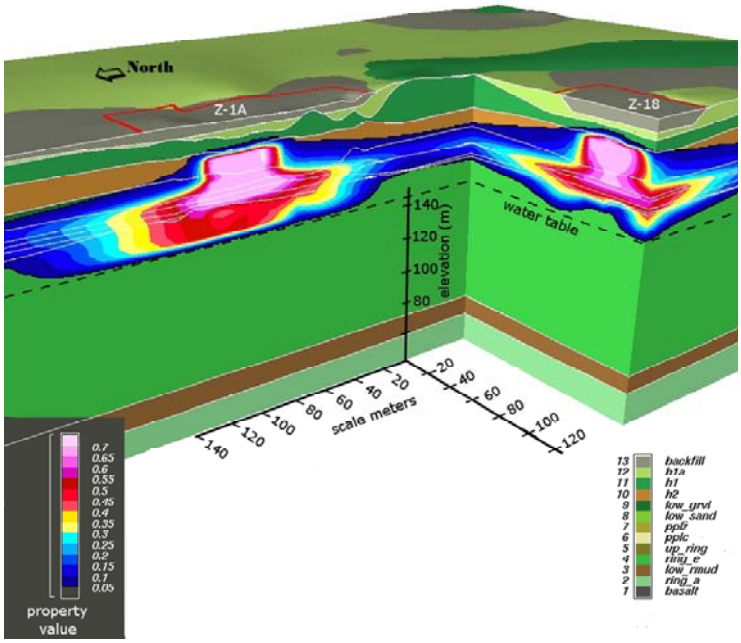

Figure 5.50. CT Gas Concentrations (in g/L) at 1993 for Sensitivity Case IV-d (0.1 g/L is equivalent to 12,000 ppmv at standard temperature and pressure)

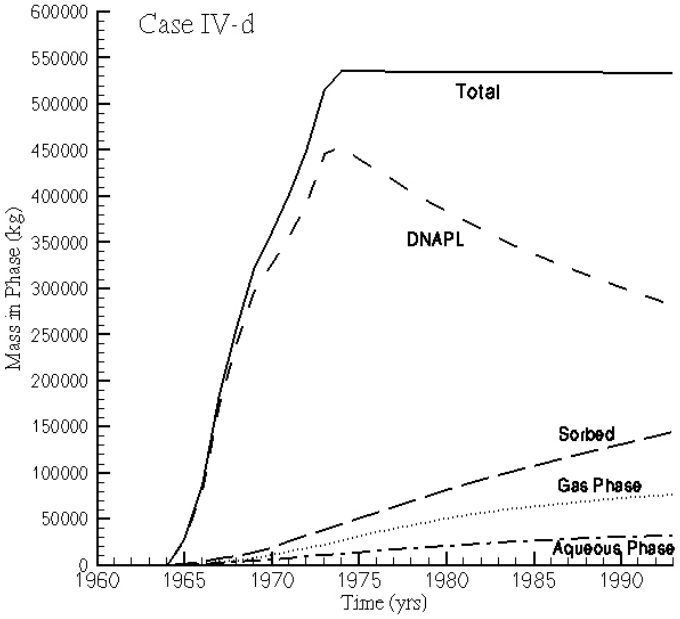

Figure 5.51. CT Mass Distribution Over the DNAPL, Sorbed, Aqueous, and Gas Phases for 1960 – 1993 (Case IV-d)

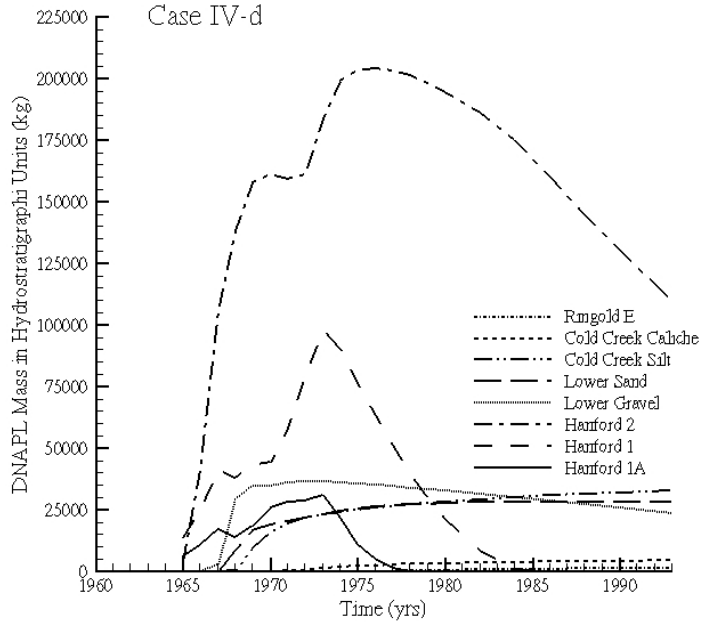

Figure 5.52. DNAPL CT Mass Distribution Over the Hydrostratigraphic Units for 1960 – 1993 (Case IV-d)

5.2.5 Porous Medium Properties of Cold Creek Unit

The permeability and air-entry pressure of the CCU were determined to be important for DNAPL movement into the subsurface of the 216-Z-9 disposal site (Oostrom et al. 2004; 2006). Four simulations were conducted in this category of which two used a lower permeability (case V-a and V-b) and two a higher permeability (case V-c and V-d). In addition, for case V-b and V-d, the permeability was increased and decreased by $\sqrt{10}$ to be consisted with the Miller and Miller (1956) scaling theory. The simulations for the category only show minor differences with the base case. As an example, the plots shown in Figures 5.53 through 5.56 are quite similar to the equivalent figures for the base case. The main differences are observed for aqueous phase transport and the associated dissolved CT transport across the water table. In case V-a and –b, no dissolved CT is transport into the saturated zone due to a lower permeability of the CCU. For cases V-c and V-d, the dissolved phase CT mass transported across the water table in the aqueous phase is approximately six times the mass transported in the base case.

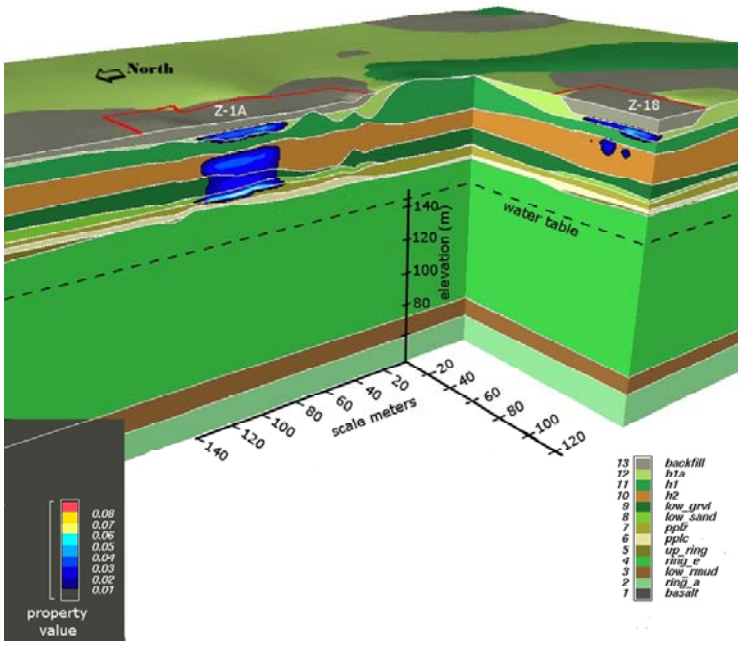

Figure 5.53. DNAPL Saturations at 1993 for Sensitivity Case V-b

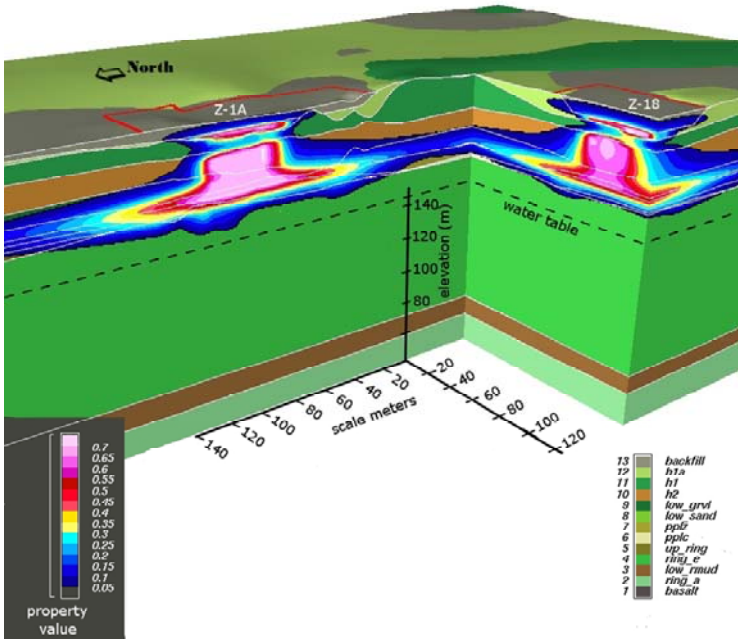

Figure 5.54. CT Gas Concentrations (in g/L) at 1993 for Sensitivity Case V-b (0.1 g/L is equivalent to 12,000 ppmv at standard temperature and pressure)

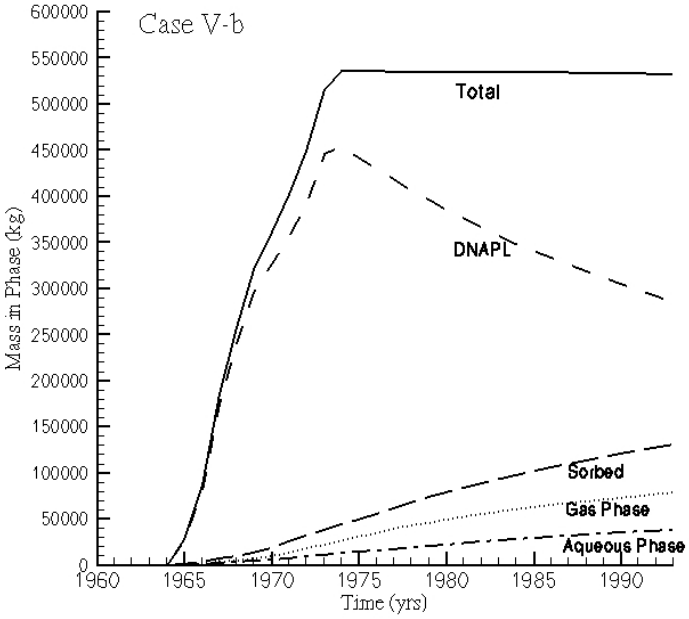

Figure 5.55. CT Mass Distribution Over the DNAPL, Sorbed, Aqueous, and Gas Phases for 1960 – 1993 (Case V-b)

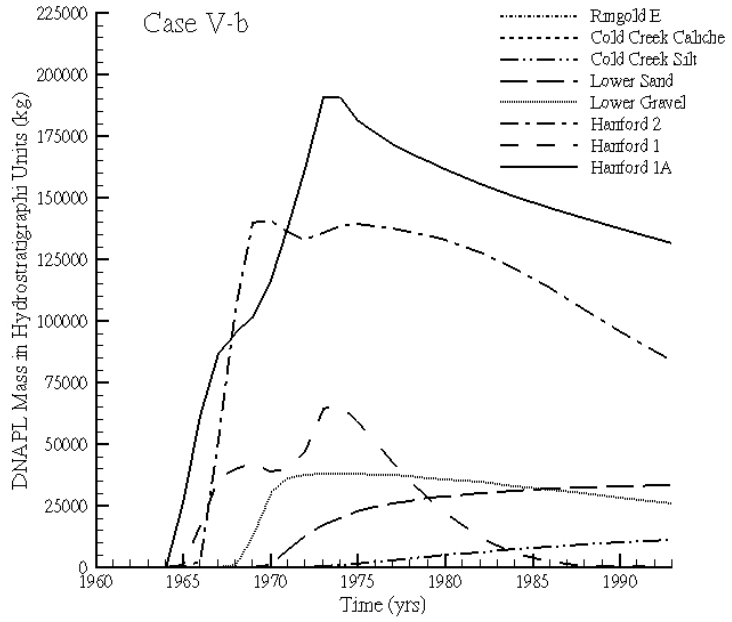

Figure 5.56. DNAPL CT Mass Distribution Over the Hydrostratigraphic Units for 1960 – 1993 (Case V-b)

5.2.6 Porous Medium Properties of all Units

A total of eight simulations were used to vary hydraulic properties of all units. The parameter value changes for the simulations compared to the based case are:

a. Anisotropy ratio of 1:1
b. Anisotropy ratio of 20:1
c. 1.25 x base case porosity
d. 0.75 x base case porosity
e. 2 x base case air-entry pressure head
f. 0.5 x base case air-entry pressure head
g. 10 x base case permeability
h. 0.1 x base case permeability

The results of case VI-a (Figures 5.57 through 5.61) are unique as it is the only simulation that predicts DNAPL disposed at the 216-Z-1A to move down all the way to the Lower Mud unit (Figure 5.57). The isotropic conditions cause more than 45,000 kg DNAPL to move across the water table by 1993 (Table 5.2). The associated gas concentration plume is shown in Figure 5.58 while aqueous phase concentrations are depicted in Figure 5.59. The latter figure shows a dissolved CT plume ranging from the water table to the top of the lower mud. The mass distribution over the phases shows that over time, the sorbed mass becomes larger than the CT DNAPL mass. The CT distribution over the hydrostratigraphic units shown in Figure 5.61 reflects the findings shown in Figure 5.57. By 1993, the CT mass in the Ringold E is more than in the H1a unit.

All other cases in this category provide expected results (Table 5.1 and 5.2), with relative minor deviations from the base case except for case VI-g and VI-h where the permeability was increased and decreased with a factor 10, respectively. Figure 5.62 shows that for case VI-g, virtually no DNAPL phase CT was left in the subsurface by 1993. This result is supported by the estimated 3% of the inventory left in the domain according to Table 5.1 and the phase distribution plot shown in Figure 5.64. The associated gas plume (Figure 5.63) is therefore also smaller than for the base case. The CT DNAPL hydrostratigraphic distribution (Figure 5.65) shows that DNAPL only appeared in the upper part of the domain, with the vast majority in the H1a. Overall, the increase in permeability by a factor 10 in all directions caused rapid lateral DNAPL spreading and gas transport. The overall reduction in permeability imposed in case VI-h resulted in a more compact DNAPL body (Figure 5.66) and CT gas plume (Figure 5.67). The reduction caused CT to primarily remain as a DNAPL (Figure 5.68) in the upper parts of the domain (Figure 5.69).

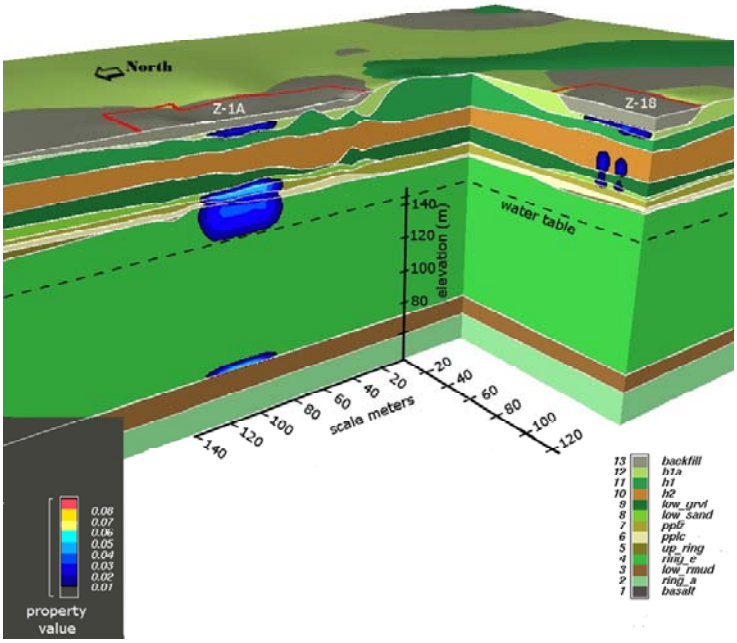

Figure 5.57. DNAPL Saturation at 1993 for Sensitivity Case VI-a

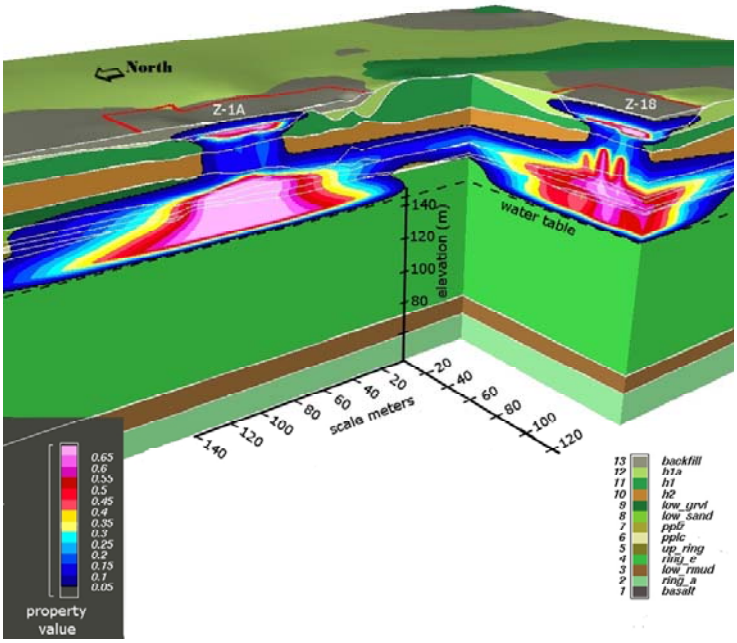

Figure 5.58. CT Gas Concentrations (in g/L) at 1993 for Sensitivity Case VI-a (0.1 g/L is equivalent to 12,000 ppmv at standard temperature and pressure)

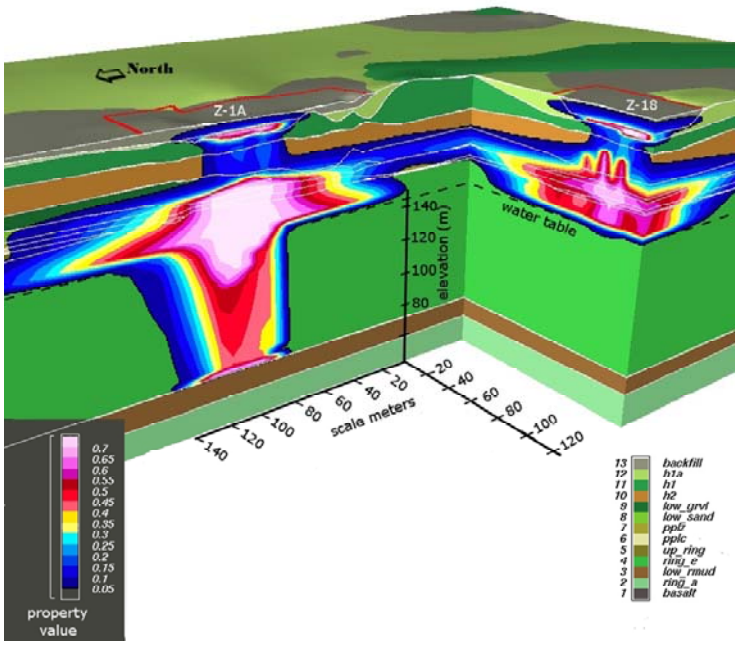

Figure 5.59. CT Aqueous Concentrations (in g/L) at 1993 for Sensitivity Case VI-a

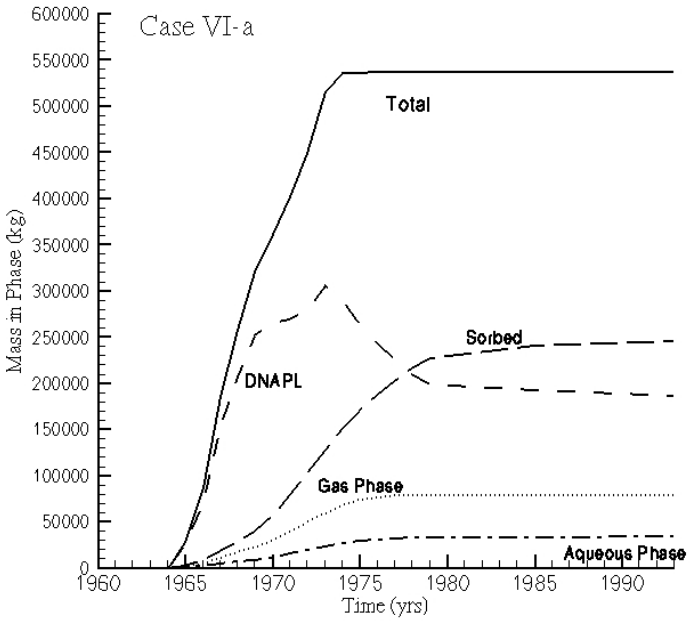

Figure 5.60. CT Mass Distribution Over the DNAPL, Sorbed, Aqueous, and Gas Phases for 1960 – 1993 (Case VI-a)

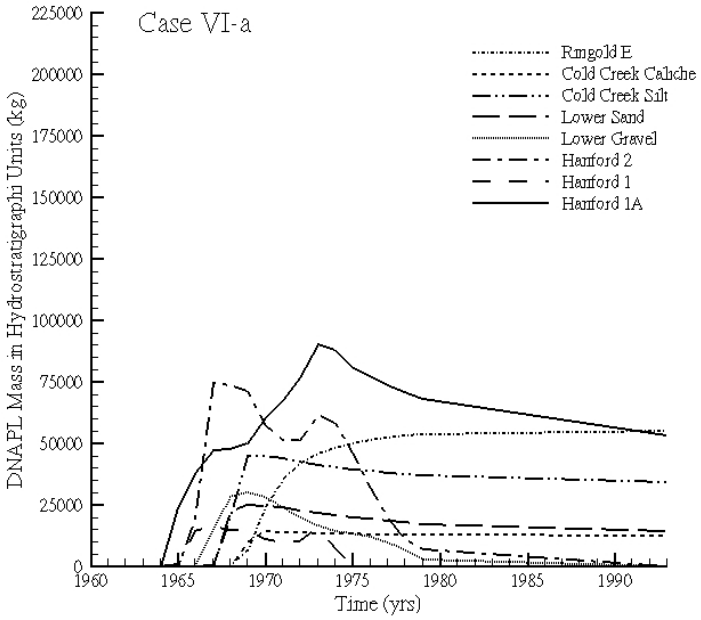

Figure 5.61. DNAPL CT Mass Distribution Over the Hydrostratigraphic Units for 1960 – 1993 (Case VI-a)

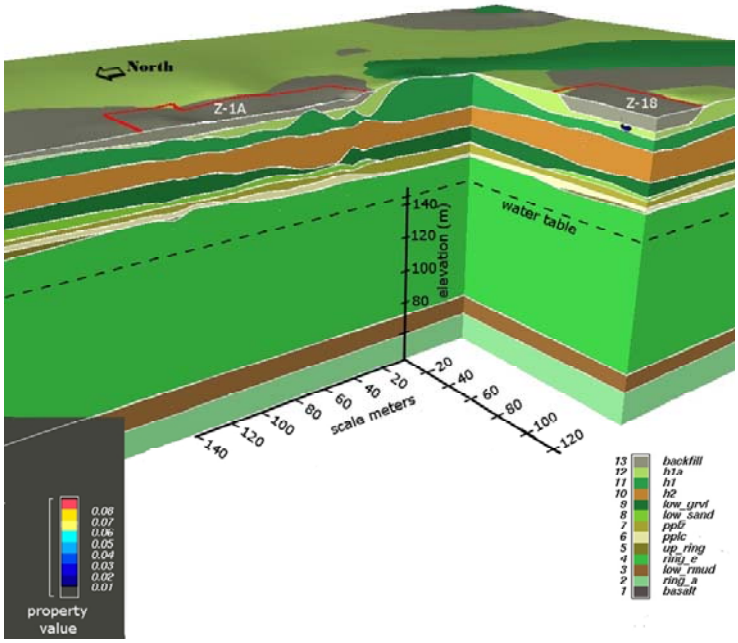

Figure 5.62. DNAPL Saturation at 1993 for Sensitivity Case VI-g

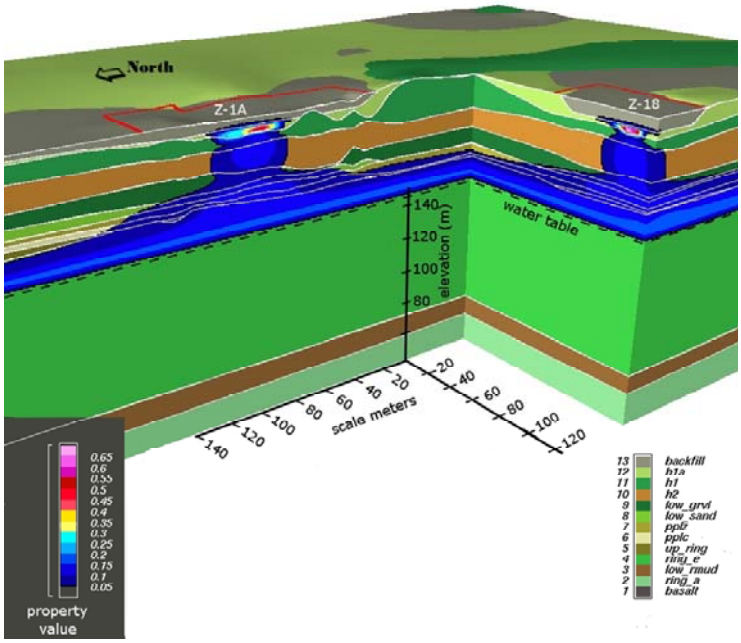

Figure 5.63. CT Gas Concentrations (in g/L) at 1993 for Sensitivity Case VI-g (0.1 g/L is equivalent to 12,000 ppmv at standard temperature and pressure)

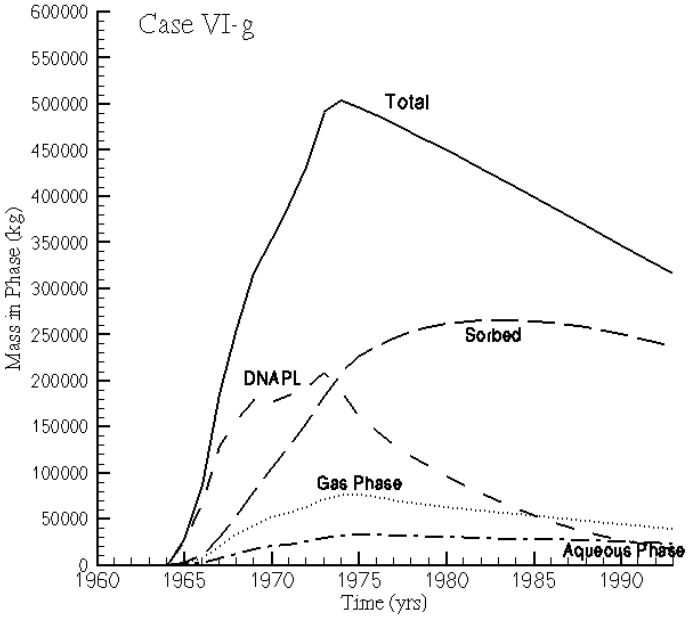

Figure 5.64. CT Mass Distribution Over the DNAPL, Sorbed, Aqueous, and Gas Phases for 1960 – 1993 (Case VI-g)

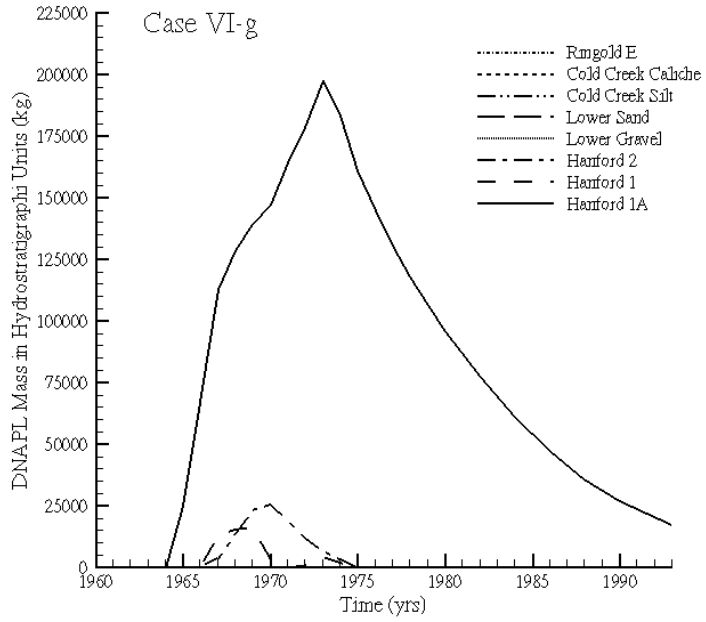

Figure 5.65. DNAPL CT Mass Distribution Over the Hydrostratigraphic Units for 1960 – 1993 (Case VI-g)

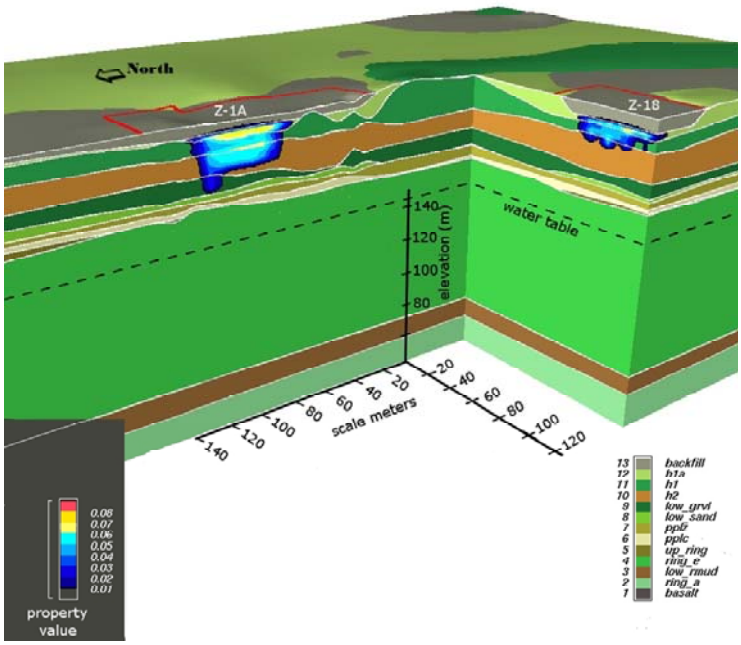

Figure 5.66. DNAPL Saturation at 1993 for Sensitivity Case VI-h

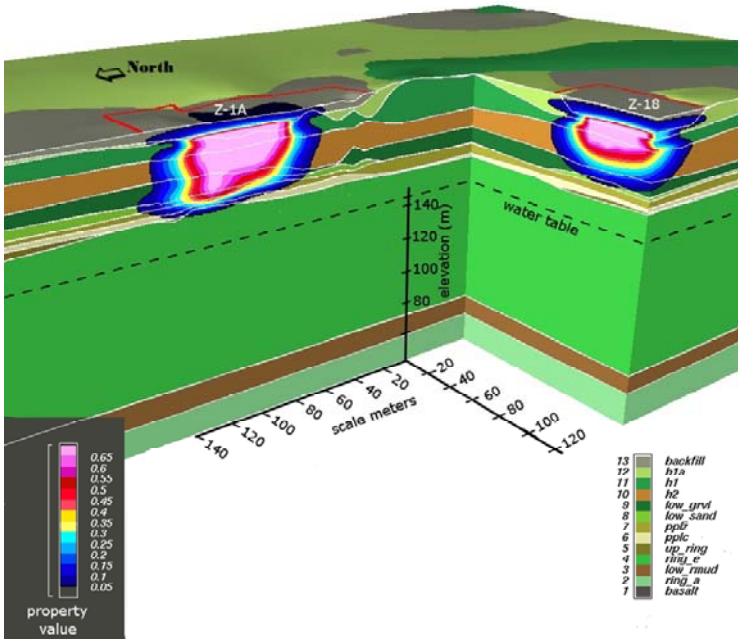

Figure 5.67. CT Gas Concentrations (in g/L) at 1993 for Sensitivity Case VI-h (0.1 g/L is equivalent to 12,000 ppmv at standard temperature and pressure)

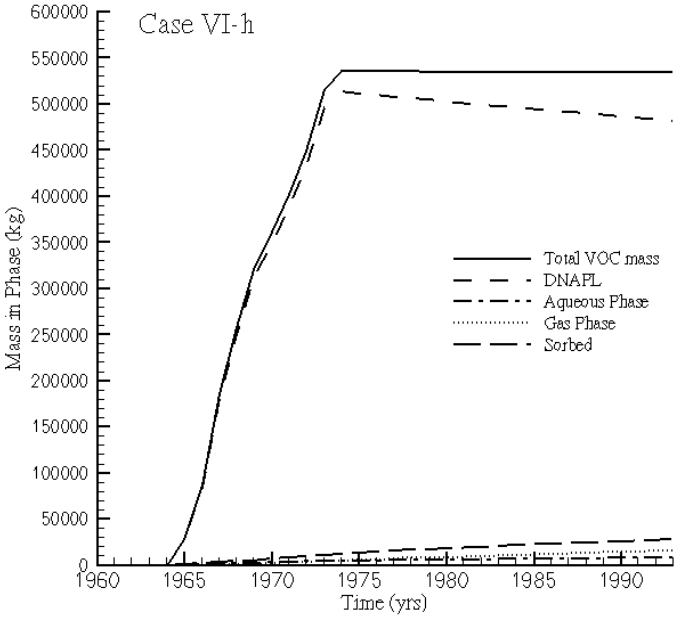

Figure 5.68. CT Mass Distribution Over the DNAPL, Sorbed, Aqueous, and Gas Phases for 1960 – 1993 (Case VI-h)

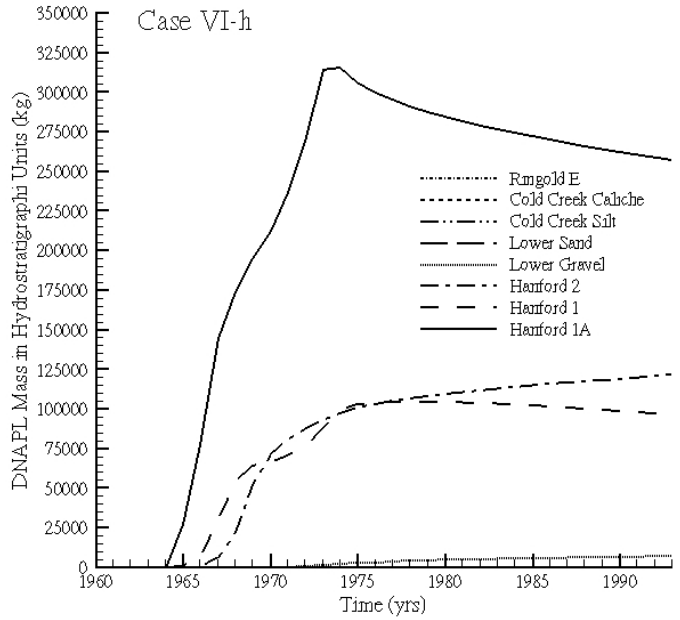

Figure 5.69. DNAPL CT Mass Distribution Over the Hydrostratigraphic Units for 1960 – 1993 (Case VI-h)

5.3 Comparison of Simulation Results

Using similar procedures used in Oostrom et al. (2004; 2006) for the 216-Z-9 simulations, normalized spatial moments of the DNAPL distribution were calculated to provide a quantitative basis for comparing the results of the different simulation cases (Freyberg 1986). The *ijk*th moment of the mass distribution in space was defined as

$$M_{ijk}(t) = \int_{-\infty}^{\infty} \int_{-\infty}^{\infty} \int_{-\infty}^{\infty} \rho_n \phi S_n(x,y,z,t) x^i y^j z^k \, dx dy dz \tag{5.1}$$

where ρ_n is the mass density of the DNAPL, ϕ is the porosity, S_n is the DNAPL saturation, and x, y, and z are the spatial coordinates. The integrals in Equation (5.1) were evaluated over the extent the DNAPL or dissolved component was transported from either the 216-Z-1A or 216-Z-18 sites.

The zeroth, first, and second (i + j + k = 0, 1, or 2, respectively) spatial moments of the DNAPL distribution were computed. These moments provide measures of the total DNAPL mass, the location of the center of mass, and spread about the center of mass. The zeroth moment, M_{000}, is equal to the total mass in the domain. The first moment, normalized by the zeroth moment, defines the location of the center of mass (x_c, y_c, z_c):

$$x_c = \frac{M_{100}}{M_{000}} \qquad y_c = \frac{M_{010}}{M_{000}} \qquad y_c = \frac{M_{001}}{M_{000}} \tag{5.2}$$

The second moment about the center of mass defines a spatial covariance tensor (Freyberg 1986):

$$\sigma^2 = \begin{bmatrix} \sigma_{xx}^2 & \sigma_{xy}^2 & \sigma_{xz}^2 \\ \sigma_{yx}^2 & \sigma_{yy}^2 & \sigma_{yz}^2 \\ \sigma_{zx}^2 & \sigma_{zy}^2 & \sigma_{zz}^2 \end{bmatrix}$$

$$\sigma_{xx}^2 = \frac{M_{200}}{M_{000}} - x_c^2 \qquad \sigma_{yy}^2 = \frac{M_{020}}{M_{000}} - y_c^2 \qquad \sigma_{zz}^2 = \frac{M_{002}}{M_{000}} - z_c^2 \tag{5-3}$$

$$\sigma_{xy}^2 = \sigma_{yx}^2 = \frac{M_{110}}{M_{000}} - x_c y_c \qquad \sigma_{xz}^2 = \sigma_{zx}^2 = \frac{M_{101}}{M_{000}} - x_c z_c \qquad \sigma_{yz}^2 = \sigma_{zy}^2 = \frac{M_{011}}{M_{000}} - y_c z_c$$

The components of the covariance tensor are directly related to the spread of the DNAPL body about its center of mass. In Table 5.3 and 5.4, the zeroth and first order moments are shown for the 216-Z-18 and 216-Z-1A, respectively. Table 5.5 and 5.6 provide an overview of the second order diagonal moments for the two sites. The listed moments are computed for 1993.

The first order moments (Table 5.3 and 5.4) show that for both disposal sites, the horizontal center of mass is located below the disposal site footprint for all simulations. The vertical center of mass for the sites is located in the H2 unit for most simulations. A vertical center of mass closer to the CCU is

predicted by the cases where the hydraulic properties of the H1a unit were altered to resemble properties of the H1 unit. The standard deviations of the second order moments, shown in Table 5.5 and 5.6, provide an indication of the DNAPL spreading. According to the moment analysis, approximately 95% of the DNAPL mass is predicted to be located between the center of mass and plus or minus the computed standard deviations. For most cases, the standard deviations in the horizontal direction are less than 50 m, limiting the mass distribution to areas with roughly the same order of magnitude as the footprints. In the vertical direction, the standard deviation for the 216-Z-1A site is typically in the order of about 10 m, while the standard deviation for the 216-Z-18 site is often less than 5 m.

Table 5.3. Zero and First Order Moments of CT DNAPL Mass at 1993 for DNAPL Disposed at the 216-Z-1A Site. (The center of 216-Z-1A Trench is set at x = 0 m, y = 0 m, and z = 199 m. The CCU below the trench is approximately located between z = 162 m and z = 170 m.)

Simulation	M_{000}	x_c (m)	y_c (m)	z_c (m)
Base Case	1.93e5	-2.1	-2.3	181
I-a	1.99e5	-1.4	-1.6	177
I-b	2.03e5	-2.1	-3.1	175
I-c	1.16e5	-2.4	-0.6	171
II-a	1.80e5	-0.4	-2.4	180
II-b	1.85e5	-0.9	1.4	176
II-c	1.41e5	-0.7	1.2	172
III-a	1.95e5	-1.1	-3.1	180
III-b	1.97e5	-3.1	-0.3	182
III-c	2.01e5	-2.1	0.4	182
III-d	2.02e5	-3.2	-3.1	180
III-e	1.43e5	-0.9	0.8	178
III-f	3.12e5	-1.2	-0.7	180
III-g	1.97e5	-1.3	0.3	180
III-h	1.89e5	-1.5	-0.2	179
III-i	1.91e5	-3.0	-1.1	181
III-j	2.01e5	-1.3	-1.0	184
III-k	2.05e5	-2.2	-3.3	183
IV-a	1.02e5	-1.2	-3.4	172
IV-b	1.81e5	-0.9	-4.5	171
IV-c	1.85e5	-1.5	-3.2	171
IV-d	1.45e5	-2.3	-6.1	167
V-a	2.01e5	-0.1	3.1	181
V-b	2.02e5	-0.4	2.6	180
V-c	1.90e5	-0.5	1.4	179
V-d	1.92e5	-0.6	4.2	180
VI-a	1.32e5	-0.8	-2.5	162
VI-b	3.31e5	-1.2	4.2	182
VI-c	2.02e5	-1.4	-1.3	181
VI-d	1.82e5	-2.5	-2.8	180
VI-e	1.85e5	-2.3	-3.7	182
VI-f	1.95e5	-2.7	-2.3	177
VI-g	5.04e3	4.2	0.4	184
VI-h	4.02e5	3.4	1.3	185

Table 5.4. Zero and First Order Moments of CT DNAPL Mass at 1993 for DNAPL Disposed at the 216-Z-18 Site. (The center of 216-Z-18 Trench is set at x = 0 m, y = 0 m, and z = 199 m. The CCU below the trench is approximately located between z = 162 m and z = 170 m.)

Simulation	M_{000}	x_c (m)	y_c (m)	z_c (m)
Base Case	0.88e5	-6.7	7.2	184
I-a	0.93e5	-5.6	7.4	180
I-b	0.9e5	-7.2	6.5	177
I-c	0.50e5	-4.6	8.2	174
II-a	0.69e5	-6.2	5.4	182
II-b	0.82e5	-5.4	4.4	179
II-c	0.58e5	-4.1	6.5	176
III-a	0.90e5	-4.9	6.4	183
III-b	0.91e5	-6.2	8.3	185
III-c	0.65e5	-5.3	5.4	184
III-d	0.64e5	-3.6	3.6	183
III-e	0.54e5	-3.7	6.3	172
III-f	1.21e5	-5.7	7.5	181
III-g	0.94e5	-6.2	8.3	182
III-h	0.77e5	-7.8	6.9	183
III-i	0.83e5	-4.3	3.9	185
III-j	0.91e5	-5.2	5.4	186
III-k	0.97e5	-5.7	7.5	187
IV-a	0.64e5	-4.3	3.5	174
IV-b	0.68e5	-6.7	6.2	172
IV-c	0.82e5	-6.7	5.4	172
IV-d	0.54e5	-5.6	6.4	168
V-a	0.84e5	-4.6	6.7	183
V-b	0.83e5	-5.9	4.3	183
V-c	0.76e5	-2.0	6.1	182
V-d	0.74e5	-6.2	5.7	182
VI-a	0.65e5	-5.8	7.4	164
VI-b	1.02e5	-7.8	6.5	185
VI-c	0.89e5	-6.4	4.5	185
VI-d	0.84e5	-6.5	4.3	182
VI-e	0.89e5	-4.2	6.5	185
VI-f	0.88e5	-5.7	6.3	181
VI-g	1.20e4	-7.6	7.4	185
VI-h	0.79e5	-5.4	7.5	186

Table 5.5. Standard Deviations of Second Order Moments (Rounded to Nearest Meter) of CT DNAPL Mass at 1993 for the 216-Z-1A Site. (The center is at x = 0 m, y = 0 m, and z = 201 m. The CCU below the trench is approximately located between z = 162 m and z = 170 m.)

Simulation	σ_{xx} (m)	σ_{yy} (m)	σ_{zz} (m)
Base Case	54	34	12
I-a	53	32	11
I-b	53	30	10
I-c	56	23	10
II-a	52	27	9
II-b	48	29	9
II-c	49	28	10
III-a	52	36	12
III-b	50	34	10
III-c	39	29	13
III-d	41	30	11
III-e	47	34	12
III-f	49	34	11
III-g	48	32	12
III-h	52	28	11
III-i	48	27	10
III-j	32	19	8
III-k	34	17	8
IV-a	38	19	7
IV-b	36	19	8
IV-c	31	15	7
IV-d	22	16	6
V-a	46	29	10
V-b	54	27	10
V-c	51	32	11
V-d	48	29	11
VI-a	9	8	41
VI-b	12	8	8
VI-c	47	29	10
VI-d	44	28	13
VI-e	43	26	12
VI-f	43	35	12
VI-g	47	31	18
VI-h	29	18	6

Table 5.6. Standard Deviations of Second Order Moments of CT DNAPL Mass at 1993 for the 216-Z-18 Site. (The center is at x = 0 m, y = 0 m, and z = 199 m. The CCU below the trench is approximately located between z = 162 m and z = 170 m.)

Simulation	σ_{xx} (m)	σ_{yy} (m)	σ_{zz} (m)
Base Case	42	22	3
I-a	42	20	3
I-b	43	21	4
I-c	44	21	4
II-a	35	18	3
II-b	36	18	3
II-c	40	21	3
III-a	43	24	4
III-b	40	21	3
III-c	31	17	5
III-d	29	18	4
III-e	37	22	4
III-f	41	24	5
III-g	42	22	5
III-h	41	22	3
III-i	38	20	4
III-j	20	14	2
III-k	21	13	2
IV-a	31	16	3
IV-b	30	15	3
IV-c	22	13	2
IV-d	16	12	3
V-a	36	24	4
V-b	40	22	4
V-c	41	23	4
V-d	42	22	4
VI-a	8	6	14
VI-b	9	5	3
VI-c	37	21	4
VI-d	38	25	4
VI-e	32	22	5
VI-f	33	24	5
VI-g	40	21	7
VI-h	19	14	2

5.4 SVE Simulation Results

In this section the results of eight SVE simulations for the period 1993 – 2007 were conducted to investigate the effect of well location, extraction rate, and vapor pressure on CT removal. The base case fluid and porous medium property values are used for all SVE simulations except for case 8. The SVE simulations are:

1. Extraction from all wells. This case is referred to as the "base case with SVE" simulation.
2. Extraction from wells with screens located in 216-Z-1A CCU silt: W18-159, -165, -166, -167, -178, and -174.
3. Extraction from wells located near water table near the 216-Z-18 trench: W18-10, -11, and -12.
4. Extraction from well W18-96 only, located below the 216-Z-18 trench.
5. Extraction from well W18-165 only, located below the 216-Z-1A tile field.
6. Extraction from well W18-246 (located west of 216-Z-1A and north of 216-Z-18)
7. Extraction with 25% of the rate.
8. Extraction from all wells and hydraulic properties of H1a the same as for H1.

The results of SVE case 1 are discussed in Section 5.4.1., while the other simulations are described in Section 5.4.2.

5.4.1 Base Case with SVE

The results of the simulation with SVE operations in the subsurface of the two disposal sites are compared with an extension of the base case from 1993 – 2007 without the inclusion of SVE. Figure 5.70 and 5.71 show the DNAPL saturation at 1995 for the base case without, and with SVE, respectively. The figures show that after two years of extraction, most of the DNAPL in the Lower Gravel unit below the 216-Z-1A site has been removed. The remediation seems to have less impact on the DNAPL in the CCU and the H1a unit, while some removal is visible in the H2 unit, especially below the 216-Z-18. Five years later, in 2000, the situation for the base case without SVE (Figure 5.72) has not changed much while the SVE operations seem to have removed most DNAPL in the H2 unit and CCU (Figure 5.73. The SVE does not seem to have a large affect the DNAPL in the H1a unit below both sites. The relative low permeability of the unit and the larger distance to the SVE well screens are important factors limiting mass removal from this unit.

The CT gas plumes at 1995 (Figures 5.74 and 5.75) and 2000 (Figure 5.76 and 5.77) show the large impact of SVE. For the base case without SVE the plumes look fairly similar for both times. However, the figures for the base case with SVE demonstrate a rapid reduction of the plume extension, even in the lower permeability units. By the year 2000, the plume extension is reduced to a size smaller than the respective footprints of the disposal facility. Top views of the CT gas plume at 1995 (Figures 5.78 and 5.79) and at 2000 (Figures 5.80 and 5.81) in the CCU show an apparent stable gas plume for simulation

without SVE, but a rapidly decreasing extension for the case where SVE is considered. In the latter case, no gaseous CT gas is predicted to be present in the CCU below the 216-Z-18 site by 2000, while the extension below the 216-Z-1A site is less than the width of the footprint (Figure 5.81). A comparison for the CT gas concentration near the water table is shown in Figures 5.82 and 5.83. For the simulation without SVE, CT in the gas phase is still being transported to the water table (Figure 5.82) while not gaseous CT is being observed near the water table for the simulation with SVE (Figure 5.83).

Figures 5.84 and 5.85 show the CT mass distribution over the phases for the cases without and with SVE, respectively, for the period 1960 – 2007. Figure 5.84 show gradual changes in phase distribution while Figure 5.85 show abrupt changes induces by the SVE operations. Figures 5.86 and 5.87 provide the same information for the period from 1993 – 2007 when SVE was employed. Again, the figures show gradual compositional changes for the simulation without SVE (Figure 5.86) and more pronounced decreases over all phases for the simulation with SVE (Figure 5.87). Figure 5.87 demonstrates a rapid decrease in gaseous, sorbed, and aqueous phase CT, and a more gradual decrease in CT DNAPL. The rapid decrease in gaseous CT and the slower reduction in CT DNAPL shown in this plot are consistent with the CT gas plumes shown in Figures 5.75 and 5.77 and DNAPL saturations shown in Figures 5.71 and 5.73. The total mass that is predicted to be removed by SVE through 2007 is almost 400,000 kg.

The CT mass distribution over the hydrostratigraphic units for the base case without and with SVE are depicted in Figures 5.88 and 5.89, respectively. The simulation without SVE shows gradual changes in composition, while the simulation with SVE indicates rapid CT DNAPL decreases in the H2, Lower Sand, and Lower Gravel units. The CT DNAPL mass reduction in the CCU appears to be a slower process, while a reduction in the H1a unit seems to be unrelated to SVE since its CT DNAPL mass behavior looks the same as for the simulation without SVE (Figure 5.88). This information becomes more pronounced in Figures 5.90 and 5.91, where the CT mass distribution is shown for the 1990 – 2007 period. Figure 5.91 shows that by 1995, all CT DNAPL mass in the Lower Gravel has disappeared and that by 1998, the SVE has removed the CT DNAPL from the Lower Sand. Complete depletion of the H2 unit is predicted to have occurred by 2004. Again, the resilience of the CT DNAPL in the H1a unit is remarkable and is associated with its low permeability, high porosity, and considerable distance to most SVE wells.

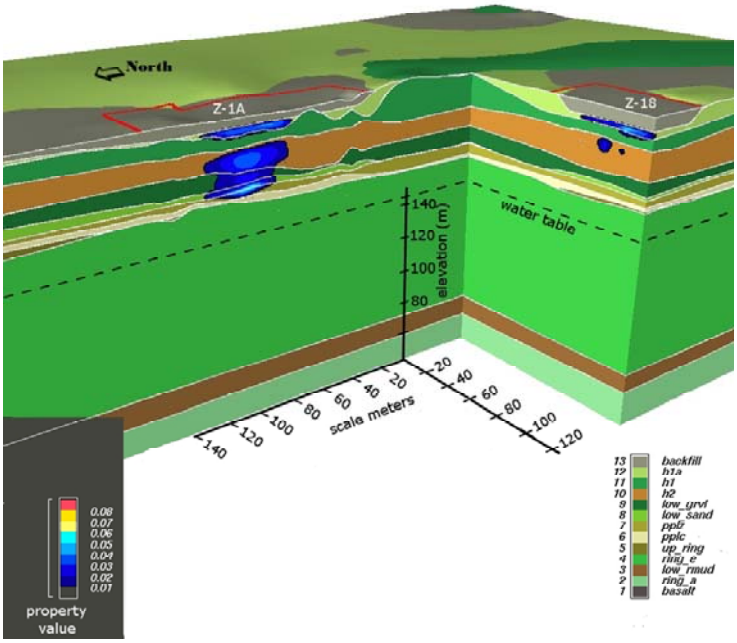

Figure 5.70. DNAPL Saturations at 1995 (Base Case)

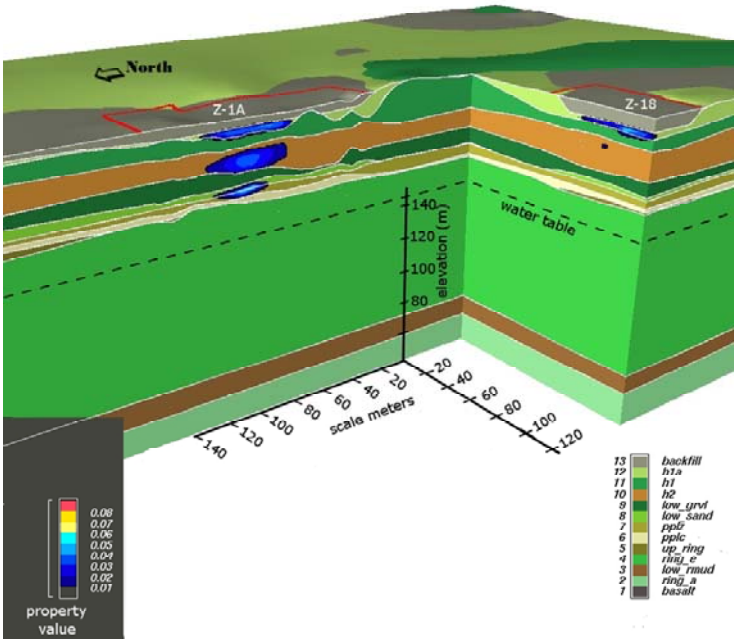

Figure 5.71. DNAPL Saturations at 1995 (Base Case with SVE)

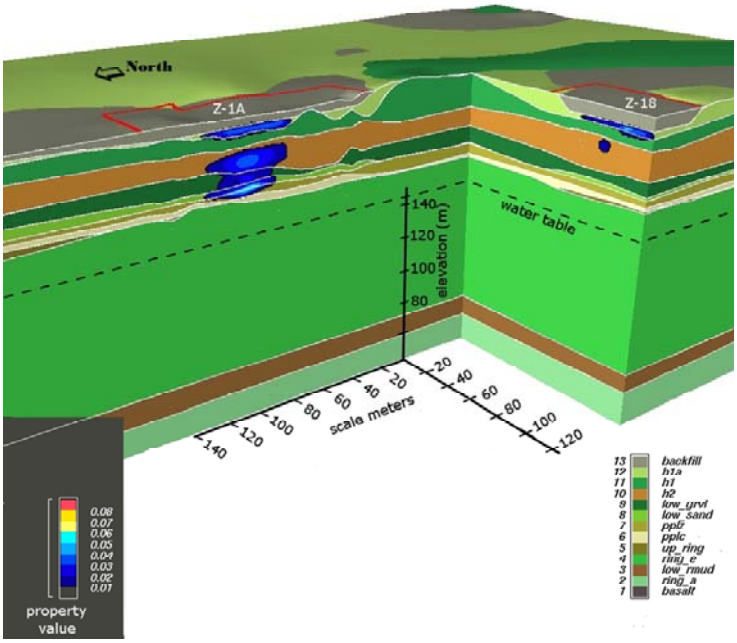

Figure 5.72. DNAPL Saturations at 2000 (Base Case)

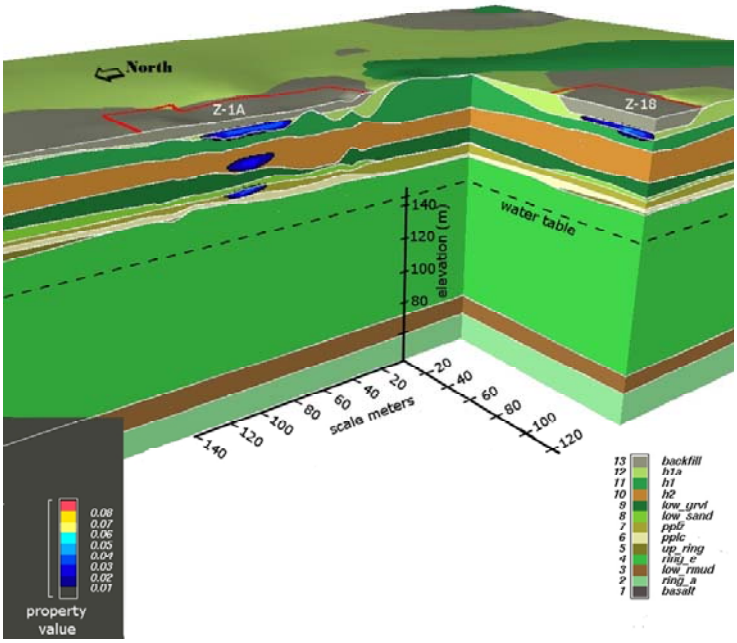

Figure 5.73. DNAPL Saturations at 2000 (Base Case with SVE)

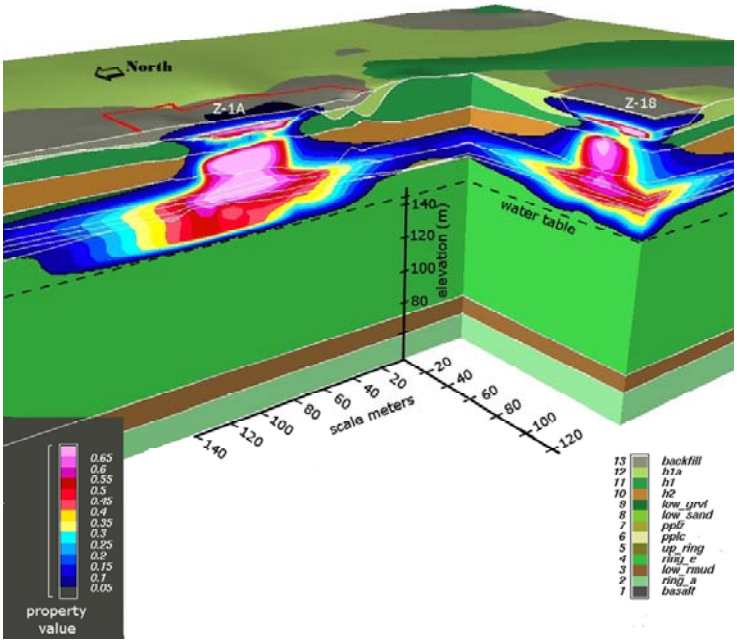

Figure 5.74. CT Gas Concentrations (g/L) at 1995 (Base Case) (0.1 g/L is equivalent to 12,000 ppmv at standard temperature and pressure)

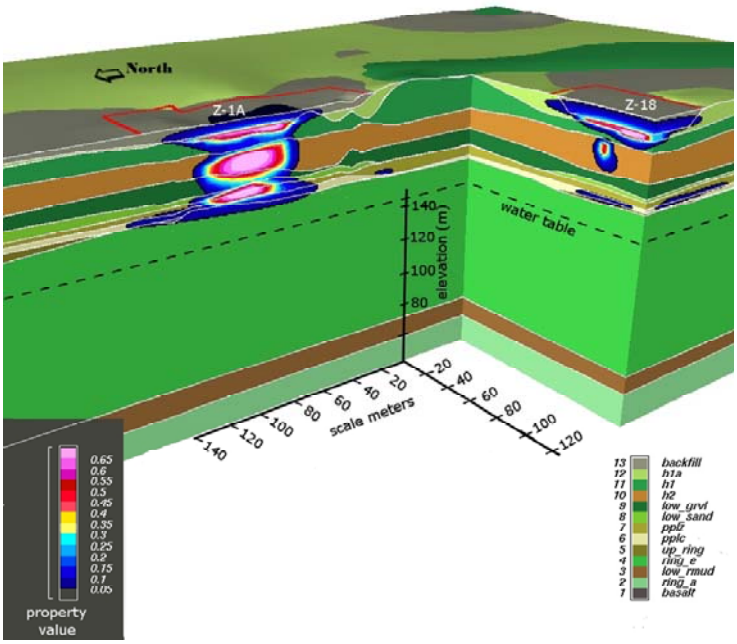

Figure 5.75. CT Gas Concentrations (g/L) at 1995 (Base Case with SVE) (0.1 g/L is equivalent to 12,000 ppmv at standard temperature and pressure)

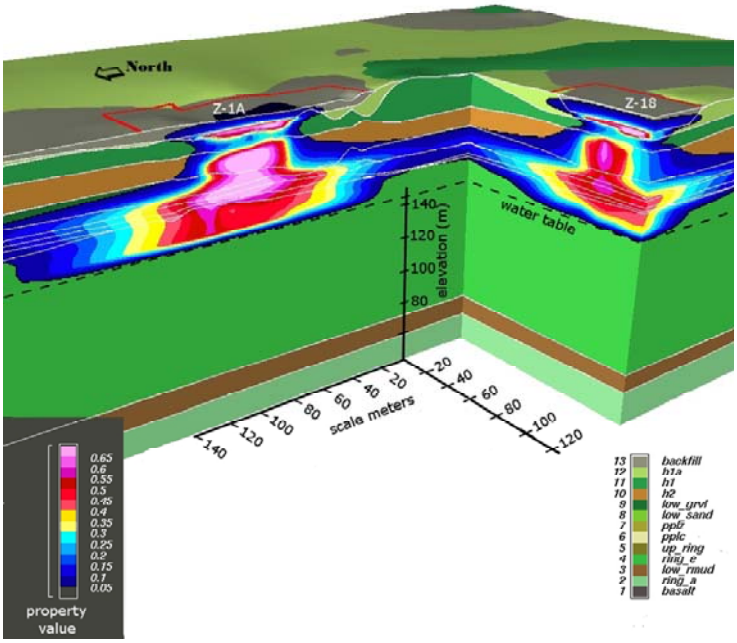

Figure 5.76. CT Gas Concentrations (g/L) at 2000 (Base Case) (0.1 g/L is equivalent to 12,000 ppmv at standard temperature and pressure)

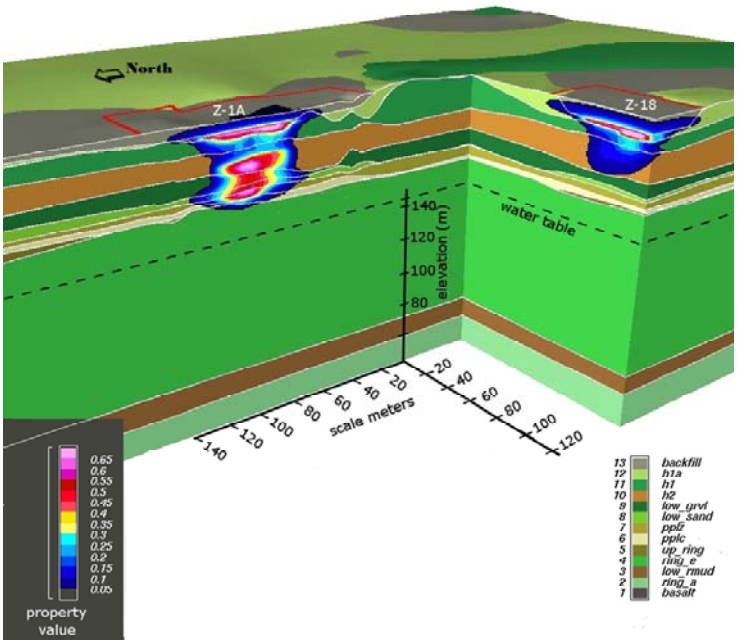

Figure 5.77. CT Gas Concentrations (g/L) at 2000 (Base Case with SVE) (0.1 g/L is equivalent to 12,000 ppmv at standard temperature and pressure)

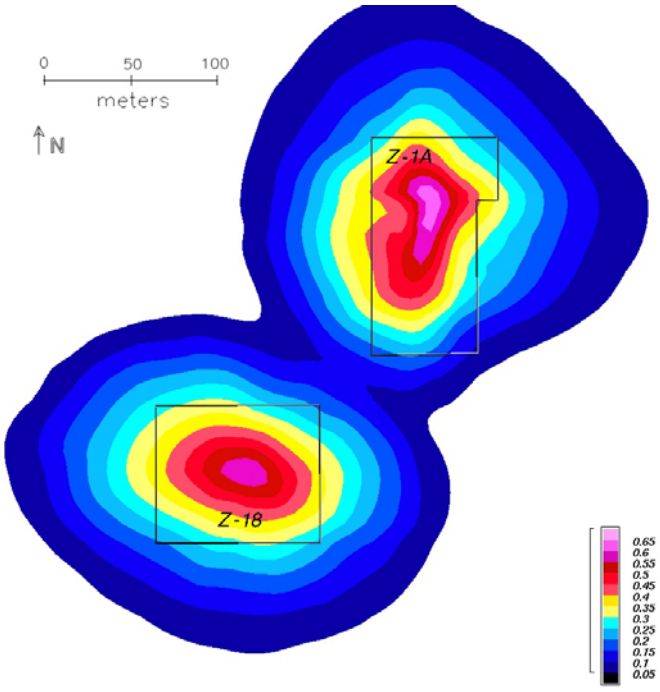

Figure 5.78. Top View of CT Gas Concentrations (g/L) in Cold Creek Unit at 1995 (Base Case) (0.1 g/L is equivalent to 12,000 ppmv at standard temperature and pressure)

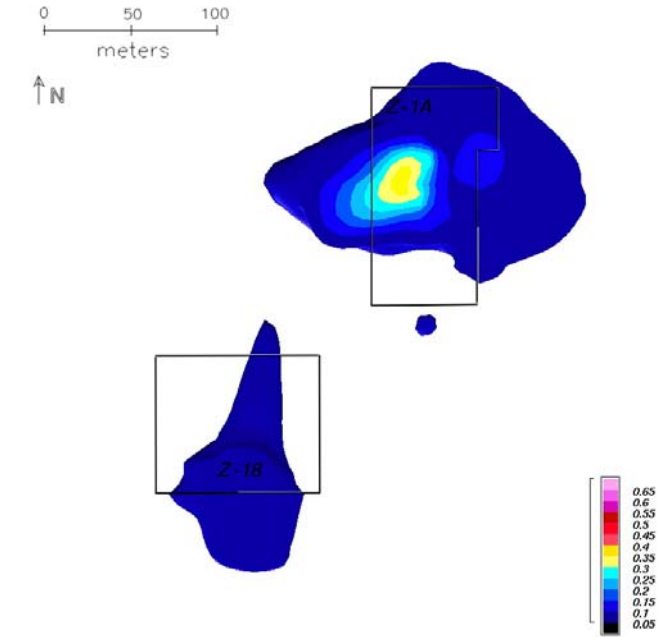

Figure 5.79. Top View of CT Gas Concentrations (g/L) in Cold Creek Unit at 1995 (Base Case with SVE) (0.1 g/L is equivalent to 12,000 ppmv at standard temperature and pressure)

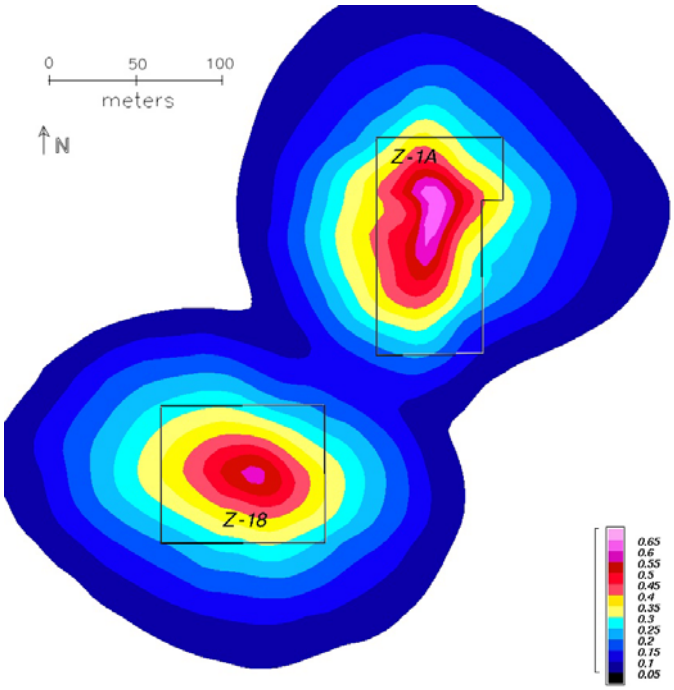

Figure 5.80. Top View of CT Gas Concentrations (g/L) in Cold Creek Unit at 2000 (Base Case) (0.1 g/L is equivalent to 12,000 ppmv at standard temperature and pressure)

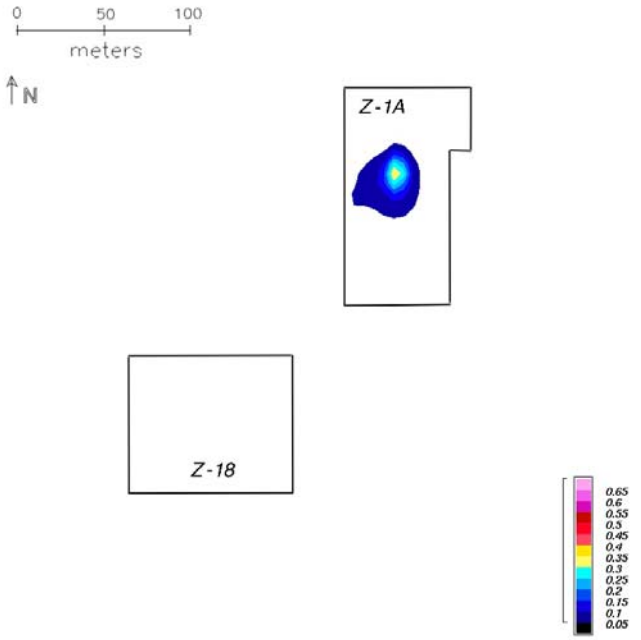

Figure 5.81. Top View of CT Gas Concentrations (g/L) in Cold Creek Unit at 2000 (Base Case with SVE) (0.1 g/L is equivalent to 12,000 ppmv at standard temperature and pressure)

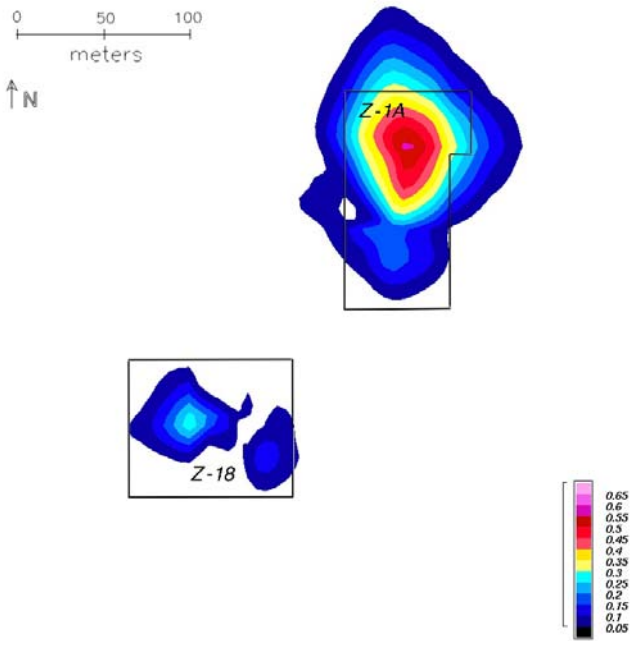

Figure 5.82. Top View of CT Gas Concentrations (g/L) Above Water Table at 2000 (Base Case) (0.1 g/L is equivalent to 12,000 ppmv at standard temperature and pressure)

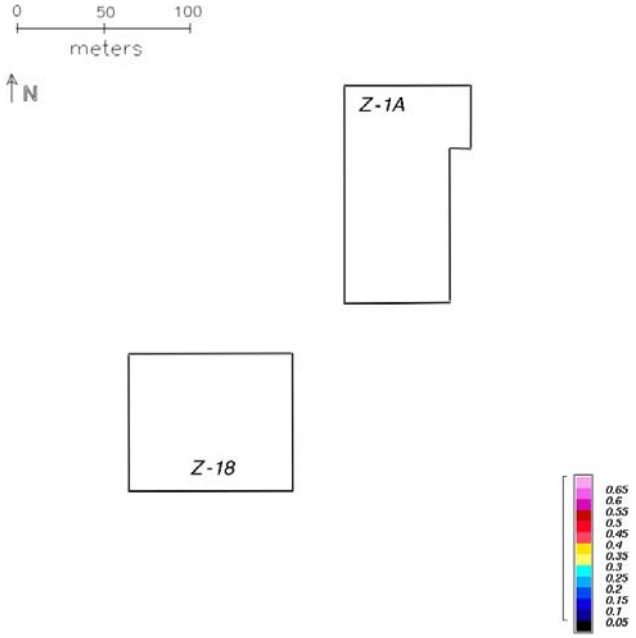

Figure 5.83. Top View of CT Gas Concentrations (g/L) Above Water Table at 2000 (Base Case with SVE) (0.1 g/L is equivalent to 12,000 ppmv at standard temperature and pressure)

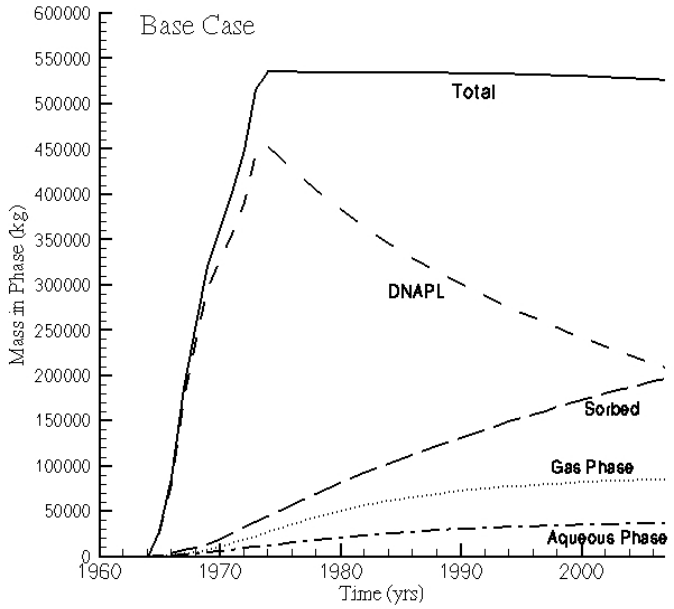

Figure 5.84. CT Mass Distribution Over the DNAPL, Sorbed, Aqueous, and Gas Phases for 1960 – 2007 (Base Case)

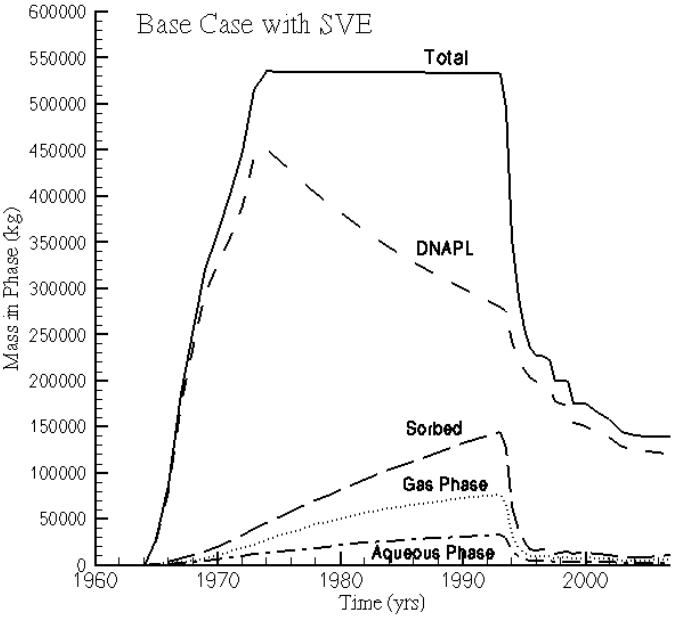

Figure 5.85. CT Mass Distribution Over the DNAPL, Sorbed, Aqueous, and Gas Phases for 1960 – 2007 (Base Case with SVE)

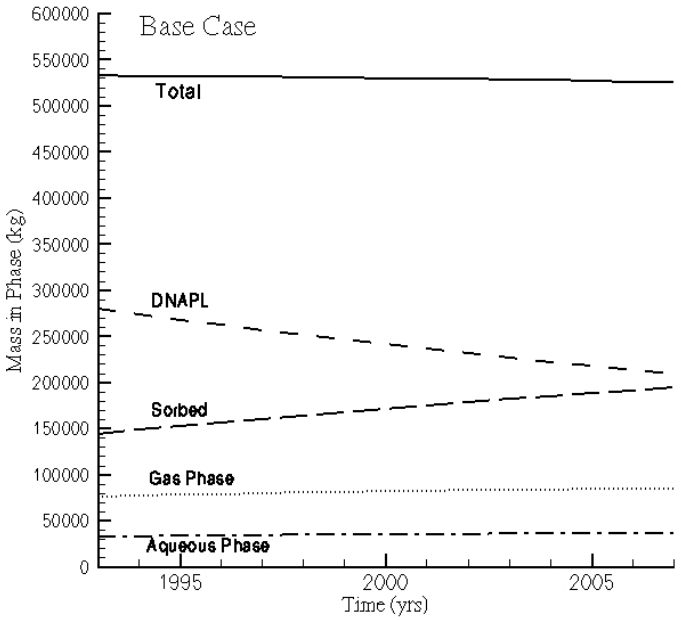

Figure 5.86. CT Mass Distribution Over the DNAPL, Sorbed, Aqueous, and Gas Phases for 1993 – 2007 (Base Case)

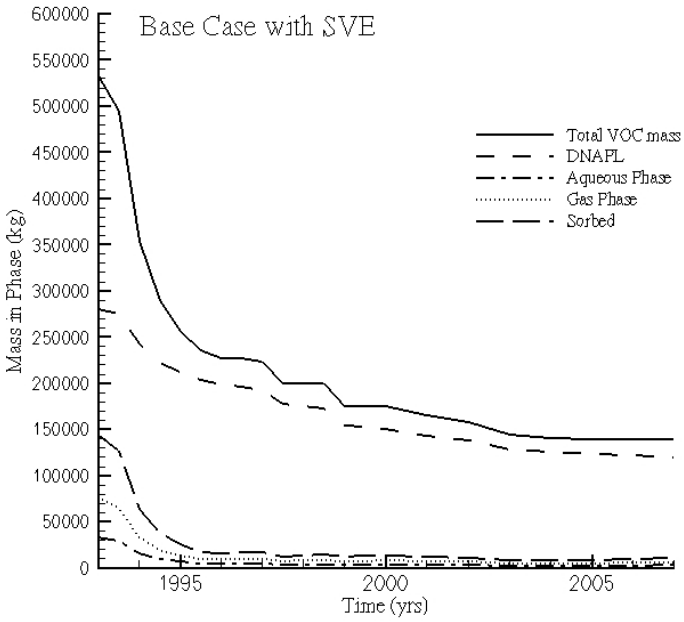

Figure 5.87. CT Mass Distribution Over the DNAPL, Sorbed, Aqueous, and Gas Phases for 1993 – 2007 (Base Case with SVE)

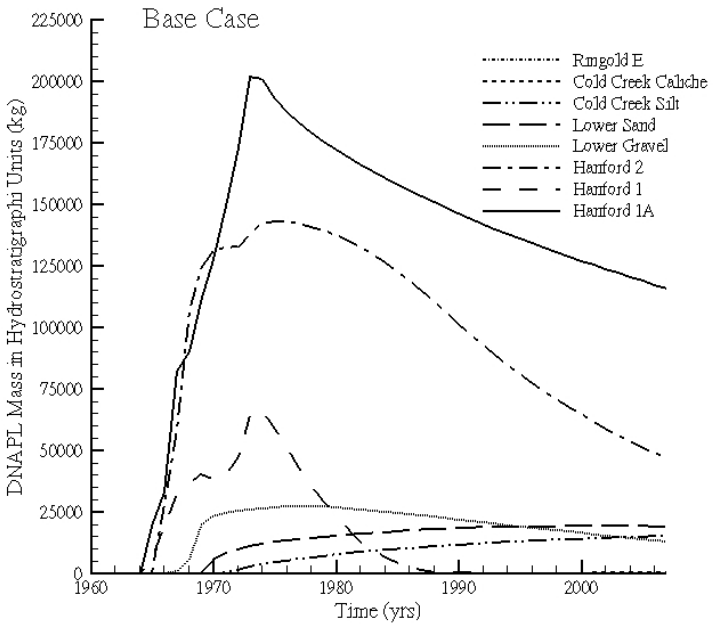

Figure 5.88. DNAPL CT Mass Distribution Over the Hydrostratigraphic Units for 1960 – 2007 (Base Case)

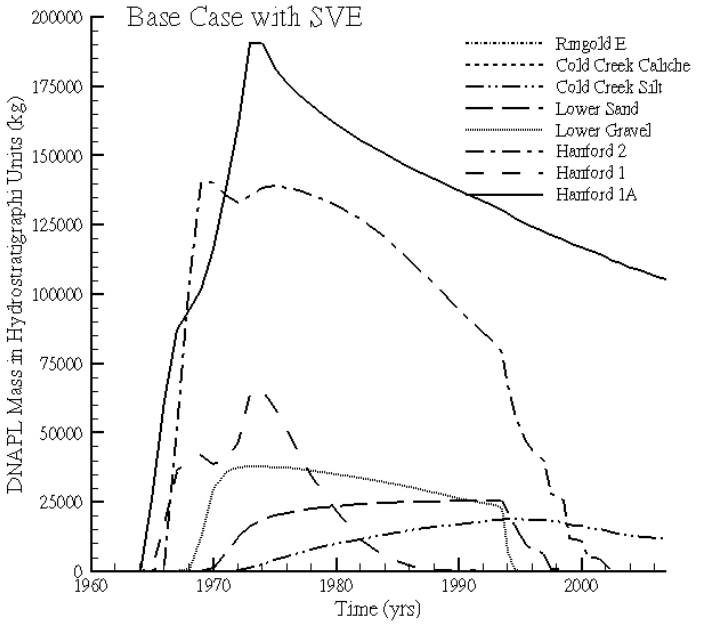

Figure 5.89. DNAPL CT Mass Distribution Over the Hydrostratigraphic Units for 1960 – 2007 (Base Case with SVE)

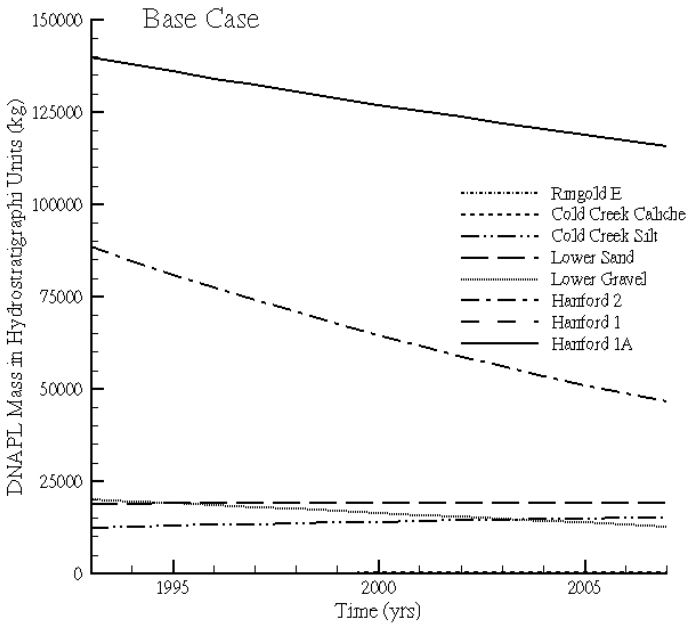

Figure 5.90. DNAPL CT Mass Distribution Over the Hydrostratigraphic Units for 1993 – 2007 (Base Case)

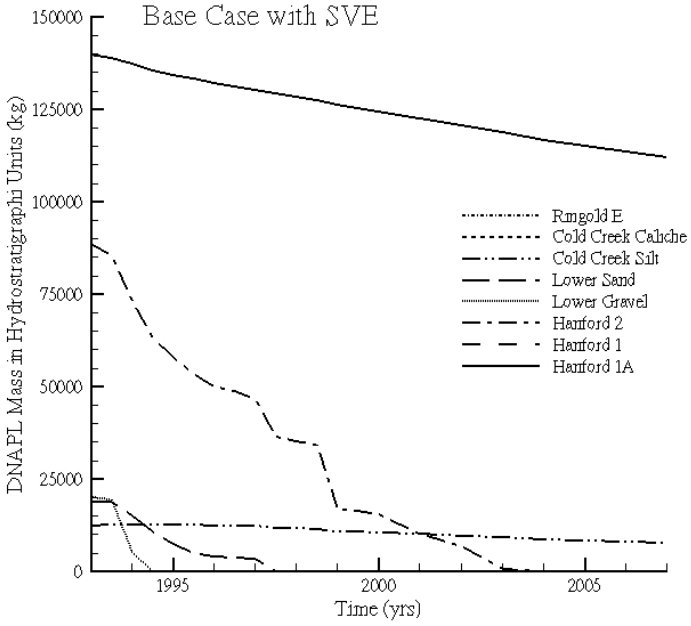

Figure 5.91. DNAPL CT Mass Distribution Over the Hydrostratigraphic Units for 1993 – 2007 (Base Case with SVE)

5.4.2 SVE Sensitivity Simulations

SVE sensitivity case 2 shows the effect of extraction from well with screen in the CCU silt below the 216-Z-1A. The CT mass distribution shows rapid changes corresponding with activation of the wells (Figure 5.92) and considerable recovery from these wells was not started until 1997. Total mass recovery was approximately 275,000 kg, which is 125,000 kg less than the base case with SVE. Removal was again the fastest from the Lower Sand, Lower Gravel, and H2 units. It is also of interest to observe that although the well screens were placed in the CCU silt, CT DNAPL removal from the unit was relatively low.

The case 3 simulations show the effect of the SVE wells located close to the water table (Figure 5.93). The predicted total mass removal is limited to approximately 50,000 kg (Figure 5.94), and most of that CT mass was removed from the Lower Sand and Lower Gravel (Figure 5.95). The distribution predicted by case 4, i.e., extraction from well W18-96 only, is shown in Figures 5.96 and 5.97. This well was only active in during the initial stages and has recovered approximately 100,000 kg from below the 216-Z-18 site. The fifth SVE case (Figures 5.98 and 5.99) looks at the recovery from a single well located below the 216-Z-1A site. This particular well was active during several periods of the campaign, yielding about 150,000 for the subsurface of this site. Most of the removed CT came from the Lower Gravel and H2 units. To investigate the effect of a well that is not located below either disposal site, a simulation was conducted (case 6) where only well W18-246 was used. This well is located west of the 216-Z-1A and north of the 216-Z-18. Although this well was located a considerable distance from both sites, the predicted removal was over 250,000 kg (Figure 5.100 and 5.101). For case 7, the effect of a 75% vapor pressure lowering on recovery was simulated (Figures 5.102 and 5.103). This simulation predicts a much slower recovery than the base case with SVE and a gradual reduction of the CT in all phases. Removal occurs primarily from the more permeable porous media, while leaving the CT mass in the H1a unit and CCU in place. The figures for SVE case 8 (Figures 5.104 and 5.105) indicate the importance of the properties of the H1a unit on CT DNAPL behavior and subsequent removal with SVE. The CT distribution over the phases (Figure 5.104) shows a larger reduction in the total VOC mass over time. The reason for the more pronounced removal is the location of the CT DNAPL at 1993. Contrary to the base case, at this point in time no CT DNAPL is located in the H1a unit because the properties of this unit are the same as for the underlying H1 unit. Most of the CT DNAPL has moved to more permeable units, allowed for a rapid removal. For this simulation, the CT DNAPL in the Cold Creek units is the most resilient (Figure 5.105).

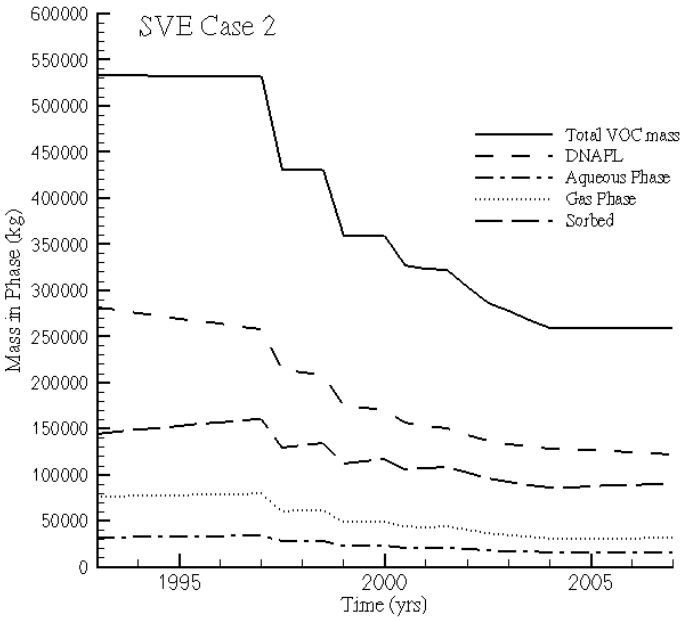

Figure 5.92. CT Mass Distribution Over the DNAPL, Sorbed, Aqueous, and Gas Phases for 1993 – 2007 (SVE Case 2)

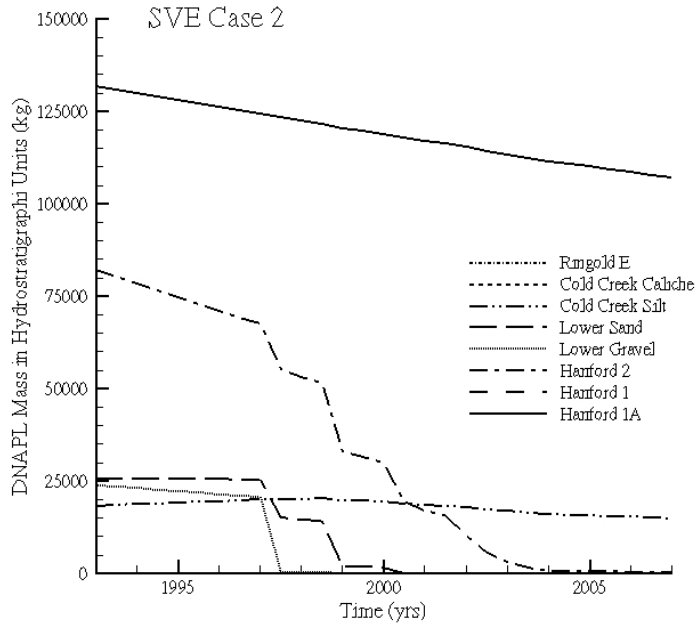

Figure 5.93. DNAPL CT Mass Distribution Over the Hydrostratigraphic Units for 1993 – 2007 (SVE Case 2)

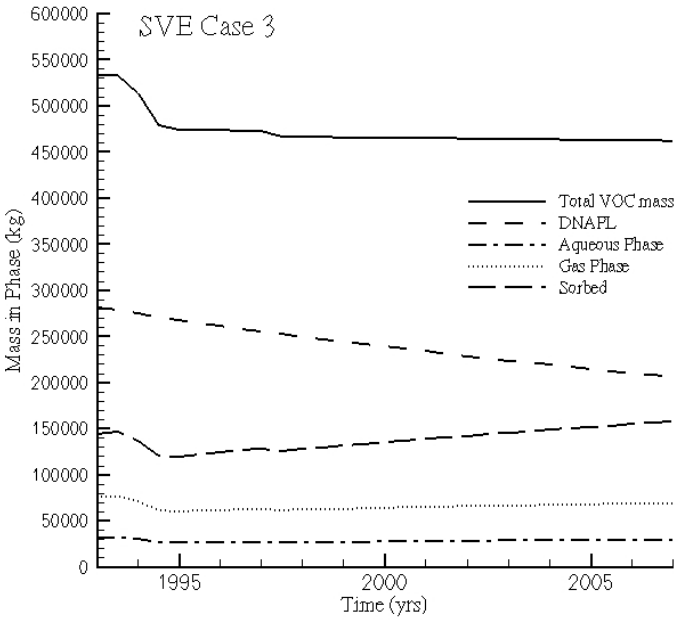

Figure 5.94. CT Mass Distribution Over the DNAPL, Sorbed, Aqueous, and Gas Phases for 1993 – 2007 (SVE Case 3)

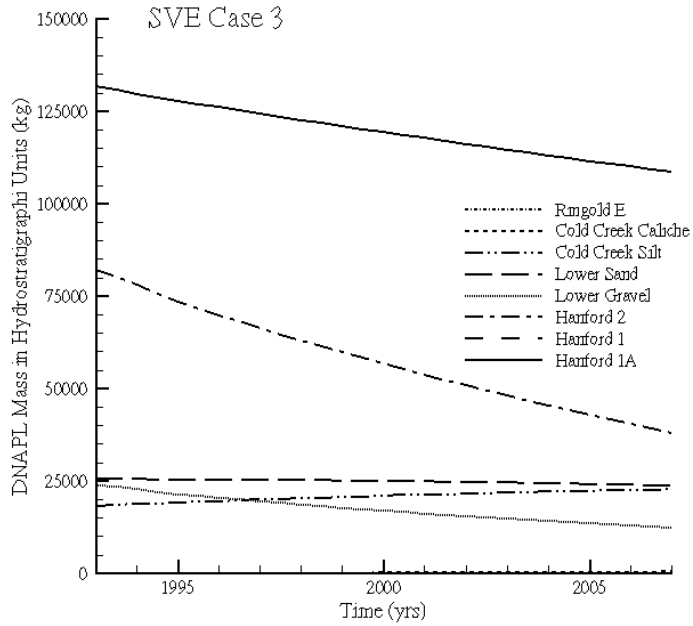

Figure 5.95. DNAPL CT Mass Distribution Over the Hydrostratigraphic Units for 1993 – 2007 (SVE Case 3)

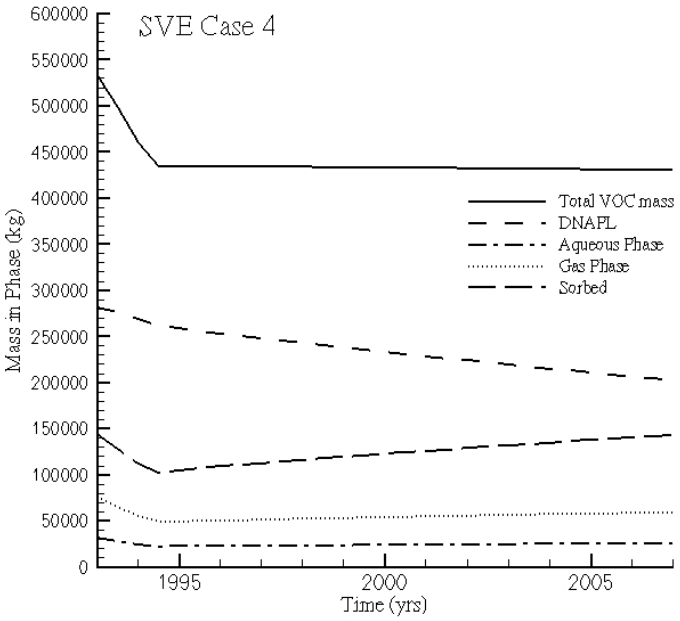

Figure 5.96. CT Mass Distribution Over the DNAPL, Sorbed, Aqueous, and Gas Phases for 1993 – 2007 (SVE Case 4)

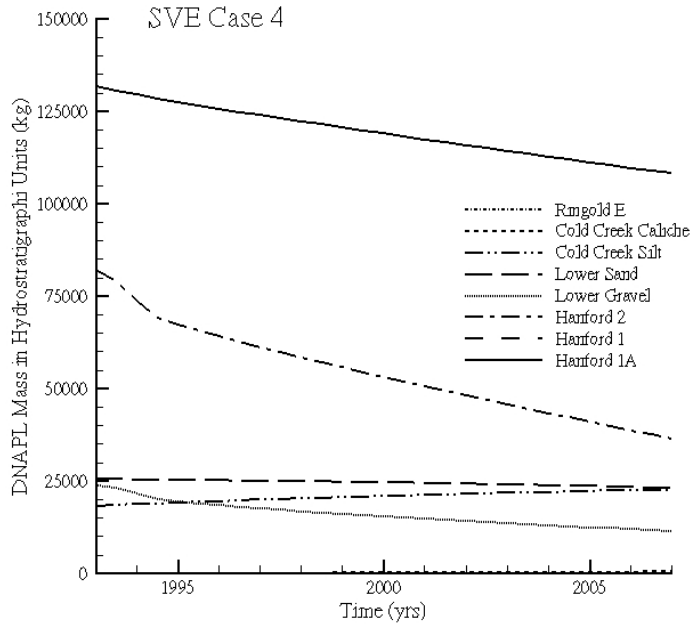

Figure 5.97. DNAPL CT Mass Distribution Over the Hydrostratigraphic Units for 1993 – 2007 (SVE Case 4)

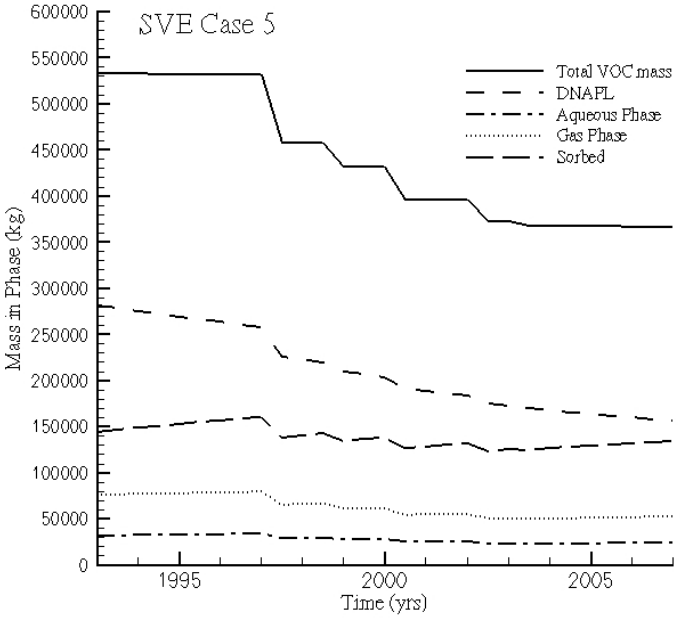

Figure 5.98. CT Mass Distribution Over the DNAPL, Sorbed, Aqueous, and Gas Phases for 1993 – 2007 (SVE Case 5)

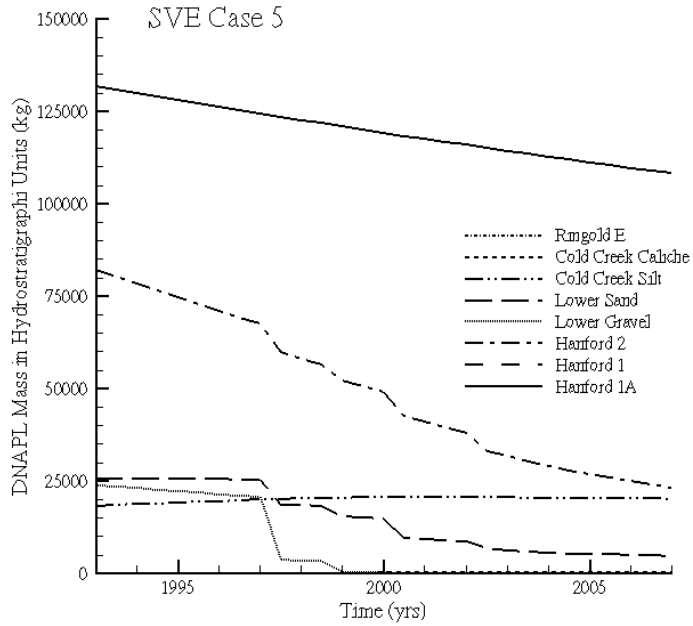

Figure 5.99. DNAPL CT Mass Distribution Over the Hydrostratigraphic Units for 1993 – 2007 (SVE Case 5)

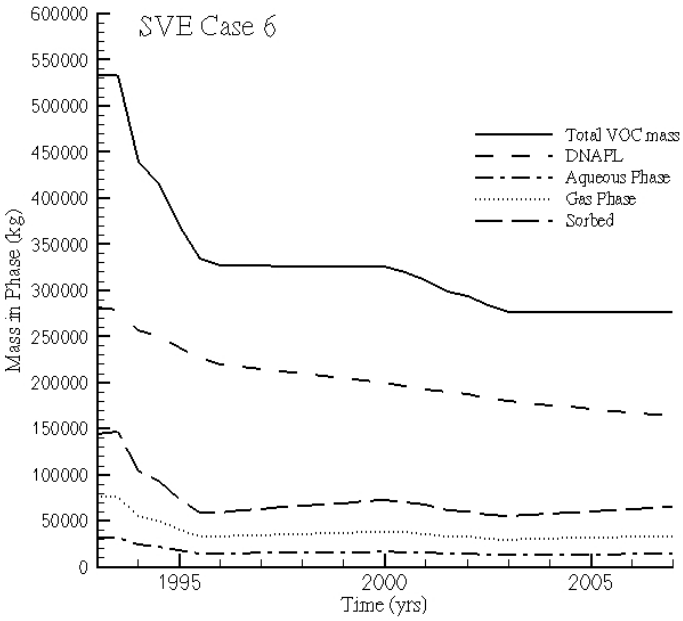

Figure 5.100. CT Mass Distribution Over the DNAPL, Sorbed, Aqueous, and Gas Phases for 1993 – 2007 (SVE Case 6)

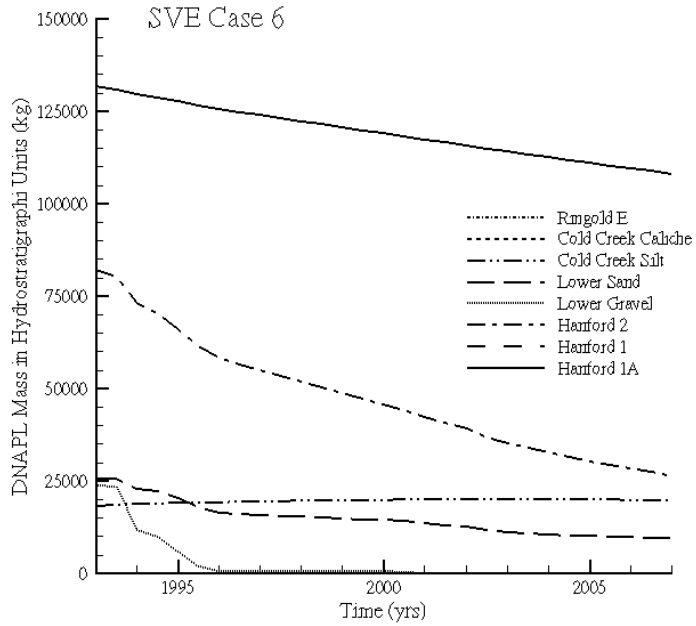

Figure 5.101. DNAPL CT Mass Distribution Over the Hydrostratigraphic Units for 1993 – 2007 (SVE Case 6)

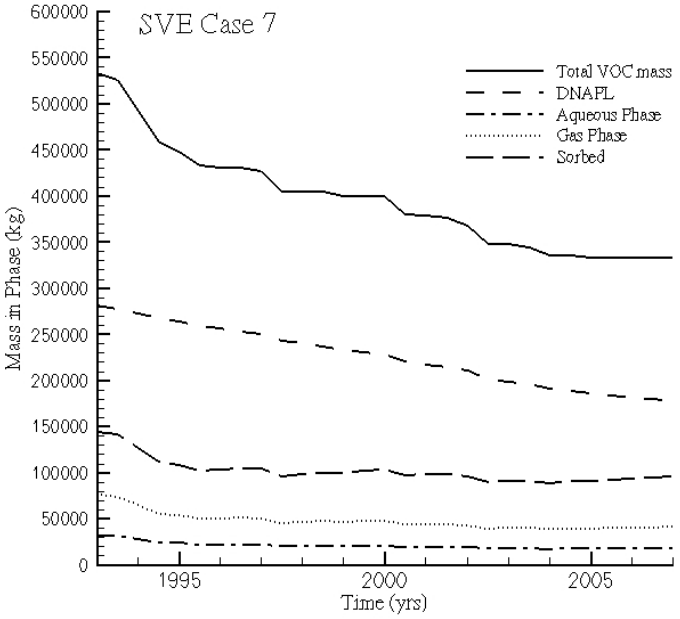

Figure 5.102. CT Mass Distribution Over the DNAPL, Sorbed, Aqueous, and Gas Phases for 1993 – 2007 (SVE Case 7)

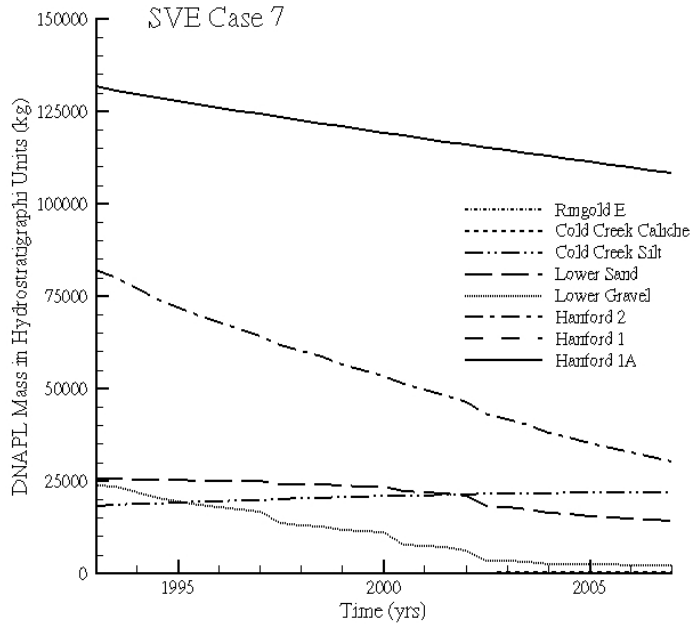

Figure 5.103. DNAPL CT Mass Distribution Over the Hydrostratigraphic Units for 1993 – 2007 (SVE Case 7)

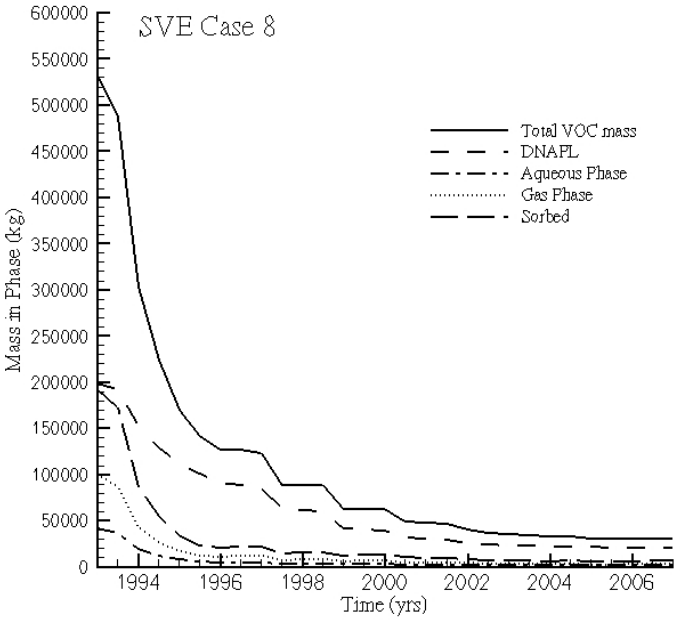

Figure 5.104. CT Mass Distribution Over the DNAPL, Sorbed, Aqueous, and Gas Phases for 1993 – 2007 (SVE Case 8)

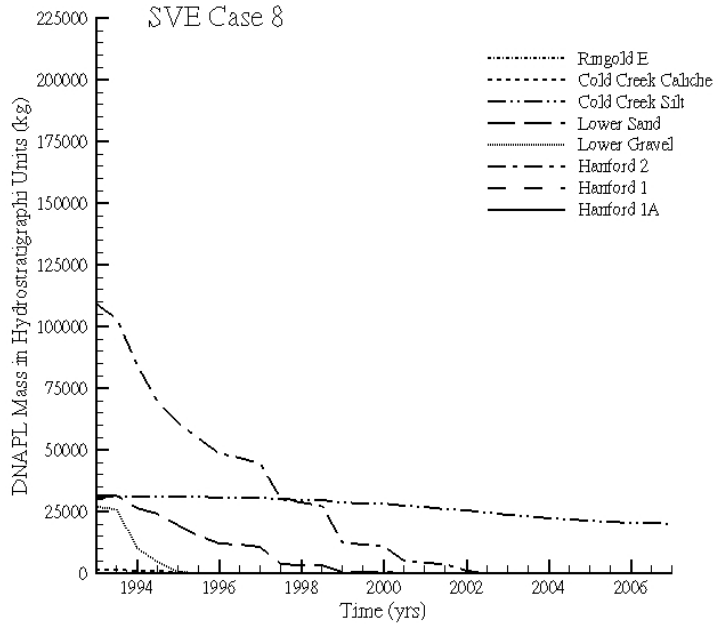

Figure 5.105. DNAPL CT Mass Distribution Over the Hydrostratigraphic Units for 1993 – 2007 (SVE Case 8)

5.5 Undocumented Discharge Simulations

A series of simulations was conducted for each of the major DNAPL sites to identify the minimum volume needed to result in DNAPL movement across the water table by 1993. The results of the iterative simulation are presented in Table 5.7. The results indicate that the minimum volume is 245 m^3, occurring at the 216-Z-9 site. The required volumes at the other two sites are approximately twice as high. The reasons for the differences are related to size of the disposal area, disposal rate, and subsurface geology. However, if the assumption is made that an undocumented discharge should have occurred at either a crib, french tile, or trench, similar to the 216-Z-9, 216-Z-1A, or 216-Z-18, volumes in the order of 250 m^3 are needed to result in DNAPL movement across the water table. Based on the available Hanford site information, additional disposal volumes of this magnitude, beyond what has been reported for the three major DNAPL sites, are not likely.

Table 5.7. Disposed DNAPL Volume at the 216-Z-9, 216-Z-1A, and 216-Z-18 Sites and the Volume Needed for Transport of a Minimum of 1 Kg CT Across the Water Table by 1993

DNAPL Site	Disposed Volume (m^3)	Disposed Volume Needed for Movement Across Water Table (m^3)
216-Z-9	316	245
216-Z-1A	242	475
216-Z-18	147	535

The results of the accidental spill simulation are listed in Table 5.8. The maximum penetration depth is 28 m, which is still above the CCU silt. The geologic domain without the H1a unit resulted in smaller penetration depths than the simulations where the H1a was included. The higher permeability of the H1 unit caused more lateral movement of the DNAPL and of the CT in the gas phase, resulting in less DNAPL available for vertical movement. The important information that may be derived from Table 5.8 regarding undocumented releases is that even fairly large spills of up to 10 m^3 do not result in DNAPL movement across the water table.

Table 5.8. Maximum Penetration Depth (m) for Several Spill Scenarios and Two Geologic Domains (The spill area is 1 m^2 for all cases.)

Spill Size (m^3)	Spill Duration	Penetration Depth Geologic Domain 1 (m)	Penetration Depth Geologic Domain 2 (m)
0.2	1 hour	6	5
0.2	1 day	5	4
0.2	10 days	3	2
1	1 hour	12	9
1	1 day	10	8
1	10 days	8	7
10	1 hour	n.d.	21
10	1 day	28	19
10	10 days	22	17
n.d.= Not determined due to excessive infiltration rate.			

6.0 Summary and Conceptual Model Update

A conceptual model of CT in the vadose zone and groundwater underlying the disposal sites defines the current understanding and the areas of uncertainty that need to be considered in characterization and modeling activities and to support remediation decisions. The conceptual model discussion for this report is focused on the subsurface near the disposal areas to provide a framework for describing the distribution of CT within the vadose zone, the source of CT for the existing groundwater plume, and the nature of any continuing source of CT to the groundwater plume from within the subsurface near the disposal areas. This discussion uses results of multi-phase modeling and assessment of published data near the disposal areas to refine the conceptual model that has been developed over time and summarized in the RI/FS Work Plan (DOE 2004). The conceptual model presented in the RI/FS Work Plan was the most recent conceptual model during the modeling effort described in this report. The conceptual model was updated for the RI report (DOE 2006). The discussion herein describes how the model results revise the conceptual model presented in the RI/FS Work Plan and how this update is consistent with and in addition to the conceptual model presented in the RI report.

Figure 6.1 illustrates the conceptual distribution of CT in the subsurface near the disposal areas as depicted in the RI/FS Work Plan (DOE 2004) and discusses the key overall components of this conceptual model. Based on the modeling results presented herein and in Oostrom et al. (2004; 2006), Figure 6.1 has been updated as a revised overall conceptual model shown in Figure 6.2. Both Figures 6.1 and 6.2 describe how CT in the DNAPL and other phases are distributed through the subsurface, but do not necessarily represent a "picture" of the CT distribution at any given time. In addition to a static picture of the conceptual model for CT, modeling provides information about the variation in CT distribution over time. Thus, the revisions to the previous conceptual model include a temporal component to interpreting CT distribution in the subsurface. A conceptual depiction of temporal variation in the CT distribution over time for the 216-Z-9 and216-Z-1A are shown in Figures 6.3 and 6.4, respectively, for the years 1966, 1974, 1993, and 2000, and for the 216-Z-18 in Figure 6.5 for the years 1974, 1993, and 2000. The key revisions to the updated overall conceptual model of the RI/FS Work Plan (DOE 2004) are listed below. These items are consistent with the conceptual model update shown in the RI report (DOE 2006). However, as discussed below, the simulation results provide additional information to further refine the conceptual model presented in the RI report (DOE 2006).

1. No lateral movement of DNAPL to under the Plutonium Finishing Plant is likely.

2. The zones of persistent CT mass in the vadose zone are primarily the CCU and H1a unit.

3. Large vertical and lateral density-driven vapor movement of occurred in the past.

4. DNAPL penetration to groundwater is likely to have occurred at the 216-Z-9 site, is possible at the 216-Z-1A site, and unlikely at the 216-Z-18 site.

5. The phase distribution of CT changes over time due to volatilization, interaction of gas-phase CT with pore water and aqueous-phase CT with sorbed phase, DNAPL dissolution in groundwater, and the impact of soil vapor extraction.

The overall revisions to the conceptual model are supported by both modeling results and existing published data. Figure 6.6 shows comparison of the simulated CT DNAPL distribution and the existing

published soil data (tabulated in Appendix A, Table A.1). The vertical distribution of CT in groundwater beneath the disposal sites from field data and a three-dimensional model of the CT distribution in groundwater developed through geostatistical modeling of the CT data (Murray et al. 2006) are shown in Figure 6.7 (data tabulated in Appendix A, Table A.2). Key conclusions from this information are listed below.

- High soil concentrations and predicted areas with high DNAPL saturations are spread vertically within a relatively small lateral area within about 30 m of the disposal area footprint.

- Measured groundwater concentrations are higher and the high groundwater concentrations are spread deeper in the aquifer beneath the 216-Z-9 site compared to the 216-Z-1A and 216-Z-18 sites. This observation correlates to modeling results where the CT flux to the groundwater at the 216-Z-9 site was significantly higher than the flux at the 216-Z-1A and 216-Z-18 sites. Modeling results showing a larger number of sensitivity simulations with DNAPL flux into groundwater and deeper penetration of DNAPL within the aquifer beneath the 216-Z-9 site, as compared to the other two disposal areas are also consistent with these observations.

While these overall changes to the conceptual model are important, it is equally important to assess the behavior of CT at key locations and interfaces in the subsurface to better understand the distribution of CT within the vadose zone, the source of CT for the existing groundwater plume, and the nature of any continuing source of CT to the groundwater plume from within the subsurface near the disposal areas.

Modeling results show accumulation within the CCU. Measured CT concentrations in vadose zone soil samples from wells within 30 m of the disposal areas are consistent with these modeling results, where the CT concentration averages 2424 µg/kg within the CCU and 444 µg/kg in other units within the vadose zone, based on samples with data above the detection limit. After initial infiltration and redistribution of the CT in the vadose zone, CT is retained in the CCU and the flux in or out of the unit is expected to be very small and only primarily via the vapor phase. While the flux in the vapor phase can be impacted by SVE above or below the CCU, the CCU is likely a location where CT will be present over the long term. Other portions of the vadose zone with a large percentage of small particle size sediments (e.g., silt lenses) would also be expected to accumulate CT based on the modeling results. Consistent with these results, for wells within 30 m of the disposal areas, the measured CT concentrations in vadose zone soil samples with an M, sM, (g)M, (g)sM, gM, gsM, or mS sediment classification average 2099 µg/kg (not including one sample that was 380,000 µg/kg) compared to an average of 528 µg/kg for all other sediment classifications (based on samples with data above the detection limit).

Modeling results also show that CT DNAPL is distributed vertically below the disposal areas with minimal lateral spreading (see Tables 5.3 – 5.6 and Oostrom et al. 2004; 2006). With this pattern of DNAPL migration, the most likely location for any DNAPL remaining in the subsurface would be vertically below the disposal areas. Measured vadose zone soil data (see Appendix A, Table A.1) also show low CT concentrations at distances greater than 30 m from the disposal areas, where CT concentrations average 79 µg/kg and within the CCU at these locations the CT averages only 81 µg/kg (based on samples with data above the detection limit) compared to the much higher CT concentrations vertically beneath the disposal areas (laterally within 30 m of the disposal area) shown above. Additionally, of 408 vadose zone soil samples from wells within 30 m of the disposal areas, only 70 were below detection limit (~17%) compared to 215 out of 258 samples below detection limit (83%) for soil samples greater than 30 m from the disposal areas.

Assessing mass flux at key interfaces provides another means to refine the conceptual model for CT. While mass flux measurements in the subsurface are difficult, modeling readily provides mass flux estimates. The mass flux estimates are related to the conceptual model and to measured data because the flux estimates can be used describe the amount of mass that has moved past an interface as a function of time. For instance, Murray et al. (2006) estimated the mass of CT within the groundwater based on recent data and how much CT would need to have been added to the groundwater to result in this mass estimate if hydrolysis were continually degrading CT at a specified rate. Using these estimates, the flux of CT across the groundwater since initial disposal that would be needed to accumulate the estimated mass of CT in the groundwater can be calculated. Model results can then be compared to this flux estimate to evaluate reasonable scenarios for how CT entered the groundwater. For instance, with 100,000 kg of CT that entered the aquifer (based on the estimate in Murray et al. 2006), only by combining the estimates of CT mass flux to the groundwater from simulation sensitivities (not the base cases) that show DNAPL crossing the water table, can a combined mass of CT (216-Z-9, 216-Z-18, and 216-Z-1A) in the aquifer near the estimated CT mass be predicted. The average CT mass of dissolved CT that has been transported across the water table (a measure of the impact of vapor phase transport to the groundwater table and pore water from the vadose zone entering the groundwater) for all three sites through 1993 is approximately 5,000-10,000 kg. The accumulated mass in the aquifer would be significantly lower than the mass of CT in the groundwater estimated by Murray et al. (2006) if only aqueous and vapor phase CT and no DNAPL phase entered the groundwater. This assessment indicates that it is likely that DNAPL CT has entered the groundwater. The simulation results herein and in Oostrom et al. (2004; 2006) show that the most likely location of significant DNAPL movement across the water table is below the 216-Z-9 site. In the base case simulation and other simulation sensitivities where DNAPL enters the groundwater, the DNAPL flux below the 216-Z-9 site ceases by 1995, when SVE was employed. Without the inclusion of SVE in the simulations, DNAPL movement across the water table is predicted to continue, though at a low flux through the present day.

The estimated amount of CT in the groundwater by Murray et al. (2006) does not include any DNAPL mass that may be in the aquifer now. For simulations where the mass of CT entering the groundwater is just equal to the mass of CT in the groundwater estimated by Murray et al. (2006), all of the DNAPL would need to be dissolved and distributed within the plume at the present time. For simulations where the mass of CT entering the groundwater is greater that the mass of CT in the groundwater estimated by Murray et al. (2006), DNAPL may still be present in the aquifer. In these cases, modeling results suggest that the DNAPL would be localized to the portion of the aquifer beneath the disposal areas (in particular at the 216-Z-9 disposal area) and laterally only within a relatively localized areal extent.

In the previous conceptual model (RI/FS Work Plan, DOE 2004), there are multiple components of the conceptual model that are included as potential mechanisms for how CT distributes through the vadose zone and groundwater near the disposal areas. The following analysis provided additional evaluation of how CT is distributed within the subsurface to help assess the importance of processes other than the CT movement simulated in the modeling effort.

Undocumented Sources – The conceptual model in the RI/FS Work Plan (DOE 2004) notes that undocumented sources may contribute to the CT plume in the groundwater. The following assessment provides information that can be used to describe the magnitude of disposal at an undocumented source that would be needed for CT for this source to have a significant impact on groundwater. A series of simulations was conducted to estimate the volume of DNAPL that is required to result in DNAPL

movement across the water table for all three sites. The simulations revealed that at least 250 m^3 of DNAPL are necessary for this movement to occur if the DNAPL would have been disposed at typical waste site in the 200 West Area. Additional DNAPL volumes of that magnitude beyond what has been commonly reported for the three major DNAPL sites, are not likely. Undocumented CT sources might have also been the result of accidental spills. The simulations outlined in Chapter 4.3 considered accidental releases ranging from 0.2 m^3 to 10.0 m^3 (approximately 1 - 50 drums) of CT DNAPL, disposed on an area of 1 m^2 for infiltration time ranging from 1 hour to 10 days. The maximum simulated infiltration depth of CT DNAPL was 28 m for the case where 50 barrels were allowed to infiltrate in 1 day. This distance is not even enough for the CT DNAPL to reach the CCU. The limited infiltration depth is directly related to sorption and mass transfer into the aqueous and gas phases as well as gaseous transport away from the infiltration zone due to advection and diffusion. Considering the size of the simulated CT DNAPL spill volumes (up to 10 m^3), it is also unlikely that an undocumented spill of CT DNAPL would have been able to reach the water table.

Effect of Water Infiltration at Other Locations – Water was disposed of at sites other than the CT disposal areas. Future modeling with a larger model that encompasses all three CT disposal areas and nearby water infiltration sites (e.g., U Pond) can be conducted to support an assessment of how these water sources can impact CT distribution. The localized models used herein and by Oostrom et al. (2004 and 2006) do not directly address this issue.

Impact of Vapor Phase CT on Distribution of CT in the Groundwater – The simulation results show that CT in the gas phase is likely to have moved considerable distances in the lateral direction due to diffusion and advection. In particular, extensive CT gas plumes are predicted to develop on top of the water table. Part of the CT from the gas phase transfers into the aqueous phase but, since the diffusion transport process in the saturated zone is much smaller than in the gas phase, the amount of CT that is able to move below the water table through this process is relatively small.

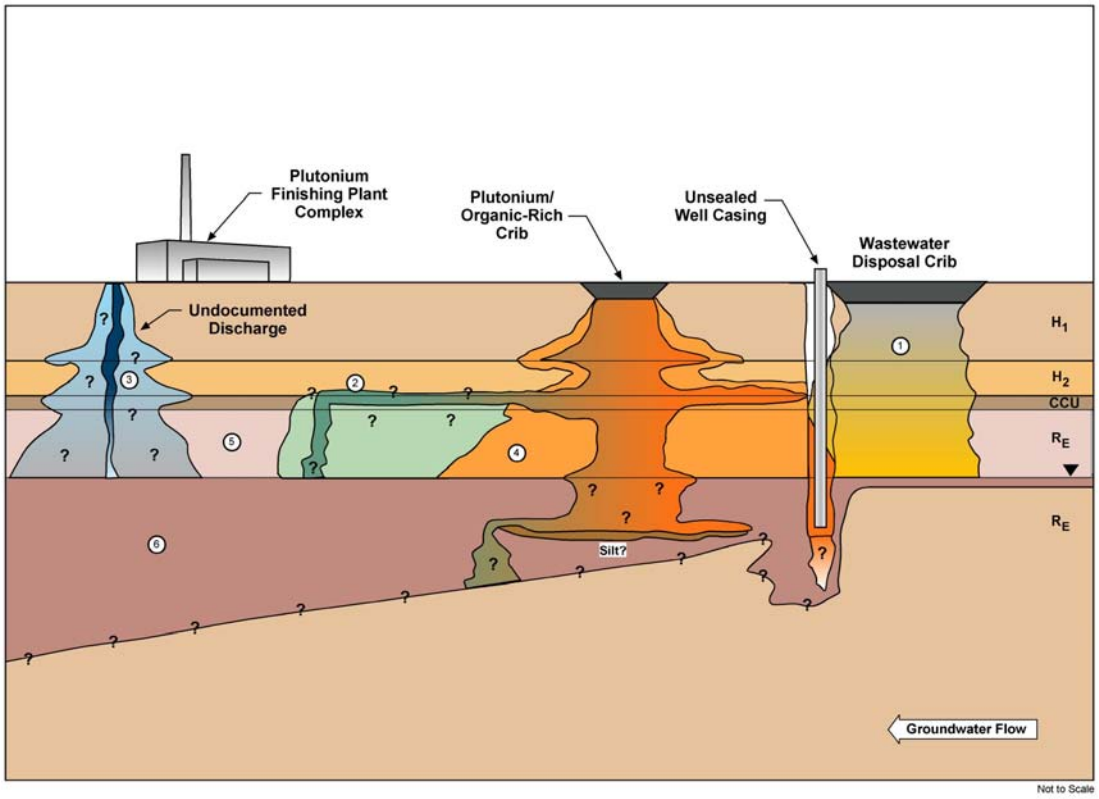

(1) Downward migration of carbon tetrachloride (aqueous and/or non-aqueous phase liquid) through plutonium/organic-rich cribs and underlying soil column to groundwater with lateral migration with groundwater.

(2) Downward migration of carbon tetrachloride (aqueous and/or non-aqueous phase liquid) through plutonium/organic-rich cribs and underlying soil column to Cold Creek unit with lateral migration along top of Cold Creek unit. Carbon tetrachloride migrates vertically through the Cold Creek unit to the groundwater with lateral migration with groundwater.

(3) Downward migration of carbon tetrachloride (aqueous and/or non-aqueous phase liquid) to groundwater from an undocumented source.

(4) Downward migration of carbon tetrachloride vapor from plutonium/organic-rich crib to groundwater in vicinity of crib, with lateral migration with groundwater, or downward and lateral migration of vapor to groundwater.

(5) Carbon tetrachloride vapor may volatilize from the carbon tetrachloride dissolved in groundwater

(6) Carbon tetrachloride dissolved in groundwater from liquid and vapor sources.

H_1	Hanford formation gravel dominated sequence
H_2	Hanford formation sand dominated sequence
CCU	Cold Creek unit silt and carbonate
R_E	Ringold Formation, Unit E gravel
▽	Water table

Figure 6.1. Conceptual Model Presented in the RI/FS Work Plan (DOE 2004)

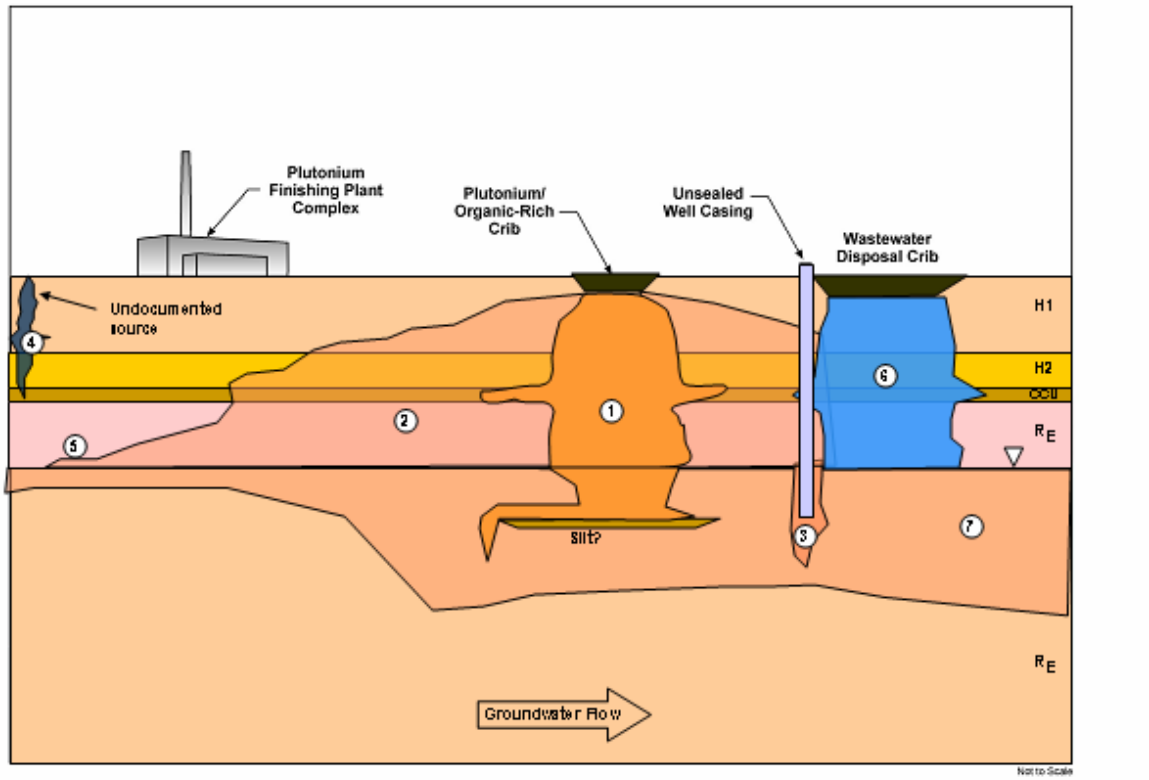

1 – Downward migration of CT in subsurface beneath disposal cribs with moderate lateral spreading in the CCU and DNAPL penetration to the groundwater likely for the 216-Z-9 site, possible for the 216-Z-1A site, and unlikely for the 216-Z-18 site. Accumulation of DNAPL in the HIA unit just below the 216-Z-1A and 216-Z-18 sites.

2 – Significant lateral spreading of CT in the vapor phase and associated aqueous and sorbed phases. Bell-shaped vapor plume due to density of plume.

3 – Potential vertical migration of aqueous or DNAPL CT in unsealed well casings. (not addressed in this modeling study)

4 – Potential vertical migration of CT from undocumented sources to groundwater is unlikely.

5 – Interaction of vapor phase and dissolved CT across the water table. Can create vapor plume or shallow groundwater plume depending on concentration gradient.

6 – Infiltrated water at other disposal cribs may impact vapor plume and carry dissolved CT to groundwater. (not directly addressed in this modeling study)

7 – Migration of dissolved phase CT with groundwater.

Figure 6.2. Revised Overall Conceptual Model for CT Migration within the Subsurface

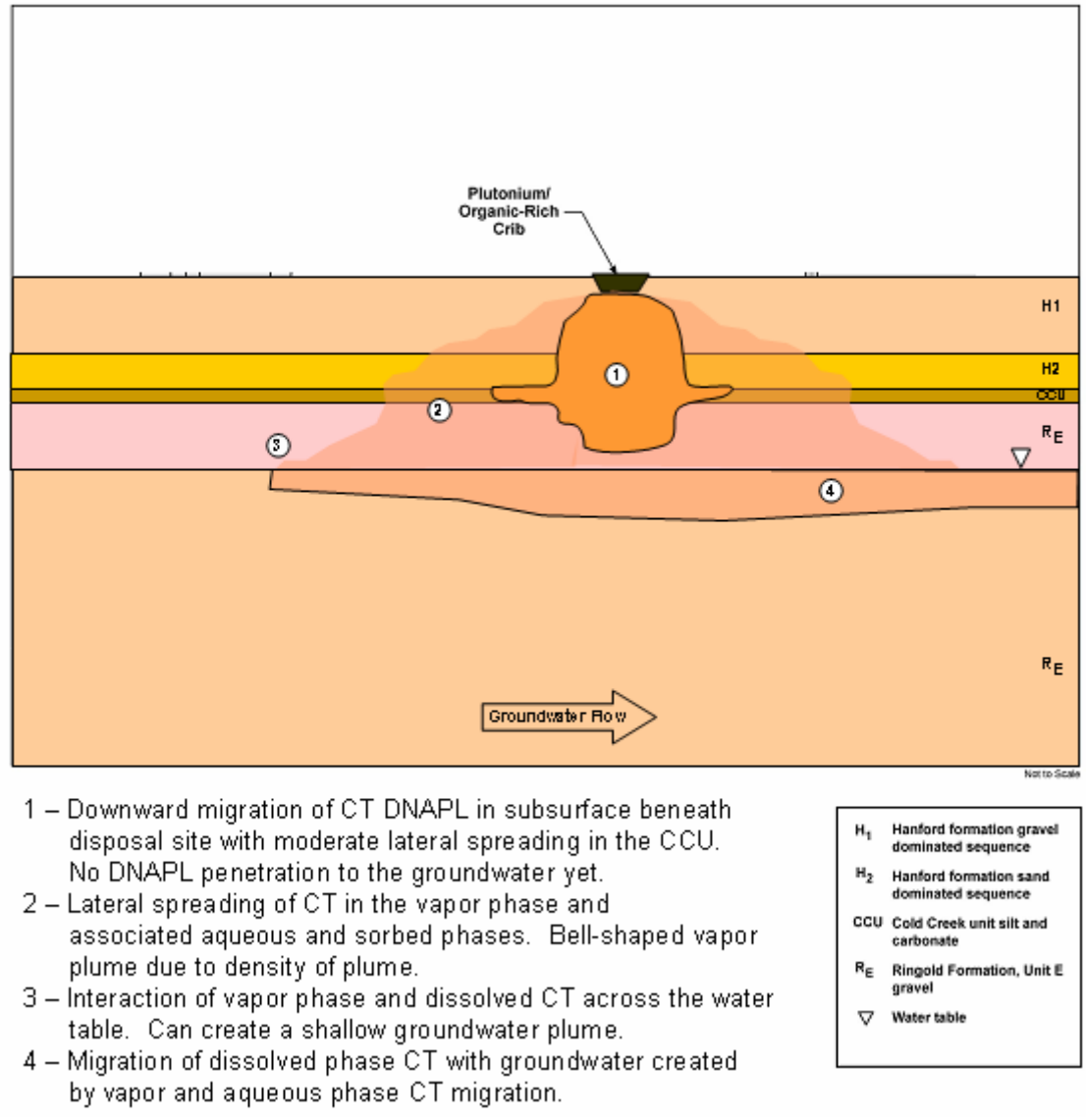

Figure 6.3a. Conceptual Distribution of Carbon Tetrachloride from Waste Disposed at the 216-Z-9 Site in the Years 1966 (a), 1974 (b), 1993 (c), and 2000 (d). (These figures are based on the results of the base case simulations. Note that some sensitivity simulations show significantly different results. The figure for the year 2000 shows the conceptual impact of soil vapor extraction remediation operations.)

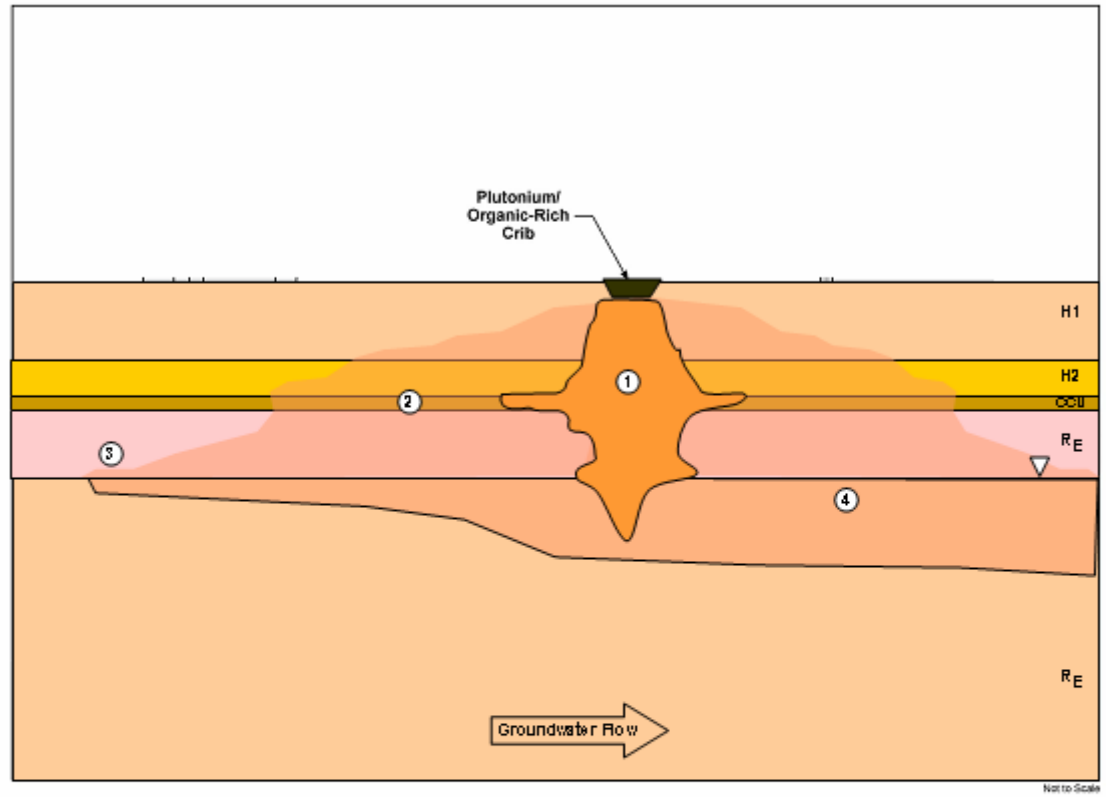

1 – Downward migration of CT DNAPL in subsurface beneath disposal site with moderate lateral spreading in the CCU. DNAPL penetration into the groundwater.
2 – Lateral spreading of CT in the vapor phase and associated aqueous and sorbed phases. Bell-shaped vapor plume due to density of plume.
3 – Interaction of vapor phase and dissolved CT across the water table. Can create a shallow groundwater plume.
4 – Migration of dissolved phase CT with groundwater created by DNAPL, vapor, and aqueous phase CT migration.

H_1	Hanford formation gravel dominated sequence
H_2	Hanford formation sand dominated sequence
CCU	Cold Creek unit silt and carbonate
R_E	Ringold Formation, Unit E gravel
▽	Water table

Figure 6.3b. Conceptual Distribution of Carbon Tetrachloride from Waste Disposed at the 216-Z-9 Site in the Years 1966 (a), 1974 (b), 1993 (c), and 2000 (d). (These figures are based on the results of the base case simulations. Note that some sensitivity simulations show significantly different results. The figure for the year 2000 shows the conceptual impact of soil vapor extraction remediation operations.)

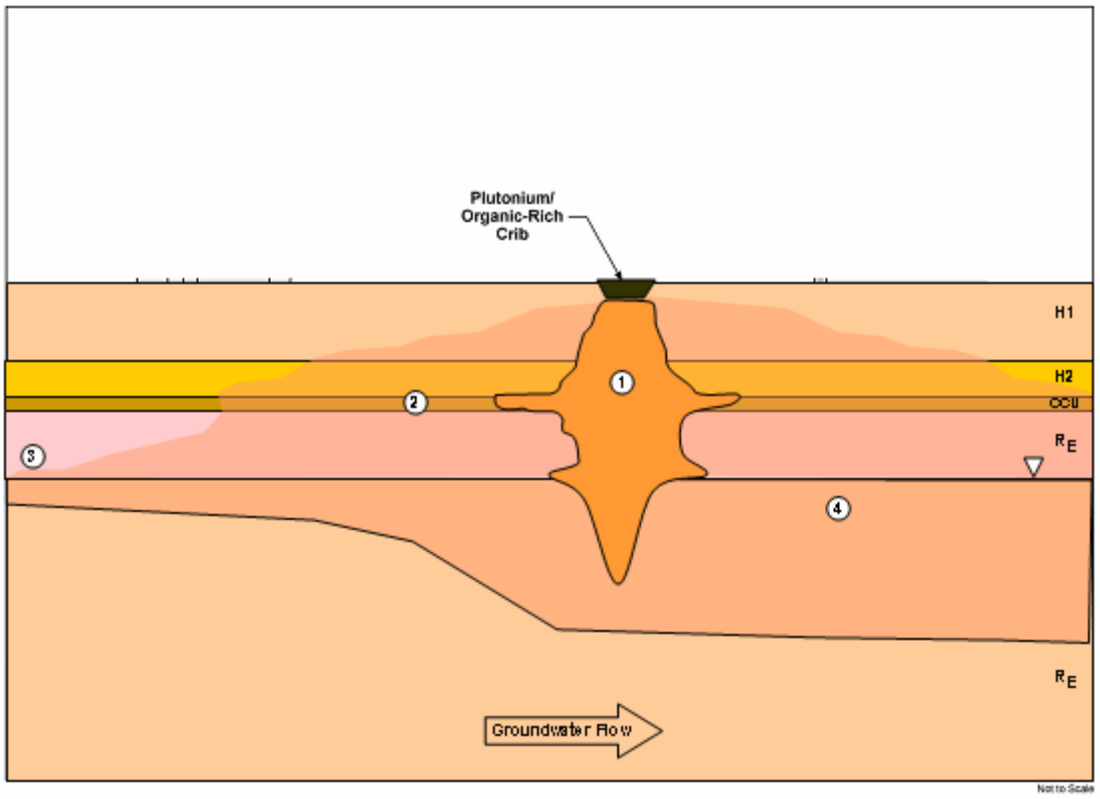

1 – Downward migration of CT DNAPL in subsurface beneath disposal site effectively ceased. Residual DNAPL in zone beneath disposal site. DNAPL penetration into the groundwater.
2 – Lateral spreading of CT in the vapor phase and associated aqueous and sorbed phases. Bell-shaped vapor plume due to density of plume.
3 – Interaction of vapor phase and dissolved CT across the water table. Can create a shallow groundwater plume.
4 – Migration of dissolved phase CT with groundwater created by DNAPL, vapor, and aqueous phase CT migration.

H_1	Hanford formation gravel dominated sequence
H_2	Hanford formation sand dominated sequence
CCU	Cold Creek unit silt and carbonate
R_E	Ringold Formation, Unit E gravel
▽	Water table

Figure 6.3c. Conceptual Distribution of Carbon Tetrachloride from Waste Disposed at the 216-Z-9 Site in the Years 1966 (a), 1974 (b), 1993 (c), and 2000 (d). (These figures are based on the results of the base case simulations. Note that some sensitivity simulations show significantly different results. The figure for the year 2000 shows the conceptual impact of soil vapor extraction remediation operations.)

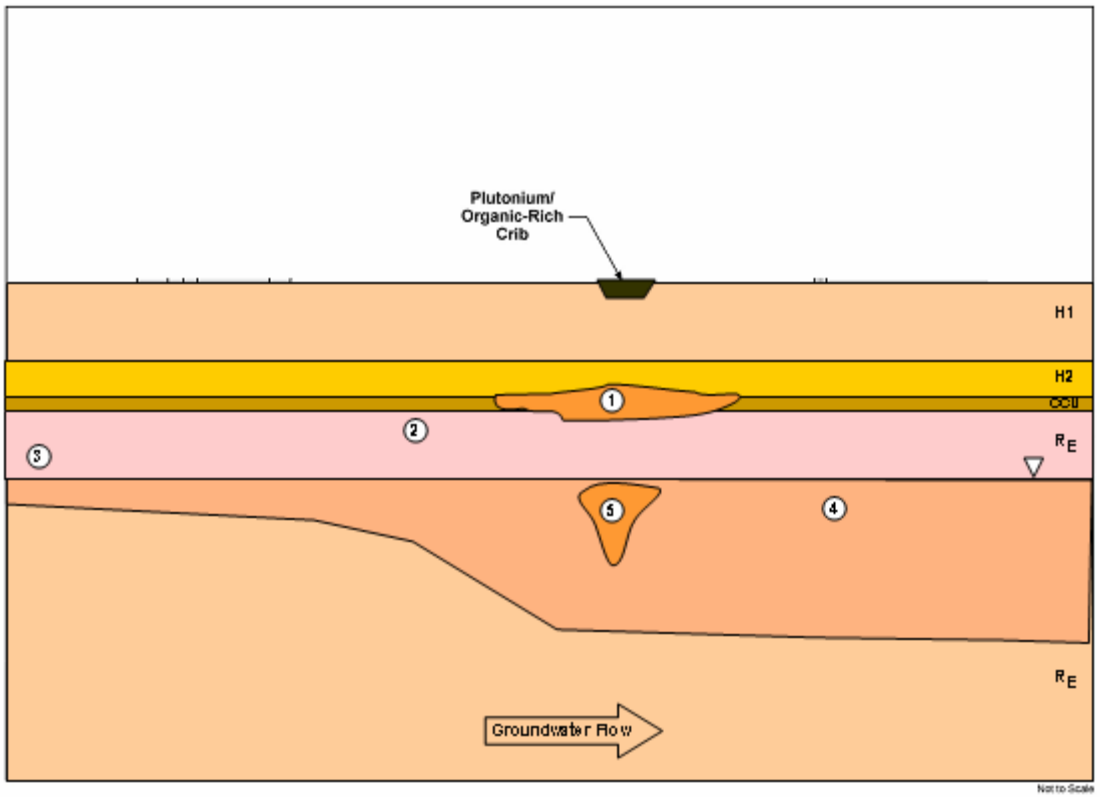

1 – Residual CT DNAPL in the subsurface, primarily in the CCU.
2 – Significantly reduced vapor plume due to SVE operations. Potentially reduced aqueous and sorbed plumes in the vadose zone.
3 – Interaction of vapor phase and dissolved CT across the water table. Can create vadose plume from groundwater contamination.
4 – Migration of dissolved phase CT with groundwater created by DNAPL, vapor, and aqueous phase CT migration.
5 – Potentially residual DNAPL in the groundwater beneath the disposal site. DNAPL extent reduced by dissolution over time.

H_1	Hanford formation gravel dominated sequence
H_2	Hanford formation sand dominated sequence
CCU	Cold Creek unit silt and carbonate
R_E	Ringold Formation, Unit E gravel
▽	Water table

Figure 6.3d. Conceptual Distribution of Carbon Tetrachloride from Waste Disposed at the 216-Z-9 Site in the Years 1966 (a), 1974 (b), 1993 (c), and 2000 (d). (These figures are based on the results of the base case simulations. Note that some sensitivity simulations show significantly different results. The figure for the year 2000 shows the conceptual impact of soil vapor extraction remediation operations.)

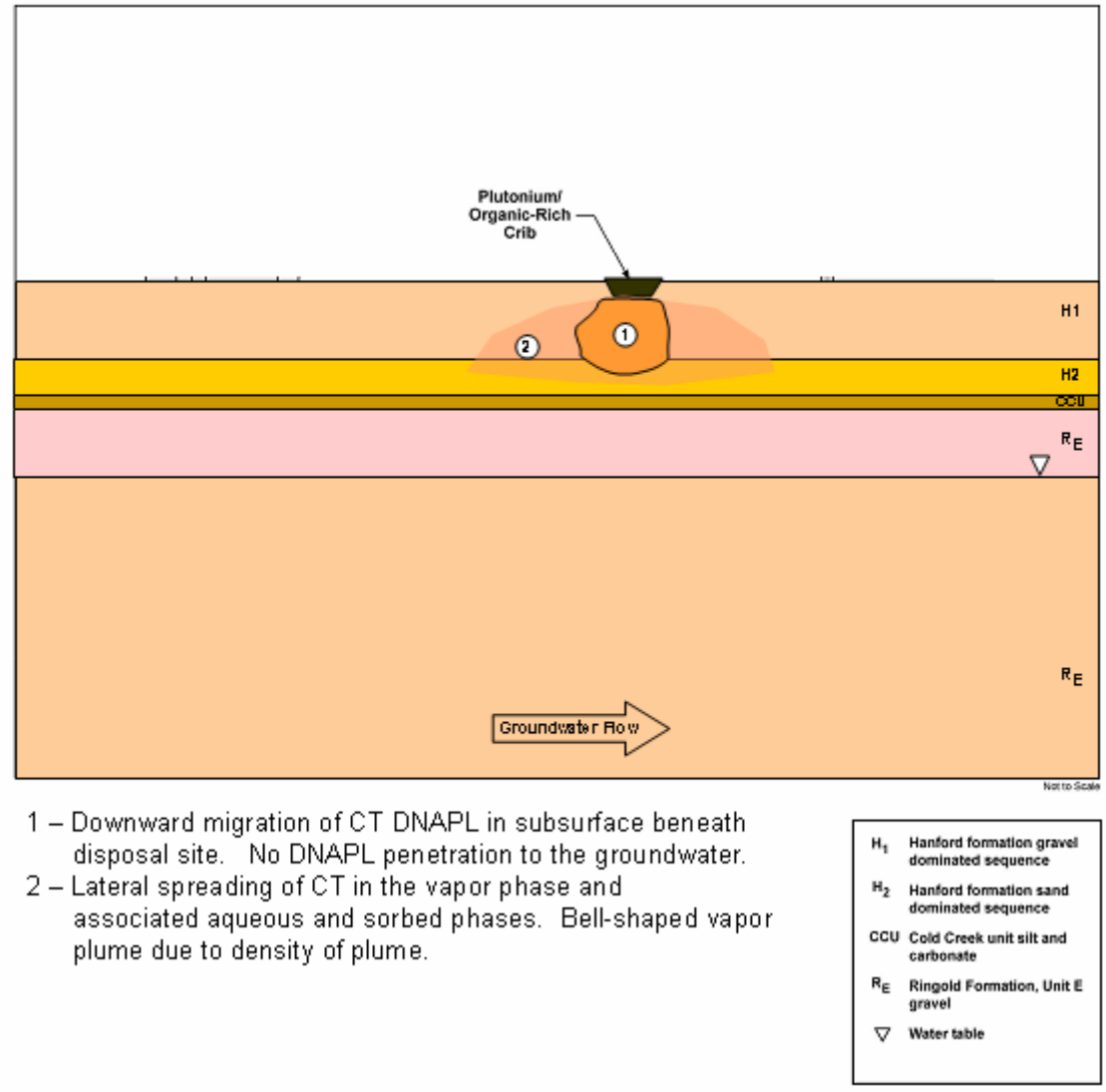

Figure 6.4a. Conceptual Distribution of Carbon Tetrachloride from Waste Disposed at the 216-Z-1A Site in the Years 1966 (a), 1974 (b), 1993 (c), and 2000 (d). (These figures are based on the results of the base case simulations. Note that some sensitivity simulations show significantly different results. The figure for the year 2000 shows the conceptual impact of soil vapor extraction remediation operations.)

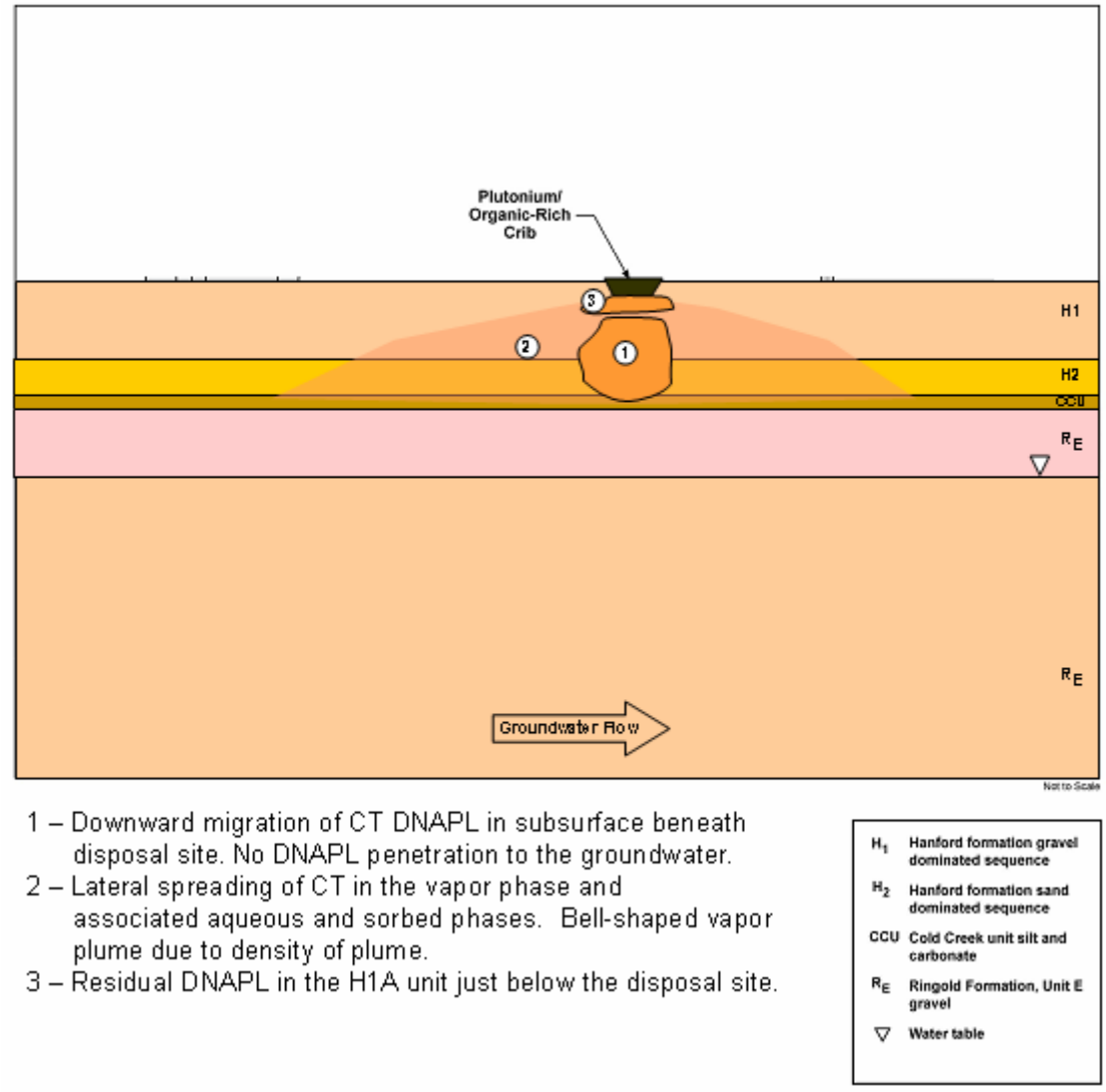

Figure 6.4b. Conceptual Distribution of Carbon Tetrachloride from Waste Disposed at the 216-Z-1A Site in the Years 1966 (a), 1974 (b), 1993 (c), and 2000 (d). (These figures are based on the results of the base case simulations. Note that some sensitivity simulations show significantly different results. The figure for the year 2000 shows the conceptual impact of soil vapor extraction remediation operations.)

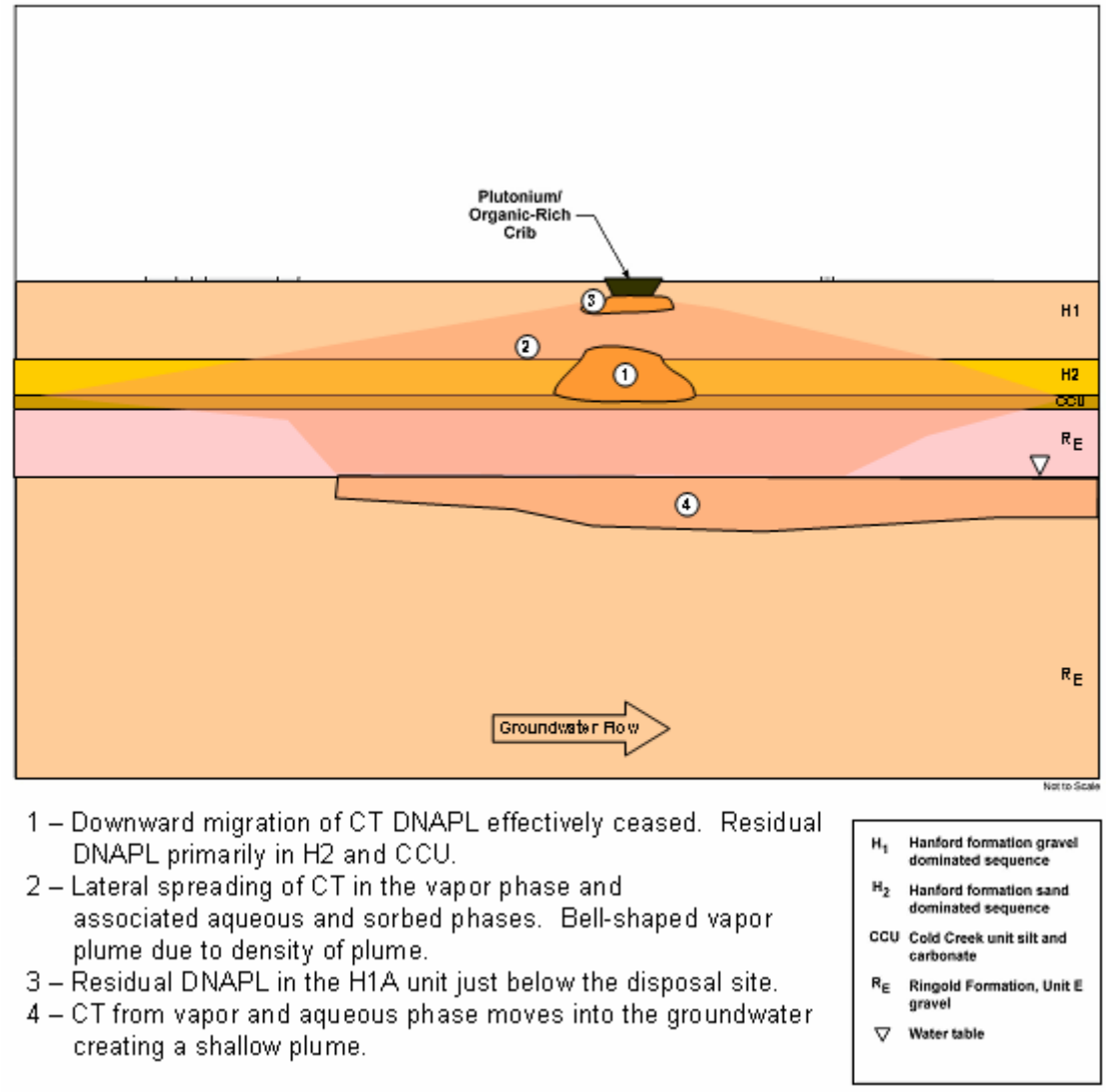

Figure 6.4c. Conceptual Distribution of Carbon Tetrachloride from Waste Disposed at the 216-Z-1A Site in the Years 1966 (a), 1974 (b), 1993 (c), and 2000 (d). (These figures are based on the results of the base case simulations. Note that some sensitivity simulations show significantly different results. The figure for the year 2000 shows the conceptual impact of soil vapor extraction remediation operations.)

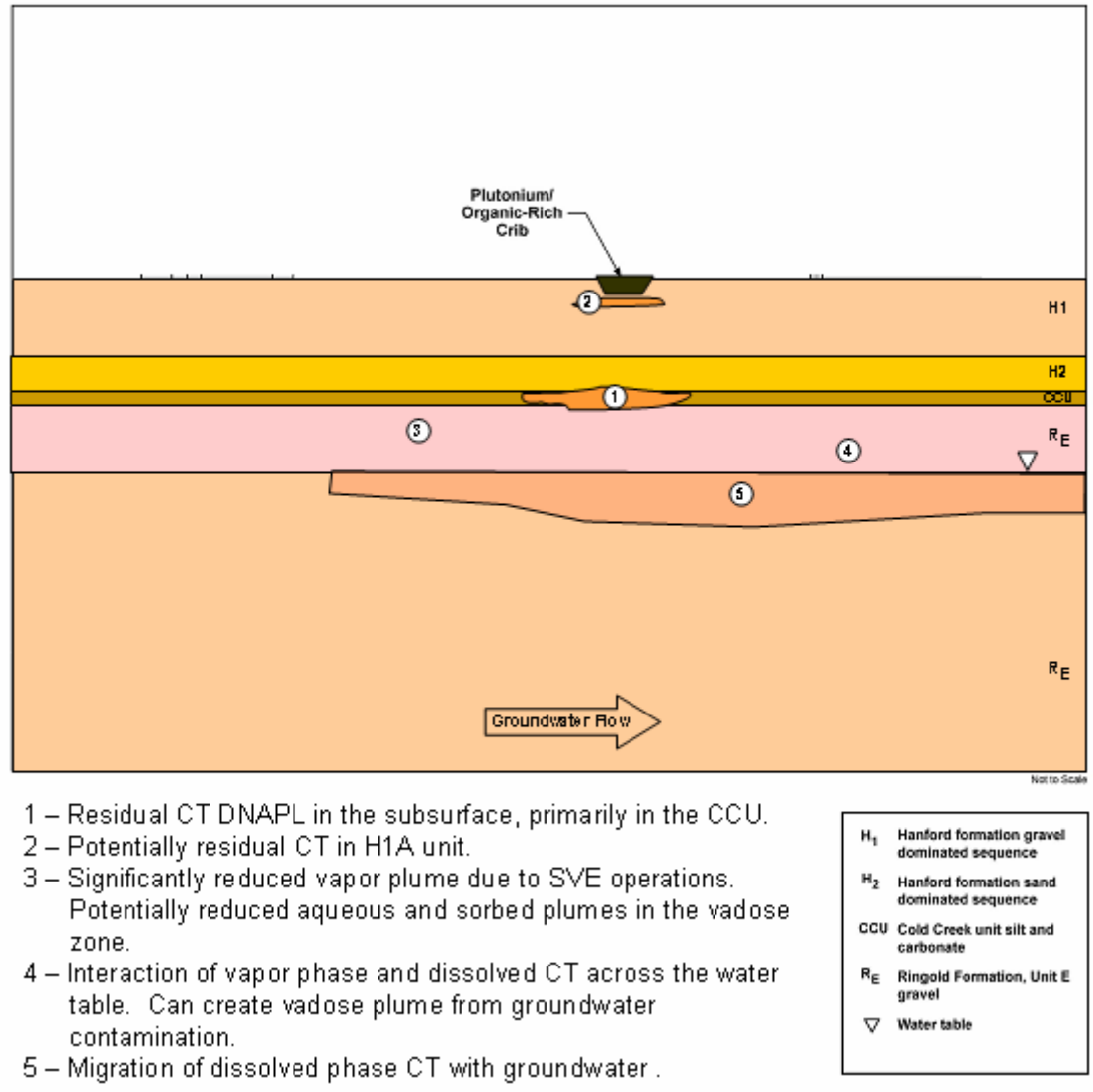

Figure 6.4d. Conceptual Distribution of Carbon Tetrachloride from Waste Disposed at the 216-Z-1A Site in the Years 1966 (a), 1974 (b), 1993 (c), and 2000 (d). (These figures are based on the results of the base case simulations. Note that some sensitivity simulations show significantly different results. The figure for the year 2000 shows the conceptual impact of soil vapor extraction remediation operations.)

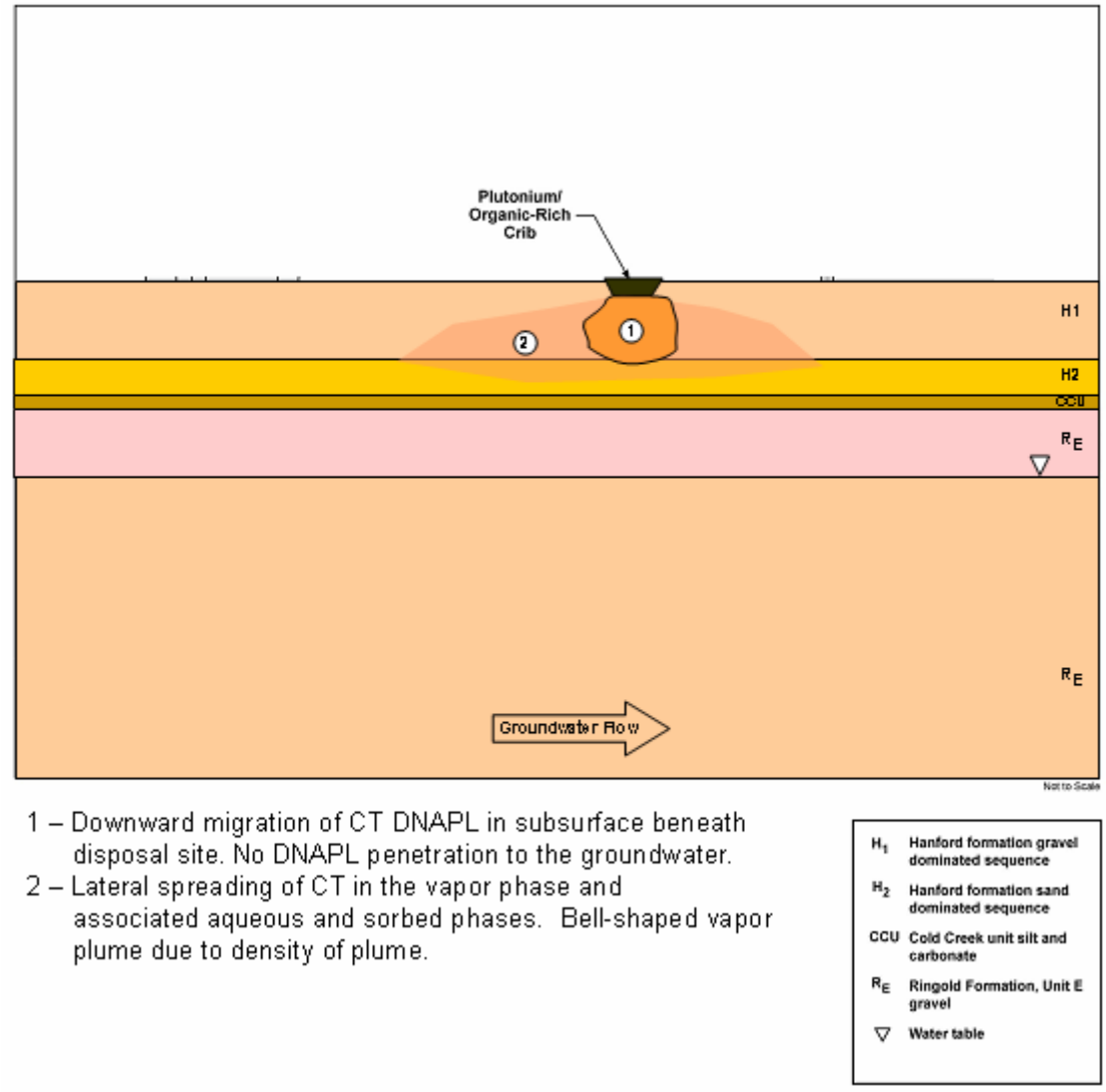

Figure 6.5a. Conceptual Distribution of Carbon Tetrachloride from Waste Disposed at the 216-Z-18 Site in the Years 1974 (a), 1993 (b), and 2000 (c). (These figures are based on the results of the base case simulations. Note that some sensitivity simulations show significantly different results. The figure for the year 2000 shows the conceptual impact of soil vapor extraction remediation operations.)

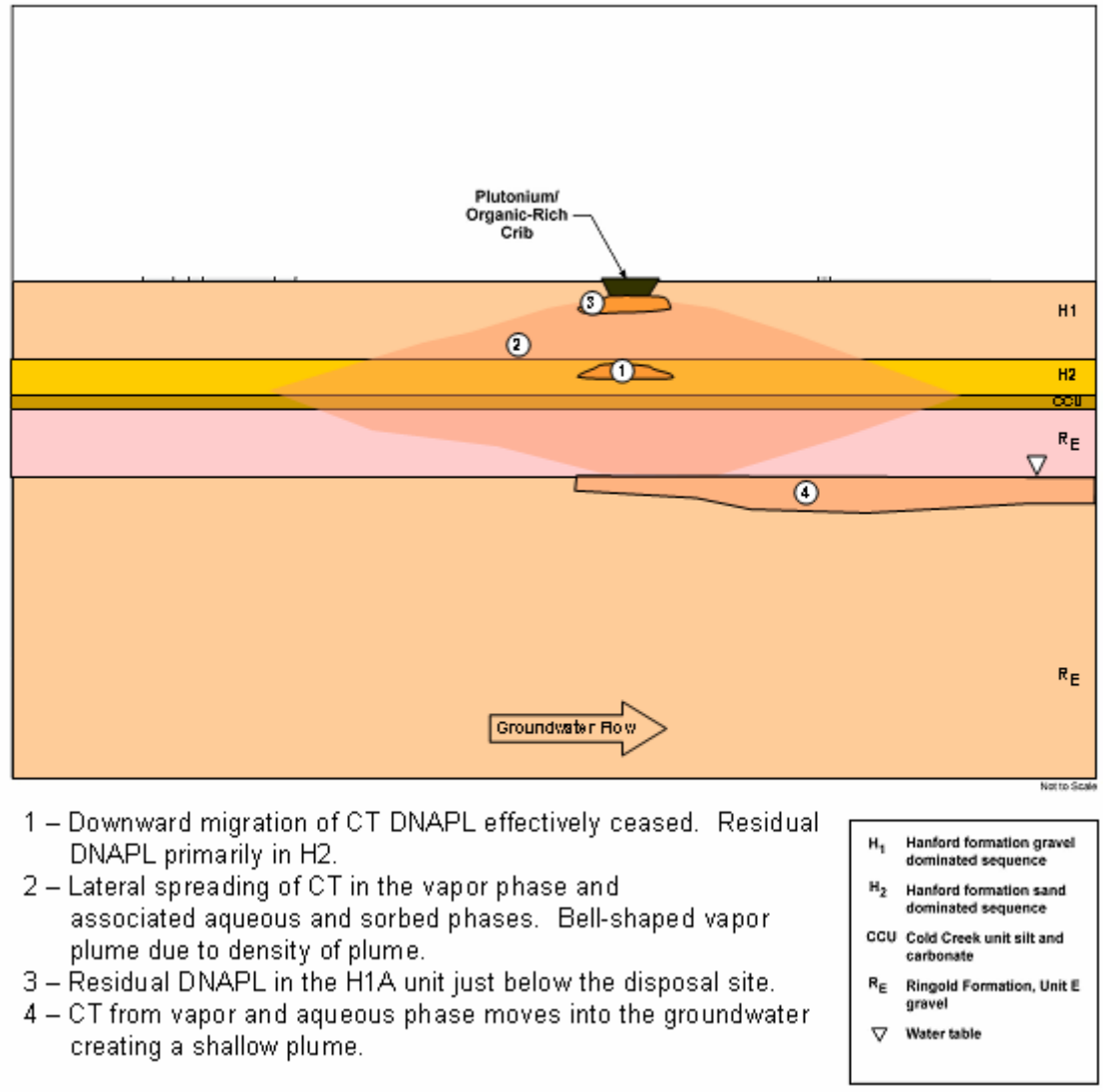

Figure 6.5b. Conceptual Distribution of Carbon Tetrachloride from Waste Disposed at the 216-Z-18 Site in the Years 1974 (a), 1993 (b), and 2000 (c). (These figures are based on the results of the base case simulations. Note that some sensitivity simulations show significantly different results. The figure for the year 2000 shows the conceptual impact of soil vapor extraction remediation operations.)

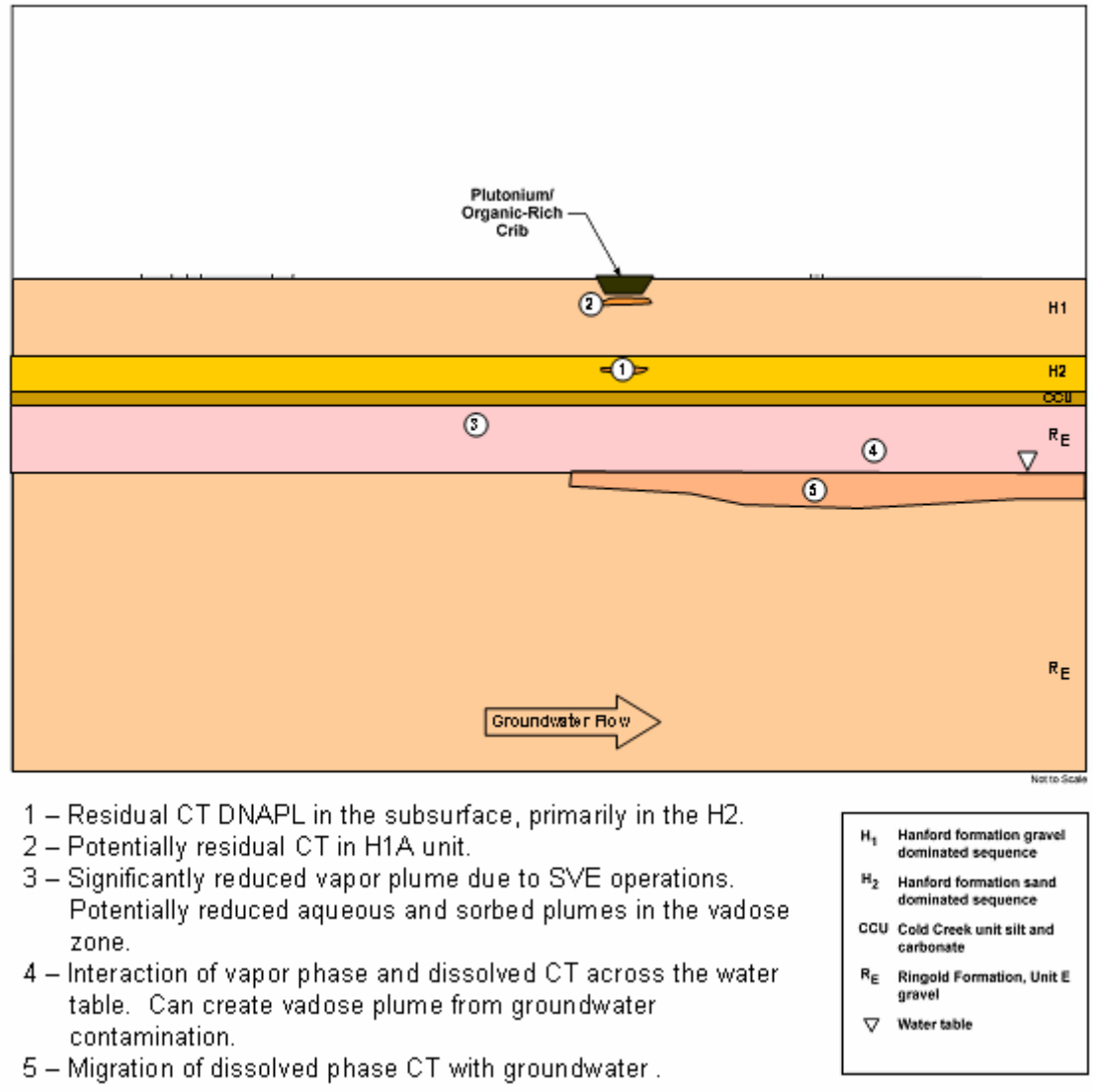

Figure 6.5c. Conceptual Distribution of Carbon Tetrachloride from Waste Disposed at the 216-Z-18 Site in the Years 1974 (a), 1993 (b), and 2000 (c). (These figures are based on the results of the base case simulations. Note that some sensitivity simulations show significantly different results. The figure for the year 2000 shows the conceptual impact of soil vapor extraction remediation operations.)

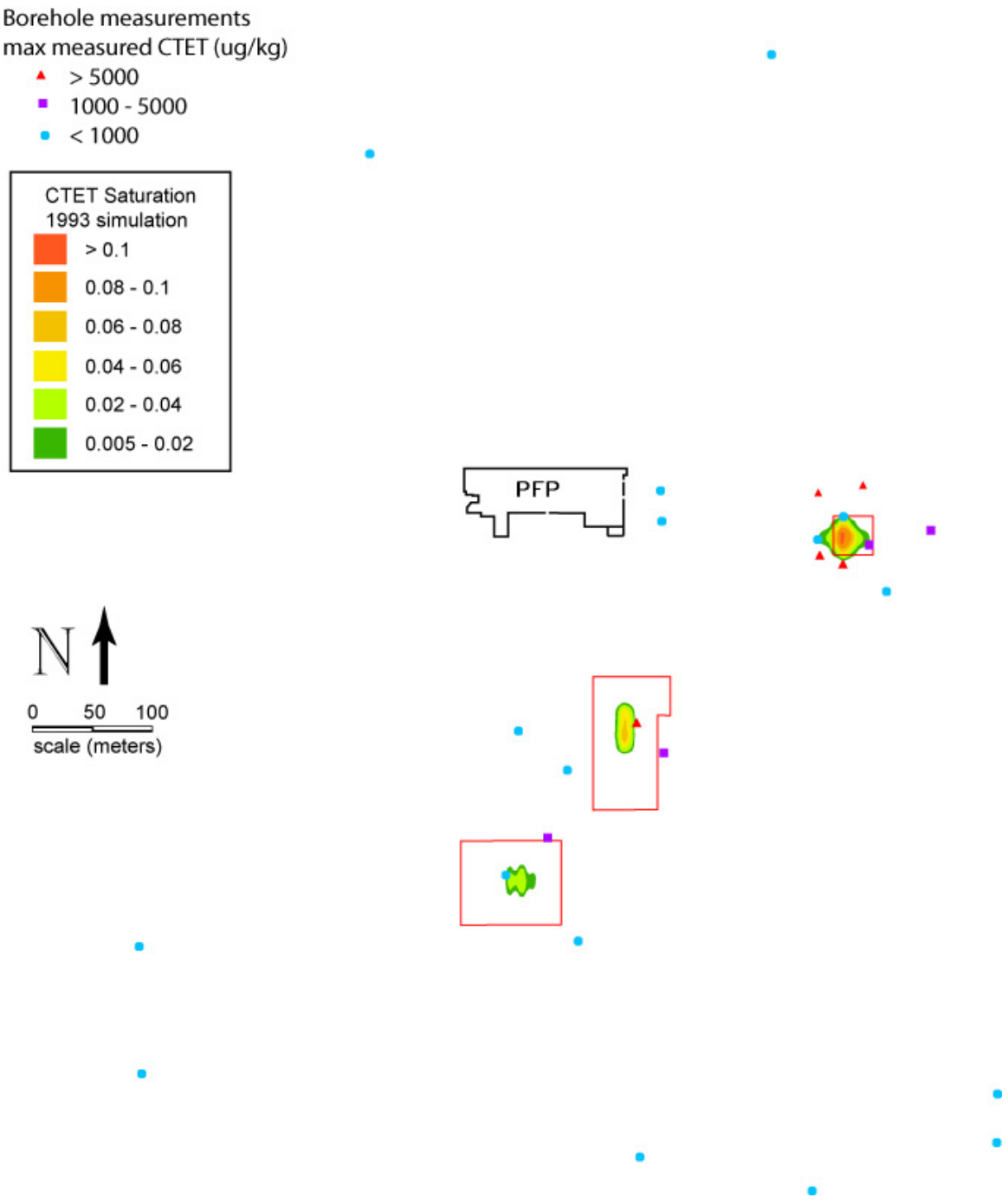

Figure 6.6. Areal Extent of the Zone with Greater than 1% DNAPL Saturation from Base-Case Simulations Compared to Measured Soil Concentrations of CT in Vadose Zone at Nearby Boreholes (The maximum concentration measured in each well is shown in the figure.)

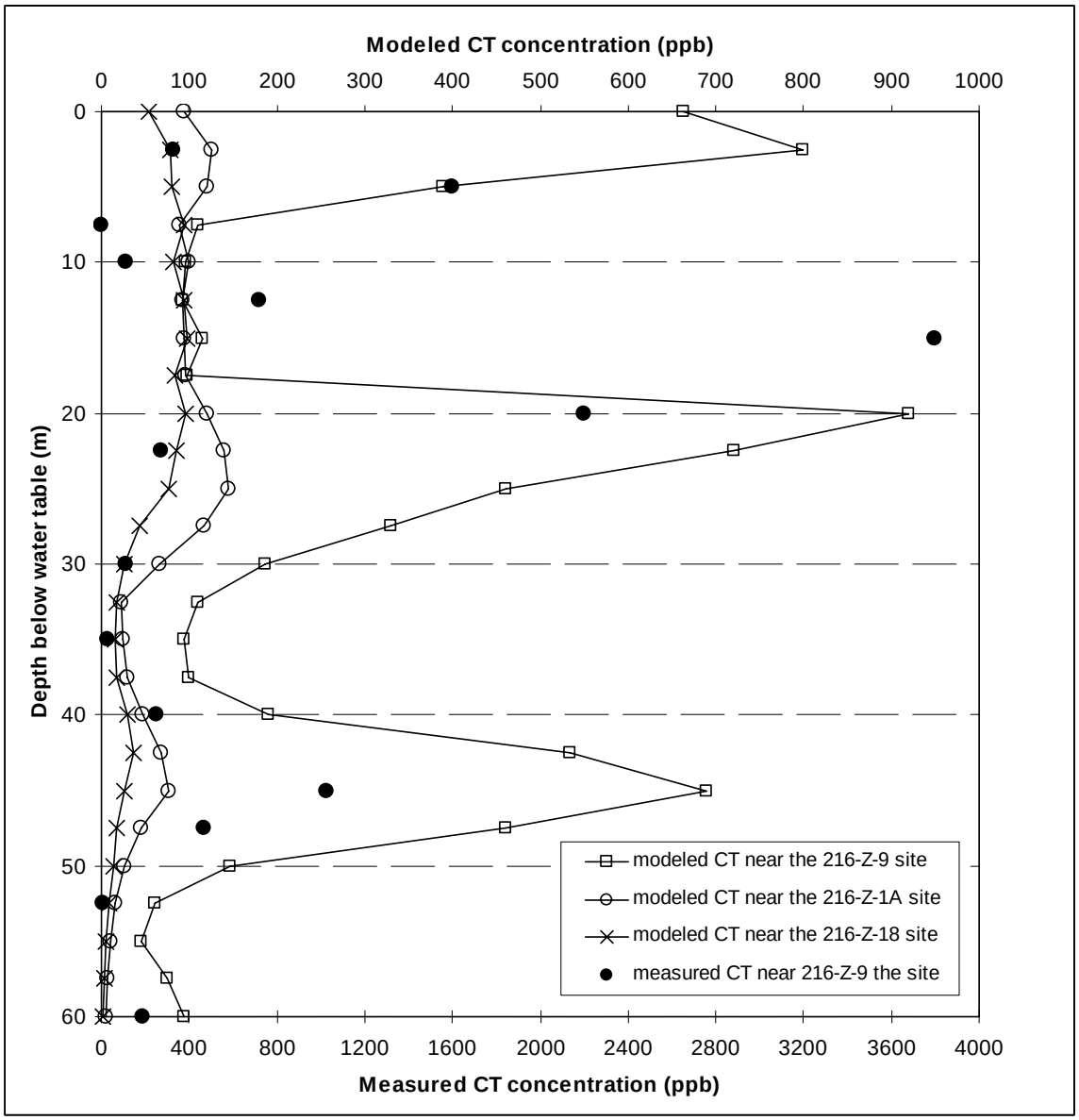

Figure 6.7. Vertical Profile of CT Concentrations in Groundwater Beneath the Disposal Sites from Depth-Discrete Sampling and from Geostatistical Modeling of Field Data (by Murray et al. [2006])

7.0 References

Anderson JD. 1976. *Input and Decayed Values of Radioactive Liquid Wastes Discharged to the Ground in the 200 Areas Through 1975*. ARH-CD-745, Atlantic Richfield Hanford Company, Richland, Washington.

Brooks RH and AT Corey. 1964. "Hydraulic Properties of Porous Media." *Hydrol. Pap. 3*, Civil Engineering Department, Colorado State University, Fort Collins, Colorado.

Burdine NT. 1953. "Relative Permeability Calculations from Pore-Size Distribution Data." *Petr. Trans., Am. Inst. Mining Metall. Eng*. 198:71-77.

CERCLA – *Comprehensive Environmental Response, Compensation, and Liability Act*. 1980. Public Law 96-150, as amended, 94 Stat. 2767, 42 USC 9601 et seq.

DOE. 2001. *Drilling, Sampling, and Analysis Plan for Installation of a Well Within the Vicinity of the Plutonium Finishing Plant*. U.S. Department of Energy, Richland Operations Office, Richland, Washington.

DOE. 2002. *Standardized Stratigraphic Nomenclature for Post-Ringold Formation Sediments Within the Central Pasco Basin*. DOE/RL-2002-39. U.S. Department of Energy, Richland, Washington.

DOE. 2004. *Plutonium/Organic-Rich Process Condensate/Process Waste Group Operable Unit RI/FS Work Plan, Includes: 200-PW-1, 200-PW-3, and 200-PW-6 Operable Units*. DOE/RL-2001-01, Rev. 0, Reissue, U.S. Department of Energy, Richland Operations Office, Richland, Washington.

DOE. 2006. *Remedial Investigation Report for the Plutonium/Organic-Rich Process Condensate/Process Waste Group Operable Unit: Includes the 200-PW-1, 200-PW-3, and 200-PW-6 Operable Units*. DOE/RL-2006-51, Draft A, U.S. Department of Energy, Richland Operations Office, Richland, Washington.

Freyberg DL. 1986. "A Natural Gradient Experiment on Solute Transport in a Sand Aquifer, 2. Spatial Moments and the Advection and Dispersion of Nonreactive Tracers. *Water Resour. Res*. 22:2031-2046.

Hofstee C, RC Walker, and JH Dane. 1998. "Infiltration and Redistribution of Perchloroethylene in Partially Saturated, Stratified Porous Media." *J. Contam. Hydrol.* 34:293-313.

Khaleel R and EJ Freeman. 1995. *Variability and Scaling of Hydraulic Properties for 200 Area Soils, Hanford Site*. WHC-EP-0883, Westinghouse Hanford Company, Richland, Washington.

Khaleel R, TE Jones, AJ Knepp, FM Mann, DA Myers, PM Rogers, RJ Serne, and MI Wood. 2001. *Modeling Data Package for S-SX Field Investigation Report (FIR).* RPP-6296 Rev. 0, CH2M HILL Hanford Group, Inc., Richland, Washington.

Klinkenberg LJ. 1941. "The Permeability of Porous Media to Liquids and Gases." *Drilling and Production Practice*, 200-213, American Petroleum Institute, New York.

Last GV, DG Horton, BN Bjornstad, TJ Gilmore, R Mackley, and C Strickland. 2002. *Prototype Geologic Database and User's Guide, FY02 Status Report*. CP-17090, Fluor Hanford, Richland, Washington.

Last GV and VJ Rohay. 1993. *Refined Conceptual Model for the Volatile Organic Compounds-Arid Integrated Demonstration and 200 West Area Carbon Tetrachloride Expedited Response Action*. PNL-8597, Pacific Northwest Laboratory, Richland, Washington.

Lenhard RJ. 1994. "Scaling Fluid Content-Pressure Relations of Different Fluid Systems in Porous Media." In *Proc. 14th Annual American Geophysical Union Hydrology Days*, HJ Morel-Seytoux (ed.), Hydrology Days Publ., Atherton, California.

Lenhard RJ, M Oostrom, and JH Dane. 2004. "A Constitutive Model for Air-NAPL-Water Flow in the Vadose Zone Accounting for Immobile Non-Occluded (Residual) NAPL in Strongly Water-Wet Porous Media." *J. of Contaminant Hydrology* 73:283-304

Lenhard RJ, JC Parker, and S Mishra. 1989. "On the Correspondence between Brooks-Corey and van Genuchten Models" *J. of Irrigation and Drainage Engineering* 115:744-751

Leverett MC. 1941. "Capillary Behavior in Porous Solids." *Trans. Soc. Pet. Eng. AIME* 142:152-169.

Lindsey, K.A., SP Reidel, KR. Fecht, JL Slate, AG Law, and AM Tallman 1994a. "Geohydrologic Setting of the Hanford Site, South-Central Washington" in *Geological Field Trips in the Pacific Northwest: 1994 Geologic Society of America Meeting*, Chapter 1C, D. A. Swanson and R. A. Haugerud (eds.), pp. 1C-1 to 1C-16, Geological Society of America, Boulder, Colorado.

Lindsey, KA, JL Slate, GK Jaeger, KJ Swett, and RB Mercer. 1994b. Geologic Setting of the Low-Level Burial Grounds. WHC-SD-EN-TI-290, Rev. 0. Westinghouse Hanford Company, Richland, Washington.

Miller EE and RD Miller. 1956. "Physical Theory for Capillary Flow Phenomena." *J. Appl. Phys.* 27:324-332.

Mualem Y. 1976. "A New Model for Predicting the Hydraulic Conductivity of Unsaturated Porous Media." *Water Resour. Res*. 12:513-522.

Murray, C., Y, Chien, and M. Truex. 2006. "Geostatistical Analysis of the Inventory of Carbon Tetrachloride in the Unconfined Aquifer in the 200 West Area of the Hanford Site". Letter report submitted to Fluor Hanford, Inc., January 4, 2006.

Oostrom M and RJ Lenhard. 1998. "Comparison of Relative Permeability-Saturation-Pressure Parametric Models for Infiltration and Redistribution of a Light Nonaqueous Phase Liquid in Sandy Porous Media." *Adv. in Water Resour*. 21:145-157.

Oostrom M and RJ Lenhard. 2003. "Carbon Tetrachloride Flow Behavior in Unsaturated Hanford Caliche Material: An Investigation of Residual NAPL." *Vadose Zone J*. 2:25-33.

Oostrom M, C Hofstee, and JH Dane. 1997. "Light Nonaqueous-Phase Liquid Movement in a Variably Saturated Sand." *Soil Science Society of America J*. 61:1547-1554.

Oostrom M, C Hofstee, RC Walker, and JH Dane. 1999. "Movement and Remediation of Trichloroethylene in a Saturated, Heterogeneous Porous Medium. 1. Spill Behavior and Initial Dissolution." *J. of Contaminant Hydrol*. 37:159-178.

Oostrom M, C Hofstee, RJ Lenhard, and TW Wietsma. 2003. "Flow Behavior and Residual Saturation Formation of Injected Carbon Tetrachloride in Unsaturated Heterogeneous Porous Media. *J. of Contaminant Hydrology* 64:93-112.

Oostrom, M, ML Rockhold, PD Thorne, GV Last, and MJ Truex. 2004. *Three-Dimensional Modeling of DNAPL in the Subsurface of the 216-Z-9 Trench at the Hanford Site*. PNNL-14895, Pacific Northwest National Laboratory, Richland, Washington.

Oostrom, M, ML Rockhold, PD Thorne, GV Last, and MJ Truex. 2006. *Carbon Tetrachloride Flow and Transport in the Subsurface of the 216-Z-9 Trench at the Hanford Site: Heterogeneous Model Development and Soil Vapor Extraction Modeling*. PNNL-15914, Pacific Northwest National Laboratory, Richland, Washington.

Rohay VJ. 2002. *Performance Evaluation Report for Soil Vapor Extraction Operations at the Carbon Tetrachloride Site, February 1992 – September 2001*. BHI-00720, Rev. 6, Bechtel Hanford, Inc., Richland, Washington.

Rohay, VJ, KJ Swett, and GV Last. 1994. *Conceptual Model of the Carbon Tetrachloride Contamination in the 200 West Area at the Hanford Site*. WHC-SD-EN-TI-248, Rev. 0, Westinghouse Hanford Company, Richland, Washington.

Schroth MH, JD Istok, JS Selker, M Oostrom, and MD White. 1998. "Multifluid Flow in Bedded Porous Media: Laboratory Experiments and Numerical Simulations." *Adv. in Water Resour*. 22:169-183.

van Genuchten M. 1980. "A Closed-Form Equation for Predicting the Hydraulic Conductivity of Unsaturated Soils." *Soil Sci. Am. J*. 44:892-898.

White MD and M Oostrom. 2000. *STOMP, Subsurface Transport Over Multiple Phases. Version 2.0. Theory Guide.* PNNL-12030, Pacific Northwest National Laboratory, Richland, Washington.

White MD and M Oostrom. 2003. *STOMP, Subsurface Transport Over Multiple Phases. Version 3.0. User's Guide.* PNNL-14286, Pacific Northwest National Laboratory, Richland, Washington.

White MD, M Oostrom, and RJ Lenhard. 2004. "A Practical Model for Mobile, Residual, and Entrapped NAPL in Porous Media." *Ground Water* 42:734-746.

White MD and M Oostrom. 2006. *STOMP Subsurface Transport Over Multiple Phases, Version 4.0, User's Guide*. PNNL-15782, Pacific Northwest National Laboratory, Richland, Washington.

Appendix

HEIS Data Used in Model

Appendix

Field Data For Comparison to Model Results

Table A.1. Compilation of Vadose Zone Soil Data Compiled from HEIS and Augmented with Geologic Unit and Sediment Classification. Geologic unit and sediment classification use the terminology presented in Section 3.

Well Name	Sample Bottom (ft)	Sample Top (ft)	Location	Geologic Unit	Sediment Classification	Sample Date	Result	Units	Data Qualifier
299-W15-216	49.6	49.1	216-Z-9	H2		5/20/1992	67	µg/kg	
299-W15-216	110.7	110.2	216-Z-9	CCUz	M	6/2/1992	54	µg/kg	
299-W15-216	110.7	110.2	216-Z-9	CCUz	M	6/2/1992	40	µg/kg	
299-W15-216	110.7	110.2	216-Z-9	CCUz	M	6/2/1992			U
299-W15-216	116.8	116.3	216-Z-9	CCUc	gS	6/3/1992	27	µg/kg	
299-W15-216	121	120.5	216-Z-9	Re	gsM	6/8/1992			U
299-W15-216	129	128.5	216-Z-9	Re	gS	6/10/1992			U
299-W15-217	5	5	216-Z-9	Hol	mS	6/8/1992			U
299-W15-217	10	10	216-Z-9	Hol	mS	6/8/1992	20	µg/kg	
299-W15-217	15	15	216-Z-9	H1	mS	6/9/1992	16	µg/kg	
299-W15-217	20	20	216-Z-9	H1	S	6/9/1992	38	µg/kg	
299-W15-217	21	20.5	216-Z-9	H1	S	6/9/1992	4	µg/kg	
299-W15-217	24.5	24.5	216-Z-9	H1	sG	6/10/1992	6	µg/kg	
299-W15-217	26	25.5	216-Z-9	H1	msG	6/10/1992	41	µg/kg	
299-W15-217	30	30	216-Z-9	H1	msG	6/11/1992	17	µg/kg	
299-W15-217	35	35	216-Z-9	H1	mgS	6/11/1992	47	µg/kg	
299-W15-217	41	40.5	216-Z-9	H1	msG	6/15/1992	60	µg/kg	
299-W15-217	45	45	216-Z-9	H1	msG	6/16/1992	61	µg/kg	
299-W15-217	50	50	216-Z-9	H1	msG	6/16/1992	239	µg/kg	
299-W15-217	54.3	53.8	216-Z-9	H2	(g)mS	6/17/1992	330	µg/kg	
299-W15-217	54.3	53.8	216-Z-9	H2	(g)mS	6/17/1992	212	µg/kg	
299-W15-217	54.3	53.8	216-Z-9	H2	(g)mS	6/17/1992			U
299-W15-217	55	55	216-Z-9	H2	(g)mS	6/17/1992	2928	µg/kg	D
299-W15-217	60	60	216-Z-9	H2	mgS	6/17/1992	705	µg/kg	
299-W15-217	65	65	216-Z-9	H2	mS	6/18/1992	5698	µg/kg	
299-W15-217	70	70	216-Z-9	H2	(g)S	6/18/1992	3068	µg/kg	D
299-W15-217	75	75	216-Z-9	H2	(g)S	6/18/1992	2333	µg/kg	D
299-W15-217	81	80.5	216-Z-9	H4	S	6/19/1992	1770	µg/kg	
299-W15-217	85	85	216-Z-9	H4	S	6/23/1992	2336	µg/kg	D
299-W15-217	90	90	216-Z-9	H4	mS	6/26/1992	9445	µg/kg	D
299-W15-217	95	95	216-Z-9	H4	S	6/26/1992	4876	µg/kg	D
299-W15-217	100	100	216-Z-9	H4	mS	6/26/1992	1280	µg/kg	
299-W15-217	101.5	101	216-Z-9	H4	mS	6/29/1992	5369	µg/kg	D
299-W15-217	105	105	216-Z-9	H4	mS	6/29/1992	906	µg/kg	
299-W15-217	110	110	216-Z-9	H4	mS	6/29/1992	1879	µg/kg	
299-W15-217	114	114	216-Z-9	CCUz	M	6/29/1992	37817	µg/kg	D
299-W15-217	115.6	115.1	216-Z-9	CCUz	M	6/30/1992	551	µg/kg	

Table A.1. (contd)

Well Name	Sample Bottom (ft)	Sample Top (ft)	Location	Geologic Unit	Sediment Classification	Sample Date	Result	Units	Data Qualifier
299-W15-217	122.1	121.6	216-Z-9	CCUc	mgS	6/30/1992	4377	µg/kg	D
299-W15-218	7	7	216-Z-9	Bf	S	2/4/1993	82	µg/kg	
299-W15-218	10	10	216-Z-9	Bf	S	2/4/1993	84	µg/kg	J
299-W15-218	15	15	216-Z-9	Bf	gS	2/5/1993	23	µg/kg	J
299-W15-218	15	15	216-Z-9	Bf	gS	2/5/1993	15	µg/kg	J
299-W15-218	20	20	216-Z-9	H1	(g)S	2/5/1993	17	µg/kg	J
299-W15-218	25	25	216-Z-9	H1	sG	2/8/1993	36	µg/kg	
299-W15-218	27	27	216-Z-9	H1	sG	2/8/1993	106	µg/kg	
299-W15-218	30	30	216-Z-9	H1	gS	2/8/1993	96	µg/kg	
299-W15-218	30	30	216-Z-9	H1	gS	2/8/1993	112	µg/kg	
299-W15-218	35	35	216-Z-9	H1	(g)S	2/9/1993	16	µg/kg	J
299-W15-218	35	35	216-Z-9	H1	(g)S	2/9/1993	11	µg/kg	J
299-W15-218	35	35	216-Z-9	H1	(g)S	2/9/1993	7	µg/kg	J
299-W15-218	35	35	216-Z-9	H1	(g)S	2/9/1993	9	µg/kg	J
299-W15-218	42	42	216-Z-9	H1	G	2/10/1993			U
299-W15-218	51	51	216-Z-9	H1	sG	2/10/1993	40	µg/kg	
299-W15-218	52.5	52.5	216-Z-9	H2	sM (clastic dike)	2/11/1993	1876	µg/kg	
299-W15-218	55	55	216-Z-9	H2	S	2/11/1993	198	µg/kg	
299-W15-218	60	60	216-Z-9	H2	S	2/11/1993	354	µg/kg	
299-W15-218	65	65	216-Z-9	H2	S	2/12/1993	75	µg/kg	
299-W15-218	70	70	216-Z-9	H2	S	2/12/1993	175	µg/kg	
299-W15-218	75	75	216-Z-9	H2	S	2/12/1993	389	µg/kg	
299-W15-218	80	80	216-Z-9	H2	S	2/12/1993	1334	µg/kg	
299-W15-218	85	85	216-Z-9	H4	S	2/16/1993	206	µg/kg	
299-W15-218	90	90	216-Z-9	H4	S	2/16/1993	810	µg/kg	
299-W15-218	95	95	216-Z-9	H4	gS	2/17/1993	11804	µg/kg	D
299-W15-218	100	100	216-Z-9	H4	gS	2/17/1993	1182	µg/kg	
299-W15-218	104.5	104.5	216-Z-9	H4	S	2/17/1993	2600	µg/kg	
299-W15-218	110	110	216-Z-9	CCUz	mS	2/17/1993	15794	µg/kg	D
299-W15-218	116.5	116.5	216-Z-9	CCUc	gS	2/24/1993	6816	µg/kg	D
299-W15-218	116.5	116.5	216-Z-9	CCUc	gS	2/24/1993	9932	µg/kg	D
299-W15-218	120	120	216-Z-9	Re	sG	2/25/1993	31	µg/kg	
299-W15-218	125	125	216-Z-9	Re	msG	3/8/1993			U
299-W15-218	130	130	216-Z-9	Re	msG	3/8/1993	19	µg/kg	
299-W15-218	140	140	216-Z-9	Re	sG	3/9/1993	244	µg/kg	
299-W15-218	145	145	216-Z-9	Re	S	3/10/1993	3915	µg/kg	D
299-W15-218	150	150	216-Z-9	Re	sG	3/10/1993	81	µg/kg	
299-W15-218	155	155	216-Z-9	Re	sG	3/10/1993	54	µg/kg	
299-W15-218	160	160	216-Z-9	Re	sG	3/11/1993	37	µg/kg	J
299-W15-218	165	165	216-Z-9	Re	sG	3/11/1993	175	µg/kg	
299-W15-218	170	170	216-Z-9	Re	sG	3/12/1993	11	µg/kg	J
299-W15-218	175	175	216-Z-9	Re	sG	3/12/1993	25	µg/kg	J
299-W15-218	180	180	216-Z-9	Re	sG	3/15/1993	45	µg/kg	J
299-W15-218	185	185	216-Z-9	Re	sG	3/16/1993	3	µg/kg	J
299-W15-218	190	190	216-Z-9	Re	sG	3/16/1993	9	µg/kg	J
299-W15-218	195	195	216-Z-9	Re	sG	3/18/1993	38	µg/kg	

Table A.1. (contd)

Well Name	Sample Bottom (ft)	Sample Top (ft)	Location	Geologic Unit	Sediment Classification	Sample Date	Result	Units	Data Qualifier
299-W15-218	200	200	216-Z-9	Re	sG	3/18/1993	323	µg/kg	
299-W15-218	205	205	216-Z-9	Re	sG	3/18/1993	308	µg/kg	
299-W15-219	25.9	25.9	216-Z-9	H1	sG	4/22/1993			U
299-W15-219	29.5	29.5	216-Z-9	H1	sG	4/23/1993	8	µg/kg	
299-W15-219	35.5	35.5	216-Z-9	H1	sG	4/23/1993	12	µg/kg	J
299-W15-219	39.75	39.75	216-Z-9	H1	gS	4/27/1993			U
299-W15-219	44.75	44.75	216-Z-9	H2	S	4/27/1993	117	µg/kg	
299-W15-219	49.5	49.5	216-Z-9	H2	S	4/27/1993	407	µg/kg	
299-W15-219	53.5	53.5	216-Z-9	H2	S	4/28/1993	182	µg/kg	
299-W15-219	54.3	54.3	216-Z-9	H2	S	4/28/1993	288	µg/kg	
299-W15-219	56.55	56.55	216-Z-9	H2	S	4/28/1993	213	µg/kg	
299-W15-219	57.9	57.9	216-Z-9	H2	S	4/29/1993	495	µg/kg	
299-W15-219	65	65	216-Z-9	H2	gS	4/29/1993	283	µg/kg	
299-W15-219	70	70	216-Z-9	H2	(m)gS	4/29/1993	679	µg/kg	D
299-W15-219	75.5	75.5	216-Z-9	H2	gS	4/29/1993	867	µg/kg	
299-W15-219	79.5	79.5	216-Z-9	H4	S	4/30/1993	9558	µg/kg	D
299-W15-219	84.5	84.5	216-Z-9	H4	S	4/30/1993	2039	µg/kg	D
299-W15-219	87	87	216-Z-9	H4	S	5/3/1993	577	µg/kg	
299-W15-219	89.5	89.5	216-Z-9	H4	S	5/3/1993	1557	µg/kg	
299-W15-219	91	91	216-Z-9	H4	S	5/3/1993	3095	µg/kg	D
299-W15-219	95.5	95.5	216-Z-9	H4	S	5/4/1993	106	µg/kg	
299-W15-219	96.5	96.5	216-Z-9	H4	S	5/4/1993	80	µg/kg	
299-W15-219	100	100	216-Z-9	H4	S	5/4/1993	198	µg/kg	
299-W15-219	105.5	105.5	216-Z-9	H4	S	5/4/1993	376	µg/kg	
299-W15-219	109.5	109.5	216-Z-9	H4	S	5/4/1993	606	µg/kg	
299-W15-219	111.1	111.1	216-Z-9	CCUz	S	5/5/1993	288	µg/kg	
299-W15-219	120	120	216-Z-9	CCUc	msG	5/5/1993	1349	µg/kg	
299-W15-219	114.5	114.5	216-Z-9	CCUz	sM	5/5/1993	10488	µg/kg	D
299-W15-219	114.5	114.5	216-Z-9	CCUz	sM	5/5/1993	11688	µg/kg	D
299-W15-219	114.9	114.9	216-Z-9	CCUz	sM	5/5/1993	9866	µg/kg	D
299-W15-219	124.5	124.5	216-Z-9	Re	sG	5/11/1993	2345	µg/kg	D
299-W15-219	129.5	129.5	216-Z-9	Re	gS	5/11/1993	4905	µg/kg	D
299-W15-219	131.5	131.5	216-Z-9	Re	gS	5/11/1993	574	µg/kg	
299-W15-219	140	140	216-Z-9	Re	sG	5/13/1993	3752	µg/kg	D
299-W15-219	145	145	216-Z-9	Re	S	5/13/1993	55	µg/kg	
299-W15-219	149	149	216-Z-9	Re	S	5/14/1993	3798	µg/kg	D
299-W15-219	150.25	150.25	216-Z-9	Re	S	5/14/1993	172	µg/kg	
299-W15-219	153.4	153.4	216-Z-9	Re	S	5/17/1993	23	µg/kg	
299-W15-219	155	155	216-Z-9	Re	sG	5/17/1993			U
299-W15-219	160	160	216-Z-9	Re	sG	5/17/1993	1305	µg/kg	D
299-W15-219	165	165	216-Z-9	Re	sG	5/18/1993	242	µg/kg	
299-W15-219	170	170	216-Z-9	Re	sG	5/18/1993	1311	µg/kg	D
299-W15-219	175	175	216-Z-9	Re	sG	5/18/1993	1620	µg/kg	D
299-W15-219	180	180	216-Z-9	Re	sG	5/19/1993	1418	µg/kg	D
299-W15-219	185	185	216-Z-9	Re	sG	5/19/1993	876	µg/kg	D
299-W15-219	187	187	216-Z-9	Re	S	5/19/1993	705	µg/kg	
299-W15-219	190.3	190.3	216-Z-9	Re	msG	5/20/1993	5	µg/kg	J

Table A.1. (contd)

299-W15-219	195	195	216-Z-9	Re	msG	5/20/1993	120	µg/kg	
299-W15-219	200	200	216-Z-9	Re	msG	5/21/1993	13	µg/kg	J
299-W15-219	205	205	216-Z-9	Re	msG	5/24/1993	382	µg/kg	
299-W15-219	210.5	210.5	216-Z-9	Re	msG	5/25/1993	107	µg/kg	
299-W15-220	24.8	24.8	216-Z-9	H1	sG	6/3/1993			U
299-W15-220	29.7	29.7	216-Z-9	H1	sG	6/5/1993	29	µg/kg	
299-W15-220	34.7	34.7	216-Z-9	H1	msG	6/7/1993	8	µg/kg	J
299-W15-220	40	40	216-Z-9	H1	msG	6/8/1993			U
299-W15-220	45	45	216-Z-9	H2	S	6/9/1993	133	µg/kg	J
299-W15-220	50	50	216-Z-9	H2	mS	6/9/1993	1052	µg/kg	
299-W15-220	55	55	216-Z-9	H2	S	6/9/1993	772	µg/kg	
299-W15-220	60	60	216-Z-9	H2	(g)S	6/10/1993	296	µg/kg	
299-W15-220	64.8	64.8	216-Z-9	H2	(g)S	6/10/1993	544	µg/kg	
299-W15-220	69.6	69.6	216-Z-9	H2	(g)S	6/11/1993	544	µg/kg	
299-W15-220	75	75	216-Z-9	H4	mS	6/14/1993	261	µg/kg	
299-W15-220	79.8	79.8	216-Z-9	H4	mS	6/14/1993	174	µg/kg	
299-W15-220	84.6	84.6	216-Z-9	H4	S	6/15/1993	107	µg/kg	
299-W15-220	90.5	90.5	216-Z-9	H4	S	6/15/1993	1132	µg/kg	
299-W15-220	94.6	94.6	216-Z-9	H4	sM	6/16/1993	699	µg/kg	
299-W15-220	100.5	100.5	216-Z-9	H4	S	6/16/1993	545	µg/kg	
299-W15-220	104.5	104.5	216-Z-9	CCUz	sM	6/16/1993	56	µg/kg	
299-W15-220	109.6	109.6	216-Z-9	CCUc	sG	6/17/1993	109	µg/kg	
299-W15-220	114.8	114.8	216-Z-9	Re	msG	6/24/1993			U
299-W15-220	120	120	216-Z-9	Re	msG	6/25/1993			U
299-W15-220	123	123	216-Z-9	Re	sG	6/25/1993	18	µg/kg	J
299-W15-220	127	127	216-Z-9	Re	sG	6/28/1993	6	µg/kg	J
299-W15-220	133	133	216-Z-9	Re	sG	6/28/1993	4	µg/kg	J
299-W15-220	138.5	138.5	216-Z-9	Re	sG	6/29/1993			U
299-W15-220	146	146	216-Z-9	Re	msG	7/9/1993	5	µg/kg	J
299-W15-220	150	150	216-Z-9	Re	msG	7/12/1993	8	µg/kg	J
299-W15-220	155	155	216-Z-9	Re	msG	7/12/1993			U
299-W15-220	160	160	216-Z-9	Re	msG	7/12/1993	5	µg/kg	J
299-W15-220	164.5	164.5	216-Z-9	Re	gS	7/14/1993			U
299-W15-220	170	170	216-Z-9	Re	sG	7/14/1993			U
299-W15-220	175	175	216-Z-9	Re	msG	7/15/1993			U
299-W15-220	180.5	180.5	216-Z-9	Re	msG	7/15/1993			U
299-W15-220	185	185	216-Z-9	Re	msG	7/19/1993			U
299-W15-220	190	190	216-Z-9	Re	msG	7/20/1993	5	µg/kg	J
299-W15-220	195	195	216-Z-9	Re	msG	7/21/1993	5	µg/kg	J
299-W15-220	200	200	216-Z-9	Re	msG	7/21/1993	101	µg/kg	
299-W15-42	2	0	Far Field	Bf	S	11/26/2001	6	µg/kg	U
299-W15-42	30.5	28	Far Field	H1	gS	11/28/2001	5	µg/kg	U
299-W15-42	62.5	60	Far Field	H2	S	11/30/2001	5	µg/kg	U
299-W15-42	62.5	60	Far Field	H2	S	11/30/2001	6	µg/kg	U
299-W15-42	119.8	117.3	Far Field	CCUz	M	12/19/2001	6	µg/kg	U
299-W15-42	125.5	123	Far Field	CCUc	mG	12/19/2001	6	µg/kg	U
299-W15-42	132		Far Field	Re	gS	1/2/2002	6	µg/kg	U
299-W15-42	138.7	136.2	Far Field	Re	msG	1/3/2002	6	µg/kg	U
299-W15-42	182.1	179.6	Far Field	Re	sG	1/8/2002	5	µg/kg	U

Table A.1. (contd)

Well Name	Sample Bottom (ft)	Sample Top (ft)	Location	Geologic Unit	Sediment Classification	Sample Date	Result	Units	Data Qualifier
299-W15-42	222.5	219	Far Field	Re	sG	1/17/2002	5	µg/kg	U
299-W15-42	233	231	Far Field	Re	sG	1/18/2002	5	µg/kg	U
299-W15-42	283	281	Far Field	Re	msG	1/23/2002	4	µg/kg	J
299-W15-43	30	0	Far Field	H1	mS/gmS	11/11/2002	5	µg/kg	U
299-W15-43	237	230	Far Field	Re	sG	11/11/2002	6	µg/kg	U
299-W15-44	30	0	Far Field	H1	gS	10/14/2002	6	µg/kg	U
299-W15-44	30	0	Far Field	H1	gS	10/14/2002	6	µg/kg	U
299-W15-44	240	225	Far Field	Re	sG	10/17/2002	5	µg/kg	U
299-W15-46	50	47.5	216-Z-9	H1	S/sG	10/20/2003	14	µg/kg	
299-W15-46	66	63.5	216-Z-9	H2	S/M	10/29/2003		µg/kg	
299-W15-46	92.5	90	216-Z-9	H4	S	3/23/2004	19	µg/kg	
299-W15-46	92.5	90	216-Z-9	H4	S	3/23/2004	5	µg/kg	U
299-W15-46	112	109.5	216-Z-9	CCUz	M	4/8/2004	240	µg/kg	U
299-W15-46	112	109.5	216-Z-9	CCUz	M	4/8/2004	260	µg/kg	
299-W15-46	117.5	115	216-Z-9	CCUz/CCUc	M/Caliche	4/19/2004	290	µg/kg	J
299-W15-46	117.5	115	216-Z-9	CCUz/CCUc	M/Caliche	4/19/2004	130	µg/kg	U
299-W15-46	119.5	117	216-Z-9	CCUc	Caliche	4/21/2004	2.1	µg/kg	U
299-W15-46	119.5	117	216-Z-9	CCUc	Caliche	4/21/2004	240	µg/kg	
299-W15-46	119.5	117	216-Z-9	CCUc	Caliche	4/21/2004	140	µg/kg	U
299-W15-46	119.5	117	216-Z-9	CCUc	Caliche	4/21/2004	92	µg/kg	
299-W15-46	122	119.5	216-Z-9	CCUc	msG	5/3/2004	2.1	µg/kg	U
299-W15-46	122	119.5	216-Z-9	CCUc	msG	5/3/2004	11	µg/kg	U
299-W15-46	176.5	174	216-Z-9	Re	sG	8/23/2004	2.1	µg/kg	U
299-W15-46	186.5	184	216-Z-9	Re	sG	8/25/2004	2.1	µg/kg	U
299-W15-46	186.5	184	216-Z-9	Re	sG	8/25/2004	2.1	µg/kg	U
299-W15-46	226.5	224	216-Z-9	Re	S	9/9/2004	2.1	µg/kg	U
299-W15-46	229	226.5	216-Z-9	Re	mS	9/9/2004	1.9	µg/kg	U
299-W15-46	230.5	228	216-Z-9	Re	mG	9/15/2004	1.8	µg/kg	U
299-W15-46	230.5	228	216-Z-9	Re	mG	9/15/2004	1.8	µg/kg	U
299-W15-46	232	230.5	216-Z-9	Re	mG	9/27/2004	2.3	µg/kg	U
299-W15-46	239.5	237	216-Z-9	Re	msG	9/29/2004	2	µg/kg	U
299-W15-46	249.5	247	216-Z-9	Re	sG	10/4/2004	2	µg/kg	U
299-W15-46	259.5	257	216-Z-9	Re	sG	10/7/2004	2.2	µg/kg	U
299-W15-46	259.5	257	216-Z-9	Re	sG	10/7/2004	2.2	µg/kg	U
299-W15-46	279.5	277	216-Z-9	Re	sG	10/13/2004	73	µg/kg	
299-W15-46	297	294.5	216-Z-9	Re	S	10/21/2004	250	µg/kg	
299-W15-46	297	294.5	216-Z-9	Re	S	10/21/2004	180	µg/kg	
299-W15-46	299.5	297	216-Z-9	Re	S	10/21/2004	22	µg/kg	
299-W15-46	319.5	317	216-Z-9	Re	S	10/28/2004	2.3	µg/kg	U
299-W15-46	340	338	216-Z-9	Re	sG	11/2/2004	1.5	µg/kg	U
299-W15-46	369.5	367	216-Z-9	Re	S	11/10/2004	8.8	µg/kg	J
299-W15-46	369.5	367	216-Z-9	Re	S	11/10/2004	13	µg/kg	
299-W15-46	379.5	377	216-Z-9	Re	sG	11/11/2004	4.5	µg/kg	J
299-W15-46	400.5	398	216-Z-9	Re	mS	11/22/2004	2.4	µg/kg	U
299-W15-46	419.5	417	216-Z-9	Rlm	M	11/30/2004	2.3	µg/kg	U
299-W15-46	421	419.5	216-Z-9	Rlm	M	11/30/2004	2.3	µg/kg	U

Table A.1. (contd)

Well Name	Sample Bottom (ft)	Sample Top (ft)	Location	Geologic Unit	Sediment Classification	Sample Date	Result	Units	Data Qualifier
299-W15-46	484.5	482	216-Z-9	Ra	gmS	1/10/2005	2.5	µg/kg	U
299-W15-46	521.5	520	216-Z-9	Ra	msG	1/21/2005	2.3	µg/kg	U
299-W15-48	54.5	52.5	216-Z-9	H2	S	3/13/2006	0.26	µg/kg	U
299-W15-48	69	67	216-Z-9	H2	S	3/20/2006	2600	µg/kg	
299-W15-48	69	67	216-Z-9	H2	S	3/20/2006	52	µg/kg	U
299-W15-48	69	67	216-Z-9	H2	S	3/20/2006	270	µg/kg	E
299-W15-48	72	70	216-Z-9	H2	S	3/22/2006	35	µg/kg	
299-W15-48	72	70	216-Z-9	H2	S	3/22/2006	520	µg/kg	
299-W15-48	75	73	216-Z-9	H2	S/M	3/27/2006	750	µg/kg	E
299-W15-48	75	73	216-Z-9	H2	S/M	3/27/2006	1500	µg/kg	
299-W15-48	75	73	216-Z-9	H2	S/M	3/27/2006	52	µg/kg	U
299-W15-48	102	100	216-Z-9	H4	M	4/4/2006	0.19	µg/kg	U
299-W15-48	102	100	216-Z-9	H4	M	4/4/2006	58	µg/kg	U
299-W15-48	102	100	216-Z-9	H4	M	4/4/2006	52	µg/kg	U
299-W15-48	105	103	216-Z-9	H4	mS	4/6/2006	0.17	µg/kg	U
299-W15-48	105	103	216-Z-9	H4	mS	4/6/2006	52	µg/kg	U
299-W15-48	105	103	216-Z-9	H4	mS	4/6/2006	57	µg/kg	U
299-W15-48	105	103	216-Z-9	H4	mS	4/6/2006	59	µg/kg	U
299-W15-48	105	103	216-Z-9	H4	mS	4/6/2006	0.16	µg/kg	U
299-W15-48	120.5	118.5	216-Z-9	H4	sM	4/13/2006	0.83	µg/kg	J
299-W15-48	124.5	122.5	216-Z-9	CCUz	M	4/18/2006	250	µg/kg	U
299-W15-48	124.5	122.5	216-Z-9	CCUz	M	4/18/2006	150	µg/kg	E
299-W15-48	124.5	122.5	216-Z-9	CCUz	M	4/18/2006	470	µg/kg	
299-W15-48	130.5	128.5	216-Z-9	CCUz	M	4/24/2006	6300	µg/kg	
299-W15-48	130.5	128.5	216-Z-9	CCUz	M	4/24/2006	150	µg/kg	E
299-W15-48	130.5	128.5	216-Z-9	CCUz	M	4/24/2006	250	µg/kg	U
299-W15-48	133	131.5	216-Z-9	CCUc	Caliche	4/27/2006	1300	µg/kg	
299-W15-48	133	131.5	216-Z-9	CCUc	Caliche	4/27/2006	130	µg/kg	U
299-W15-48	133	131.5	216-Z-9	CCUc	Caliche	4/27/2006	4100	µg/kg	
299-W15-48	140	135	216-Z-9	Re	msG	5/3/2006	0.16	µg/kg	U
299-W15-48	140	135	216-Z-9	Re	msG	5/3/2006	3	µg/kg	U
299-W15-48	140	135	216-Z-9	Re	msG	5/3/2006	320	µg/kg	U
299-W15-48	140	135	216-Z-9	Re	msG	5/3/2006	190	µg/kg	U
299-W15-49	262	260	Far Field	Re	sG	12/2/2004	2.3	µg/kg	U
299-W15-49	262	260	Far Field	Re	sG	12/9/2004	2.3	µg/kg	U
299-W15-49	335	330	Far Field	Re	msG	12/10/2004	2.2	µg/kg	U
299-W15-49	406	401	Far Field	Re	msG	12/14/2004	2.2	µg/kg	U
299-W15-49	440	435	Far Field	Re	msG	12/15/2004	2.7	µg/kg	U
299-W15-49	440	435	Far Field	Rlm	gsM	12/15/2004	2.7	µg/kg	U
299-W15-762			Far Field			11/14/2000	1.3	µg/kg	U
299-W15-762			Far Field			12/5/2000	6	µg/kg	U
299-W15-763			Far Field			12/5/2000	6	µg/kg	U
299-W15-764	2	0	Far Field	Bf	backfill	10/4/2001	5	µg/kg	U
299-W15-764	28		Far Field	H1	sG	10/10/2001	5	µg/kg	U
299-W15-764	60		Far Field	H2	S	10/12/2001	5	µg/kg	U
299-W15-764	123.5	121	Far Field	CCUz	M	10/17/2001	4	µg/kg	J

Table A.1. (contd)

Well Name	Sample Bottom (ft)	Sample Top (ft)	Location	Geologic Unit	Sediment Classification	Sample Date	Result	Units	Data Qualifier
299-W15-764	125.5	125.5	Far Field	CCUz	M	10/18/2001	6	µg/kg	U
299-W15-765			Far Field			10/10/2001	5	µg/kg	U
299-W15-765			Far Field			10/10/2001	5	µg/kg	U
299-W15-765	228	220	Far Field	Re	msG	4/16/2002	1	µg/kg	U
299-W15-84	111.8	110	Far Field	H4	sM	6/8/2001	6	µg/kg	U
299-W15-84	114.5	112.5	Far Field	H4/CCUz	sM	6/8/2001	5	µg/kg	U
299-W15-84	116.5	114.5	Far Field	CCUz	M	6/11/2001	5	µg/kg	U
299-W15-84	119	117	Far Field	CCUz	M	6/11/2001	2	µg/kg	J
299-W15-84	121	119.5	Far Field	CCUz	M	6/11/2001	9	µg/kg	
299-W15-84	123.5	121.5	Far Field	CCUc	Caliche	6/11/2001	6	µg/kg	U
299-W15-84	125.4	123.5	Far Field	CCUc	Caliche	6/11/2001	5	µg/kg	U
299-W15-84	127	125.5	Far Field	CCUc	Caliche	6/11/2001	5	µg/kg	U
299-W15-84	129	127	Far Field	Re	msG	6/11/2001	5	µg/kg	U
299-W15-84	132.3	130	Far Field	Re	sG	6/12/2001	6	µg/kg	U
299-W15-84	134.3	132	Far Field	Re	sG	6/12/2001	5	µg/kg	U
299-W15-84	143.5	141.5	Far Field	Re	S	6/12/2001	5	µg/kg	U
299-W15-84	153	151	Far Field	Re	S	6/12/2001	6	µg/kg	U
299-W15-84	173	171	Far Field	Re	sG	6/13/2001	5	µg/kg	U
299-W15-84	162.5	161	Far Field	Re	sG	6/13/2001	5	µg/kg	U
299-W15-84	195	193.5	Far Field	Re	msG	6/15/2001	6	µg/kg	U
299-W15-95	104.5	102.5	Far Field	H4	(m)S	5/21/2001	5	µg/kg	
299-W15-95	107		Far Field	CCUz	mS	5/21/2001	6	µg/kg	U
299-W15-95	109.5		Far Field	CCUz	sM	5/21/2001	6	µg/kg	U
299-W15-95	112	109.5	Far Field	CCUz	sM	5/22/2001	6	µg/kg	U
299-W15-95	114.5	112	Far Field	CCUc	Caliche	5/22/2001	6	µg/kg	U
299-W15-95	116	114.5	Far Field	CCUz	Caliche	5/22/2001	6	µg/kg	U
299-W15-95	118	116	Far Field	Re	msG	5/22/2001	5	µg/kg	U
299-W15-95	118.5	118	Far Field	Re	msG	5/22/2001	5	µg/kg	U
299-W15-95	122	120	Far Field	Re	sG	5/22/2001	5	µg/kg	U
299-W15-95	125	122.5	Far Field	Re	sG	5/23/2001	6	µg/kg	U
299-W15-95	132.5	130	Far Field	Re	S	5/25/2001	6	µg/kg	U
299-W15-95	146.5	145	Far Field	Re	mS	5/25/2001	6	µg/kg	U
299-W15-95	157.5	155	Far Field	Re	msG	5/29/2001	5	µg/kg	U
299-W15-95	187.5	185	Far Field	Re	S	5/31/2001	5	µg/kg	U
299-W18-174	53	53	216-Z-1A	H2	S	3/19/1993	28	µg/kg	J
299-W18-174	53	53	216-Z-1A	H2	S	3/22/1993	31	µg/kg	
299-W18-174	56	56	216-Z-1A	H2	S	3/22/1993	95	µg/kg	
299-W18-174	56	56	216-Z-1A	H2	S	3/22/1993	41	µg/kg	
299-W18-174	57.5	57.5	216-Z-1A	H2	S	3/24/1993	143	µg/kg	
299-W18-174	57.5	57.5	216-Z-1A	H2	S	3/24/1993	75	µg/kg	
299-W18-174	61	61	216-Z-1A	H2	S	3/24/1993	83	µg/kg	
299-W18-174	61	61	216-Z-1A	H2	S	3/24/1993	126	µg/kg	
299-W18-174	66	66	216-Z-1A	H2	S	3/25/1993	150	µg/kg	
299-W18-174	65.75	65.75	216-Z-1A	H2	S	3/25/1993	69	µg/kg	
299-W18-174	71.5	71.5	216-Z-1A	H2	S	3/25/1993	349	µg/kg	
299-W18-174	71.25	71.25	216-Z-1A	H2	S	3/25/1993	52	µg/kg	

Table A.1. (contd)

Well Name	Sample Bottom (ft)	Sample Top (ft)	Location	Geologic Unit	Sediment Classification	Sample Date	Result	Units	Data Qualifier
299-W18-174	74.5	74.5	216-Z-1A	H2	S	3/25/1993	337	µg/kg	
299-W18-174	74.5	74.5	216-Z-1A	H2	S	3/25/1993	151	µg/kg	
299-W18-174	76	76	216-Z-1A	H2	S	3/26/1993	67	µg/kg	
299-W18-174	75.8	75.8	216-Z-1A	H2	S	3/26/1993	67	µg/kg	
299-W18-174	80.6	80.6	216-Z-1A	H2	S	3/29/1993	51	µg/kg	
299-W18-174	80.5	80.5	216-Z-1A	H2	S	3/29/1993	56	µg/kg	
299-W18-174	86.6	86.6	216-Z-1A	H3	sG	3/29/1993	60	µg/kg	
299-W18-174	86.1	86.1	216-Z-1A	H3	sG	3/29/1993	35	µg/kg	
299-W18-174	90.45	90.45	216-Z-1A	H3	sG	3/29/1993	6	µg/kg	J
299-W18-174	90.45	90.45	216-Z-1A	H3	sG	3/29/1993	18	µg/kg	J
299-W18-174	93.5	93.5	216-Z-1A	H3	sG	3/30/1993	15	µg/kg	J
299-W18-174	93.5	93.5	216-Z-1A	H3	sG	3/30/1993	13	µg/kg	J
299-W18-174	95.95	95.95	216-Z-1A	H3	sG	3/30/1993	19	µg/kg	J
299-W18-174	95.95	95.95	216-Z-1A	H3	sG	3/30/1993	13	µg/kg	J
299-W18-174	101.1	101.1	216-Z-1A	H3	sG	4/1/1993	2	µg/kg	J
299-W18-174	101.1	101.1	216-Z-1A	H3	sG	4/1/1993	3	µg/kg	J
299-W18-174	105	105	216-Z-1A	H3	sG	4/2/1993			U
299-W18-174	105	105	216-Z-1A	H3	sG	4/2/1993	3	µg/kg	J
299-W18-174	111.5	111.5	216-Z-1A	H4	S	4/2/1993	103	µg/kg	
299-W18-174	111.5	111.5	216-Z-1A	H4	S	4/2/1993	24	µg/kg	J
299-W18-174	114.2	114.2	216-Z-1A	H4	mS	4/5/1993	498	µg/kg	
299-W18-174	114.2	114.2	216-Z-1A	H4	mS	4/5/1993	246	µg/kg	
299-W18-174	116.1	116.1	216-Z-1A	H4	sM	4/5/1993	230	µg/kg	
299-W18-174	115.8	115.8	216-Z-1A	H4	sM	4/5/1993	34	µg/kg	
299-W18-174	118.5	118.5	216-Z-1A	H4	mS	4/5/1993	68	µg/kg	
299-W18-174	118.5	118.5	216-Z-1A	H4	mS	4/5/1993	37	µg/kg	
299-W18-174	122.1	122.1	216-Z-1A	CCUz	M	4/6/1993	26	µg/kg	
299-W18-174	122.1	122.1	216-Z-1A	CCUz	M	4/6/1993	20	µg/kg	
299-W18-174	122.2	122.2	216-Z-1A	CCUz	M	4/6/1993	357	µg/kg	
299-W18-174	122.2	122.2	216-Z-1A	CCUz	M	4/6/1993	427	µg/kg	
299-W18-174	124.9	124.9	216-Z-1A	CCUz	M	4/6/1993	1247	µg/kg	
299-W18-174	124.9	124.9	216-Z-1A	CCUz	M	4/6/1993	796	µg/kg	
299-W18-174	124.9	124.9	216-Z-1A	CCUz	M	4/6/1993	890	µg/kg	
299-W18-174	124.9	124.9	216-Z-1A	CCUz	M	4/6/1993	789	µg/kg	
299-W18-174	127.1	127.1	216-Z-1A	CCUz	M	4/7/1993	6561	µg/kg	D
299-W18-174	126.8	126.8	216-Z-1A	CCUz	M	4/7/1993	749	µg/kg	
299-W18-174	128.9	128.9	216-Z-1A	CCUz	M	4/7/1993	4124	µg/kg	D
299-W18-174	128.9	128.9	216-Z-1A	CCUz	M	4/7/1993	3088	µg/kg	D
299-W18-174	131	131	216-Z-1A	CCUc	Caliche	4/8/1993	317	µg/kg	
299-W18-174	130.4	130.4	216-Z-1A	CCUc	Caliche	4/8/1993	374	µg/kg	
299-W18-246	56.8	56.3	216-Z-1A	H1	S	3/27/1992	133	µg/kg	
299-W18-246	107	106.5	216-Z-1A	H3	sG	4/13/1992	10	µg/kg	
299-W18-246	142.3	141.8	216-Z-1A	CCUz	M	4/16/1992	261	µg/kg	
299-W18-246	146.5	146	216-Z-1A	CCUc	mS	4/20/1992	772	µg/kg	
299-W18-246	194.9	194.4	216-Z-1A	Re	S	4/30/1992			U
299-W18-247	56.1	55.6	216-Z-18	H2	S	3/4/1992	13	µg/kg	

Table A.1. (contd)

Well Name	Sample Bottom (ft)	Sample Top (ft)	Location	Geologic Unit	Sediment Classification	Sample Date	Result	Units	Data Qualifier
299-W18-247	111	110.5	216-Z-18	H2	S	3/18/1992	17	µg/kg	
299-W18-247	135.4	134.9	216-Z-18	CCUz	M	3/19/1992	717	µg/kg	
299-W18-247	148.5	148	216-Z-18	CCUc	gsM	3/20/1992	47	µg/kg	
299-W18-247	154.7	154.2	216-Z-18	CCUc	S	3/25/1992	0.3	µg/kg	J
299-W18-248	20	19.5	216-Z-1A	H1	gS	5/4/1992	3	µg/kg	J
299-W18-248	40	39.5	216-Z-1A	H1	gS	5/6/1992	26	µg/kg	
299-W18-248	60.1	59.6	216-Z-1A	H2	mS	5/11/1992	126	µg/kg	
299-W18-248	65	65	216-Z-1A	H2	(m)S	5/12/1992	360	µg/kg	
299-W18-248	70	70	216-Z-1A	H2	S	5/12/1992	147	µg/kg	
299-W18-248	75	75	216-Z-1A	H2	S	5/12/1992	115	µg/kg	
299-W18-248	79.9	79.9	216-Z-1A	H2	S	5/12/1992	137	µg/kg	
299-W18-248	81.5	81	216-Z-1A	H2	(g)S	5/15/1992	95	µg/kg	
299-W18-248	85	85	216-Z-1A	H2	(g)S	5/18/1992	99	µg/kg	
299-W18-248	90	90	216-Z-1A	H3	msG	5/19/1992	74	µg/kg	
299-W18-248	95	95	216-Z-1A	H3	msG	5/19/1992	44	µg/kg	
299-W18-248	100	100	216-Z-1A	H3	msG	5/20/1992	16	µg/kg	
299-W18-248	102.5	102	216-Z-1A	H4	gS	5/21/1992	61	µg/kg	
299-W18-248	105	105	216-Z-1A	H4	S	5/21/1992	35	µg/kg	
299-W18-248	110	110	216-Z-1A	H4	S	5/21/1992	116	µg/kg	
299-W18-248	115	115	216-Z-1A	H4	S	5/21/1992	50	µg/kg	
299-W18-248	120	120	216-Z-1A	H4	S	5/21/1992	63	µg/kg	
299-W18-248	121.5	121	216-Z-1A	H4	S	5/22/1992	32	µg/kg	
299-W18-248	125	125	216-Z-1A	H4	S	5/22/1992	72	µg/kg	
299-W18-248	127	126.5	216-Z-1A	CCUz	M	5/22/1992	45	µg/kg	
299-W18-248	130	130	216-Z-1A	CCUz	M	5/26/1992	24	µg/kg	
299-W18-248	135	135	216-Z-1A	CCUz	M	5/26/1992	1093	µg/kg	
299-W18-248	140.5	140	216-Z-1A	CCUc	(g)mS	5/26/1992	644	µg/kg	
299-W18-248	140	140	216-Z-1A	CCUc	(g)mS	5/26/1992	51	µg/kg	
299-W18-249	22.9	22.4	216-Z-18	H1	sG	7/7/1992			U
299-W18-249	26	26	216-Z-18	H1	sG	7/7/1992	3	µg/kg	
299-W18-249	30	30	216-Z-18	H1	S	7/7/1992	4	µg/kg	
299-W18-249	31.3	30.8	216-Z-18	H1	S	7/8/1992			U
299-W18-249	33.5	33	216-Z-18	H1	S	7/8/1992	3	µg/kg	
299-W18-249	35.5	35	216-Z-18	H1	G	7/8/1992	6	µg/kg	
299-W18-249	37.5	37	216-Z-18	H1	G	7/8/1992	6	µg/kg	
299-W18-249	39.3	38.9	216-Z-18	H1	G	7/9/1992	7	µg/kg	
299-W18-249	45	45	216-Z-18	H1	msG	7/10/1992	9	µg/kg	
299-W18-249	50	50	216-Z-18	H1	msG	7/10/1992	15	µg/kg	
299-W18-249	55	55	216-Z-18	H1	msG	7/13/1992	24	µg/kg	
299-W18-249	59	59	216-Z-18	H2	(m)S	7/13/1992	122	µg/kg	
299-W18-249	59.6	59.1	216-Z-18	H2	(m)S	7/13/1992	39	µg/kg	
299-W18-249	65	65	216-Z-18	H2	(m)S	7/13/1992	31	µg/kg	
299-W18-249	70	70	216-Z-18	H2	(m)S	7/13/1992	74	µg/kg	
299-W18-249	75	75	216-Z-18	H2	S	7/13/1992	216	µg/kg	
299-W18-249	80	80	216-Z-18	H2	mS	7/13/1992	184	µg/kg	
299-W18-249	81.4	80.9	216-Z-18	H2	mS	7/14/1992	139	µg/kg	

Table A.1. (contd)

Well Name	Sample Bottom (ft)	Sample Top (ft)	Location	Geologic Unit	Sediment Classification	Sample Date	Result	Units	Data Qualifier
299-W18-249	85	85	216-Z-18	H2	mS	7/14/1992	133	µg/kg	
299-W18-249	90	90	216-Z-18	H2	(m)S	7/14/1992	566	µg/kg	
299-W18-249	95	95	216-Z-18	H2	mS	7/14/1992	188	µg/kg	
299-W18-249	99	99	216-Z-18	H2	(m)S	7/16/1992	168	µg/kg	
299-W18-249	100.5	100	216-Z-18	H2	(m)S	7/16/1992	53	µg/kg	
299-W18-249	100.5	100	216-Z-18	H2	(m)S	7/16/1992			U
299-W18-249	100.5	100	216-Z-18	H2	(m)S	7/16/1992	4	µg/kg	
299-W18-249	107	107	216-Z-18	H3	sG	7/16/1992	14	µg/kg	
299-W18-249	110	110	216-Z-18	H3	sG	7/16/1992	44	µg/kg	
299-W18-249	115	115	216-Z-18	H3	G	7/16/1992	34	µg/kg	
299-W18-249	120	120	216-Z-18	H3	G	7/17/1992	28	µg/kg	
299-W18-249	125	125	216-Z-18	H3	G	7/17/1992	9	µg/kg	
299-W18-249	128.3	127.8	216-Z-18	H4	mS	7/21/1992	58	µg/kg	
299-W18-249	133	133	216-Z-18	CCUz	M	7/21/1992	1618	µg/kg	
299-W18-249	135	135	216-Z-18	CCUz	M	7/21/1992	134	µg/kg	
299-W18-249	140	140	216-Z-18	CCUz	M	7/21/1992	481	µg/kg	
299-W18-249	145	145	216-Z-18	CCUc	mS	7/21/1992	1957	µg/kg	
299-W18-249	146.7	146.2	216-Z-18	CCUc	mS	7/21/1992	1755	µg/kg	
299-W18-252	4.5	4.5	Far Field	Hol	S	5/3/1993	6	µg/kg	J
299-W18-252	9.5	9.5	Far Field	H1	gS	5/3/1993	2	µg/kg	J
299-W18-252	15	15	Far Field	H1	sG	5/3/1993			U
299-W18-252	20	20	Far Field	H1	S	5/3/1993			U
299-W18-252	25	25	Far Field	H1	gS	5/4/1993			U
299-W18-252	30.6	30.6	Far Field	H1	gS	5/4/1993			U
299-W18-252	35	35	Far Field	H1	gS	5/5/1993	7	µg/kg	J
299-W18-252	39.5	39.5	Far Field	H1	S	5/5/1993	57	µg/kg	
299-W18-252	44.7	44.7	Far Field	H1	sG	5/6/1993	18	µg/kg	J
299-W18-252	49.5	49.5	Far Field	H1	sG	5/10/1993			U
299-W18-252	55	55	Far Field	H2	S	5/10/1993	16	µg/kg	J
299-W18-252	59.5	59.5	Far Field	H2	S	5/11/1993			U
299-W18-252	65.5	65.5	Far Field	H2	S	5/11/1993	48	µg/kg	
299-W18-252	70.5	70.5	Far Field	H2	S	5/12/1993	77	µg/kg	
299-W18-252	75.5	75.5	Far Field	H2	S	5/12/1993	62	µg/kg	
299-W18-252	80.2	80.2	Far Field	H2	S	5/12/1993	84	µg/kg	
299-W18-252	85.5	85.5	Far Field	H2	S	5/13/1993	25	µg/kg	J
299-W18-252	89.7	89.7	Far Field	H2	S	5/13/1993	155	µg/kg	
299-W18-252	96	96	Far Field	H2	S	5/13/1993	101	µg/kg	
299-W18-252	99.5	99.5	Far Field	H2	S	5/14/1993	22	µg/kg	
299-W18-252	105	105	Far Field	H3	sG	5/14/1993	9	µg/kg	J
299-W18-252	115	115	Far Field	H3	G	5/17/1993			U
299-W18-252	121.25	121.25	Far Field	H3	sG	5/18/1993	6	µg/kg	J
299-W18-252	126.5	126.5	Far Field	CCUz	sM	5/19/1993	519	µg/kg	
299-W18-252	129.5	129.5	Far Field	CCUz	sM	5/19/1993	74	µg/kg	
299-W18-252	134.8	134.8	Far Field	CCUz	mS	5/19/1993	307	µg/kg	
299-W18-252	142.1	142.1	Far Field	Re	sG	5/25/1993	53	µg/kg	
299-W18-252	145.5	145.5	Far Field	Re	sG	5/25/1993	140	µg/kg	

Table A.1. (contd)

Well Name	Sample Bottom (ft)	Sample Top (ft)	Location	Geologic Unit	Sediment Classification	Sample Date	Result	Units	Data Qualifier
299-W18-252	149.7	149.7	Far Field	Re	S	5/26/1993	56	µg/kg	
299-W18-252	154.5	154.5	Far Field	Re	S	5/26/1993	281	µg/kg	
299-W18-252	159.5	159.5	Far Field	Re	sG	5/26/1993	205	µg/kg	
299-W18-252	164.5	164.5	Far Field	Re	gS	5/27/1993	177	µg/kg	
299-W18-252	164.5	164.5	Far Field	Re	gS	5/27/1993	377	µg/kg	
299-W18-252	172	172	Far Field	Re	G	5/28/1993	10	µg/kg	J
299-W18-252	175.5	175.5	Far Field	Re	sG	6/1/1993	116	µg/kg	
299-W18-252	191.7	191.7	Far Field	Re	sG	6/1/1993	8	µg/kg	J
299-W18-252	182	182	Far Field	Re	G	6/1/1993			U
299-W18-252	185.1	185.1	Far Field	Re	S	6/1/1993	159	µg/kg	
299-W18-252	195.8	195.8	Far Field	Re	sG	6/3/1993			U
299-W18-252	199.5	199.5	Far Field	Re	sG	6/3/1993	130	µg/kg	
299-W18-252	206.1	206.1	Far Field	Re	sG	6/7/1993	24	µg/kg	J
299-W18-252	211.1	211.1	Far Field	Re	sG	6/7/1993			U
299-W18-252	214.7	214.7	Far Field	Re	sG	6/8/1993			U
299-W18-252	220.2	220.2	Far Field	Re	sG	6/8/1993			U
299-W18-252	225.6	225.6	Far Field	Re	sG	6/9/1993			U
299-W18-27	142	140	Far Field	H2/CCUz	S/M	4/5/1991	5	µg/kg	U
299-W18-27	142	140	Far Field	H2/CCUz	S/M	4/5/1991	5	µg/kg	U
299-W18-27	81		Far Field	H1	msG	4/10/1991	6	µg/kg	U
299-W18-27	81		Far Field	H1	msG	4/10/1991	6	µg/kg	U
299-W18-27	102	100	Far Field	H1/H2	sG	4/12/1991	5	µg/kg	U
299-W18-27	102	100	Far Field	H1/H2	sG	4/12/1991	5	µg/kg	U
299-W18-27	121	119	Far Field	H2	S	4/12/1991	5	µg/kg	U
299-W18-27	121	119	Far Field	H2	S	4/12/1991	5	µg/kg	U
299-W18-27	161	159	Far Field	Re	gS	4/18/1991	5	µg/kg	U
299-W18-27	161	159	Far Field	Re	gS	4/18/1991	5	µg/kg	U
299-W18-27	185	183	Far Field	Re	sG	4/25/1991	5	µg/kg	U
299-W18-27	185	183	Far Field	Re	sG	4/25/1991	6	µg/kg	U
299-W18-27	201	198	Far Field	Re	gS	4/30/1991	5	µg/kg	U
299-W18-27	201	198	Far Field	Re	gS	4/30/1991	6	µg/kg	U
299-W18-28	27		Far Field	H1a	(g)S	4/9/1991	5	µg/kg	U
299-W18-28	27		Far Field	H1a	(g)S	4/9/1991	5	µg/kg	U
299-W18-28	47		Far Field	H1a	S	4/10/1991	5	µg/kg	U
299-W18-28	47		Far Field	H1a	S	4/10/1991	5	µg/kg	U
299-W18-28	69	67	Far Field	H1	G	4/11/1991	5	µg/kg	U
299-W18-28	69	67	Far Field	H1	G	4/11/1991	5	µg/kg	U
299-W18-28	89	87	Far Field	H2	(m)S	4/15/1991	6	µg/kg	U
299-W18-28	89	87	Far Field	H2	(m)S	4/15/1991	6	µg/kg	U
299-W18-28	114	112	Far Field	H2	S	4/16/1991	5	µg/kg	U
299-W18-28	114	112	Far Field	H2	S	4/16/1991	6	µg/kg	U
299-W18-28	135	133	Far Field	H2	mS	4/17/1991	6	µg/kg	U
299-W18-28	135	133	Far Field	H2	mS	4/17/1991	6	µg/kg	U
299-W18-28	155	153	Far Field	CCUc	sG	4/23/1991	5	µg/kg	U
299-W18-28	155	153	Far Field	CCUc	sG	4/23/1991	6	µg/kg	U
299-W18-28	174	173	Far Field	Re	gS	4/26/1991	6	µg/kg	U
299-W18-28	174	173	Far Field	Re	gS	4/26/1991	5	µg/kg	U

Table A.1. (contd)

Well Name	Sample Bottom (ft)	Sample Top (ft)	Location	Geologic Unit	Sediment Classification	Sample Date	Result	Units	Data Qualifier
299-W18-28	195	193	Far Field	Re	sG	4/30/1991	5	µg/kg	U
299-W18-28	195	193	Far Field	Re	sG	4/30/1991	6	µg/kg	U
299-W18-28	130		Far Field	H2	mS	5/6/1991	6	µg/kg	U
299-W18-28	130		Far Field	H2	mS	5/6/1991	5	µg/kg	U
299-W18-29	80		Far Field	H3	sG	4/5/1991	5	µg/kg	U
299-W18-29	80		Far Field	H3	sG	4/5/1991	5	µg/kg	U
299-W18-29	100		Far Field	H3	sG	4/9/1991	5	µg/kg	U
299-W18-29	100		Far Field	H3	sG	4/9/1991	5	µg/kg	U
299-W18-29	120		Far Field	H4	S	4/10/1991	6	µg/kg	U
299-W18-29	120		Far Field	H4	S	4/10/1991	6	µg/kg	U
299-W18-29	128		Far Field	CCUz	M	4/11/1991	22	µg/kg	
299-W18-29	128		Far Field	CCUz	M	4/11/1991	23	µg/kg	
299-W18-29	131	129	Far Field	CCUz	sM	4/11/1991	4	µg/kg	J
299-W18-29	131	129	Far Field	CCUz	sM	4/11/1991	4	µg/kg	J
299-W18-29	133	131	Far Field	CCUz	sM	4/12/1991	6	µg/kg	U
299-W18-29	133	131	Far Field	CCUz	sM	4/12/1991	6	µg/kg	U
299-W18-29	135	133	Far Field	CCUz	sM	4/12/1991	5	µg/kg	J
299-W18-29	135	133	Far Field	CCUz	sM	4/12/1991	4	µg/kg	J
299-W18-29	152	150	Far Field	Re	(m)sG	4/23/1991	6	µg/kg	U
299-W18-29	152	150	Far Field	Re	(m)sG	4/23/1991	6	µg/kg	U
299-W18-40	7	0	Far Field	Bf	mS	9/19/2001	6	µg/kg	U
299-W18-40	230	218	Far Field	Re	msG	9/19/2001	8	µg/kg	U
299-W18-40	230	218	Far Field	Re	msG	4/16/2002	0.9	µg/kg	U
299-W18-96	84.5	84	216-Z-18	H2	S	2/10/1993	89	µg/kg	
299-W18-96	86.5	86.5	216-Z-18	H2	S	2/11/1993	93	µg/kg	
299-W18-96	86.5	86.5	216-Z-18	H2	S	2/11/1993	79	µg/kg	
299-W18-96	90	90	216-Z-18	H2	S	2/12/1993	440	µg/kg	
299-W18-96	90	90	216-Z-18	H2	S	2/12/1993	332	µg/kg	
299-W18-96	92.35	92.35	216-Z-18	H2	S	2/12/1993	99	µg/kg	
299-W18-96	92.35	92.35	216-Z-18	H2	S	2/12/1993	56	µg/kg	
299-W18-96	95	95	216-Z-18	H2	(m)S	2/12/1993	124	µg/kg	
299-W18-96	98	98	216-Z-18	H2	(m)S	2/12/1993	111	µg/kg	
299-W18-96	98	98	216-Z-18	H2	(m)S	2/12/1993	193	µg/kg	
299-W18-96	100.5	100.5	216-Z-18	H2	(gm)S	2/12/1993	242	µg/kg	
299-W18-96	100.5	100.5	216-Z-18	H2	(gm)S	2/12/1993	127	µg/kg	
299-W18-96	104	104	216-Z-18	H2	gS	2/12/1993	140	µg/kg	
299-W18-96	110.15	110.15	216-Z-18	H3	sG	2/16/1993	10	µg/kg	J
299-W18-96	110.15	110.15	216-Z-18	H3	sG	2/16/1993	4	µg/kg	J
299-W18-96	116	116	216-Z-18	H3	sG	2/16/1993	12	µg/kg	
299-W18-96	119	119	216-Z-18	H3	sG	2/17/1993	6	µg/kg	J
299-W18-96	120	120	216-Z-18	H3	sG	2/17/1993	2	µg/kg	J
299-W18-96	120	120	216-Z-18	H3	sG	2/17/1993	7	µg/kg	J
299-W18-96	123.5	123.5	216-Z-18	H3	G	2/17/1993	52	µg/kg	
299-W18-96	123.5	123.5	216-Z-18	H3	G	2/17/1993	41	µg/kg	
299-W18-96	125.5	125.5	216-Z-18	H3	G	2/18/1993	41	µg/kg	
299-W18-96	125.5	125.5	216-Z-18	H3	G	2/18/1993	68	µg/kg	
299-W18-96	125.5	125.5	216-Z-18	H3	G	2/18/1993	8	µg/kg	J

Table A.1. (contd)

Well Name	Sample Bottom (ft)	Sample Top (ft)	Location	Geologic Unit	Sediment Classification	Sample Date	Result	Units	Data Qualifier
299-W18-96	125.5	125.5	216-Z-18	H3	G	2/18/1993	5	µg/kg	J
299-W18-96	129	129	216-Z-18	H4	mG	2/22/1993	43	µg/kg	
299-W18-96	129	129	216-Z-18	H4	mG	2/22/1993	65	µg/kg	
299-W18-96	129	129	216-Z-18	H4	mG	2/22/1993	39	µg/kg	
299-W18-96	129	129	216-Z-18	H4	mG	2/22/1993	28	µg/kg	
299-W18-96	130.5	130.5	216-Z-18	H4	mG	2/22/1993	16	µg/kg	
299-W18-96	130.5	130.5	216-Z-18	H4	mg	2/22/1993	5	µg/kg	J
299-W18-96	130.5	130.5	216-Z-18	H4	mG	2/22/1993	4	µg/kg	J
299-W18-96	130.5	130.5	216-Z-18	H4	mG	2/22/1993	14	µg/kg	
299-W18-96	134.5	134.5	216-Z-18	H4	sM	2/22/1993	111	µg/kg	
299-W18-96	134.5	134.5	216-Z-18	H4	sM	2/22/1993	17	µg/kg	J
299-W18-96	136.5	136.5	216-Z-18	H4	sM	2/23/1993	786	µg/kg	
299-W18-96	136.5	136.5	216-Z-18	H4	sM	2/23/1993	759	µg/kg	
299-W18-96	138.5	138.5	216-Z-18	CCUz	M	2/24/1993	334	µg/kg	
299-W18-96	138.5	138.5	216-Z-18	CCUz	M	2/24/1993	494	µg/kg	
299-W18-96	143.84	143.84	216-Z-18	CCUz	M	2/25/1993	861	µg/kg	
299-W18-96	143.84	143.84	216-Z-18	CCUz	M	2/25/1993	626	µg/kg	
299-W18-96	143.84	143.84	216-Z-18	CCUz	M	2/25/1993	714	µg/kg	
299-W18-96	144.45	144.45	216-Z-18	CCUz	M	2/25/1993	28	µg/kg	
299-W18-96	144.45	144.45	216-Z-18	CCUz	M	2/25/1993	24	µg/kg	J
299-W18-96	146.5	146.5	216-Z-18	CCUc	Caliche	2/25/1993	33	µg/kg	
299-W18-96	146.5	146.5	216-Z-18	CCUc	Caliche	2/25/1993	33	µg/kg	
299-W19-34B	170.5	168	Far Field			4/14/1994	11	µg/kg	U
299-W19-34B	170.5	168	Far Field			4/14/1994	11	µg/kg	U
299-W19-34B	188.5	186	Far Field			4/18/1994	11	µg/kg	U
299-W19-34B	244.5	242.5	Far Field			4/26/1994	16	µg/kg	U
299-W19-34B	334	332	Far Field			6/1/1994	12	µg/kg	UJ
299-W19-34B	417.5	416	Far Field			6/30/1994	12	µg/kg	U
299-W19-34B	442	440	Far Field			8/1/1994	12	µg/kg	U
299-W19-34B	462	460	Far Field			8/5/1994	12	µg/kg	U
299-W19-34B	481.5	480.5	Far Field			8/11/1994	13	µg/kg	U
299-W19-34B	531.3	530	Far Field			8/24/1994	11	µg/kg	U
299-W19-35	160.5	158	Far Field			3/7/1994	12	µg/kg	U
299-W19-35	181	179	Far Field			3/8/1994	11	µg/kg	U
299-W19-35	238.5	236	Far Field			3/16/1994	10	µg/kg	U
299-W19-35	238.5	236	Far Field			3/16/1994	10	µg/kg	U
299-W19-35	247	245	Far Field			3/18/1994	11	µg/kg	U
299-W19-43	25		Far Field			7/2/2001	6	µg/kg	U
299-W19-43	25		Far Field			7/2/2001	6	µg/kg	U
299-W19-43	262	260	Far Field			7/17/2001	5	µg/kg	U
299-W19-44	233		Far Field			8/30/2001	6	µg/kg	U
299-W19-44	50		Far Field			8/30/2001	5	µg/kg	U
299-W19-44	245	233	Far Field			4/16/2002	0.8	µg/kg	U
299-W19-45			Far Field			8/17/2001	6	µg/kg	U
299-W19-45			Far Field			8/17/2001	6	µg/kg	U

Table A.1. (contd)

Well Name	Sample Bottom (ft)	Sample Top (ft)	Location	Geologic Unit	Sediment Classification	Sample Date	Result	Units	Data Qualifier
299-W19-45	234	228	Far Field			4/16/2002	1	µg/kg	U
299-W19-46	267	260	Far Field			11/20/2002	6	µg/kg	U
299-W19-46	30	0	Far Field			12/2/2002	5	µg/kg	U
299-W19-48	290	285	Far Field			11/24/2004	2	µg/kg	U
299-W19-48	340		Far Field			12/9/2004	2.4	µg/kg	U
299-W19-48	340		Far Field			12/9/2004	2.3	µg/kg	U
299-W19-48	407	402	Far Field			12/13/2004	2.4	µg/kg	U
299-W19-48	429	424	Far Field			12/15/2004	2.5	µg/kg	U
299-W19-94	32	30	Far Field			11/15/1993	25	µg/kg	U
299-W19-94	6	4	Far Field			12/3/1993	11	µg/kg	U
299-W19-94	17.5	15.5	Far Field			12/6/1993	11	µg/kg	U
299-W19-94	36	33.5	Far Field			12/8/1993	25	µg/kg	U
299-W19-94	40	38	Far Field			12/13/1993	13000	µg/kg	U
299-W19-94	59.5	57.5	Far Field			12/14/1993	5100	µg/kg	U
299-W19-94	50	48	Far Field			12/14/1993	4900	µg/kg	U
299-W19-94	70	68	Far Field			12/15/1993	10	µg/kg	U
299-W19-94	91.5	89.5	Far Field			12/16/1993	1300	µg/kg	U
299-W19-94	116	114	Far Field			1/3/1994	12	µg/kg	U
299-W19-94	130	128	Far Field			1/4/1994	11	µg/kg	U
299-W19-94	150	148	Far Field			1/6/1994	10	µg/kg	U
299-W19-94	150	148	Far Field			1/6/1994	10	µg/kg	U
299-W19-94	167.5	165.5	Far Field			1/7/1994	11	µg/kg	U
299-W19-94	167.5	165.5	Far Field			1/7/1994	11	µg/kg	U
299-W19-94	189	187	Far Field			1/13/1994	11	µg/kg	U
299-W19-94	199	197	Far Field			1/17/1994	13	µg/kg	U
299-W19-95	16.5	14.5	Far Field			9/3/1993	11	µg/kg	U
299-W19-95	32.5	30	Far Field			9/7/1993	11	µg/kg	U
299-W19-95	47.5	45	Far Field			9/8/1993	11	µg/kg	U
299-W19-95	62.5	60	Far Field			9/9/1993	11	µg/kg	U
299-W19-95	77.3	74.8	Far Field			9/10/1993	10	µg/kg	U
299-W19-95	92.25	90.25	Far Field			9/13/1993	11	µg/kg	U
299-W19-95	107.5	105	Far Field			9/15/1993	10	µg/kg	U
299-W19-95	107.5	105	Far Field			9/15/1993	11	µg/kg	U
299-W19-95	142.5	140	Far Field			9/16/1993	11	µg/kg	U
299-W19-95	122.5	120	Far Field			9/16/1993	11	µg/kg	U
299-W19-95	167.5	165	Far Field			9/16/1993	12	µg/kg	U
299-W19-95	182	181	Far Field			9/20/1993	10	µg/kg	U
299-W19-95	171.5	169	Far Field			9/20/1993	10	µg/kg	U
299-W19-95	171.5	169	Far Field			9/20/1993	11	µg/kg	U
299-W19-96	6	4	Far Field			11/5/1993	10	µg/kg	U
299-W19-96	17	15	Far Field			11/10/1993	5	µg/kg	U
299-W19-96	24	22	Far Field			11/12/1993	5	µg/kg	U
299-W19-96	27	24.5	Far Field			11/15/1993	20	µg/kg	U
299-W19-96	29.5	27	Far Field			11/16/1993	21	µg/kg	U
299-W19-96	32	29.5	Far Field			11/17/1993	23	µg/kg	U
299-W19-96	42.5	40.5	Far Field			12/9/1993	13000	µg/kg	U
299-W19-96	52	50	Far Field			12/13/1993	10	µg/kg	U

Table A.1. (contd)

Well Name	Sample Bottom (ft)	Sample Top (ft)	Location	Geologic Unit	Sediment Classification	Sample Date	Result	Units	Data Qualifier
299-W19-96	62	60	Far Field			12/15/1993	10	µg/kg	U
299-W19-96	82	80	Far Field			12/16/1993	10	µg/kg	U
299-W19-96	101.5	99.5	Far Field			12/20/1993	11	µg/kg	U
299-W19-96	122	120	Far Field			1/3/1994	12	µg/kg	U
299-W19-96	142	140	Far Field			1/3/1994	11	µg/kg	U
299-W19-96	142	140	Far Field			1/3/1994	11	µg/kg	U
299-W19-96	170	168	Far Field			1/5/1994	10	µg/kg	U
299-W19-96	168	166	Far Field			1/5/1994	12	µg/kg	U
299-W19-96	168	166	Far Field			1/5/1994	12	µg/kg	U
299-W19-96	161	159	Far Field			1/5/1994	11	µg/kg	U
299-W19-96	177	175	Far Field			1/11/1994	10	µg/kg	U
299-W19-97	6	4	Far Field			9/7/1993	11	µg/kg	U
299-W19-97	22.5	20	Far Field			9/8/1993	11	µg/kg	U
299-W19-97	32	30	Far Field			9/8/1993	10	µg/kg	U
299-W19-97	12.5	10	Far Field			9/8/1993	11	µg/kg	U
299-W19-97	52.5	50	Far Field			9/10/1993	12	µg/kg	U
299-W19-97	72.5	70	Far Field			9/13/1993	11	µg/kg	U
299-W19-97	103.3	101	Far Field			9/15/1993	11	µg/kg	U
299-W19-97	103.3	101	Far Field			9/15/1993	11	µg/kg	U
299-W19-97	132.5	130	Far Field			9/16/1993	11	µg/kg	U
299-W19-97	148.5	146	Far Field			9/17/1993	11	µg/kg	U
299-W19-97	148.5	146	Far Field			9/17/1993	11	µg/kg	U
299-W19-97	158.5	156	Far Field			9/17/1993	12	µg/kg	U
299-W19-97	170	167.5	Far Field			9/20/1993	12	µg/kg	U
299-W19-97	177	175.7	Far Field			9/21/1993	11	µg/kg	U
299-W19-98	5.4	4.4	Far Field			1/13/1994	11	µg/kg	U
299-W19-98	13.5	11	Far Field			3/2/1994	10	µg/kg	U
299-W19-98	17.25	15	Far Field			3/3/1994	11	µg/kg	U
299-W19-98	26.5	24	Far Field			3/4/1994	10	µg/kg	U
299-W19-98	49	47	Far Field			3/8/1994	10	µg/kg	U
299-W19-98	62.2	60	Far Field			3/9/1994	11	µg/kg	U
299-W19-98	82.1	80	Far Field			3/10/1994	10	µg/kg	U
299-W19-98	102.5	100	Far Field			3/14/1994	11	µg/kg	U
299-W19-98	132	130	Far Field			3/15/1994	11	µg/kg	U
299-W19-98	175.3	172	Far Field			3/17/1994	11	µg/kg	U
299-W19-98	185.5	183.5	Far Field			3/17/1994	11	µg/kg	U
299-W19-98	175.3	173	Far Field			3/17/1994	11	µg/kg	U
299-W19-98	185.5	183.5	Far Field			3/17/1994	11	µg/kg	U
299-W19-98	193	191.1	Far Field			3/22/1994	10	µg/kg	U

Table A.2. Compilation of Modeled (Murray et al. 2006) and Measured (HEIS) Concentrations of Carbon Tetrachloride in Groundwater Beneath the Disposal Areas (ND = No data)

Depth Below Water Table (m)	Modeled CT at 216-Z-9 (ppb)	Modeled CT at 216-Z-1A (ppb)	Modeled CT at 216-Z-18 (ppb)	Measured CT at 216-Z-9 (ppb)
0	663	93	54	ND
2.5	800	127	78	330
5	389	120	80	1600
7.5	110	89	95	0
10	96	100	82	115
12.5	92	92	95	720
15	116	95	97	3800
17.5	98	97	83	ND
20	920	120	96	2200
22.5	720	139	86	270
25	460	145	78	ND
27.5	330	116	44	ND
30	186	66	26	110
32.5	110	23	17	nd
35	95	25	16	29
37.5	99	29	17	nd
40	190	47	29	250
42.5	534	68	36	ND
45	690	76	26	1025
47.5	460	46	17	470
50	147	26	13	ND
52.5	61	16	9	8.7
55	46	11	6	ND
57.5	75	8	4	ND
60	93	4	1	190

Distribution

No. of Copies

OFFSITE

Wes Bratton
Vista Engineering
8203 West Quinault Avenue
Kennewick, WA 99336

Rick Dinicola
U.S. Geological Survey
Washington Water Science Center
1210 Pacific Avenue, Suite 600
Tacoma, WA 98402

ONSITE

6 **DOE Richland Operations Office**

B. L. Foley*	A6-38
J. G. Morse*	A6-38
K. M. Thompson*	A6-38
A. C. Tortoso*	A6-38
Public Reading Room (2*)	H2-53

11 **Fluor Hanford, Inc.**

J. V. Borghese	E6-35
M. E. Byrnes	E6-35
D. B. Erb	E6-35
T. W. Fogwell*	E6-35
B. H. Ford	E6-35
D. S. Miller*	E6-35
S. W. Petersen	E6-35
V. J. Rohay (2*)	E6-35
A. F. Shattuck*	E6-35
L. C. Swanson	E6-35
M. E. Todd-Robertson*	E6-35

No. of Copies

U.S. Environmental Protection Agency

D. A. Faulk*	B1-46

Washington State Department of Ecology

D. Goswami*	H0-57

15 **Pacific Northwest National Laboratory**

R. W. Bryce	E6-35
A.R. Felmy	K8-96
M. D. Freshley	K9-33
N.J. Hess	K8-96
C. T. Kincaid	K9-33
G. V. Last*	K6-81
M. Oostrom (2*)	K9-33
M. L. Rockhold*	K9-36
P. D. Thorne*	K9-33
M. J. Truex*	K6-96
S. B. Yabusaki	K9-33
M. D. White	K9-33
Hanford Technical Library (2*)	P8-55

*Hard copy distribution; all others receive electronic file.